ACTA UNIVERSITATIS SZEGEDIENSIS

ACTA MINERALOGICA-PETROGRAPHICA

Tomus XXXVI.

SZEGED, HUNGARIA
1995

NOTE TO CONTRIBUTORS

General

The Acta Mineralogica–Petrographica publishes original studies on the field of geochemistry mineralogy and petrology, first of all studies Hungarian researches, papers resulted in by cooperation of Hungarian researches and those of other countries and, in a limited volume, papers from abroad on topics of global interest.

Manusrcipts should be written in English and submitted to the Editor-in-chief, Institute of Mineralogy, Geochemistry and Petrography, Attila József University, H–6701 Szeged, Pf. 651 Hungary.

The authors are responsible for the accuracy of their data, references and quotations from other sources.

Manuscript

Manuscript should be typewritten with double spacing, 25 lines on a page and space for 50 letter in a line. Each new paragraph should begin with an indented line. Underline only words that should be typed in italics.

Manusrcipt should be generally be organized in the following order:

Title
Name(s) of author(s) and their affiliations, in foot-note the address of the author to whom the correspondence should be sent.
Abstract
Introduction
Methods, techniques, material studied, description of the area investigated, etc.
Results
Discussion or conclusions
Acknowledgement
Explanation of plates (if any)
Tables
Captions of figures (drawings, photomicrographs, etc.)

Abstract

The abstract cannot be longer than 500 words.

Tables

The tables should be typewritten on separate sheets and numbered according to their sequence in the text, which refers to all tables.

The title of the table as well as the colum headings must be brief, but sufficiently explanatory.

The tables generally should not exceed the type-area of the journal, i.e. 12,5x18,5 cm. Foldouts can only exceptionally be accepted.

(continuation on the inner side of verso)

ACTA UNIVERSITATIS SZEGEDIENSIS

ACTA MINERALOGICA-PETROGRAPHICA

Tomus XXXVI.

SZEGED, HUNGARIA
1995

HU ISSN 0365–8006
HU ISSN 0324–6523

SERIES NOSTRA AB INSTITUTIS MINERALOGICIS, GEOCHEMICIS PETROGRAPHICS UNIVERSITATUM HUNGARICUM ADIUVATUR

Nota

Acta Miner. Petr., Szeged

Szerkeszti

SZEDERKÉNYI TIBOR

a szerkesztőbizottság tagjai

KUBOVICS IMRE
EGERER FRIGYES
SZÖŐR GYULA
KLEB BÉLA

Kiadja

a József Attila Tudományegyetem Ásványtani, Geokémiai és Kőzettani Tanszéke
H–6722 Szeged, Egyetem u. 2–6.

Kiadványunk címének rövidítése
Acta Miner. Petr., Szeged

SOROZATUNK A MAGYARORSZÁGI EGYETEMEK ROKON TANSZÉKEINEK TÁMOGATÁSÁVAL JELENIK MEG

Printed in JUHÁSZ NYOMDA, Szeged

CONTENTS

Acta Mineralogica-Petrographica, Szeged, XXXVI, 5–15, 1995

SILVER MINERALS FROM RUDABÁNYA (N-HUNGARY)

S. SZAKÁLL* –Á. KOVÁCS**

Herman Ottó Museum, Department of Mineralogy
University of Miskolc, Department of Metallurgy

ABSTRACT

Numerous silver minerals were found recently in the primary and in the secondary oxidation zone of the hydrothermal-metasomatic iron ore deposit at Rudabánya, Northern-Hungary.

In the baritized zone bound to the carbonatic ore - primary in the galena-rich orebodies - silver, acanthite, proustite, pyrargyrite and xanthoconite? were found. The limonitic and siliceous limonitic ores of the oxidation zone contains acanthite, moschellandsbergite, bromargyrite, chlorargyrite and iodargyrite. These minerals are the resultant products of the recrystallization of the silver-bearing phases of the baritized zone, i.e. of secondary origin. This paper is on the description of the minerals referred to above.

INTRODUCTION

The professional literature refers to only one silver mineral, pyrargyrite from Rudabánya. This is surprising, having regard to the fact that Rudabánya was famed for its medieval silver mining. According to PODÁNYI (1956), the mineral under mining was silver-bearing galena. The earlier examinations proved that silver was present almost in every ore type as a trace element (KOCH, GRASSELLY and DONÁTH, 1956; PANTÓ, 1956; CSALAGOVITS, 1973). From the examinations of Csalagovits it turned out however, that the richest in silver is the baritized zone. It was also proved that silver enrichments are always bound to lead, therefore to galena. The only described silver mineral, pyrargyrite was observed by KOCH (1966), by ore microscope in a galena specimen from the primary zone. According to his description it occurs at the boundary of galena and barite as narrow strips.

RESULTS OF THE EXAMINATIONS

Primary silver minerals

Silver

It was found several times in the Polyánka and Vilmos areas of the deposit. In case of the specimen from Polyánka, the correct place of occurrence is not known, because it was found on the waste dump. The carbonatic ore consist of calcite, siderite and quartz grains, according to the microprobe analysis.

* H–3525 Miskolc, Kossuth u. 13.
** H–3515 Miskolc, Egyetemváros

The microprobe analyses and the SEM examinations were made by AMRAY 1803 I equipment with connected energy dispersive sensor at the Dept. of Metallurgy, University of Miskolc. Accelerating voltage: 20 kV, test current 10^{-10}, SiLi detector, W cathode, EDAX-EDS system, analyses by supplied softwares.

Disseminated pyrite and galena were also observed in the carbonatic ore. Silver occurred as shining white scales in fissures of the ore. At the edge of the grains thorn-like crystals were observed by SEM. According to analyses the grains are formed by xenomorphous silver and acanthite in its gaps and on the edges (*Fig. 1.*). Acanthite was often observed as acicular aggregates and as silver-form grains in cases alteration had completed. The greatest silver grains which size of 20 μm. Based on the EDX studies it contains no other element. It also occurs in the cavities of the galena-bearing barite of a Vilmos area as 1-3 mm hair-like aggregates and tufted bunches (*Fig. 2.*). On the surfaces of these aggregates acanthite appears as acicular crystals. This mineral association is supposedly of secondary origin.

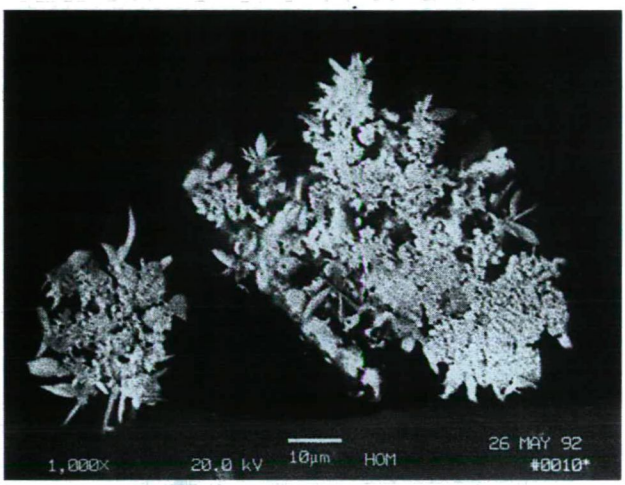

Fig. 1. Silver, grained appearance with acicular acanthite. Rudabánya-Polyánka. Back-scattered electron image. (Herman Ottó Museum (HOM) collection)

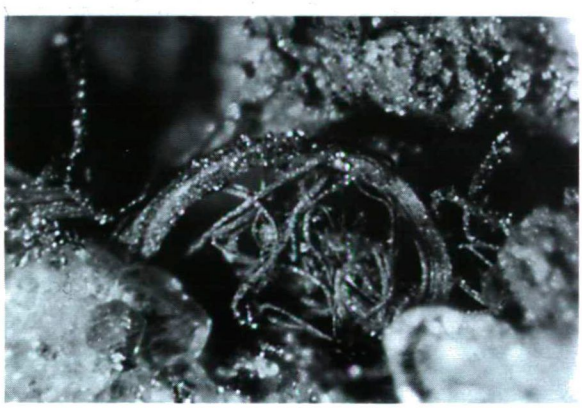

Fig. 2. Silver, hair-like aggregates. Rudabánya-Vilmos. Width of the picture: 5 mm. (S. Klaj collection).

Acanthite

As a widely distributed silver mineral acanthite was observed in the primary and the secondary zone as well in numerous openings, always in small quantities. When occurring in the primary zone it is always bound to galena (Polyánka, Andrássy-I, Andrássy-II, and Vilmos areas). Its 2-40 mm grains are enclosed in galena, and it was also observed on the edge of galena accompanied by pyrite and sphalerite. Thus, the prime material of the medieval mining may have been acanthite-bearing galena. Apart from this primary acanthite occurrence, a second generation acanthite formed from silver is also known from Rudabánya. Acicular acanthite crystals were observed on and among the silver grains and the tufted bunches as well. In several cases, the entire grain altered into acanthite. The microprobe analyses of the acanthite is entirely corresponds to those of other localities. Acanthite frame crystals of similar appearance (*Fig. 3.*) are well known from the professional literature (WALENTA, 1984). Its formation can be credited to the alteration of silver.

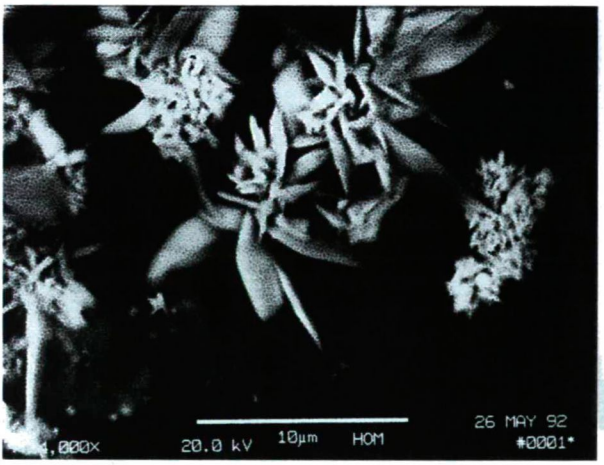

Fig. 3. Acanthite, acicular crystals. Rudabánya-Polyánka. Back-scattered electron image.(HOM collection).

Proustite

It is found in the galena-bearing ore of the Andrássy-I, Andrássy-II and Vilmos areas mostly as xenomorphous grains. It occurs in the galena-bearing ore of the spar edge accompanied by galena, sphalerite, tetrahedrite, pyrargyrite, barite, calcite. It is found as some mm rufous patches. Its presence was proved by ore microscopic studies during which its strong inner reflection was detected, and by microprobe analyses, either (Table 1). Its composition, derived from the analysis is $Ag_{3,58}$ $AsS_{3,44}$, thus showing somewhat less As compared to the theoretical composition. Small crystals of poustite were also found in cavities, which are of short, columnar habit, reaching 1-2 mm (*Fig. 4.*), with faces of (1120, 0112). This is the only locality of idiomorphous proustite in Rudabánya so far.

TABLE 1

Chemical composition of proustite from Rudabánya-Vilmos (Wt%)

Ag	66,8	67,5
As	13,4	13,2
S	19,8	19,3
	100,0	100,0

Analyst: Á. KOVÁCS

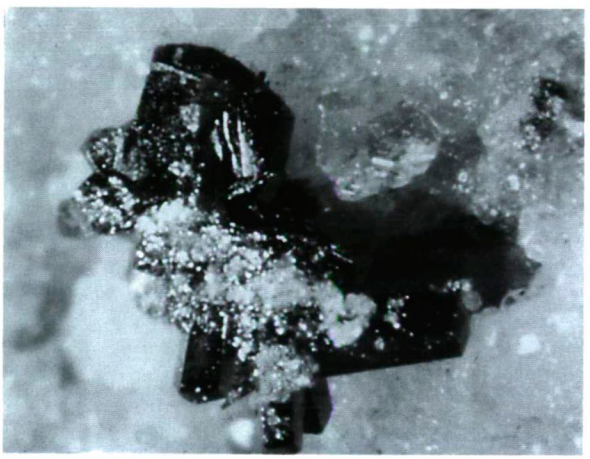

Fig. 4. Proustite, stubby columnar crystals. Rudabánya-Vilmos. Width of the picture: 4 mm. (S. Klaj collection).

Pyragyrite

It was often observed together with proustite in the galena-bearing ore of the Vilmos area. Its colour is dark red, showing dark red inner reflection in ore microscope, and occurs as 30-80 μm grains and also disseminated in sphalerite and barite (*Fig. 5.*). It was also found in columnar crystals reaching 1-2 mm in small cavities. The microprobe analyses assured its presence (Table 2) as its chemical composition corresponds to those of the literature (ANTHONY et al., 1990), the Ag content higher, and the sulphur content is lower, than the reference, however.

TABLE 2

Chemical composition of pyragyrite from Rudabánya-Vilmos (Wt%)

Ag	62,8	65,5
Sb	23,3	19,8
S	13,9	14,7
	100,0	100,0

Analyst: Á. KOVÁCS

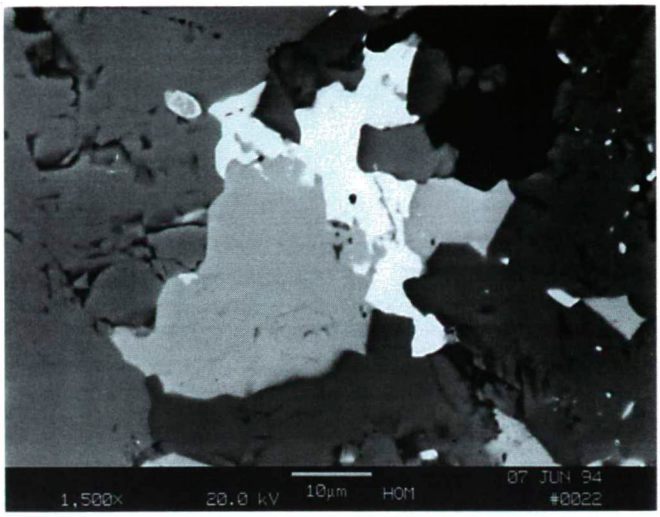

Fig. 5. Pyrargyrite (light grey), anhedral appearance with barite (white), galena (grey) and calcite (dark grey). Rudabánya-Vilmos. Back-scattered electron image. (HOM collection).

Xanthoconite?

A dark yellow mineral containing Ag, As, S elements according to the EDX studies was rarely found in the silver mineral rich ore of the Vilmos area. It was very rarely observed as short crystals reaching 1 mm. Its lustre was bright, the scratch was lemon-yellow. The extremely small sample quantity was not enough for an X-ray powder study, therefore its presence is not proved yet.

Secondary silver minerals

Acanthite

As referred above, the acicular acanthite on the surface of the silver precipitations in siderite and barite in the Polyánka and Vilmos areas are supposed to be secondary phase. The acanthite described in this paragraph however, is surely of secondary origin. In the Andrássy-I area, near the surface, the galena-rich baritized zone was exposed to strong weathering processes, changing the originally massive ore into hollow texture and making the primary ore minerals dissolve and precipitate again in different appearance and phase. These processes formed the thin tabular crystals of barite, the 2-3 mm rhombohedras of calcite and the short crystals of quartz. As a typical oxidation zone mineral, anglesite was also found as tabular and columnar crystals, smaller than 1 mm. Similarly, the sulphides were observed as small crystals or thin crystalline crusts instead of the original massive appearance. Finally, resembling to galena, appearing as tin-like crusts, coatings and branchy aggregates, a bright grey silver and sulphur-bearing phase also observed, which is considered to be acanthite, judging by its appearance, composition and genetics (*Fig. 6.*).

It occurred as a member of an intriguing mineral assembly in the Adolf area. In the secondary ore, along occasionally 0,5 m thick siliceous veins, a diverse mineral assemblage rich in various elements (Pb, Fe, Cu, Sb, Hg, Ag, S, As, Cl, Br, I) and minerals was found. In this material cinnabar aggregates reaching 1-2 mm were found, which are of zonal structure according to the microprobe studies, with concentric precipitations of an Ag, S containing phase considered to be acanthite.

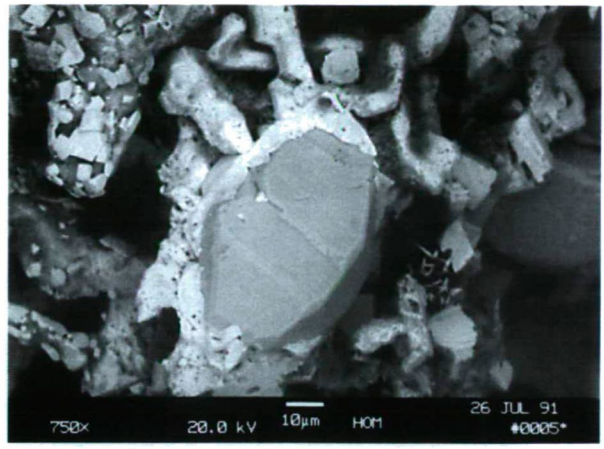

Fig. 6. Acanthite, crusts on calcite. Rudabánya-Andrássy I. Scanning electron micrograph. (HOM collection)

Moschellandsbergite

In the siliceous limonitic ore of the Adolf area referred to above silver coloured 1 mm grains were observed in the environs of cinnabar enrichments. The grains are mostly of xenomorphous appearance, but rarely occur as idiomorphous crystals with smooth edges, mainly of dodecahedral habit. Its 4-8 mm hexahedral crystals and crystal aggregates were also observed in thin sections. The grains and crystals are commonly found as pathes black with tennantite and their surfaces encrusted by malachite. The crystals are often accompanied by mercury drops. Thus, moschellandsbegite is likely to be considered to have formed from the Hg, content of the tennantite and the high Ag content of the formation. The results of the microprobe studies show a right correspondence to those in the literature (ANTHONY et al., 1990) is seen (Table 3). The strongest reflections of moschellandsbergite have appeared on the X-ray powder diffraction image (Table 4).

TABLE 3

Chemical composition of moschellandsbergite from Rudabánya-Adolf (Wt%)

Hg	68,8	70,2
Ag	31,2	29,8
	100,0	100,0

Analyst: Á. KOVÁCS

TABLE 4

X-ray powder diffraction data of bromargyrite and chlorargyrite from Rudabánya-Adolf

bromargyrite, chlorargyrite Rudabánya-Adolf		bromargyrite JCPDS 6-438		chlorargyrite, bromian JCPDS 14-255	
d(Å)	int (obs)	d(Å)	int	d(Å)	int
2.866	100	2.886	100		
2.826	69			2.810	100
2.029	76	2.041	55		
2.005	41			1.989	60
1.662	25	1.667	16		
1.625	17			1.623	30
1.256	15			1.258	40

Made in Dept. of Mineralogy, Landesmuseum Joanneum (Graz)

Chlorargyrite

Chlorargyrite is a member of the mineral assemblage of the siliceous limonitic ore type of the Adolf area with other silver halides. It was found in the small cavities of the ore, as clear, greenish-yellow or light magenta mostly octahedral crystals and amorphous aggregates. The crystals change colour exposed to light and turn grey and black. Oriented intergrowths are common (*Fig. 7*), fine grained aggregates and crust-like coatings were also found. Based on the EDX images the chlorargyrite of Rudabánya sometimes contains bromium (*Fig. 8a*). The four strongest reflections of chlorargyrite have appeared on the X-ray powder diffraction image that corresponds to the chlorargyrite, bromian of the JCPDS standards, though (Table 5). Its accessory minerals are dominantly quartz, cuprite, cerussite, malachite, barite, goethite, calcite, rarely sulphur, mercury, and according to X-ray and microprobe studies pale yellow powder-like bindheimite. The matrix of the ore also consists of hematite ans cinnabar.

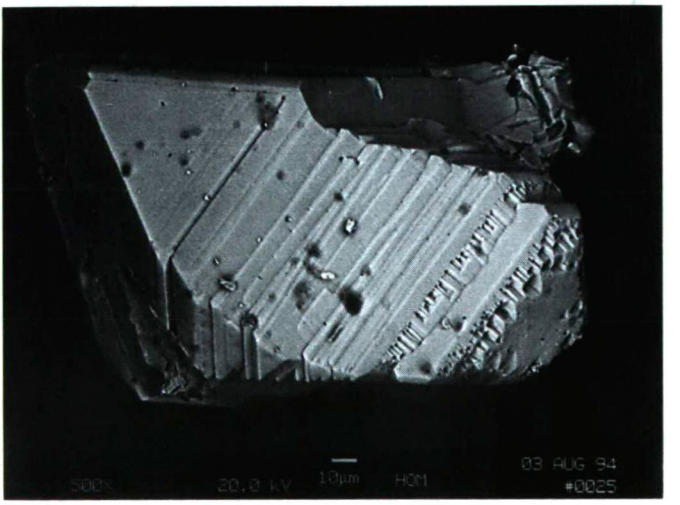

Fig. 7. Chlorargyrite, epitaxial octahedral crystals. Rudabánya-Adolf. Scanning electron micrograph. (HOM collection)

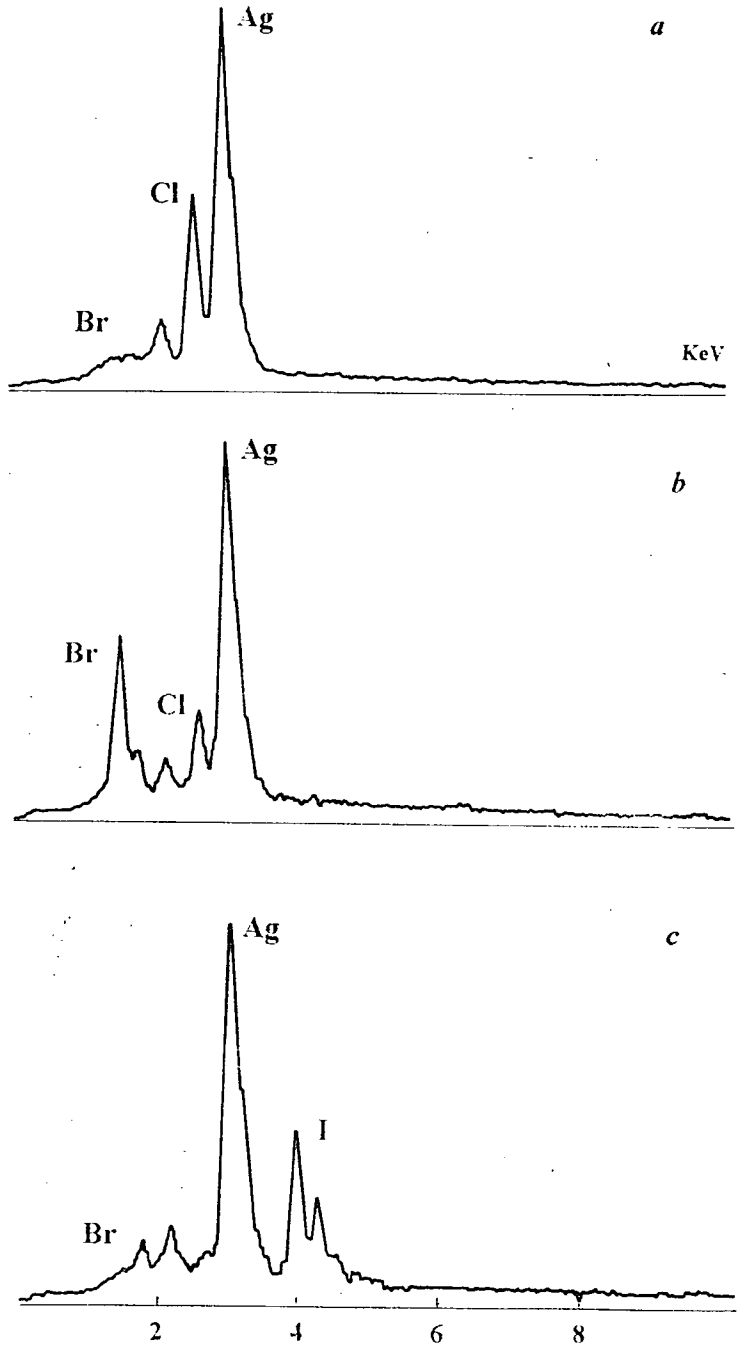

Fig. 8. Energy dispersive X-ray spectrum of chlorargyrite, bromargyrite and iodargyrite from Rudabánya-Adolf.

TABLE 5

X-ray powder diffraction data of moschellandsbergite from Rudabánya-Adolf.

moschellandsbergite			moschellandsbergite	
Rudabánya-Adolf			JCPDS 11-0067	
d(Å)	int (obs)		d(Å)	int
			4.080	10
			3.530	10
3.34	15	Q		
2.89	10		2.880	30
2.68	12		2.670	40
2.41	31	Q		
2.36	100		2.360	100
2.270	8	Q		
2.239	6		2.240	30
2.137	6		2.130	30
1.966	8		1.965	40
1.831	4		1.828	20
1.669	9		1.667	40
			1.629	10
1.586	2		1.583	10
1.541	3		1.547	20
1.481	5		1.478	30
1.449	5		1.447	40
1.417	6		1.419	40
1.376	7	Q		
1.366	15		1.365	70
1.341	13		1.341	20

Made in ALUTERV-FKI (Budapest)
Q= quartz

A different chlorargyrite occurrence in the oxidation zone is also known. The X-ray powder diffraction and chemical studies revealed the presence of pale green, massive paratacamite in the fissures of limonitic ore on a rock specimen the accurate place of occurrence of which is not known (SZAKÁLL, 1992). During the SEM examinations chlorargyrite dendrite aggregates were observed on the surfaces of the tabular paratacamite crystals.

Bromargyrite

Accompanying chlorargyrite, bromargyrite occurs as clear or greyish-white aggregates, crusts and rarely cubooctahedral crystals, reaching 1 mm (*Fig. 9.*). According to EDX studies chlorargyrite always contains more or less bromium, but phases containing dominantly bromium also occur (*Fig. 8b*). By the microprobe studies made on sections of crystal aggregates it was pointed out that the crystals had grew in several stages, with formation gaps between each generation. These studies did not show any order in the chlorine and bromium content, i.e. the bromium distribution image on wich among chlorargyrite reflexions of three highest peaks of bromargyrite are seen (Table 5).

Iodargyrite

In the cavities of the silicious limonitic ore containing chlorargyrite, bromargyrite, yellow, hexagonal tabular crystals greater than 1 mm with very intense lustre can be

observed very rarely. The colour of the crystals does not change exposed to light. The forms of the hexagonal base and prism are present on the crystals (*Fig.10*). Crystal growth phenomena can be seen on the base faces. Even rarer, its short, columnar crystals, reaching 0,5 mm were observed.

By EDX studies, I, (Br) and Ag are the only compounds of the crystals (*Fig. 8c*). Having regard to the chemical composition and the physical characteristic, the crystal morphology and the paragenesis, these crystals are considered to be iodargyrite.

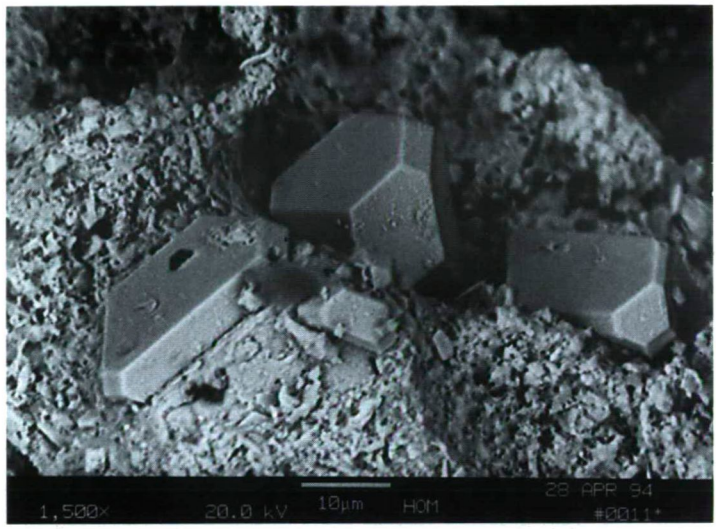

Fig. 9. Bromargyrite, cubooctahedral crystals. Rudabánya-Adolf. Scanning electron micrograph. (HOM collection)

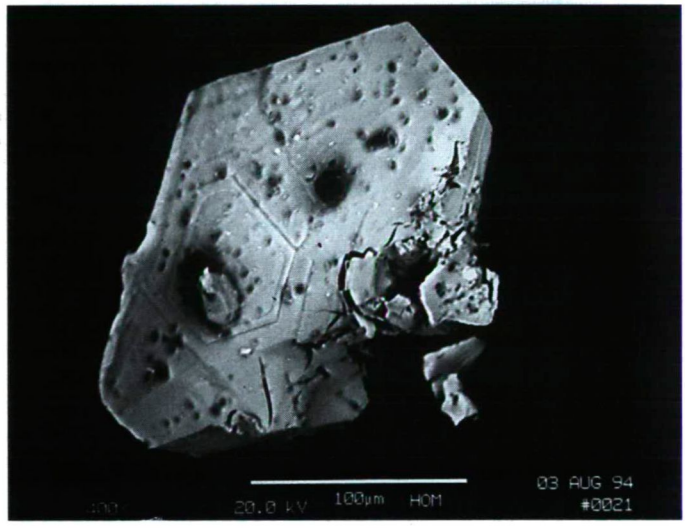

Fig. 10. Iodargyrite, tabular crystal. Rudabánya-Adolf. Scanning electron micrograph. (HOM collection)

Unidentified silver sulfhalides

AgHgSCl mineral (RB-01)

A mineral occurring in clear or yellowish, elongated, columnar crystals smaller than 1 mm with diamond lustre is found very rarely in Ag halide paragenesis (Adolf area). According to the EDX analysis, Ag, Hg, S, Cl are present in the crystals. Unfortunately, structure examinations were not made on the sample, because of its extremely small quantity.

AgHgSBr mineral (RB-02)

On the southern side of the Andrássy-I area in lower Villanytető openings, the below paragenesis was observed in barite veins. Galena, sphalerite, tennantite, heteromorphite? occur as primary minerals forming patches and veins in the barite mass. The weathering of these minerals resulted in the formation of the secondary cerussite, bindheimite, goethite, cinnabar, hematite, malachite and rarest a greenish-yellow powder-like mineral, the surface of which turns dark grey when exposed to light. This phase contains Ag,Hg,S,Br according to the EDX analyses.

Further examinations are still made on these interesting samples.

ACKNOWLEDGEMENTS

We thank ISTVÁN SAJÓ (ALUTERV-FKI, Budapest) and WALTER POSTL (Landesmuseum Joanneum, Graz) for the X-ray diffraction studies. We are grateful to MIKLÓS GÁL (Komló), SÁNDOR KLAJ (Pécs), CSABA PAPP (Pécs) and GYŐZŐ VÁRHEGYI (Budapest) for providing us with some of the samples examined.

The helpful cooperation of GÁBOR HERNYÁK (Rudabánya), retired chief geologist, during the groundwork through years is also gratefully ackowledged

REFERENCES

ANTHONY, J. W. - BIDEAUX, R. A. - BLADH, K. W. - NICHOLS, M. C. (1990): Handbook of Mineralogy I. Mineral Data Publishing, Tucson, Arizona. 588.

CSALAGOVITS I. (1973): Results of the geochemical and ore genetical investigations of a Triassic sequence in the vicinity of Rudabánya. (in Hungarian with English summary). MÁFI Évi Jel. az 1971. évről. 61-91.

KOCH S. (1966): Minerals of Hungary (in Hungarian). Akadémiai kiadó, Budapest. 419.

KOCH S.-GRASSELLY GY.-DONÁTH É. (1950): The minerals of the Hungarian iron ore deposites (in Hungarian with English summary). Acta Miner. Petr., **4**, 1-41.

PANTÓ G. (1956): The geologic structure of the iron ore range at Rudabánya (in Hungarian with French summary). MÁFI Évk., 44, 637.

PODÁNYI T. (1957): Early ore mining at Rudabánya. in: Ore mining of Rudabánya (in Hungarian). OMBKE, Budapest, 66-102.

SZAKÁLL S. (1992): Newly discovered minerals in Hungarian geologic formations (in Hungarian). Manuscript. Herman Ottó Múzeum, Miskolc.

WALENTA , K. (1984): Whiskerartige Bildungen von Silberglanz und Kupfersulfiden. Aufschluss, **35**, 113-117.

Manuscript received 21. Aug. 1994.

Acta Mineralogica-Petrographica, Szeged, XXXVI, 17–33, 1995

CRYSTALLIZATION OF AMPHIBOLES IN THE KID VOLCANIC COMPLEX, SOUTHERN SINAI, EGYPT: IMPLICATIONS FOR MAGMA EVOLUTION

I. KUBOVICS* and A. M. ABDEL-KARIM**

*Department of Petrology and Geochemistry, Eötvös University
and **Geology Department, Zagazig University

ABSTRACT

The Kid volcanics consist of three main suites namely, basaltic andesite-andesite (BA-A), trachydacite-dacite (TD-D) and rhyodacite-alkali rhyolite (RD-AR). Microprobe analyses of phenocrysts and groundmass of the amphiboles from rocks of these volcanic suites are presented in this paper. Amphiboles from BA-A suite range from tschermakite phenocryst cores to ferro tschermakitic hornblende phenocryst rims and groundmass. TD-D suite has ferroan pargasite phenocrysts and ferroan pargasitic hornblende groundmass. Amphiboles from RD-AR suite range from kaersutite and ferroan pargasite phenocryst cores to magnesian hastingsitic hornblende phenocryst rims and magnesian hastingsite groundmass.

The amphiboles of Kid volcanics are Ti-rich, calcic-type. In most cases, amphibole phenocrysts from BA-A and RD-AR suites have the same evolution, reflect their cognate magmas. Moreover, both the TD-D and RD-AR suites have close genetic relationship. The progressive evolutionary trend from phenocryst cores to phenocryst rims and groundmass and from intermediate (BA-A) to felsic (RD-AR) suite are responsible for the magmatic evolution of the Kid volcanic suites. In contrast, the concentration of amphibole composition as a function of pressure and temperature suggest an opposite trend for the grade of metamorphism of these suites. These calcic amphiboles are expected to be formed at high temperature (~700–1000 °C) and low pressure (~0.2–3 Kb.) conditions.

INTRODUCTION

Amphibole represents the dominant mafic mineral phase in many rocks of intermediate and felsic compositions. Due to its importance, a large body of miscellaneous work on amphibole is scattered throught the scientific literature. More recently, amphibole in intermediate and felsic compositions has been thoroughly studied by several investigators including LEAKE (1978), CAMERON and PAPIKE (1979), WONES and GILBERT (1981), HAWTHORNE (1983), SCHULZ-KUHNT et al. (1990).

Generally, the Precambrian volcanic rocks in the Egyptian basement belong to the three major geotectonic units (RIES et al., 1983 and EL-GABY et al., 1988); namely, the lower unit comprises low-K tholeiitic basalts which are integral part of an ophiolite association. The second unit belongs to the island arc association of andesite, dacite and volcanoclastics with subordinate basalt overthrusted on the former unit (EL-GABY et al., 1988), and the third unit manifested by a vast subaerial, calc-alkaline volcanics (Dokhan-type) rhyolites and rhyodacites are dominant rock types of this unit.

* H–1088 Budapest, Múzeum krt. 4/A
** Zagazig, Egypt

Amphibole is represent in diverse varieties in many volcanics of the Kid segment of southeastern Sinai (*Fig. 1.*). In this study, a number of fresh amphibole samples have been analyzed to enable us to examine the mineralogical variations with each volcanic unit and, to examine the compositional zoning of individual amphibole grains. The purpose of this work is: 1. to study the amphibole chemistry using new microprobe analytical data, 2. to illustrate the compositional trends, crystallization history and evolution of the amphibole of the various rocks, and 3. to discuss the role of amphibole on magma evolution.

GENERAL GEOLOGY

The Kid supracrustal segment, southeastern Sinai (*Fig. 1.*), is largely occupied by a volcano-sedimentary succession intruded by a number of igneous intrustions including layered gabbro, quartz monzodiorite, G2 and G3 younger granites and minor albitite (EL-GABY et al., 1991). The succession is overprinted by a low-pressure metamorphism (REYMER et al., 1984). It lies unconformably above partially migmatized gneisses.

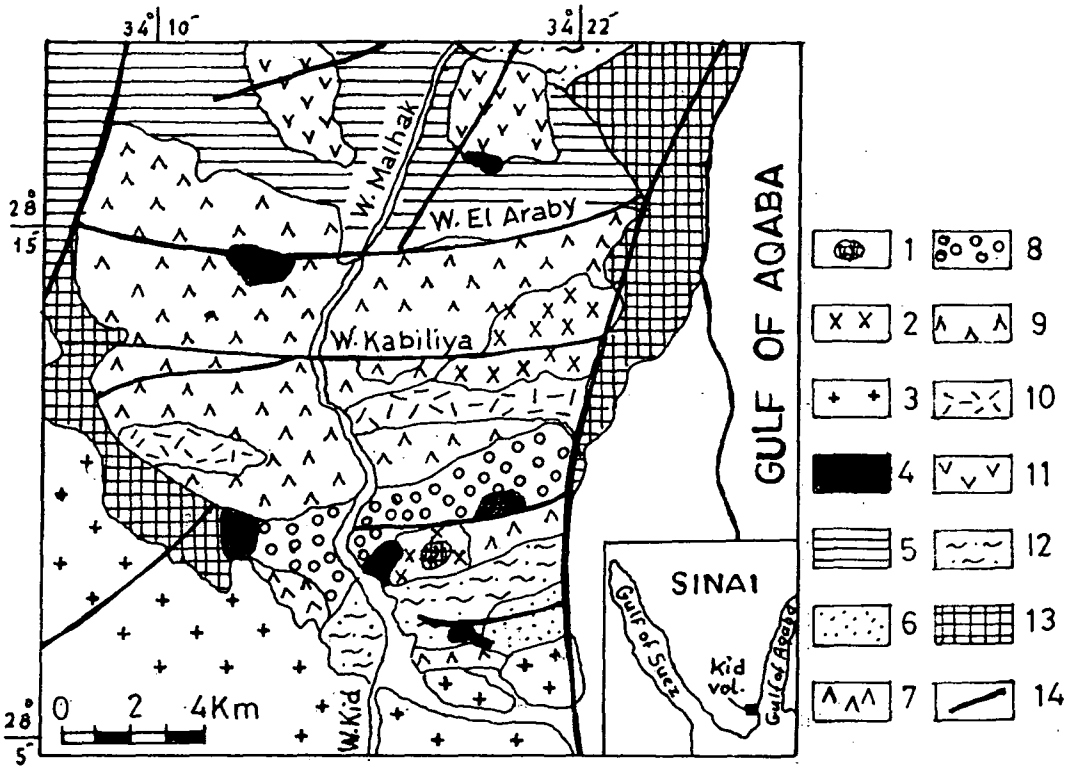

Fig. 1. Geologic map of the Kid volcanics (after HASSANEN, 1992).
1 = albitite; 2 = younger granite; 3 = gneissose granite; 4 = Upper Volcanic Sequence (basaltic rocks); 5 = Hammamate clastic sediments; Middle Volcanic Sequence [upper unit (6 = high K-dacite with pyroclastics, 7 = alkali rhyolite), 8 = Kid metaconglomerate, lower unit (9 = rhyolite and dacite with pyroclastics, 10 = andesite)]; 11 = Lower Volcanic Sequence (metabasalt and metabasaltic andesite); 12 = marine sediments, 13 = gneissose diorite, gneiss and amphibolite, 14 = fault lines.

The geology and geochemistry of the Kid volcanics have been discussed elsewhere (SHIMRON, 1984; GHONEIM et al., 1985; EL-GABY et al., 1991; HASSANEN, 1992). Nevertheless, the magmatic evolution of these rocks is still a matter of great dispute. This work represents the first mineralogical study in the Wadi Kid area. The following is a synopsis of the geology of the volcanics in question.

The main volcanic components of the Kid volcanics are lava flows, sheets, subvolcanics and pyroclastics of a wide composition range from basalt to rhyolite. The associated sedimentary rocks vary in lithology and deposition including metagreywackes, metaconglomerates, epiclastics, mudstone and turbidites. The Kid volcanics can be subdivided into three main volcanic sequences. These are: lower, middle and upper volcanic sequences.

The lower volcanic sequence consists of slightly to moderately metamorphosed intermediate and minor mafic volcanics. The rocks of this sequence occur as sheets, flows and sills. The middle sequence, on the other hand, are fresh and weakly metamorphosed, and occured as subvolcanic dyke-like intrusions and sheets intruded into the former volcanic unit. The rocks of this unit comprises felsic and minor intermediate volcanics. The middle sequence is separated into two stratigraphic units by thick beds of Kid metaconglomerate belonging to Hammamate clastic type sediments. The lower unit is dominated by rhyolite and less common andesite and their pyroclastic equivalents. The upper unit consists mainly of felsic volcanics and pyroclastics. HASSANEN (1992) added a new sequence (e. g., upper volcanic sequence) to Kid volcanics. This sequence is locally distributed and comprises mafic and intermediate alkaline volcanics and is separated from the middle sequence by Hammamate clastic sediments. Most of these volcanic sequences are cut by doleritic dykes. The intermediate rocks of the lower sequence and the felsic rocks of middle volcanic sequences which constitute the main volcanic rocks are the amphibole bearing volcanic suites of the region, and are the subject of this mineralogical study.

PETROGRAPHY

The lower volcanic unit is variably metamorphosed aphyric to phyric basaltic andesite, andesite, trachydacite and dacite. The pyroclastics comprise ignimberite, tuffs and agglomerate of the same compositions. The middle volcanic unit, on the other hand, is unmetamorphosed aphyric and phyric rhyolite and less abundant rhyodacite and their compositionally equivalent tuffs and lava flows. Detailed petrographic description is given by EL-GABY et al. (1991) and HASSANEN (1992).

The following account summarizes the main petrographic features of the amphibole-bearing volcanic rocks in question.

a) Basaltic andesite-andesite (BA-A) suite constitutes the main components of the lower volcanic unit. They are fine grained, commonly porphyritic greyish green in colour. Intergranular and porphyritic textures are the most common rock textures. They are composed of plagioclase (An_{40-50}) and amphibole phenocrysts embedded in pilotaxitic groundmass composed of the same minerals and subordinate Fe-oxides and apatite. Augite is present in some rock samples. Secondary metamorphic products include epidote, chlorite and sphene. Amphibole occurs as pale green-brown prismatic phenocrysts (0.4–1.9 mm long) and as anhedral crystals in the groundmass. It is occasionally zoned (*Fig. 2*). Zoned phenocrysts exhibit pleochroic pale green to deep brown-green colour outer rims, and blueish green colour outermost rims. Chlorite, epidote and Fe-oxide are the main alteration products of the amphibole.

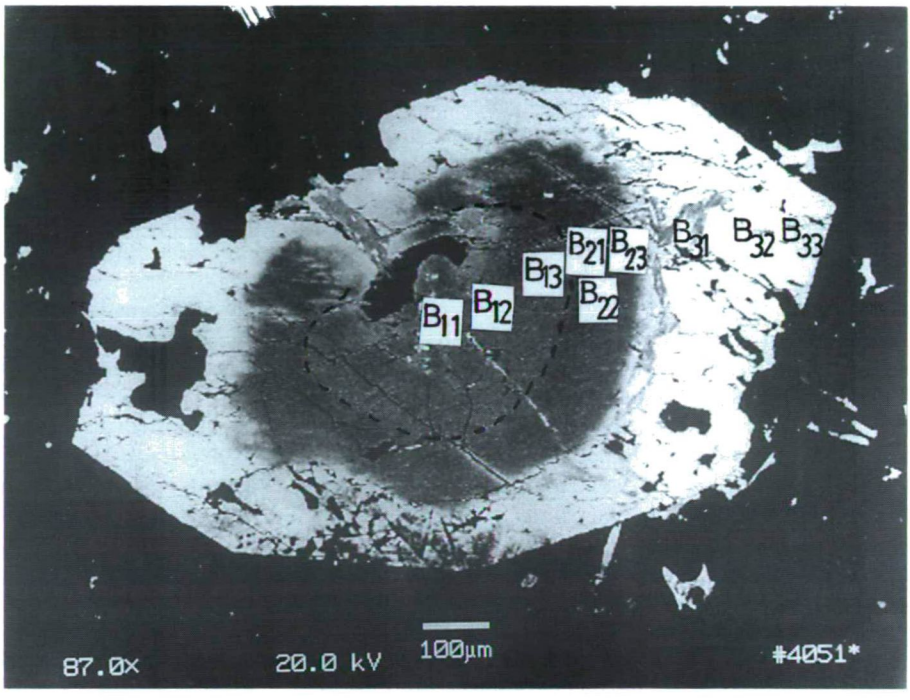

Fig. 2. Photomicrograph of a zoned phenocryst from basaltic andesite-andesite (BA-A) suite showing tschermakite inner and outer cores and ferro tschermakitic hornblende rim.
B_{11}, B_{12}, ... = Locations of analyses

b) Trachydacite-dacite (TD-D) suite is recorded in the lower unit of the middle volcanic sequence are fine grained, light green, yellowish green or grey and frequently porphyritic. They consist of phenocrysts of plagioclase (An_{30-44}) and less abundant amphibole, disposed in a fine grained flow banding and trchytoid groundmass composed of the same composition and potash feldspar, quartz and biotite and subordinate Fe-oxides, sphene and apatite. Amphibole occurs as idiomorphic prismatic and rhombic-shape phenocrysts (0.3–1.8 mm long) or as subhedral crystals in the groundmass. It is relatively homogeneous in colour (mainly yellow to brown tint), and does not show compositional zoning (*Fig. 3*). Amphibole crystals occasionally rimmed by thick alteration margin composed of uralite, chlorite and Fe-oxides, are recorded.

c) Rhyodacite-alkali rhyolite (RD-AR) suite is the dominant rock types in the upper unit of middle volcanic sequence. These two rock types are fine grained, leucocratic of buff, reddish brown and light grey colour and show the same textural features (flow and porphyritic). They are composed of phenocrysts (0.6–2.8 mm across) of plagioclase (An_{23-35}), potash feldspar and less frequent amphibole embedded in a fine grained flow banded groundmass consisted of the same minerals together with biotite and minor apatite and sphene. Amphibole forms subedral prismatic phenocrysts and as fine grains in the groundmass. Compositionally, the amphibole phenocrysts are sometimes zoned (*Fig. 4*), showing yellow to brown cores and brown to brownish green colour rims. On the other

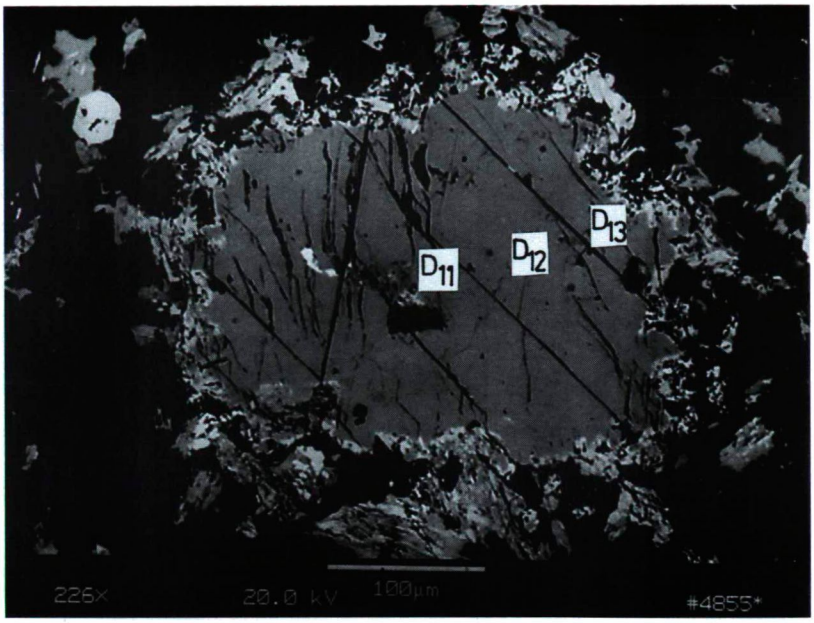

Fig. 3. Photomicrograph of a homogenous phenocryst from trachydacite-dacite (TD-D) suite showing ferroan pargasite composition, occasionally rimmed by a thick alteration margin consists of uralite, chlorite and Fe-oxide

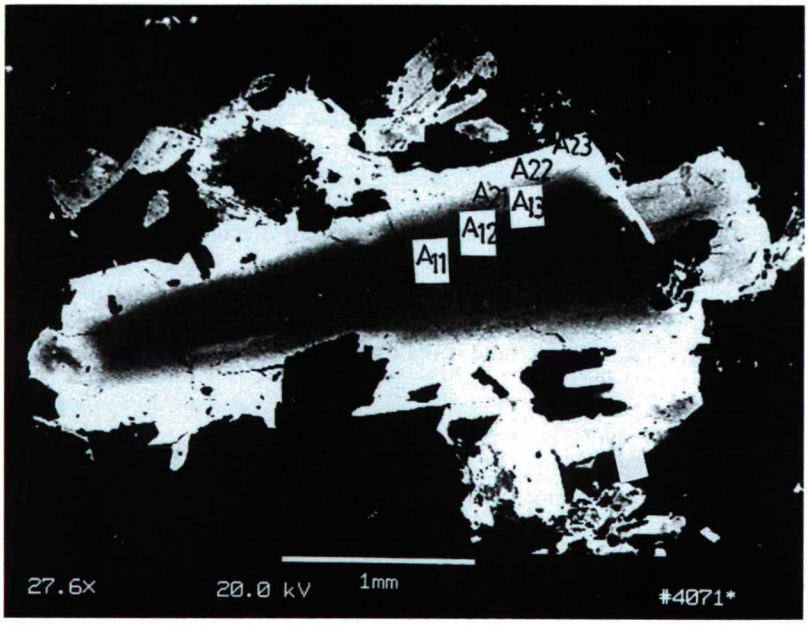

Fig. 4. Photomicrograph of a zoned phenocryst from rhyodacite-alkali rhyolite (RD-AR) suite showing kaersutite inner core, ferroan pargasite outer core and magnesian hastingsitic hornblende rim.

TABLE I

Representative whole-rock chemical compositions (wt. %) of the Kid volcanics

	Lower volcanic sequence		Middle volcanic sequence			
	Bas. andesite-andesite		Trachydacite-dacite		Rhyodacite-rhyolite	
	1	2	3	4	5	6
SiO_2	58.50	60.30	65.05	67.44	69.30	71.05
TiO_2	0.84	0.71	0.32	0.25	0.20	0.17
Al_2O_3	15.80	15.50	14.20	13.70	13.83	13.04
Fe_2O_3	1.20	1.04	1.15	1.02	0.73	0.65
FeO	5.23	4.98	2.70	2.40	2.10	2.05
MnO	0.06	0.07	0.04	0.04	0.04	0.03
CaO	4.95	4.80	1.98	1.75	1.78	1.65
MgO	2.54	2.22	1.20	0.93	1.10	1.04
Na_2O	4.25	4.37	4.45	4.55	4.66	4.73
K_2O	2.28	2.33	4.90	4.73	4.85	4.50
H_2O^-	0.54	0.48	0.72	0.61	0.19	0.20
P_2O_5	0.13	0.20	0.05	0.06	0.04	0.05
LOI	2.08	2.11	1.90	1.80	1.00	0.75
Sum.	99.12	99.09	98.66	99.28	99.82	99.91

hand, the grains of the groundmass are homogenous and show colours analogous to outer rims of the phenocrysts. A few amphibole grains are cracked and partially altered to chlorite and Fe-oxides or to biotite.

WHOLE ROCK CHEMISTRY

For the purpose of this study, it may useful to outline some chemical features and range of compositions of the amphibole host rocks to support field and mineralogical distinctions. Table 1 shows the results of the chemical analysis. A plot of the K_2O versus SiO_2 (*Fig. 5a*, PECCERILLO and TAYLOR, 1976) gives the best chemical classification of the studied volcanic sequences. Rocks represent the lower sequence fall into the andesite field, while those from the middle sequence correspond to trachyte, dacite and rhyolite. Most of these rocks belong to K-rich calc-alkaline series. A plot of (Na+K) versus Si (*Fig. 5b*) provides the best discriminant between the Kid volcanic sequences. Rocks of BA-A suite have low silica and alkalis and exhibit a positive trend. On the other hand, the TD-D and RD-AR suites have higher contents of silica and alkalis compared to the BA-A suite with a negative slope. The RD-AR suite contains the highest Si values.

ANALYTICAL TECHNIQUE

Mineral analyses were obtained using polished thin sections, which were vacuum-ccoated with carbon. A total of 30 amphibole analyses for the phenocrysts and groundmass of three samples representative the BA-A, TD-D and RD-AR suits of the Kid volcanics, were analyzed and given in Table 2. The analyses were carried out using the computerized Amray-1830 I electron microprobe under operating condition of 20kV and 1–2 nA. The structural formulae were calculated on the basis of 23 oxygens. In most cases, core and rim compositions were determined for zoned amphibole grains.

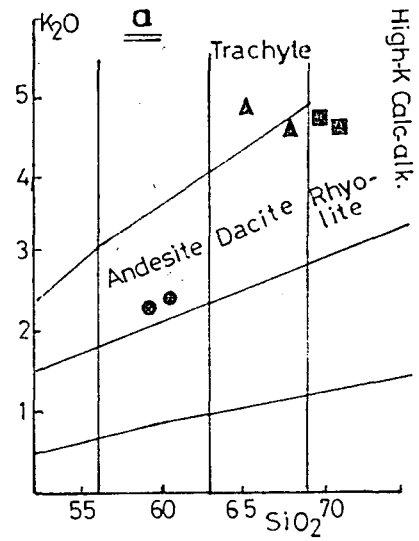

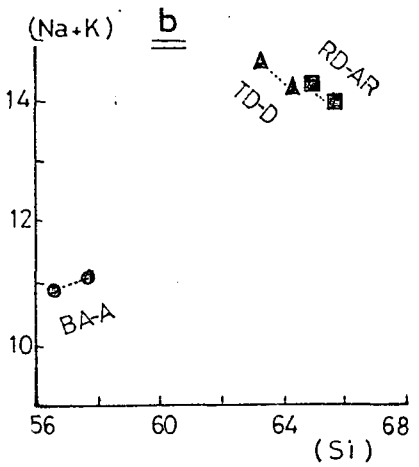

Fig. 5. Plots show the chemical characters of the whole rock samples from Kid volcanic suites.
A) K20 vs SiO_2 diagram after PECCERILLO and TAYLOR (1976). B) (Na+K) vs Si variation diagram (in cation percent).

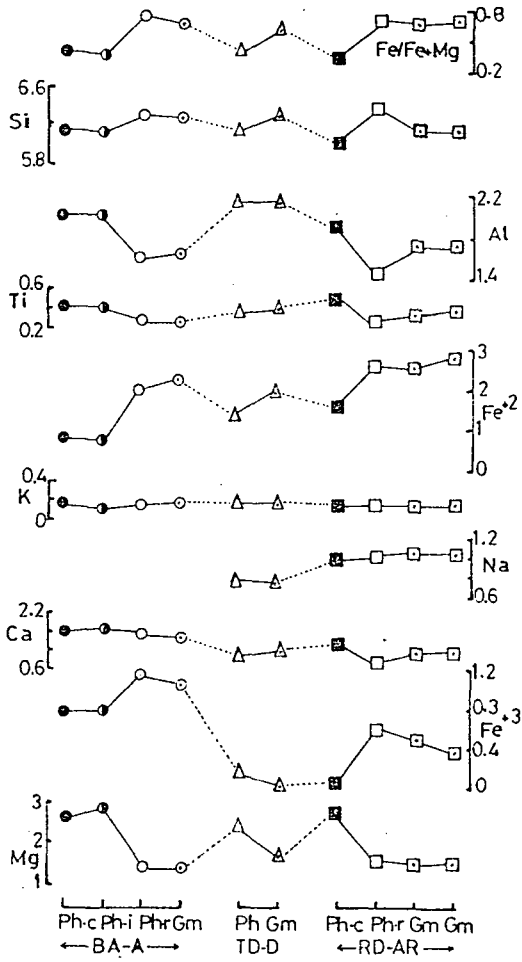

Fig. 6. Microprobe traverse through the amphibole phenocrysts (Ph) of *Fig. 2, 3 and 4* and groundmass (Gm) from Kid volcanic suites. The horizontal scale is arbitrary. Ph-c, -i, -r: present averages of phenocryst cores, intermediate portions and rims. Gm: averages of groundmass.

Chemical composition of amphiboles in the Kid volcanics

	Basaltic andesite-andesite (BA-A)												Trachydac-Dacite (TD-D)					
	Ph-c B-11	Ph-c B12	Ph-c B13	Ph-i B21	Ph-i B22	Ph-i B23	Ph-r B31	Ph-r B32	Ph-r B33	Gm-c A11	Gm-i A12	Gm-r A13	Ph-c D11	Ph-i D12	Ph-r D13	Gm-c F11	Gm-i F12	Gm-r F13
SiO_2	41.70	41.84	41.81	41.66	41.52	41.82	40.89	40.68	41.06	40.85	40.90	40.93	41.80	41.55	41.29	41.95	41.53	41.75
TiO_2	4.13	4.21	4.03	4.03	3.94	4.04	2.77	2.71	2.56	2.75	2.72	2.76	3.84	3.81	3.83	3.94	3.87	3.90
Al_2O_3	11.61	11.92	11.65	11.67	11.70	11.96	8.60	8.25	8.60	8.70	8.65	8.75	12.70	12.91	13.04	11.98	12.21	12.50
FeO_t	13.59	13.75	13.42	12.84	12.89	12.72	27.70	27.61	27.39	27.80	27.05	27.25	13.10	13.35	13.40	15.32	15.75	15.80
MnO	–	–	–	–	–	–	–	–	–	–	–	–	–	–	–	–	–	–
CaO	12.66	12.60	12.56	12.68	12.55	12.84	11.01	11.31	11.25	11.32	11.25	11.50	11.23	11.33	11.40	11.20	11.12	11.35
MgO	12.46	12.58	12.90	12.96	13.12	12.97	5.65	5.52	6.11	5.72	5.78	5.83	12.11	11.44	11.46	7.55	7.35	7.58
Na_2O	–	–	–	–	–	–	–	–	–	–	–	–	–	–	–	–	–	–
K_2O	0.70	0.89	0.62	0.60	0.63	0.69	0.99	0.92	0.90	0.95	0.92	0.97	0.84	0.77	0.80	0.93	0.94	0.90
Cr_2O_3	–	–	–	–	–	–	–	–	–	–	–	–	–	–	–	–	–	–
Sum	96.85	97.79	96.99	96.44	96.35	97.04	97.61	97.00	97.87	98.56	98.12	98.64	98.21	97.74	97.98	95.62	95.65	96.71
Si	6.131	6.091	6.106	6.120	6.092	6.114	6.276	6.314	6.270	6.252	6.301	6.275	6.129	6.149	6.112	6.417	6.372	6.336
Al_4	1.869	1.909	1.894	1.880	1.908	1.886	1.556	1.509	1.548	1.569	1.471	1.581	1.871	1.851	1.888	1.583	1.628	1.664
Fe^{3+}	0.000	0.000	0.000	0.000	0.000	0.000	0.168	0.177	0.182	0.179	0.128	0.144	–	–	–	–	–	–
Sum	8.000	8.000	8.000	8.000	8.000	8.000	8.000	8.000	8.000	8.000	8.000	8.000	8.000	8.000	8.000	8.000	8.000	8.000
Al_6	0.143	0.136	0.111	0.140	0.115	0.175	0.000	0.000	0.000	0.000	0.000	0.000	0.324	0.401	0.387	0.577	0.580	0.572
Cr	–	–	–	–	–	–	–	–	–	–	–	–	–	–	–	–	–	–
Ti	0.457	0.461	0.443	0.445	0.435	0.444	0.320	0.316	0.294	0.316	0.315	0.318	0.423	0.424	0.426	0.435	0.447	0.445
Fe^{3+}	0.684	0.744	0.837	0.734	0.845	0.663	1.224	1.074	1.239	0.946	0.895	0.832	0.277	0.124	0.090	–	–	–
Mg	2.730	2.730	2.808	2.838	2.869	2.826	1.293	1.277	1.391	1.315	1.327	1.332	2.647	2.523	2.528	1.721	1.681	1.715
Fe^{2+}	0.986	0.929	0.801	0.843	0.736	1.892	2.163	2.333	2.076	2.433	2.462	2.518	1.329	1.528	1.569	1.964	2.021	2.005
Mn	–	–	–	–	–	–	–	–	–	–	–	–	–	–	–	–	–	–
Sum	5.000	5.000	5.000	5.000	5.000	5.000	5.000	5.000	5.000	5.000	4.999	5.000	5.000	5.000	5.000	4.715	4.730	4.737
Fe^{2+}	0.001	0.001	0.001	0.000	0.001	0.001	0.000	0.000	0.001	–	–	–	–	–	–	–	–	–
Ca	1.994	1.965	1.965	1.996	1.973	2.011	1.811	1.881	1.841	1.856	1.857	1.889	1.764	1.796	1.808	1.836	1.828	1.846
Na	–	–	–	–	–	–	–	–	–	0.144	0.143	0.111	0.236	0.204	0.192	0.164	0.172	0.154
Sum	1.995	1.966	1.966	1.996	1.974	2.012	1.811	1.881	1.841	1.856	1.857	1.889	1.764	1.796	1.808	1.836	1.828	1.846
Na	–	–	–	–	–	–	–	–	–	0.099	0.111	0.157	0.500	0.536	0.600	0.652	0.685	0.708
K	0.131	0.165	0.115	0.112	0.118	0.129	0.194	0.182	0.175	0.185	0.181	0.190	0.157	0.145	0.151	0.181	0.184	0.174
total	15.13	15.13	15.08	15.11	15.09	15.14	15.00	15.06	15.02	15.28	15.29	15.35	15.66	15.68	15.75	15.55	15.60	15.62

Ph = phenocrysts, Gm = groundmass, c = core, i = intermediate portion, r = rim, All = number of analysis.

TABLE 2 contd.

	Rhyodacite-rhyolite (RD-AR)											
	Ph-c A11	Ph-c A12	Ph-c A13	Ph-c A21	Ph-c A22	Ph-c A23	Gm-c C11	Gm-i C12	Gm-r C13	Gm-c E11	Gm-i E12	Gm-r. E13
SiO_2	40.26	40.68	40.42	41.56	41.23	41.75	39.49	39.55	39.22	38.60	39.10	39.14
TiO_2	4.52	4.15	4.32	2.15	2.20	2.08	2.76	2.86	2.87	3.27	3.12	3.22
Al_2O_3	10.83	10.87	10.96	7.36	7.41	7.51	9.14	8.84	9.30	9.32	9.17	9.23
FeO_t	12.93	12.89	12.60	25.99	25.96	25.75	24.03	24.44	24.11	23.40	24.12	24.14
MnO	0.00	0.00	0.00	0.35	0.35	0.40	0.36	0.41	0.35	0.32	0.28	0.21
CaO	11.84	12.08	12.06	10.34	10.37	10.49	10.65	10.77	10.59	10.71	10.80	10.63
MgO	12.73	12.63	12.60	6.69	6.58	6.78	6.96	7.00	6.97	6.80	6.85	6.42
Na_2O	3.33	3.17	3.64	3.31	3.40	3.58	3.66	3.53	3.63	3.87	3.44	3.58
K_2O	0.68	0.67	0.68	0.86	0.83	0.80	0.82	0.82	0.80	0.86	0.85	0.81
Cr_2O_3	0.29	0.28	0.25	0.00	0.00	0.00	0.00	0.00	0.00	0.00	0.00	0.00
Sum	97.41	97.42	97.35	98.61	98.33	99.14	97.87	98.22	97.84	97.15	97.73	97.38
Si	6.054	6.107	6.068	6.443	6.424	6.450	6.177	6.169	6.129	6.118	6.134	6.177
Al_4	1.919	1.893	1.932	1.345	1.361	1.367	1.685	1.625	1.713	1.741	1.695	1.717
Fe^{3+}	0.000	0.000	0.000	0.212	0.215	0.183	0.188	0.206	0.158	0.141	0.171	0.106
Sum	8.000	8.000	8.000	8.000	8.000	8.000	8.000	8.000	8.000	8.000	8.000	8.000
Al_6	0.000	0.030	0.007	0.000	0.000	0.000	0.000	0.000	0.000	0.000	0.000	0.000
Cr	0.034	0.033	0.030	–	–	–	–	–	–	–	–	–
Ti	0.511	0.469	0.488	0.251	0.258	0.242	0.325	0.335	0.337	0.390	0.368	0.382
Fe^{3+}	0.000	0.000	0.000	0.446	0.397	0.356	0.326	0.322	0.384	0.100	0.279	0.204
Mg	2.853	2.826	2.819	1.546	1.528	1.561	1.623	1.628	1.624	1.606	1.602	1.510
Fe^{2+}	1.626	1.618	1.582	2.712	2.772	2.788	2.679	2.660	2.609	2.860	2.714	2.876
Mn	0.000	0.000	0.000	0.046	0.046	0.052	0.048	0.054	0.046	0.043	0.037	0.028
Sum	4.997	4.976	4.926	5.000	5.000	4.999	5.000	4.999	5.000	4.999	5.000	5.000
Fe^{2+}	–	–	–	–	–	–	–	–	–	–	–	–
Ca	1.908	1.943	1.940	1.718	1.731	1.736	1.785	1.800	1.773	1.819	1.815	1.797
Na	0.092	0.057	0.060	0.281	0.269	0.264	0.214	0.200	0.227	0.181	0.185	0.203
Sum	2.000	2.000	2.000	2.000	2.000	2.000	2.000	2.000	2.000	2.000	2.000	2.000
Na	0.879	0.866	0.999	0.714	0.758	0.808	0.896	0.868	0.873	1.008	0.861	0.892
K	0.130	0.128	0.130	0.170	0.165	0.158	0.164	0.164	0.159	0.174	0.170	0.163
total	16.00	15.97	16.05	15.88	15.92	15.97	16.06	16.03	16.03	16.18	16.03	16.05

AMPHIBOLE CHEMISTRY

Microprobe analytical results of the amphiboles from the Kid volcanics, along with the calculated number of ions per unit cell, are reported in Table 2. All the amphibole compositions from the different sequences of the Kid volcanics are, in general, characterized by $(Ca+Na)_B$ > or = 1.34 and Na_B < 0.67 (i. e., calcic-type amphibole), and rich in Ca, Mg and Al. Moreover, the present amphibole is characterized by their high Ti contents (Ti = 0.24–0.51) (Table 2) probably reflect their derivation from Ti-rich pyroxene.

The analyzed calcic amphiboles of various volcanic suites are exhibited wide compositional variations (*Fig. 6*) and classified according to the IMA classification (LEAKE, 1978, *Fig. 7*).

The analyzed amphiboles of the basaltic andesite-andesite (BA-A) suite of the lower sequence comprise phenocrysts and groundmass. The phenocrysts exhibit normal zoning towards Fe-K-Si-rich and Mg-Ti-poor rims (*Fig. 6*). Both the inner and outer parts of the phenocryst cores (i. e., Ph-c and Ph-i; *Fig. 6*) are generally similar in composition, but the outer core is richer in Mg and Ca contents. Phenocrysts of the BA-A suite are tschermakite cores and ferro tschermakitic hornblende rims (*Fig. 7a*). In this case, significant substitution of Fe^{3+} of ferro tschermakitic hornblende for Al, i. e. $[Al^6]$ of tschermakite, can occur. The present phenocrysts contain the highest values of Fe^{3+}/Fe^{2+} ratio among the Kid volcanics, which are probably the result of highly oxidizing conditions that may have dominated, locally during the hydrothermal stage at relatively lower temperature. The groundmass amphiboles and the outermost rims of phenocrysts are commonly analogous, but with a less Fe^{3+}/Fe^{2+} ratio, probably corresponded to the decrease of oxidizing process as well as the differences in their condition of crystallization. The groundmass amphiboles are homogenous, showing ferro tschermakitic hornblende (*Fig. 7a*).

The analyzed amphiboles of the Trachydacite-dacite (TD-D) suite of lower unit of the middle sequence are compositonally homogeneous. The phenocrysts are ferroan pargasite, whereas the groundmass amphiboles are ferroan pargasitic hornblende (*Fig. 7b*). Amphibole phenocrysts from TD-D suite tend to be poorer in Mg and Ca and richer in Fe^{2+}, K and Na than are those from BA-A suite, suggesting a progressive magmatic evolution. Furthermore, Fe^{2+}, Si and K increase and Mg decreases from phenocrysts toward the groundmass (*Fig. 6*), indicating a more evolutionary groundmass amphiboles. Moreover, the ferroan pargasite phenocryst contains contents of Fe^{3+}, probably indicate an oxidizing condition probably during hydrothermal stage. Conversely, the ferroan pargasitic hornblende groundmass is free from Fe^{3+}.

The analyzed amphiboles of the rhyodacite-alkali rhyolite (RD-AR) of upper unit of the middle sequence represent the phenocrysts and groundmass. The phenocrysts exhibit normal zoning showing a wide range of composition towards Fe-, Mn-, Na- and Si-rich and Cr-Mg-poor rims (*Fig 6*; Table 2). The amphibole phenocrysts from RD-AR suite tend to have the same trends of the BA-A suite but poorer in Al and Fe^{3+} and more rich in Fe^{2+} (*Fig. 6*) probably suggest cognate magma. The cores of phenocrysts consist of kaersutite inner part (*Fig. 7c*) and ferroan pargasite outer part (*Fig. 7b*), whereas the rims are magnesian hastingsitic hornblende (*Fig. 7c*). Kaersutite is Ti-rich (Ti > 0.5) version of pargasite. In this case, substitution of Fe^{3+} of the magnesian hastingsitic hornblende rims for Al^6 of the ferroan pargasite cores, can occur. These cores (i. e., kaersutite and ferroan pargasite) contain Mn. Furthermore, these phenocryst cores are similar to the phenocryst of the TD-D suite (i. e., ferroan pargasite). The groundmass amphiboles, on the other hand, are magnesian hastingsites (*Fig. 7d*), and are nearly equivalent to the phenocryst

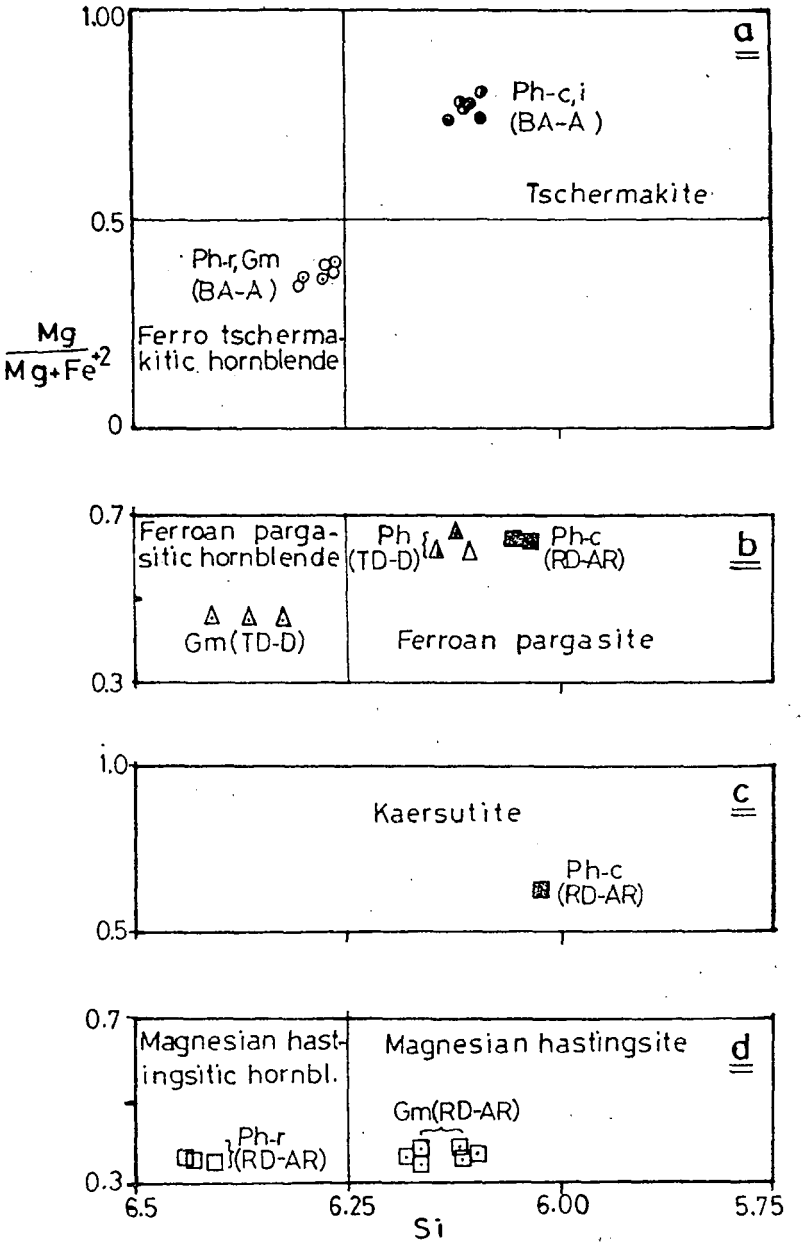

Fig. 7. Classification of calcic amphiboles (LEAKE, 1978) of Kid volcanic suites.
a) $(Na+K)_A < 0.5$; $Ti < 0.5$; b) $(Na+K)_A \geq 0.5$, $Ti < 0.5$, $Fe^{3+} \leq Al6$; c) $Ti \geq 0.5$; d) $(Na+K)A \geq 0.5$, $Ti < 0.5$, Fe3+ > Al6. BA-A = Basaltic andesite-andesite, TD-D = trachydacite-dacite, RD-AR = rhyodacite-alkali rhyolite. Symbols as in *Fig. 6*.

rims, with less Si and Ti and more Mg. The magnesian hastingsites are equivalent to Fe^{3+} rich ferroan pargasites (Fe^{3+} > $[Al^{6}]$). The entry of Fe^{3+} into hornblende can also be balanced by the substitution of O for [OH] (DEER et al., 1992). The amphibole groundmass form RD-AR suite tend to be lowest in Ti and Ca and highest in Na, Mn and Fe/(Fe+Mg) ratio among the other amphibole groundmasses of the Kid volcanics (*Fig. 6*), suggesting that they are the highest differentiated volcanic phase.

DISCUSSION

The data presented here allow some interpretations to be made concerning: a) the tschermakite-kaersutite-ferroan pargasite-magnesian hastingsite end-member relationships, b) evolutionary trends for amphiboles, c) metamorphism and geobarometer, d) implications for magma evolution.

The tschermakite-pargasite-hastingsite relationships

These relationships have been studied by several investigators, including HAWTHORNE (1983), HAMMARSTROM and ZEN (1986), FLEET et al. (1987), BEDARD (1988), HENDERSON et al. (1989), SCHULZ-KUHNT et al. (1990) and DEER et al. (1992). Oxy-hornblendes have a wide range of compositions which constitute the main calcic amphiboles in volcanic rocks. In this case, the iron-rich version usually with $Fe^{2+}/(Fe^{2+}+Mg) > 0.5$ can be indicated by the prefix „ferro". Within the calcic-amphiboles, as a whole the range of Fe/(Fe+Mg) ratio is complete but those with high Si content tend to be more „Mg-rich", whereas among tschermakitic and pargasitic hornblende, iron-rich members are more common. In the more iron-rich hornblendes, the Fe^{3+}-rich equivalents (Fe^{3+} > $[Al]^{6}$) of pargasite and ferroan pargasite are respectively called magnesian hastingsite. Ti-rich (Ti>0.5 atom) version of pargasite is kaersutite (DEER et al., 1992).

Kaersutite has a formula similar to that of pargasite, but Ti replaces Al in C-sites. Kaersutite, like oxyhornblende, it mostly Mg-rich with substitution of Mg by (Fe^{2+}+Fe^{3+}). Kaersutite can be oxidized during eruption, converting Fe^{2+} to Fe^{3+} and OH to O. It is a typical constituent of alkaline volcanic rocks, occurs as phenocrysts and can be replaced Ti-augite (DEER et al., 1992). Hastingsite (usually primary hornblende) occurs in the rocks of the calc-alkaline series, where the f_{H_2O} and f_{O_2} are high. The typical hastingsite of the intermediate rocks of the calc-alkaline series have Mg/(Mg+Fe) ratio ~0.5 and a moderate content of Al (~1.5). The hastingsite of andesitic rocks tend to richer in alkalis and Fe^{3+} (DEER et al., 1992).

The amphibole of Kid volcanics is characterized by compositional changes, i. e. tschermakite → Fe-tschermakitic hornblende in BA-A suite, Fe-pargasite → Fe-pargasitic hornblende in TD-D suite and Kaersuite → Fe-pargasite → Mg-hastingsitic hornblende in RD-AR suite. The overall compositional change of the Kid hornblende is characterized by the change of tschermakite → pargasite and hastingsite.

Evolutionary trend of the amphibole

Amphiboles of Kid volcanics have a wide range of compositions. *Fig. 8* displays the major element chemical variation as a function of the evolution index Fe/(Fe+Mg). The Fe/(Fe+Mg) ratio varies from 0.36–0.74 and a trend of increasing Si+Na+K, corresponding to a decrease in Ca+Al4 from phenocryst cores to phenocryst rims and

groundmass (*Fig. 9a*), is apparent as the amphiboles become more Fe-rich. The evolution index [Fe/(Fe+Mg) ratio] of the amphibole phenocrysts increases from cores (0.36–0.38) towards the rims (0.40–0.74). However, the cores of phenocrysts of BA-A, TD-D and RD-AR suites have similar values of Fe/(Fe+Mg) raito and Ca+Al4 (*Fig. 8., 9a*), suggesting a cognate magma for these suites. This ratio ranges from 0.53–0.68 in the groundmass of these suites, which are indistinguishable from the rims of phenocrysts. The evolution of these amphiboles was mainly controlled by the Fe ↔ Mg and Al6 ↔ Fe3+ substitution schemes.

The amphiboles of Kid volcanics range from tschemakite and ferroan tschermakitic hornblende in the BA-A suite, through ferroan pargasite and ferroan pargasitic hornblende in T-D suite to kaersutite, ferroan pargasite, magnesian hastingsitic hornblende and magnesian hastingsite in the RD-R suite (Table 2). The evolutionary trend is characterized by decreasing Ca, Mg, Cr, Fe^{3+} and Al, increasing Na and Fe^{2+}, and almost constant K, Ti and Si (*Fig. 6*). The variations in amphiboles (i. e., from BA-A suite of the lower sequence to RD-AR suite in the upper unit of the middle sequence) are responsible for the magmatic evolution of the Kid volcanics. Furthermore, the decrease in $Ca+Al_4$ and increase in Si+Na+K are gradually increased from BA-A suite of the lower sequencesuite to RD-D and RD-AR suite of the middle sequence (*Fig. 9a*), indicating again the progressive fractionation trend of the amphiboles. On the other hand, ferric-ferrous (Fe^{3+}/Fe^{2+}) ratio in these amphiboles is gradually decreased in the same direction. This suggest a gradual decrease in f_{O_2} (i. e., the melt becomes less oxidized) with differentiation of the volcanic suites.

The data presented show that there is only a calcic-type trend of the amphibole. This is probably due to the stability of the early formed Ca-rich amphibole phenocrysts, with the progressive increase in the alkalinity of the melt. Consequently, the absence of a gap miscibility in this amphibole. However, a probable small gap may be existed between amphiboles of lower and middle volcanic sequence.

Amphibole Metamorphism and Geobarometer

Hornblende is one of the most common constituens of regionally metamorphosed basic-intermediate rocks and is stable under a wide range of pressure-temperature conditions. The amphibole assemblage of the Kid volcanics as well as the probable metamorphic facies are summarized (Table 3). Both of BA-A and TD-D suites are overprinted by upper epidote amphibolite and lower amphibolite facies, whereas the RD-AR suite shows mineral assemblage similar to the upper greenschist and lower epidote amphibolite facies. Increasing grade of metamorphism tends to produce changes in amphibole composition, i. e. increases in Al, Ti, Na and K, but rock composition and oxygen fugacity are influential as well as temperature (DEER et al., 1992).

HAMMARSTROM and ZEN (1986) reported the compositional dependence of amphibole on temperature (T), pressure (P), oxygen fugacity (f_{O_2}) and bulk composition. T tends to increase with increasing Al^4, Ti, and $Mg/(Mg+Fe^{2+})$ ratio and decreasing Al^{6+}, Mn and $Fe^{3+}/(Fe^{3+}+Fe^{2+})$ ratio. P increases with increasing Al^6 and Al^T. F_{O_2} appears to increase with increasing Al^T and $Mg/(Mg+Fe^{2+})$ ratio and decreasing Ti. The bulk composition usually increases with increasing concentration of Si, Ti, alkalis and $Mg/(Mg+Fe^{2+})$ ratio in the system.

In the Kid volcanics, the amphibole phenocrysts of both BA-A and RD-AR suites are characterized by decrease in Ti, Al^4 and $Mg/(Mg+Fe^{2+})$ ratio from cores to rims (*Fig. 8, 9a and 9b*), suggest a decrease in T of crystallization toward the phenocryst rims. Also,

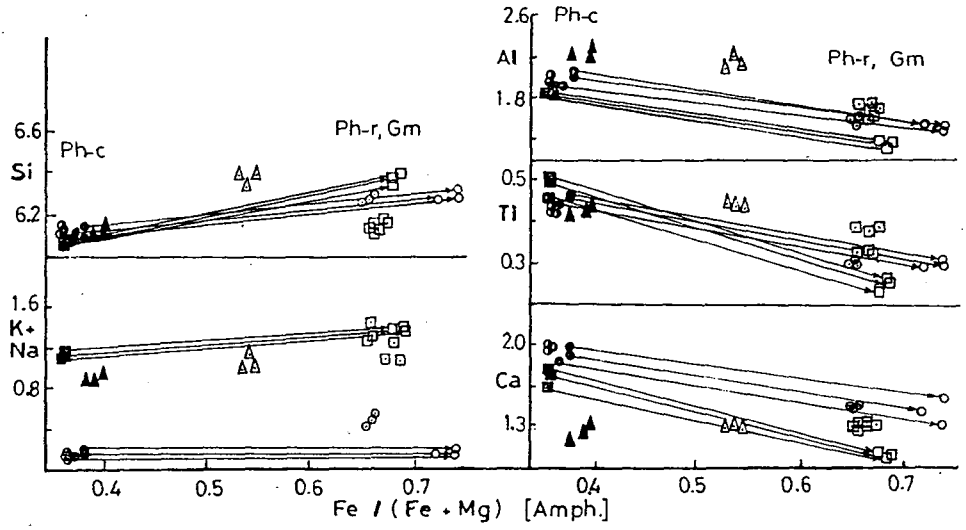

Fig. 8. Variation of Si, K+Na, Al, Ti and Ca versus Fe/(Fe+Mg) ratio of the amphiboles from Kid volcanics. The tie lines join the phenocryst cores and phenocryst rims. Symbols as in *Fig. 6.*

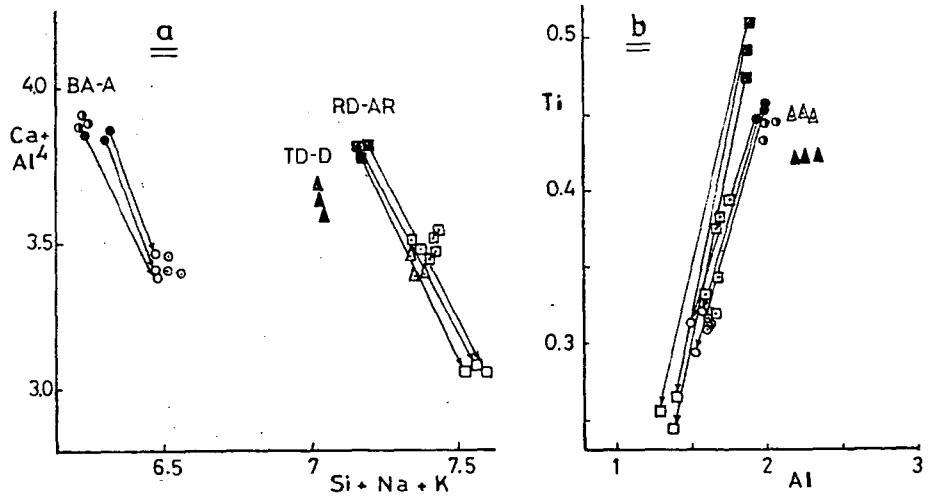

Fig. 9. Plots show the compositional variations of the phenocryst cores and rims and groundmass of the amphiboles of Kid volcanics.
a) (Ca+Al4) vs. (Si+Na+K) diagram. b) Ti vs. Al diagram. Symbols as in *Fig. 6.*

P appears to be decreased with decreasing Al^6 and Al^T. F_{O_2} tends to increase with decreasing Ti from cores to rims of phenocrysts. Furthermore, metamorphic grade of these rocks decrease with decreasing Al^T, Ti and alkalis from BA-A suite of the lower sequence to RD-AR suite of the middle volcanic sequnce and from cores to rims of phenocrysts, revealing that the early formed stage (e. g., BA-A suite) is more affected by metamorphism than the latter. These features are consistent with the higher metamorphic grade of the Old Dokhan volcanics or the lower volcanic sequence (e. g., BA-A suite) reported by EL-GABY et al. (1991) and HASSANEN (1992).

Implications for magma evolution

Petrographic studies (e. g., *Fig. 2, 3 and 4*) combined with the microprobe analytical data presented, have decumented the presence of compositional normal zoning in the amphibole grains. The dominant substitution mechanisms in amphiboles from mafic to intermediate silica-saturated and oversaturated alkaline rocks are thought to be (Na, K)^{A}Al^4 ↔ [ ]^{A}Si, Ca(Mg, Fe^{2+}) ↔ Na^MFe^{3+vi} and Mg = Fe^{2+} (NEUMANN, 1976; GIRET et al., 1980; STEPHENSON and UPTON, 1982).

Amphibole phenocrysts. Amphibole phenocrysts from the basaltic andesite-andesite (BA-A) suite range from tschermakite core to ferro tschermakitic hornblende rims and display a strongly increase in Si, Fe and K and decrease in Al, Mg, Ca and Ti toward the rims (*Fig. 6, 8 and 9a*), together with decrease Fe^{3+}/Fe^{2+} ratio (average of 0.84 core – 0.61 rim), suggests that the BA-A suite of the lower sequence has evolved from an early (subalkaline) melt that started its crystallization under oxidizing conditions. However, these compositional relations are believed to represent normal magmatic zoning. The substitution mechanisms in amphiboles of the BA-A suite are thought to be $[Al]^6$ ↔ Fe^{3+}, Mg ↔ Fe and Ca+Al ↔ Na+Si.

TABLE 3

Amphibole mineral assemblages in Kid volcanic complex

Mineral assemblage	Suite	Greenschist facies	Epidote amphibolite facies		Amphibolite facies
		A2	B1	B2	C1
Tschermakite	BA-A				----------
Tsch. hornbl.	BA-A			----------	----------
Pargasite	TD-D			----------	----------
Parg. hornbl.	TD-D			----------	
Kaersutite	RD-AR			----------	----------
Hastingsite	RD-AR	----------	----------		
Hast. hornbl.	RD-AR	----------	----------		

Amphibole phenocrysts from rhyodacite-alkali rhyolite (RD-AR) suite in the lower unit of the middle sequence range from kaersutite and ferroan pargasite core to magnesian hastingsitic hornblende rims, displaying compositional trends analogue to that from BA-A suite above (e. g., strongly increase of Si, Fe, K, Na and Mn and decrease of Al, Ti, Mg, Cr and Ca toward the rims (*Fig. 6, 8 and 9a*), suggests the genetic links of their parental magma. Furthermore, the compositional trend of the RD-AR suite may reflect a progressive fractionated magma. The substitution mechanisms in these amphiboles are

thought to be $Ti+O \leftrightarrow Fe^{3+}+OH^-$. The RD-AR suite magma probably had low silica activities. This would inhibit substitution such as $CaAl^4 \leftrightarrow Na^MSi$ and should result in a limited range of $Ca+Al^4$ vs. Si+Na+K variation, as is observed. RD-AR suite amphiboles show limited Na-enrichment and Ca-depletion. This implies that the substitutions like Ca (Mg, Fe^{2+}) Na^MFe^{3+vi} did not occur to great extent. Both the TD-D and RD-AR suites of the middle sequence are characterized by a quite similarity in composition and evolution, suggest a genetic relationship of their cognate magma.

Amphibole groundmass. Amphibole groundmass from BA-A suite is ferro tschermakitic hornblende which is quite similar to the phenocryst rims of the same rocks. Groundmass and phenocryst amphiboles from TD-D suite are also analogous. However, groundmass amphiboles are slightly enriched in Si and Fe^{2+} and depleted in Mg and Fe^{3+}, probably reflect their fractionation. On the other hand, the groundmass amphiboles from RD-AR suite are magnesian hastingsites and tend to be depleted in Cr, Fe^{3+} and $Ca+Al^4$ and enriched in Fe^{2+} and Na compared with the phenocryst rims of the same rocks reflecting their intermediate crystallization between the phenocryst cores and rims.

Although the stability of tschermakite at high-P conditions has been studied (e. g., GILBERT et al, 1981), its thermal stability at low-P conditions has yet to be defined. However, results of experimental studies applied to phase equilibrium of tremolite, which is similar to tschermakite, is available. BOYD (1969) has studied the P-T stability of tremolite. On his phase diagram, tremolite (as well as tschermakite-tschemakitic hornblende of BA-A suite) appears in a field, between T of ~ 800 °C and 900 °C at P of 0.5–3 Kbar. On the other hand, HANDERSON et al. (1989) have established, by means of amphibole composition, that the range of T of crystallization is 950–1000 °C for kaersutite and 750–800 °C for hastingsite. The stability limits of the pargasite. Fe-pargasite, Mg-hastingsite and hastingsite as a function of T and P have been studied by GILBERT et al. (1981). On the T side of his phase diagram, Fe-pargasite has maximum stability at f_{O_2} of the wustite-magnetite buffer (e. g., T: < 700–870 °C and P: 0.5–2.2 Kb.), whereas the more Fe^{3+}-rich Mg hastingsite has maximum stability with the hematite-magnetite buffer (e. g., T: 900–1030 °C and P: 0.2–0.6 Kb). These results seem to be concordant with the decrease of T and P as well as the metamorphic grade from BA-A suite of the lower sequence to RD-AR suite of the middle sequence (e. g., from cores to rims of phenocrysts and groundmass).

It is common to see a sharp optical and compositional boundary (*Fig. 2, 3, 4, 8 and 9a*) between the core and rims of the phenocrysts. The sharp discontinuity suggests a sudden transition from one growth environment to another and may reflect rapid ascent or sudden change in equilibrium caused by volatile exsolution (BEDARD, 1988) in the Ca-amphibole group itself.

In summary, the role of amphibole during magmatic differentiation may control the composition of the derivative melt. For example, the $Mg \leftrightarrow Fe$, $CaFe^{2+} \leftrightarrow NaFe^{3+}$ and $CaAl \leftrightarrow NaSi$ substitution mechanisms in the Ca-amphiboles of the Kid volcanics, have led to magma evolution from intermediate to felsic compositions (e. g. from BA-A suite of the lower seuence to TD-D and RD-AR suite of the middle volcanic sequence). The phenocrysts of both BA-A nd RD-AR suites show a same compositional trend; this implies that they are cognate with higher temperature and f_{O_2} and lower pressure cores than the rims. Amphiboles that characterize these suites (e. g., tschermakite, kaersutite, Fe-pargasite and Mg-hastingsite) are breakdown to form discontinuous zoned, calcic-type amphibole with a progressive increase in the alkalinity, silica and iron of the melt. These amphiboles are expected to be formed at high temperature (~700-1000 °C) and low pressure (~0.2-3 Kb.).

REFERENCES

BEDARD, J. H. (1988): Comparative amphibole chemistry of the Moteregian and White Mountain alkaline suites, and the origin of amphibole megacrysts in alkaline basalts and lamprophyres. Min. Mag., **52**, 91–103.

BOYD, F. R. (1959): Hydrothermal investigations of the amphiboles. In: Research Geochemistry, P. H. Ableson (ed.), 377–396.

CAMERON, M., J. J. PAPIKE (1979): Amphibole crystal chemistry: a review. Fortschr. Miner., **57**, 28–67.

DEER, W. A., R. A. HOWIE, J. ZUSSMAN (1992): An introduction to the rock-forming minerals. Long. Sci. & Tech., England.

EL-GABY, S., A. A. KHUDEIR, M. ABDEL-TAWAB, R. F. ATALLA (1991): The metamorphosed volcano-sedimentary succession of Wadi Kid, Southeastern Sinai, Egypt. Annals Geol. Surv. Egypt, XVII, 19–35.

EL-GABY, S., F. K. LIST, R. TEHRANI (1988): Geology, evolytion and metallogenesis of the Pan-African belt in Egypt. The Pan-African belt of Northeastern Africa and adiacent countries. In: S. EL-GABY and R. GREILING (eds.). 17–68.

FLEET, M. F., R. L. BARNETT, W. M. MORRIS (1987): Prograde metamorphism of the Sudbury igneous complex. Can. Mineral., **25**, 499–514.

GHONEIM, M. F., S. M. ALY, M. H. EL-BARAGA (1985): Geochemistry of the Malhag metavolcanics, South Sinai Peninsula, Egypt. Annals Geol. Surv. Egypt., XV, 171–182.

GILBERT, M. C., R. T. HELZ, R. K. POPP, F. S. SPEAR (1981): Experimental studies of amphibole stability. Mineral. Soc. Amer., Rev. Mineral., **9B**, 279–353.

GIRET, A., B. BONIN, J.-M. LEGER (1980): Amphibole compositional tennds in oversaturated and under-saturated alkaline plutonic ring complexes. Can. Mineral., **18**, 481–495.

HASSANEN, M. H. (1992): Geochemistry and petrogenesis of the late Precambrian Kid volcanis: evidence relevant to arc-intra-arc rifting volcanism in Southern Sinai, Egypt. J. Afr. Earth Sci., **14**, 131–145.

HAMMARSTROM, J. M., E-AN ZEN (1986): Aluminium in hornblende: An empirical igneous geobarometer. Amer. Mineral., **71**, 1297–1313.

HENDERSON, C. M. B., K. PENDLENURY, K. F. FOLAND (1989): Mineralogy and petrology of the Red Hill alkaline igneous complex. New Ampshire, U. S. A. J. Petrol., **30**, 627–666.

HOWTHORNE, F. C. (1983): The crystal chemistry of amphiboles. Can. Mineral., **21**, 173–480.

LEAKE, B. E. (1978): Nomenclature of amphiboles. Can. Mineral., **16**, 501–520.

NEUMANN, E.-R. (1976): Two refinaments for the calculation of structural formulae for pyroxenes and amphiboles. Norsk Geol. Tidsske., **56**, 1–6.

PECCERILLO, A., S. R. TAYLOR (1976): Geochemistry of Eocene calc-alkaline volcanic rocks from Kastamonu area, northern Turkey. Contrib. Min. Petrol. , **58**, 63–81.

REYMER, A. P. S., A. MATHEWS, O. NAVON (1984): Pressure-temperature conditions in the Wadi Kid metamorphic complex: Implications for the Pan-African event in the southeastern Sinai. Contrib. Mineral. Petrol., **85**, 336–345.

RIES, A. C., R. M. SCHACKLETON, R. H. GRAHAM, W. R. FITCHES (1983): Pan-African structures, ophiolites and melanges in the Eastern Desert of Egypt: A traverse at 26 N. J. Geol. Soc. London, **140**, 75–95.

SCHULZ-KUHNT, D., G. MULLER, J. HOEFS (1990): Petrology of high-grade metamorphic terrains in the Abre Campo-Jequeri Quadrangle, Eastern Minas Gerais, Brazil. Chem. Erde, **50**, 225–245.

SHIMRON, A. E. (1984): Evolution of the Kid Group, Southeast Sinai Peninsula. Thrusts, Melanges and implications for accretionary tectonics during the late Proterozoic of the Arabian-Nubian Shield. Geology, **12**, 242–247.

Manuscript received 22 August 1995.

Acta Mineralogica-Petrographica, Szeged, XXXVI, 35–54, 1995

CHEMISTRY OF BIOTITE AS A GUIDE TO THE NATURE OF MAGMAS, HAJJA GRANITOID COMPLEX. YEMEN REPUBLIC

E. R. EL NASHAR*, M. L. KABESH*

Earth Sciences Dept., National Research Centre

ABSTRACT

Biotites separated from Hajja granatic rocks, Yemen Republic, have been examined. The chemical data of 14 analysed biotites show that the biotites are ferrous iron varieties. The behaviour of major elements in the examined biotites discussed according to different variation diagrams and elemental ratios. The significance of $Fe^{(t)}$ ($Fe^{(t)}$+Mg) ratio as a relative measure of biotite crystallization suggests that the biotites may be formed under a temperature range of 815°–950°C. In the present study since Fe shows little variation with Al in biotites in both calc-alkaline and peralumios magmas, the substitution $2Al \rightarrow 3Fe^{2+}$ does not play an important role during the crystallization of biotites in these two types. On the other hand the substitution $3Mg \rightarrow 2Al$ is vital. The contrasting behaviour of Fe and Mg with respect to Al during the crystallization of biotites is partly governed by the various physicochemical conditions including the behaviour of volatiles in these magmas.

INTRODUCTION

Biotite is an important ferromagnesian mineral in most intermediate and felsic igneous rocks. Its potential to reveal both the nature and the physicochemical conditions of source magmas from which it formed is high. Igneous biotite can also be used to provide valuable petrogenetic information.

Althought numerous studies have been carried out on biotites from individual igneous complexes and granitoids in particular, very little work has been done to characterize biotite in the spectrum of igneous rocks or to find a possible tectonic linkage of biotite compositions to magma types from various sources and distinct petrogenetic histories.

Recently ABDEL-RAHMAN (1994) succesfully introduced several discrimination diagrams based on major-element composition of biotites in igneous rocks world-wide crystallized from three distinct magma types. He defined 3 magma suites, namely: 1. Alkaline complexes (A), 2. Peraluminous suites (P), 3. Calc-Alkaline complexes (C).

The present work is the first attempt to apply ABDEL-RAHMAN'S (op. cit.) scheme on biotites from Hajja granatic complex, Yemen Republic.

In a previous study the petrochemical characters and chemical classification of Hajja granitoid rocks were studied by SALEM et al. (1986).

The granatic rocks of Hajja *(Fig. 1)* comprise two field types represented by greyish white and pinkish granites. They are medium to coarse grained and may be porphyritic, composed essentially of quartz, alkali feldspar, plagioclase, biotite, in addition to fair amount of muscovite; iron oxide minerals epidote, sphene; magnetite and zircon are the common accessories. Biotite occurs as the dominant mafic mineral, it forms subhedral

* Dokki Cairo, Egypt

crystals ranging from 0.9 mm to 2.6 mm in length and from 0.3 mm to 1 mm in breadth. Biotite forms stout flakes with torn ends, sometimes exhibiting sub-parallel arrangement. It often displays pleochroism with X=straw yellow and Y=Z=dark brown.

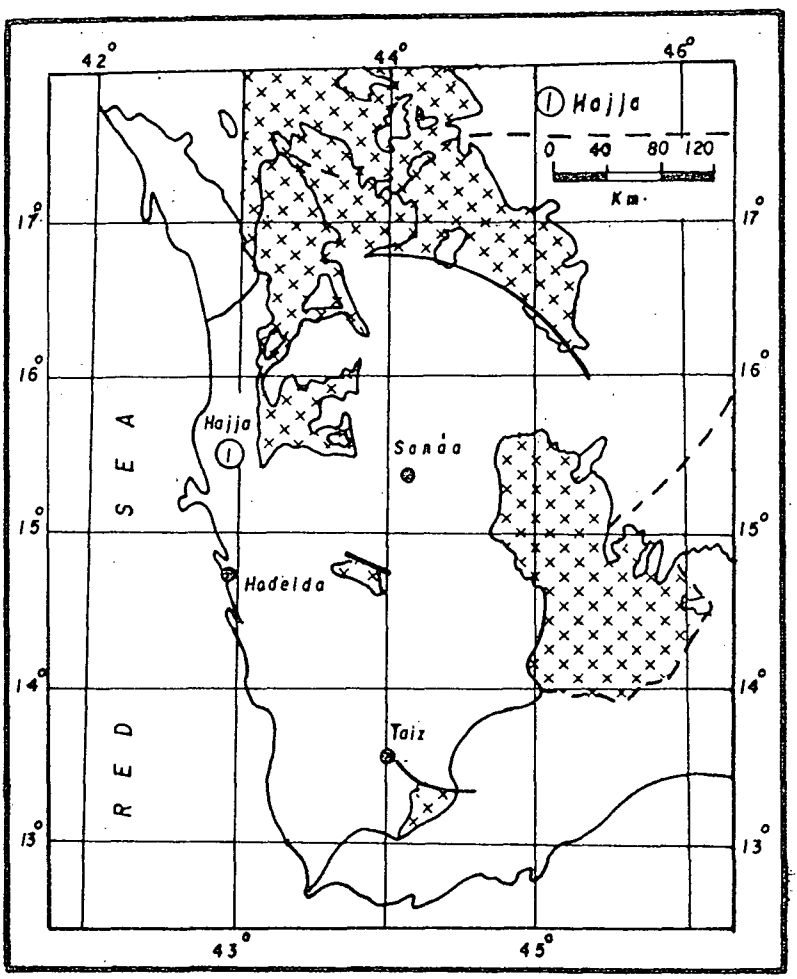

Fig. 1. Map showing distribution of the basement complex in the Yemen Arab Republic and Location of Hajja.

COMPOSITION OF BIOTITES

The chemical analyses* of the recovered biotites are given in Table 1 with some analyses from other localities for comparison. The chemical data are used in different

* Measurements of samples from 1–11 were carried out by using the scanning electron micro-analyser M.S. 46 camesa and teletype printing unit in the lab. of petrography department Leningrad Mining Institute, Russia, samples 12, 13, 14 by wet analysis.

TABLE 1

Chemical analyses of biotites from Hajja granitoids

Samples No.	1	2	3	4	5	6	7	8	9	10	11	12	13	14	A	B	C
SiO_2	37.40	38.27	37.92	38.74	39.79	38.78	38.77	35.85	34.75	37.64	37.70	38.40	37.25	38.90	35.40	35.99	36.90
Al_2O_3	14.30	13.18	13.67	13.33	11.81	13.53	13.47	16.60	15.85	16.42	15.90	15.66	16.88	16.32	16.66	14.94	115.40
Fe_2O_3	5.74	9.20	9.39	7.92	10.27	9.48	7.97	6.10	4.83	2.15	1.90	12.73	8.25	12.24	5.17	6.11	3.90
FeO	12.10	7.23	8.32	9.18	4.19	6.92	9.29	13.84	16.32	18.60	18.90	13.53	15.72	13.34	21.61	16.91	16.60
MnO	0.65	0.82	0.56	0.65	0.95	0.63	0.72	–	–	–	–	0.28	0.40	0.28	0.45	0.14	0.52
MgO	12.65	14.36	13.93	13.58	16.96	14.91	13.91	10.64	11.44	10.22	10.29	6.25	6.84	5.91	6.23	12.90	10.90
CaO	–	–	0.16	–	–	–	0.30	–	–	0.52	0.49	1.23	1.29	1.41	1.40	0.14	0.22
Na_2O	–	0.35	0.41	0.40	–	–	–	0.94	1.13	–	–	0.13	0.18	Trace	0.34	0.12	0.04
K_2O	9.53	9.95	9.25	9.59	10.04	10.00	9.66	10.13	9.54	9.48	8.89	6.78	7.13	6.78	6.34	7.81	9.10
TiO_2	4.34	3.39	2.94	3.25	2.35	2.38	2.58	2.90	2.61	2.51	2.72	2.52	3.42	2.40	2.18	2.73	2.90
H_2O	–	–	–	–	–	–	–	–	–	–	–	2.06	2.24	1.99	2.83	2.50	3.10
Total	96.79	90.75	96.52	96.95	96.35	96.60	96.67	96.99	96.47	96.99	96.81	99.60	99.60	99.57	98.99	99.43	98.98

– = Not detected
A = Biotite from Kadabora granites (KABESH and SALEM 1981)
B = Biotite from Ras Barud granites (KABESH et al., 1977)
C = Biotite from granodiorite, Sierra Nevada Batholith, California (DODGE et al., 1969)

petrochemical parameters and variation diagrams in order to elucidate the petrochemical and petrogenetic characteristics of the studied biotites.

Nockolds diagram

According to NOCKOLDS (1942) the biotite composition is different for different mineral associations, I-Biotites associated with muscovite and topaz, II-Biotites unaccompanied by other mafic minerals. III-Biotites associated with hornblende, pyroxene, and/or olivene. The chemical data are plotted on NOCKOLDS variation diagram (Fig. 2) which shows the fields (I, II, III); it is evident that the analysed biotites fall within field II of biotites unaccompanied by other mafic minerals.

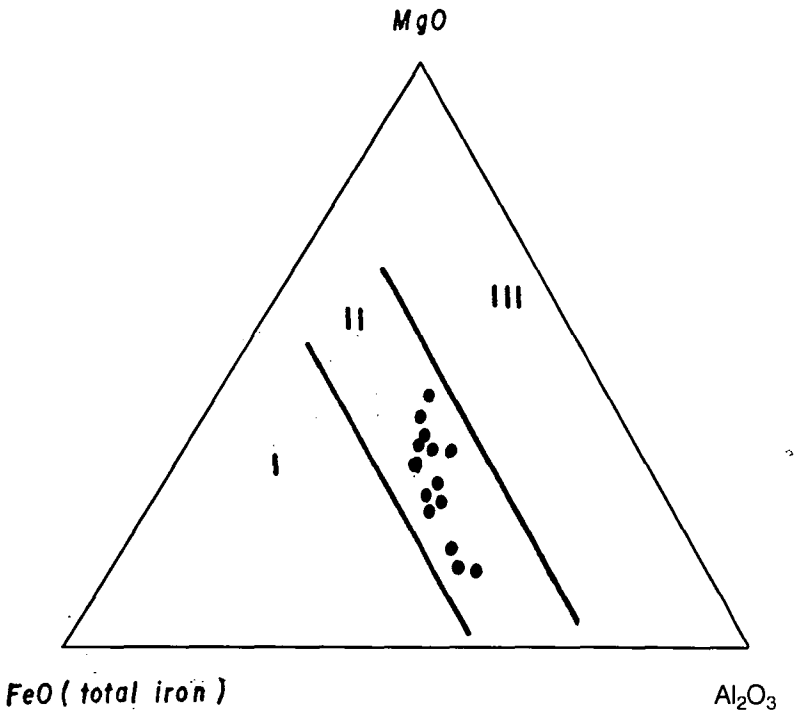

Fig. 2. Plots of biotites on the ternary diagram of NOCKOLDS (1947)
I – Biotites associated with muscovite, topaz etc. II – Biotites unaccompanied by other mafic minerals.
III – Biotities associated with hornblende, pyroxene and or olivine.

Heinrich variation diagram

The values Fe_2O_3+TiO_2–MgO–FeO+MnO are taken into account. *Fig. 3*, it is evident that the examined biotites share the fields of magmatic and metamorphic metasomatic, which indicate that the Hajja granatic mass might have suffered some postmagmatic metasomatic processes.

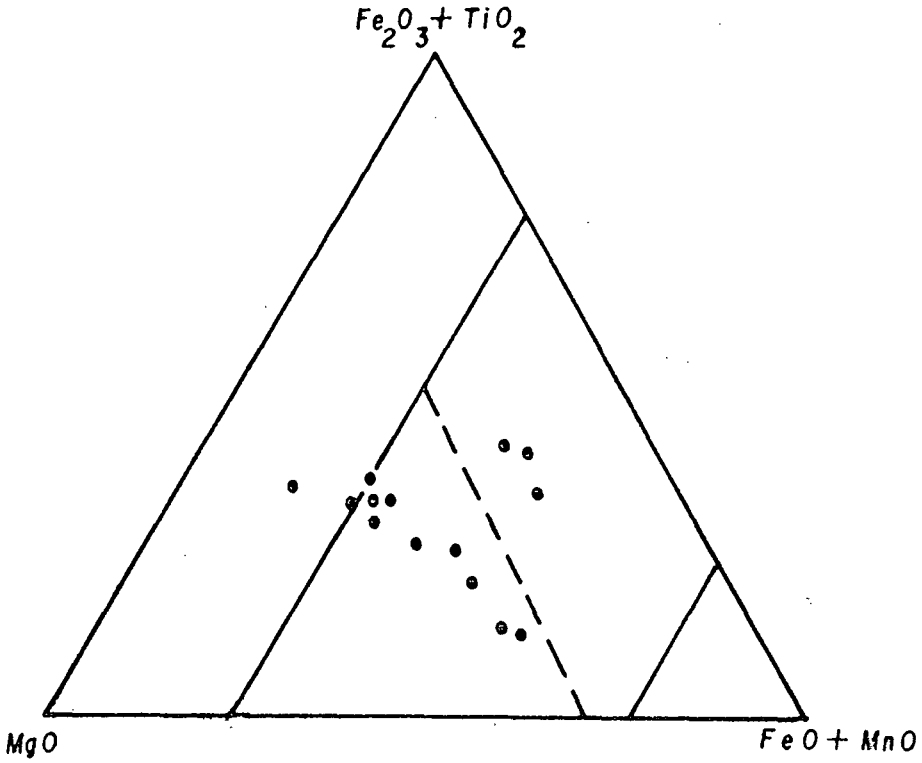

Fig. 3. Heinrich variation diagram

STRUCTURAL FORMULAE OF BIOTITES

The chemical analyses (Table 2) are recalculated on the basis of 23 (O), (DEER et al., 1966), and the results are given in (Table 2) which gives the following picture: The coordinated large cations Ca, Na, K of X group have values reanging from 1,55–2,28, in all cases K cation constitutes over 75% of the total X values, while both Na, Ca contents in the biotites are low and sometimes are not present. The wide range of X values is due to the wide range of the alkalinity of the host granatic rocks. The Y group cations consist mainly of iron and magnesium, the relation between cations of the Y group is shown in *Fig. 4.* It is obvious that the studied biotites are magensio-ferrous rich varieties, the composition ranges from Mg biotites to Fe+2 biotites.

Experimental work by WONES and EUGSTER (1965) demonstrate the effect of oxygen fugacity on the formation and resultant composition of biotites, if it is assumed that substitution other than Fe → Mg will not materially influence biotite stability. Application of the experimental data to the studied biotites permits an evaluation of the variation during the course of crystallization of Hajja granitic magma. WONES and EUGSTER (1965) considered two contrastive trends of crystallization of biotites. Trend I representes a magma in which oxygen fugacity remains constant or somewhat increases whereas in trend II oxygen fugacity decreases.

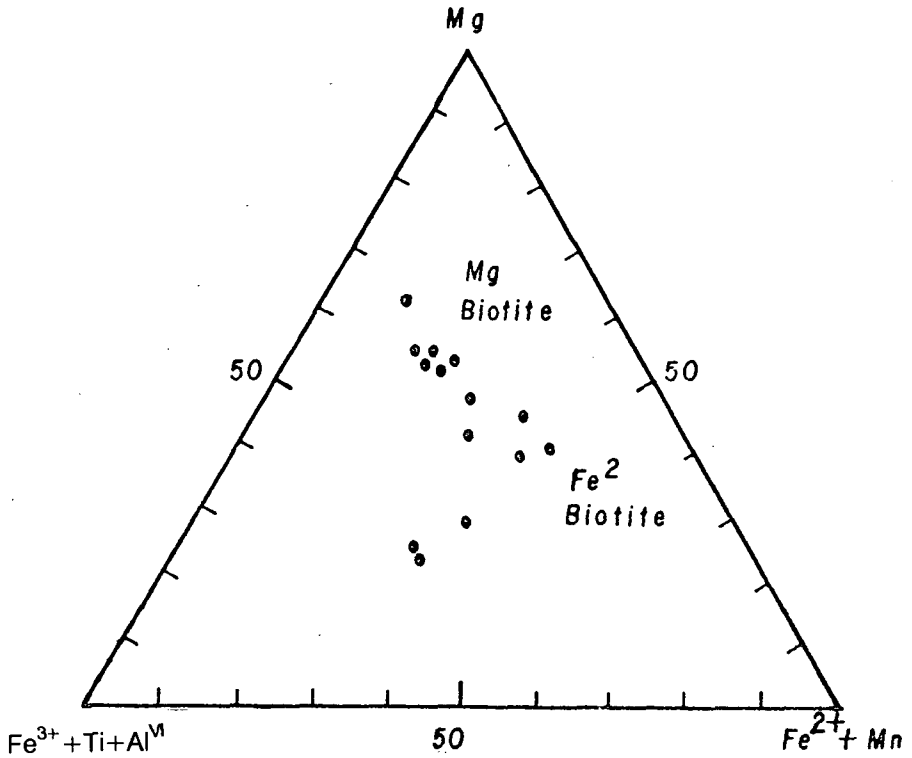

Fig. 4. Relation between octahedral cations of the investigated biotites

The trend of the Hajja biotites within the compositional triangle Fe^{3+}, Fe^{2+}, Mg (*Fig. 5*) rather closely paralells WONES and EUGSTER'S (op. cit.) estamited composition of biotites solid solution in the ternary system $KFe_3^{3+}AlSi_3O_{12}OH$–$KFe^{2+}{}_3AlSiO_3O_{10}(OH)_2$–$KMg_3AlSi_3O_{10}(OH)_2$, which are stable at oxygen fugacities controlled by individual buffer equilibria. The correlation suggests the composition of the examined biotites as defined by oxygen fugacities greater than those of the Ni–NiO buffer thus, the biotite composition suggests oxygen fugacities for the biotites of Hajja area as largely following a buffer curve during crystallization i.e. oxygen fugacities decreased with decreasing temperature. All the biotites analyzed belong to the assemblage potash feldspar – magnetite biotite, the buffering effect of magnetite was recognized in controlling oxygen fugacities in the crystallizing magma.

KENNEDY (1955) and OSBORN (1962) have suggested that the calc-alkaline or „Bowen trend" of late silica enrichment in contrast to the „Fenner trend" of late iron enrichment is caused by a relatively high constant oxygen fugacity during crystallization. However, because oxygen fugacity will decrease as temperature decreases i.e. was defined by buffering reaction, trend II of WONES and EUGSTER (1965).

The plotting of 100 Fe (total)/(Fe total+Mg) ratio of the studied biotites on the stability diagram (*Fig. 6*) according to EUGSTER (1965) reveals that these ratios of the analyzed biotites range between 32–69.96 which correspond to temperature about 815°C–950°C and oxygen frugacity of about 10^{-14}–10^{-8}.

TABLE 2

Structural Formulae of Biotites

Formula No.	1		2		3		4		5		6		7		8		9		10		11		12		13		14	
Si	5.75	Z 8	5.8	8	5.77	8	5.90	7.99	5.98	8	5.87	8	5.90	8	5.55	8	5.38	8	5.77	8	5.77	8	5.90	8	5.73	8	5.96	8
Al^{IV}	2.25		2.2		2.23		2.09		2.02		2.13		2.10		2.45		2.62		2.32		2.23		2.10		2.27		2.04	
Al^{VI}	0.34		.16		0.22		0.31		0.07		0.27		0.31		0.58		0.27		0.74		0.54		0.74		0.79		0.91	
Fe^{3+}	0.75		1.17		1.20		1.00		1.29		1.20		1.02		0.80		0.64		0.28		0.25		1.47		0.95		1.41	
Fe^{2+}	1.55		0.92		1.06		1.15		0.53		0.88		1.18		1.82		2.15		2.36		2.40		1.74		2.02		1.71	
Mn	Y 0.08	6.13	0.10	5.99	.07	6.04	.08	5.99	0.12	6.08	0.08	6	0.09	6	–	6	–	6	–	6.01	–	5.85	.04	5.72	0.05	5.77	.04	5.69
Mg	2.90		3.24		3.16		3.09		3.80		3.86		3.16		2.46		2.64		2.34		2.35		1.44		1.57		1.34	
Ti	0.51		0.39		0.34		0.37		0.27		0.27		0.30		0.34		0.30		0.29		0.31		0.29		0.39		0.28	
Ca	–	X 1.89	–	1.89	0.03		–		–		–		0.31		0.58		0.27		0.74		0.54		0.74		0.79		0.91	
Na	–		0.11	2.03	0.12	1.94	0.37	2.24	–	1.93	1.20		1.02		0.80		0.64		0.28		0.25		1.47		0.95		1.41	
K	1.89		1.92		1.80		1.87		1.93		0.27		0.30		0.34		0.30		0.29		0.31		0.29		0.39		0.28	

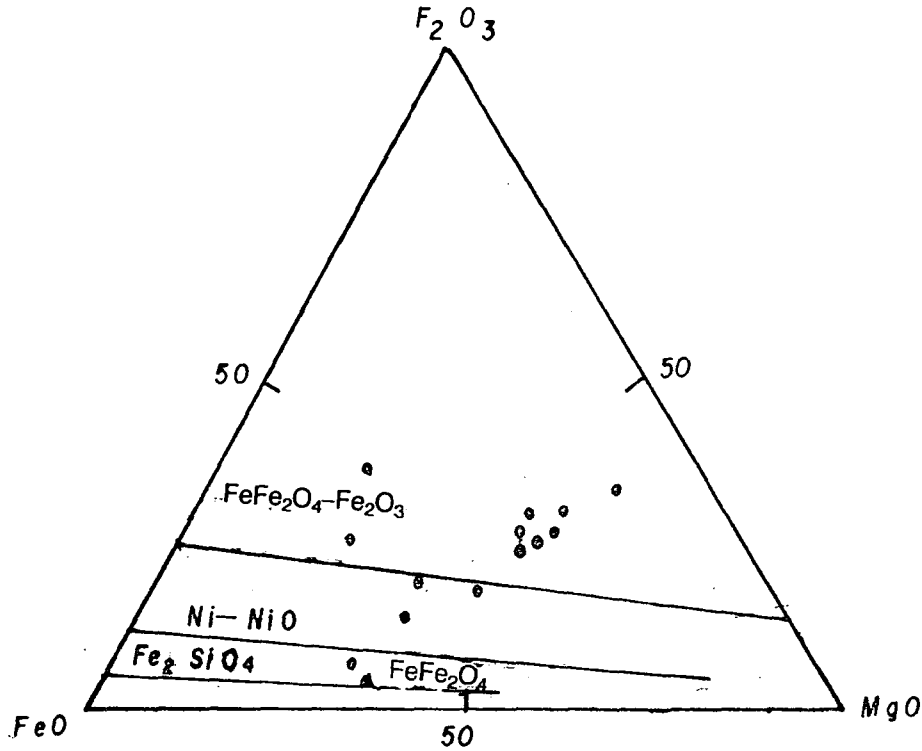

Fig. 5. Relation between Fe^{3+}, Fe^{2+} and Mg in the investigated biotites

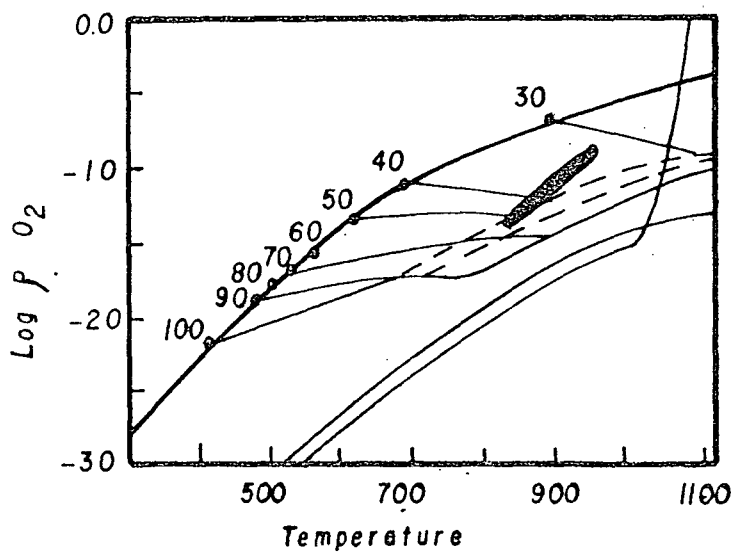

Fig. 6. Biotite stability diagram of specific 100 Fe/(Fe+Mg) values as a function of oxygen fugacity and temperature at 20, 70 bars total pressure (after WONES and EUGSTER 1965). Heavily shaded area represents the investigated biotites.

Magma type

Chemistry and crystallization conditions of the granitic magma essentially affect the composition of the biotites derived from this magma.

Al content plays an important role in the alkalinity of the magma and could be used as a factor controlling alkalinity, acidity and as an indicator for pressure prevailing during the process of crystallization.

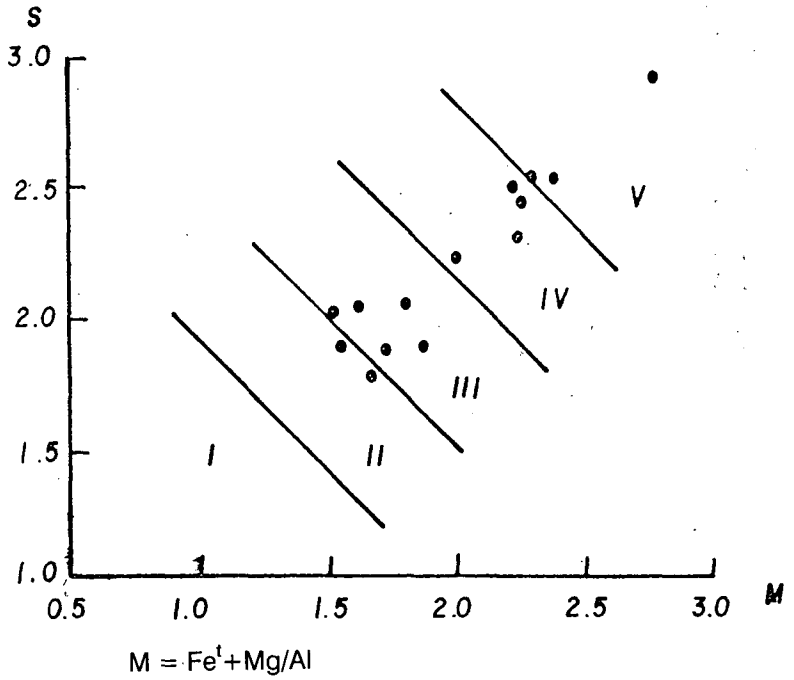

Fig. 7. Acidity-Alkalinity diagram of Hajja granitoids with biotite composition

On the diagram alkalinity–aluminosity of biotites (*Fig. 7*) the values Si/Al vs. (Mg+Fe)/Al was suggested by MARACHUCHIEV (1966). He divided the fields of crystallization of the biotites host rocks into five fields in order of increasing alkalinity:

I. Calcic magma, II. Calc alkaline magma,
III. Subalkaline magma, IV. Alkaline magma,
V. Peralkaline magma.

Plots of the examined biotites fall in the fields of subalkaline to alkaline granite. The above mentioned elements were used also by IVANOV (1970) for revealing the relationship and illustrating alkalinity and temperature of crystallization of biotites and water fugacity of crystallizing liquid. He suggested the following relationship

L=AlX100/Si+Al+Fe+Mg,

F=100FeO$^+$/(FeO$^+$+Mg).

The values of Hajja biotites range from 15.3 to 23 for L) and from 32 to 69.96 for F, these values occupy the fields of moderate to high alkalinity and of high to moderate termpature of crystallization (*Fig. 8*).

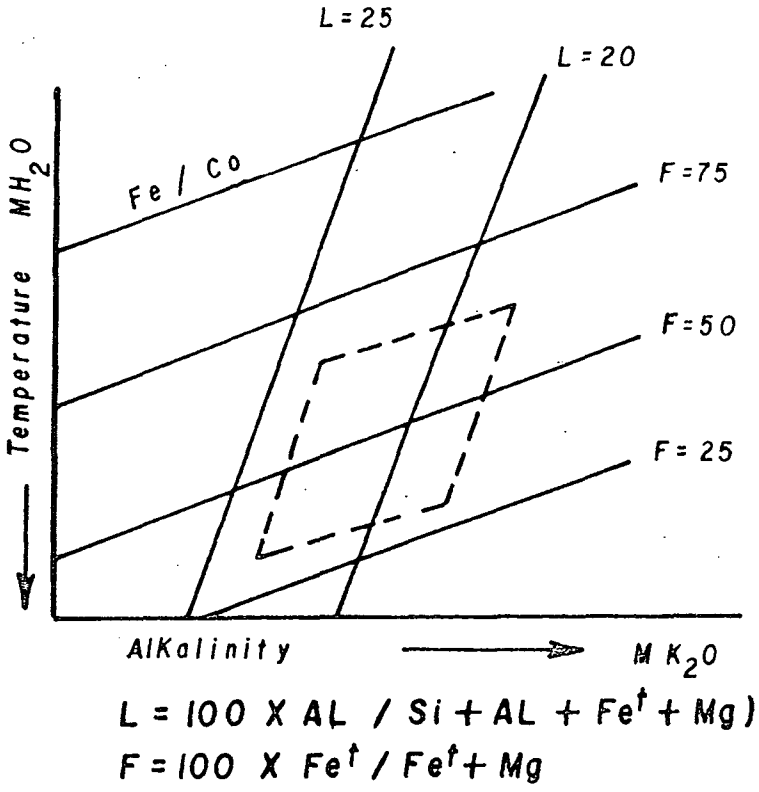

Fig. 8. Relation between water activity and potassium activity in granitoids of Hajja.

According to SMITH (1968) increasing temperature gives possibilities for Al to replace Si in the tetrahedral position while increasing pressure gives favourable condition for this replacement to take place on the octahedral coordination. Diagram (*Fig. 9*) illustrates the relation between Al^{IV} ad Al^{VI} coordinations.

The diagram shows that in the tetrahedral Al is not great from (2.020 to 2.618) while variations in octahedral Al are more or less clear from (0.02 to 0.92), this may indicate that these granites are allochtonous, where the pressure decrease through the magma ascending upwards intruding country rocks of different composition.

Relation of Pleochroism to chemistry

The formulae of biotites have been discussed by HAYAMA (1959, 1964) and ENGEL and ENGEL (1962). HAYAMA (1959) has correlated the change in the absorption colour of biotite to the behaviour of TiO_2 and $Fe_2O_3/(FeO+Fe_2O_3)$ values. He concluded that biotites of high Ti content and lower $Fe^{3+}/(Fe^{+2}+Fe^{+3})$ values are characterized by red brown absorption colour in Y and Z direction while those of lower Ti and higher $Fe^{3+}/Fe^{3+}/(Fe^{+2}+Fe^{+3})$ values show brown absorption colours in Y and Z directions. The examined biotites are strongly pleochroic with X straw yellow and Y=Z dark brown (SALEM et al., 1986).

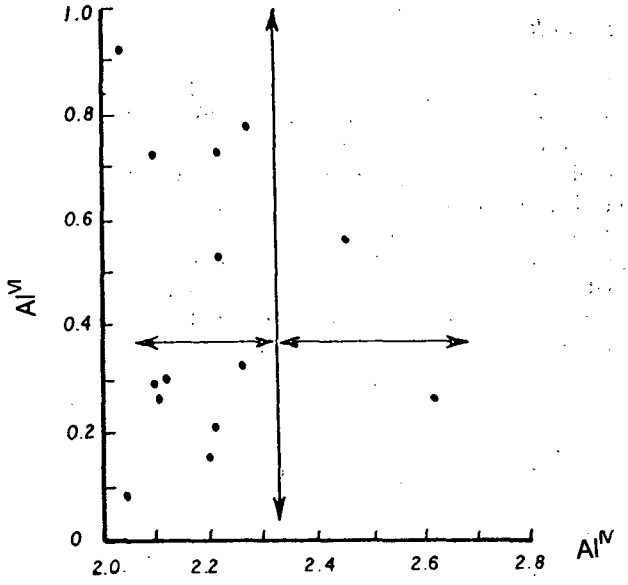

Fig. 9. Content of Al in tetrahedral and octahedral positions in biotites of Hajja

According to the structural formulae Table 2 of the examined biotites the Ti/Fe^{+2} ratios are low whereas the ratios of $Fe^{3+}/(Fe^{3+}+Fe^{2+})$ are high. Therefore the Hajja biotites fall in the field of brown absorption or Y and Z direction (*Fig. 10*).

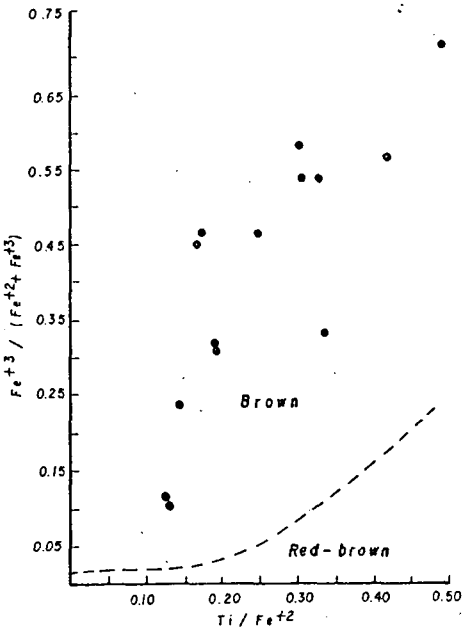

Fig. 10. Relation between the Y and Z absorption colours of biotites and their $Fe^{+3}/(Fe^{+2}+Fe^{+3})$ and Ti/Fe^{+2} ratios (after HAYAMA, 1959)

This feature has been extensively reviewed by FOSTER (1960) HANZEN and WONES (1972) DYMEK (1983), HEWITT and ABRECTH (1986) AL-DAHAN et al. (1988). In the present work it is proposed to give only an outline of the main substitution mechanism govering tetrahedral and octahedral compositional changes.

As mentioned before Al plays a dominant role in the nature of Fe^{2+} Mg, Ti substitutional relations. Some of these relations have been studied to demonstrate this feature in the examined biotites, the most clear substitution is the relation between the four cations Ba Al^{IV} SiK, the binary diagram (*Fig. 11*) shows a good relation which indicate the process of substitution through th crystallization of the magma forming biotites. It is obvious that by lowering temperature and oxygen frugacity the SiK pair is substituting Ba Al^{IV}.

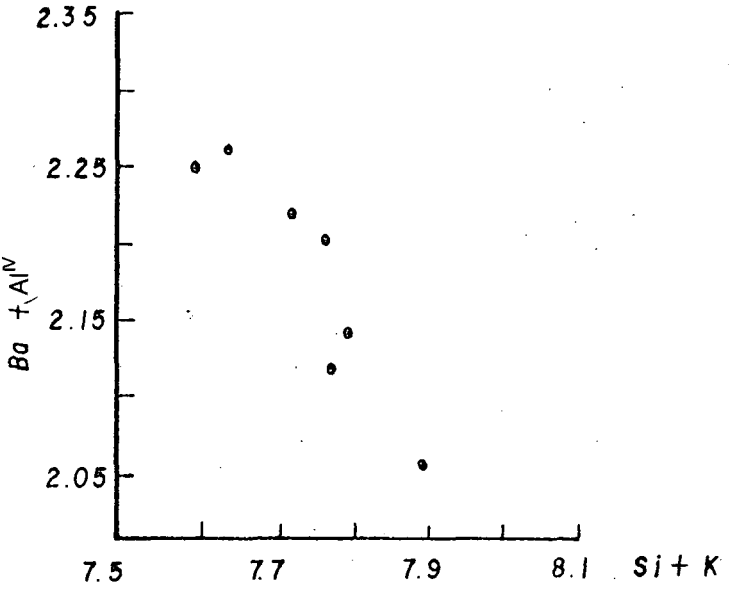

Fig. 11. Plots of Ba+Al^{IV} against Si+K

There is also a good relation in substitution between Al^{VI} and Mg ion (*Fig. 12*) which have greater values at high temperature and are by decreasing temperature. Ti cation is correlated with both Al^{IV} and Al^{VI} but with no clear relation with both cations of Alumina (*Fig. 13 and 14*). On the other hand if we divided the relation of Al^{IV} into two values Al^{IV} < 0.5 and , Al^{IV}>0.5, shows a positive relation in the first portion while in the second where Al^{IV}>0.5 a negative relation exists. This means that the Al content in biotite is the main factor in most of the substitutional processes, because of the dual role of Al ions, since Ti is slightly higher with low oxygen fugacity.

As regards the relation between Ti and Mg it is clear from the diagram (*Fig. 15*) that there is moderate correlation except at high values of Mg which means high temperature.

The following two relations are regarded as the dominant Ti substitution mechanism for Mg-biotites, which are suggested by ABRECHT and HEWITT (1988), FOLEY (1989).

1. $2Mg^{VI}=Ti^{VI}+Al^{VI}$ 2. $Mg^{VI}+2S^{IV}=Ti^{VI}+2Al^{IV}$

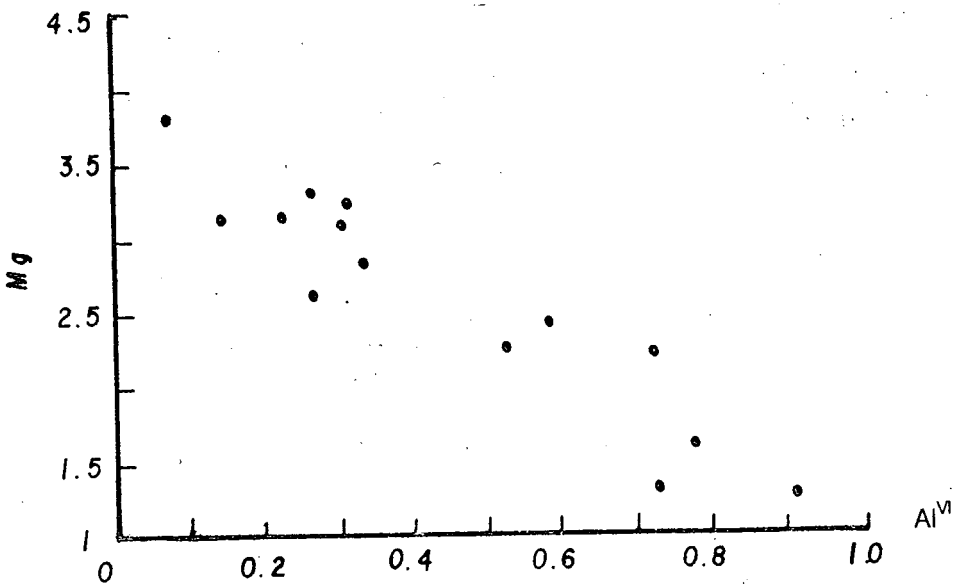

Fig. 12. Plots of Mg against Al^{VI}

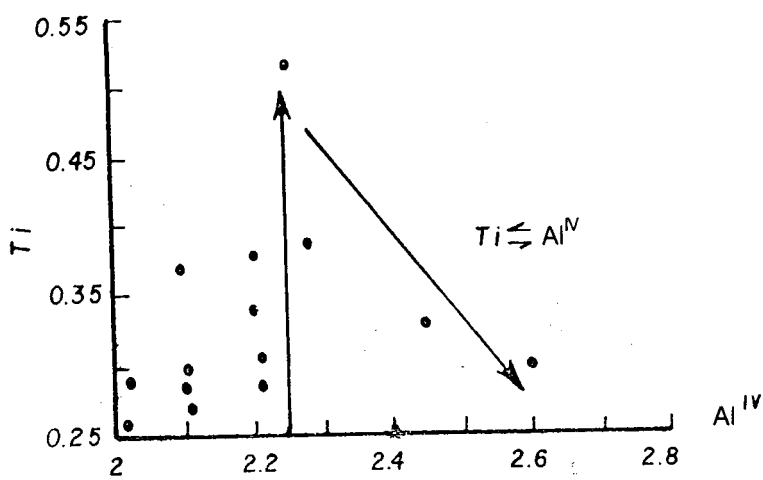

Fig. 13. Plots of Al^{IV} against Ti

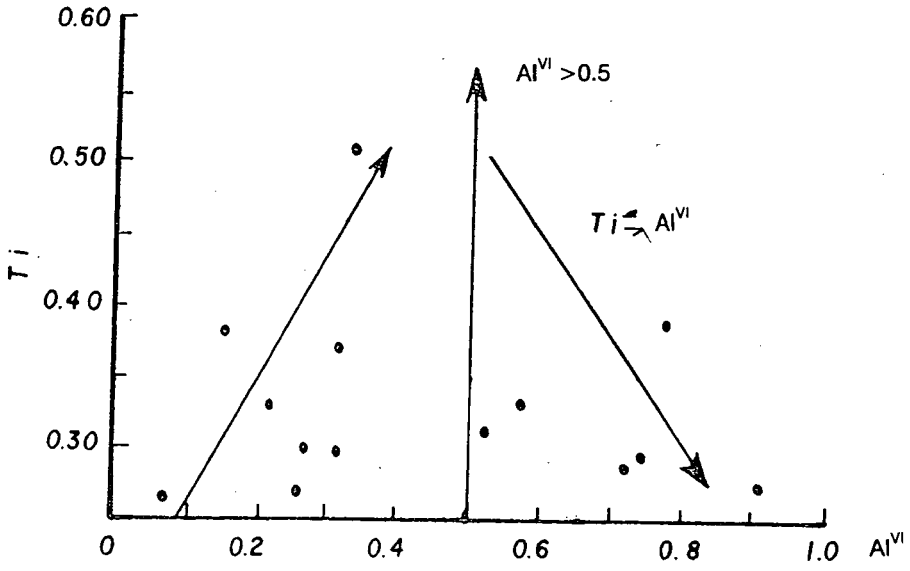

Fig. 14. Plots of Al^{VI} against Ti

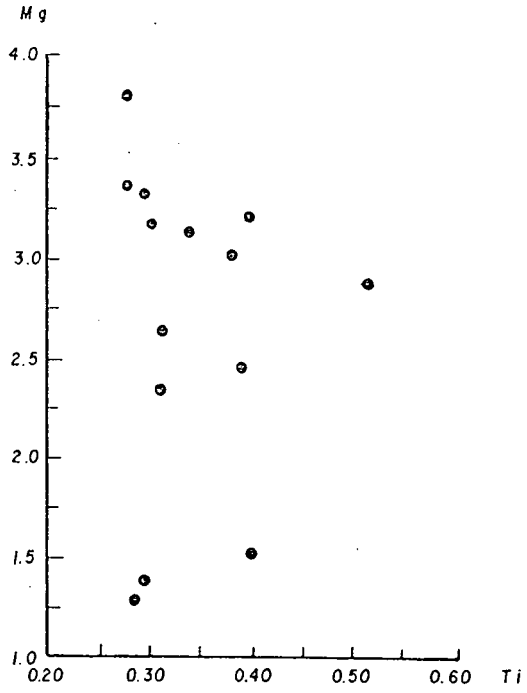

Fig. 15. Plots of Ti against Mg

BIOTITE DISCRIMINATION DIAGRAMS

Discrimination on the basis of biotite composition can be summarized as follows:

1. Discrimination FeO^t–Al_2O_3:– the FeO^t Al_2O_3 diagram (*Fig. 16*) shows that there is virtually no overlap between the 3 magmatic fields A, P, C only 3 samples plot in field P. FeO^t shows slight variation with increasing Al_2O_3 this may suggest that the substitution $2Al \rightarrow 3Fe^{2+}$ is not vital during biotite crystallization in calc alkaline magmatic systems.

2. Discrimination in MgO–Al_2O_3: – However some overlap occurs between a few biotite samples (3) in peraluminous (P) and calc-alkaline (C) rocks. Biotites which occupy fields P and C exhibit a general trend showing a gradual increase in MgO with decreasing Al_2O_3 (*Fig. 17*). This negative relation shows a substitution between Mg and Al in octahedral sites $3Mg \rightarrow Al$ within biotites in both gneous groups.

3. Discrimination in FeO^t–MgO: In this MgO–FeO^t diagram *Fig. 18* biotites plot in calc-alkaline orogenic field (C) are moderately enriched in Mg (FeO^t/MgO 1.63 on average) occupying a narrow sector (C) with an FeOt–MgO negative trend. Few biotites (3 samples) plot below that general trend within a separate field (P) this is because they are significantly depleted in Mg (wt% MgO 6.33 on average) compared with biotites in calc alkaline suite (–wt% MgO=13 on average). The well defined trend observed in (*Fig. 18*) reveals the fact that the FeOt → MgO substitution governs biotite composition in calc-alkaline (C) magmas, but it it less important for biotites in peraluminous rocks (P).

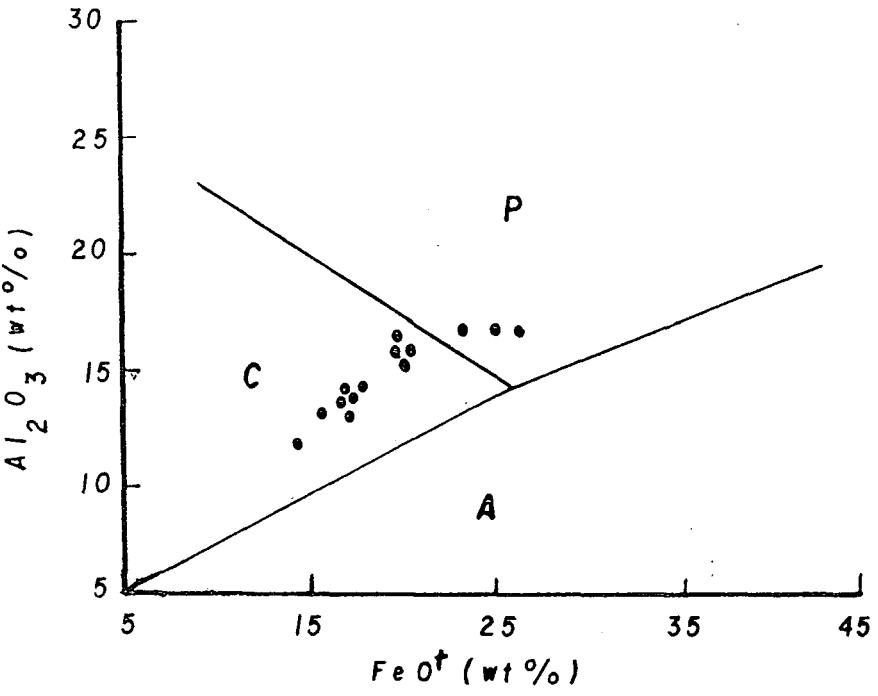

Fig. 16. FeO^t – Al_2O_3 biotite discriminant diagram (A – alkaline, P – Peraluminous, C – Calcalkaline)

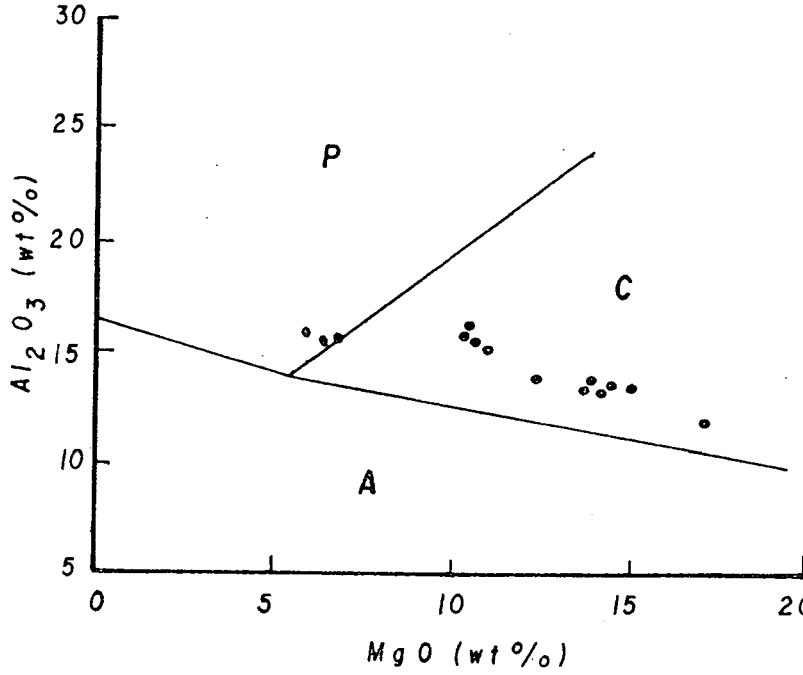

Fig. 17. MgO–Al_2O_3 biotite discriminant diagram (symbols A, P, C as in *Fig. 16.*)

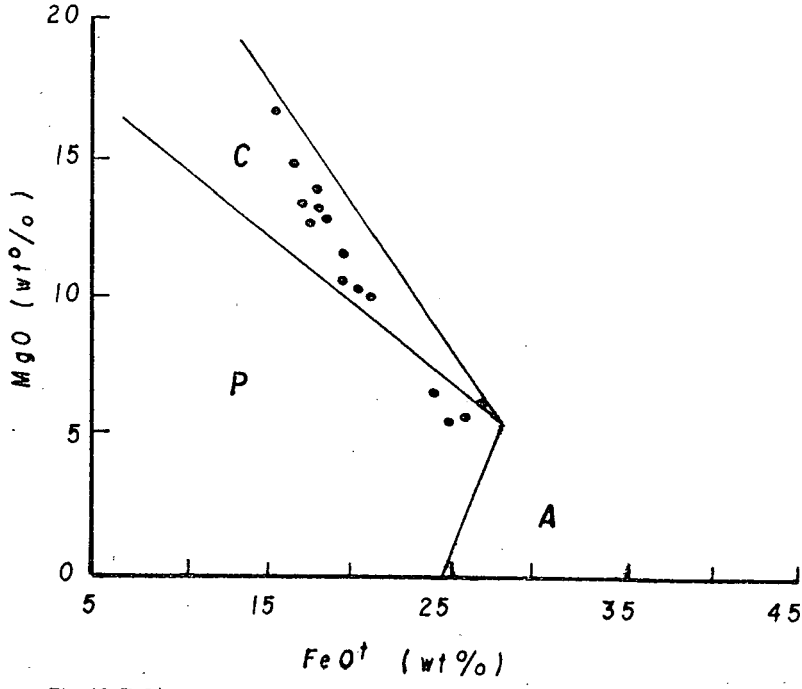

Fig. 18. FeO^t – MgO biotite discriminant diagram (symbols A, P, C as in *Fig. 16.*)

TABLE 3

Trace elements in ppm of biotites from Hajja granitoids with some localities for comparison, and some elemental ratios of the examined biotites

Sample	1	2	3	4	5	6	7	A	B	C
Sn	10	50	30	15	5	10	5	–	–	–
Ga	50	15	15	70	70	100	50	95	90	44
V	50	70	30	30	150	20	50	90	100	180
Cu	50	20	15	500	50	20	10	–	25	50
Co	20	50	20	15	70	50	30	60	40	34
Ni	30	70	20	20	10	20	5	95	25	10
Zr	50	200	500	1000	1000	1000	50	–	57	60
Sr	50	50	70	70	70	70	50	6	6	20
Ba	100	200	200	100	300	100	50	450	340	–
Pb	5	20	10	–	20	10	10	–	–	–
103 Ba/K	1.3	2.41	2.6	1.26	3.6	1,2	0.62	–	–	–
Ni/Co	1.5	1.4	1	1.3	0.1	0,4	0.15	–	–	–
103 Ni/Mg	0.39	0.81	0.24	0.24	0.1	0,22	0.06	–	–	–

A, B, C as in TABLE 1

Trace elements distribution

Some trace elements for seven samples of the examined biotites are determined and given in (Table 3), with some analyses of biotites from Egyptian granites.

Distribution of trace elements depend mainly on the presence of this element in the magmatic source from which the biotite crystallized. Many studies confirmed that enrichment of one or another element is used as indicator or pathfinder for metallogenic potentilalites, or petrogenesis of the host rocks of the biotites.

In the case of the investigated biotites, the number of samples analyzed limited the possibilities to give a good picture for the course of trace elements relations and distribution within the examined biotites. Some elemental ratios are calculated and given in (Table 3). The comparison of the trace elements values with other Egyptian biotites (KABESH et al., 1981) show that the examined biotites are similar to biotites from non mineralized pink granatic rocks. The comparison with biotites of Ras Barud (KABESH et al., 1977) shows that the present biotites have less values in the following trace elements (Ga, Cr, Ni, Ba, Sn, V) and higher values in (Cu, Zr, Sr).

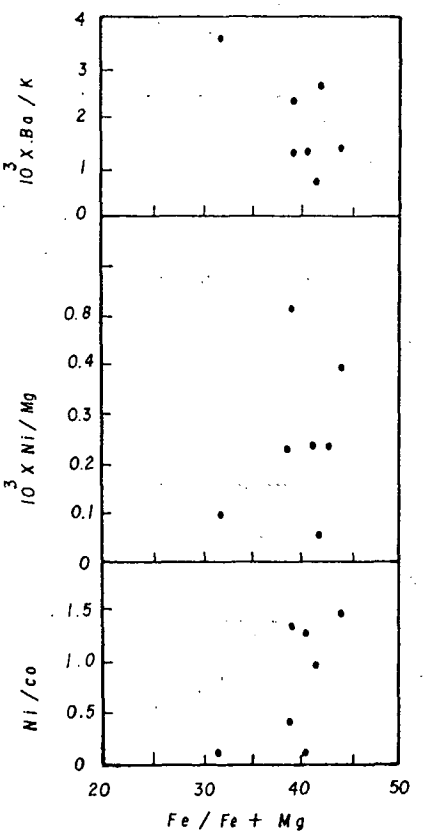

Fig. 19. Plots of Fe/Fe+Mg against some elemental ratios for biotites of Hajja granites

The ratio $FeO^t/(FeO^t+MgO)$ has been plotted against different elemental ratios such as 10^3xBa/K, 10^3 Ni/Mg, Ni/Co; (*Fig. 19*) it is clear that Ba/K ratio decrease with increasing the former value which means increasing of K content with increasing Fe total values and decreasing oxygen fugacity and temperature as well as increasing acidity of the examined biotites while the value Ni/Mg increases i.e. increasing Ni and decreasing Mg which is compatible with the previous conclusion. Ni increase may be attributed to contamination or hybridization with some basic xenolithes or magma with the granitoid magma, the same thing applies with the Ni/Co value. The value Ga $\times$ 10^3 Al is compared with some Russian studies, BARABANOF (1985) which were found to be about 6 for granodiorites; this means that the biotites of Hajja were possibly derived from magma of granodioritic composition.

REFERENCES

ABDEL-RAHMAN, A. M. (1994): Nature of Biotites from Alkaline, Calc-Alkaline, and Peraluminous Magmas. J. Petrology, **35**, Part 2, 525–541.

ABRECHT J. and HEWITT, D. A. (1988): Experimental evidence on the substitution of Ti in biotite. Amer. Mineral, **73**, 1275–1284.

AL DAHAN, A. A. QUNCHANUM, P. and MORAD, S. (1988): Chemistry of micas and chlorite in proterozoic acid metavolcanics and associated rocks from Hästefält area, Norberg ore district, central Sweden. Contrib. Mineral. Petrol. **100**, 19–34.

BARABANOF, V. F. (1985): Geochemistry, Leningrad Nedra pp 344 in Russian.

DEER, W. A., HOWIE, R. A. ZUSSMAN (1966): Introduction to Rock-Forming Minerals, Longmans, London, pp. 528.

DODGE, F. C., SMITH, V. C. and MAYS, R. E. (1969): Biotite from granatic rocks of the central Sierra Nevada Batholith, California, J. Petrology. **10**, p. **2**, 250–71.

DYMEK, R. F. (1983): Titanium, Aluminium and interlayer cation substitution in biotite from high grade gneisses, West Greenland. Amer. Mineral, **68**, 80–899.

ENGEL, A. E. J., and ENGEL, G. G. (1960): "Progressive metamorhism and granitization of the major paragenesis", Northwest Adirondack Mountains, New York. Part II, Mineralogy. Geol. Soc. Am. Bull. **71**, 1–57.

EUGSTER, H. P. and WONES, D. R. (1963): Stability relations of the ferruginous biotite, annite. J. Petrol. **3**, 82–125.

FOSTER, M. D. (1960): "Interpretation of the composition of trioctahedral micas." U. S. Geol. Surv. Prof. Pap. **354-B**, 11–49.

FOLEY, S. F. (1989): Experimental constraints on phlogopite chemistry in lamproites: 1. The effect of water activity and oxygen fugacity. Eur. J. Mineral. **1**, 411–426.

HAZEN, R. M., and WONES, D. R. (1972): Predicted and observed compositional limits of trioctahedral micas. Am. Mineral. **63**, 885–92.

HAYAMA, Y. (1959): Some consideration on the colour of biotites and its relation to metamorphism. J. Geol. Soc. Japan. **65**, 21–30.

HEINRICH, E. W. (1946): "Studies in the mica group, the biotite phlogopite series" Am. J. Sci. **244**, 836–848.

IVANOF V. S. E. (1970): On the effect of temperature and chemical activities of K in the composition of biotites of granitoids. IZV. A. N. USSR Ser. Geol. **7**, 20–30.

KABESH, M. L, ALI, M. M. (1980): The chemistry of biotites as a guide to the Petrogenesis of some Precambrian grantic rocks Yemen Arab Republic, Chem. Erde **39**, 313–324.

KABESH, M. L., HILMY, M. E., REFAAT, A. M., ABDULLAH, Z. M. (1977): Geochemistry of biotites from Ras Barud Granitic Rocks, Eastern Desert, Egypt. N. JB. Mineral. Abh. **129**, **2**, 201–210.

KENNEDY, G. C. (1955): Some aspects of the role of water in the rock melts. Spec. Geol. Soc. Amer. **62**, 498–503.

MARACUCHIEV A. A., TARARIN, I. A. (1966): Mineralogical criteria for alkalinity of granitoids, IZV. A. N. USSR,T Seria, Geol. **3**, 20–38.

NOCKOLDS, S. R. (1947): The relation between chemical composition and paragenesis in the biotite micas of igneous rocks. Am. J. Sci. **245**. 401–420.

OSBORN, E. F. (1962): Reaction series for subalkaline Igneous rocks based on different oxygen pressure conditions. Amer. Miner. **47** S, 211–226.

SALEM, A. A., KABESH, M. L., ATTAWIYA, M. Y., ALY. M. M. (1986): Petrology of Hajja Grantic Pluton, Y. A. R. Bull, NRC. Egypt. **11**, 344–357.

SMITH, G. F. (1968): Physical Geochemistry, M. Nedra (in Russian).

SOLIMAN, M. (1979): Distribution of selected elements in biotites from some Egyptian granites in relation to mineralization, Egypt. J. Geol. **23**, No. 1–2, 125–134.

WONES, D. R., EUGSTER, H. P. (1965): Stability of biotite, experimental, theory and application. Amer. Mineral. **50**, 1228–1272.

Manuscript received 15. Nov. 1994.

Acta Mineralogica-Petrographica, Szeged, XXXVI, 55–72, 1995

GEOCHEMICAL ASPECTS AND ORIGIN OF TIN-BEARING GRANITES IN THE EASTERN DESERT, EGYPT

M. A. HASSANEN*, N. A. SAAD*, O. M. KHALEFA*

Alexandria University, Geology Department

ABSTRACT

Three granitic plutons belonging to the younger granite province in the Eastern Desert of Egypt were selected for detailed petrological and geochemical studies. These granatic masses (Homr Akarem, Igla and Mueilha) are associated with Sn-W-Mo-F mineralization and selectively affected by post-magmatic albitization and greisenization processes. The granitic rocks of the three plutons have alkaline affinity with some metaluminous to moderately peraluminous character. They show pronounced enrichment in Sn, Nb, W, Rb, Y, Zr, Be, Zn and Ga coupled with moderate depletion in Ca, Mg, Fe, Ti, Sr, Ba, Eu and elemental ratios Ba/Sr and K/Rb. These chemical aspects are consistent with the metallogenetically specialized granites that elsewhere are often associated with deposits of Sn, W, Mo and rare metals. Despite the close similiarity of the studied granites with the intra-plate magmatism, yet the field occurence and many chemical features of post-collision granites are considered.

The origin of these granitic rocks is largely controlled by low-pressure crystal-melt fractionation from a source close to a within-plate magma. Although, the mineral fractionation could explain the rock chemistry, the abundances of HFS elements and HREE require the contribution of a fluorine-bearing fluid phase at a late stage of differentiation. These chemical features characterize the widespread metasomatic alteration and represent the potential economic source of Sn-W-Mo-F in the granitic rocks. The role of crustal contamination on such granites neither proved nor being exluded due to the lack of isotopic data.

Keywords: Eastern Desert, Egypt, Tin-bearing granites, Geochemistry

INTRODUCTION

During the past decade, intense geological and geochemical studies have been carried out on the main granitoid groups in the Egyptian Basement complex: the synorogenic granitoids (older granites) and the late to post-orogenic younger granites (AKAAD and EL-RAMLY 1960; EL-GABY 1975; AKAAD and NOWEIR 1980; EL-GABY et al. 1988; GREENBERG 1981). The older granites represent calc-alkaline, I-type mantle derived magmatism developed in subduction environment (HUSSEIN et al. 1982; STERN et al. 1984; DIXON 1981). Concerning the younger granites, it has been speculated that these rocks belong to the post collision granite group as a terminal phase of Pan-African orogeny. Other workers are biased to consider the younger granites as anorogenic rift-related magmatism (Stern et al. 1984). Some granitic plutons which belong to the younger granite group are commonly associated with Sn, Mo, W, F, Be and Nb-Ta mineralization (SABET and TSOGOEV 1973; SABET et al. 1973; HUSSEIN et al. 1982). They show many chemical characteristics of the specialized granites or correspond to the A-type granite (RENNO et al.

* Alexandria, Egypt

1993; MOHAMED et al. 1994). Despite the interest, these mineralized granitic plutons have recieved little attention.

This paper presents a trial to reevaluate the gheochemical data of three Sn-bearing granitic plutons that crop out in the central part of the Eastern Desert (*Fig. 1*): the Mueilha, Igla and Homr Akarem plutons. These data are used to characterize the plutons, reevaluate their genesis, and finally to elucidate the geochemical aspects of the tin-bearing granites in Egypt.

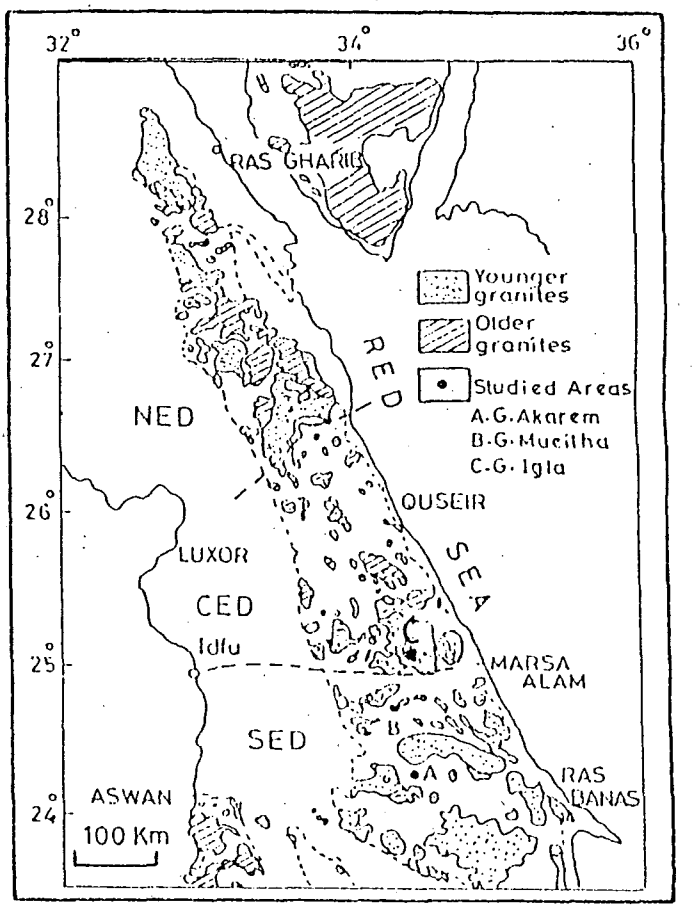

Fig. 1. Geologic map showing the distribution of older and younger granitoids in the Eastern Desert, Egypt. (After EL-RAMLY, 1972). Field circles indicate the location of (A) Homr Akarem; (B) Mueilha; (C) Igla plutons

GEOLOGICAL SETTING

Granitoid rocks constitute about 40% of the crystalline basement complex in Egypt (*Fig. 1.*). This granitic province include two major groups. The synorogenic calc alkaline intrustives (older granites) of wide compositional variation, range from quartz diorite, tonalite, granodiorite to granite. The second group comprises highly differentiated LIL-enriched alkaline granites forming shallow level intrustions of limited extension. Recent

mapping activities by the Geological Survey of Egypt (EL-RAMLY 1972) have demonstrated the homogenity of this granitic group, although local variations in mineralogy and chemistry are commonly recorded. They are now referred to as younger granites or late- and post-orogenic granites. The younger granites have Rb-Srages ranging from 662 to 430 Ma (HASHAD et al. 1972; FULLAGAR and GREENBERG 1978; MENEISY and LENZ 1982; ROGERS and GREENBERG 1981; STERN and HEDGE 1985). Some of the granitic masses of this group are mineralized and commonly affected by post magmatic alterations (eg. albitization and greisenization) and have many chemical pecularities corresponding to specialized granites (MOHAMED et al. 1994).

The three granitic plutons which are selected for the present work represent the major tin-bearing granites in the Eastern Desert. Similar to many other mineralized granites, they are spatially related to major structure trends (MOHAMED, 1993). These granitic masses intruded thick succession of highly foliated metasediments (metasiltston, slate, phyllite metagreywacke and metatuffs) and basic metavolcanics. This volcano-sedimentary sequence contains minor serpentinite and is further intruded by metagabbro-diorite complex (*Fig. 2A,B*). The emplacement of these granitic masses was diapiric resulting in sharp contacts against the enclosing country rocks with development of thin hornfelsic aureoles (1–3 m) around Homr Akarem and Mueilha. Most of the mineralized granitic plutons in the Eastern Desert are of small sizes (1–10 km^2) with isometric outlines and have oval (Mueilha), subtriangular (Homr Akarem) or rarely irregular (Igla) shapes. They are commonly located along N30°W deep-seated fracture system and at or near its intersection with block faults striking N60°E (KRS et al. 1973; GARSON and KRS 1976).

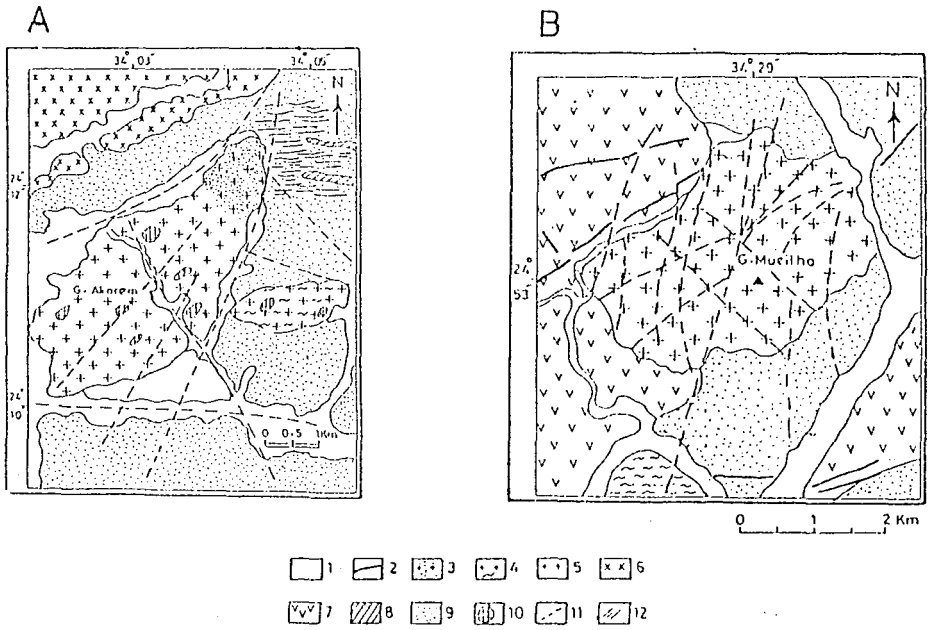

Fig. 2. Geologic maps of A, Homr Akarem and B, Mueilha granitic plutons
1. wadi deposits; 2. post-granatic dykes; 3. albitized granite; 4. greisenized granite; 5. medium-grained pink granite; 6. granodiorite; 7. basic metavolcanics; 8. metagabbro; 9. metasediments; 10. greisen pockets; 11. faults; 12. quartz veins

The studied granitic plutons are also dissected by two main sets of joints and faults trending NE-SW AND NW-SE which follow the major structure trends in the Eastern Desert of Egypt (MESHREF et al. 1980). The field relationships, such as sharp and mainly discordant intrusive contacts, and the internal isotropic fabrics, suggest that the granitic plutons were emplaced at high crustal level. The granitic rocks are locally affected by intense albitization and greisenization processes. The albitized rocks form the apical portion of the Homr Akarem pluton, the outer margin of Mueilha pluton and also occuras dykes and apophyses in Igla area. The rocks show bleached appearance, white colour with seriate to porphyritic textures. Greisens of pervasive and vein-types are erratically distributed in the granitic rocks. Greisen occurs as pockets, along fractures and often delineating the mineralized quartz veins. Some greisen pockets are mineralized and contain appreciable amounts of cassiterite as in Homr Akarem and Igla. The mineral transformation and geochemical aspects of all the metasomatic rocks associated with the mineralized granites in Egypt are treated in a further publication (HASSANEN et al. in prep.). Besides, the detailed mineralogical investigations of these area are carried out by SAAD et al. (1994).

PETROGRAPHY

The major granitoid phases and rock facies encountered in the investigated plutons include, 1) the older (synorogenic) granodiorite, 2) medium-grained pink (younger) granites and 3) metasomatites (albitized and greisenized rock facies). These rocks are briefly described as follows:

1. Granodiorite

This rock type is encountered in Homr Akarem and Igla Areas. The rock is medium grained with equigranular hypidiomorphic texture, often develop gneissose texture. The granodiorite consists of plagioclase, quartz, potash feldspar and biotite with minor hornblende. Apatite is the most common accessory besides zircon, titanite and irox oxides. Intensity of alteration is highly variable. Green chlorotized biotite, and different degrees of saussuritization are observed even within a single thin section. Plagioclase feldspar (An_{25}–An_{30}) constitutes about 38% of the rock mode. The crystals are medium-grained, polysynthetically twinned and strongly zoned with highly altered core. Potash feldspar (35% of the average rock mode) is mostly of microcline with rare perthite. Quartz usually forms anhedral interstitial crystals often display undulose extinction. Biotite occurs in subhedral fine grained pleochroic flakes (X=straw yellow; Y=brown; Z=reddish brown). Some large crystals represent a late-crystallized phase found to contain inclusions of quartz, feldspar, zircon and apatite.

2. Medium-grained pink granite

This granite type constitutes the main mass of Gabal Homr Akarem and Mueilha but has a restricted occurrence in Igla pluton. The granite outcrops are fairly uniform in appearance, consisting predominantly of medium-to coarse-grained pink biotite-(muscovite) granite. A porphyritic variety is recorded in Homr Akarem pluton with K-feldspar and quartz as common phenocrysts. The modal composition (*Fig. 3*) shows slight variation in the relative proportion of quartz and feldspar but with a higher variation in type and amount of mica. The rocks consist of K-feldspar (microline and perthite),

plagioclase, quartz, biotite and muscovite. Accessory minerals are frequently abundant including zircon, apatite, fluorite, topaz, beryl, cassiterite and ilmenite.

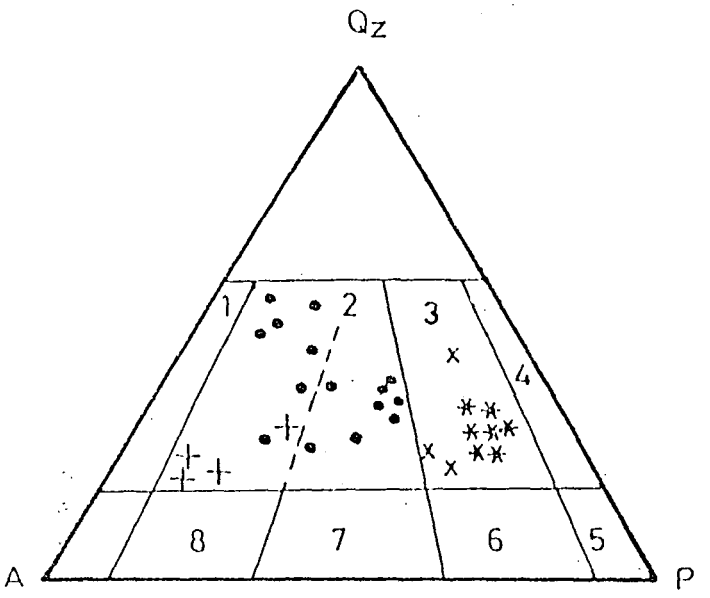

Fig. 3. Modal analysis of younger granites and metasomatized rocks plotted on the classification diagram recommended by Streckeisen (1976). Alkali feldspar granite (1); Granite (2); Granodiorite (3) and Tonalite (4)

Alkali feldspar is medium-grained represented by microline, patch and flame perthites. The crystals are clouded and turbid due to argillic-type alteration. Quartz (30.3% on the average mode) occurs in two distinct forms and sizes. The first is coarse grained (up to 2.5×1.8 mm) anhedral and display undulose extinction. The second is less abundant and occur as fine grained, undeformed crystals that paragenetically represent post-deformation recrystallization during subsolidus rock-fluid interaction. The latter process is rather effective at the apical part of the plutons particularly in Homr Akarem pluton. Plagioclase (An_{10}–An_{15}) occurs as subhedral polysynthetically twinned crystals forming on average about 24.7% of the rock mode. Some crystals are zoned and show patchy, irregular and selectively sericitized core with fresh albite rim. Biotite and minor hornblende are common mafic phases in Igla granite, while Homr Akarem granite contains biotite and muscovite. The latter is the only mica type found in Mueilha granite. The biotite crystals are subhedral, pleochroic from X, pale yellow to Y and Z reddish brown. The muscovite is also subhedral and displayserratic abundance and distribution in the different samples. Most of the muscovite crystals are secondary formed at the expense of biotite and feldspar, but few are of primary magmatic nature.

3. Albite-rich granite

Albite rich granite (albitized granite) occurs as small outcrops randomly distributed at the outer margin of the plutons (Mueilha), as apophyses (Igla) and forming the apical

portion of Homr Akarem pluton. This rock facies is fine-grained, white in colour with inequigranular to seriate texture. It is similar to their parent medium grained pink granite but with minor amounts of biotite and larger amounts of plagioclase and muscovite. The latter is mostly developed at the expense of biotite. Plagioclase is of albite composition (An_5–An_{10}) representing the most abundant constituent of the rock (57% of the average mode). The albite crystals are fine grained with subhedral prismatic form and rarely show zoning. Few crystals of anhedral form are formed as reaction rim around K-feldspar. The abundant secondary muscovite, fluorite and bleached appearance of this granitic type indicate the high rock-fluid interaction during the alteration process.

GEOCHEMISTRY

Analytical Techniques

Thirty two samples were chosen for whole-rock major and trace element analyses by full automatic energy dispersive X-ray fluorecence spectrometer. Two representative samples from Mueilha granite pluton were analysed for REE and Hf by inductively coupled plasma emission spectrometer (ICP). The analyses were performed at the Technical University of Berlin, Germany. Precisions for major elements (except REE) range from 5–10%. Sn, Be and Mo were measured by optical emission spectroscopy using d.c. are emission source. FeO and H_2O (as LOI) in the rocks were determined by the classical wet method with a precision of ±2%.

Major element characteristics

The post magmatic alteration and metasomatic processes that probably have disturbed the primary igneous signature of the rocks put some constraints when we attempt to interpret the chemistry of these rocks and their possible derivation. These processes such as albitization, greisenization and extraction of residual pegmatitic fluids will be considered in relation to mineralization process is subsequent sections. Chemical analyses of typical samples from the three granitic plutons and associated metasomatites are presented in Table 1. The samples have been classified in *Fig. 4* using the Q-P diagram of DEBON and LEFORT (1982). Most of the studied samples range from K-rich granites to adamellite while the older grey granite fall in the granodiorite field. This diagram is sensitive to feldspar alteration (e.g., alkali metasomatism) and therefore the albitized rocks are shifted to lower Q and P values. The major element chemistry of the less altered samples from the investigated granitic pluton display a restricted major element variations (SiO_2 68.32 to 76.05%) with a relatively high Al_2O_3 and total alkali contents but with a marked depletion of CaO, TiO_2, MgO and P_2O_5 (*Fig. 6., 7*). The pink granitic rocks are collectively of alkaline character (*Fig. 5A*) and comparable to the Group II alkaline. Younger granites (*Fig. 5B*) defined by ROGER and GREENBERG (1981). The albitized rocks show a noticeable enrichment in Na_2O, Al_2O_3 and SiO_2 and slight impovershment in K_2O, CaO and Fe_2O_3. The granitic rocks from Homr Akarem, Igla and Mueilha plutons are metaluminous to weakly peraluminous (*Fig. 5C*) with percent normative corundum between 0.16 and 4.58. On the variation diagrams (*Fig. 6*) the three granitic plutons have defined chemically specific compositional areas, with no direct chemical link.

The $K_2O/(Na_2O+K_2O)$ ratio of the granitic samples range from 0.38 to 0.72. This wide variation in K_2O and Na_2O concentrations within the granitic instrusions resulted from the

TABLE I

Representative major and trace element analyses of Tin-bearing granitic plutons, Eastern Desert, Egypt

	Granodiorite		Medium grained pink granite							Albitized granite			Greisens	
Sample#	A–1	A–2	M–5	M–6	M–7	A–15	A–16	I–20	I–21	M–23	A–28	A–29	M–30	A–32
SiO_2	69.50	69.55	76.05	74.25	73.86	75.03	75.02	75.53	73.50	71.84	74.90	75.07	73.10	75.65
TiO_2	0.80	0.85	0.12	0.01	0.05	Bd	0.16	0.01	0.15	Bd	0.02	0.08	0.09	0.09
Al_2O_3	14.95	14.48	13.64	13.74	13.45	14.31	12.91	11.84	14.41	15.39	14.43	12.68	14.18	14.05
Fe_2O_3	1.23	0.83	0.93	0.74	4.61	0.69	0.41	1.54	1.39	0.30	0.38	1.29	0.29	0.19
FeO	1.90	2.93	0.51	0.58	0.12	0.13	0.13	1.76	1.44	0.23	0.59	1.08	1.36	1.25
MnO	0.08	0.05	0.05	0.03	0.04	0.30	0.08	0.04	0.03	0.01	0.07	0.01	0.07	0.07
MgO	0.90	0.91	0.23	0.10	0.10	0.72	0.63	0.10	0.20	0.51	0.20	0.13	0.23	0.24
CaO	2.85	2.79	1.35	0.89	0.71	0.79	0.99	0.79	0.79	0.56	0.12	0.79	1.00	0.11
Na_2O	3.61	3.43	2.10	2.88	4.43	2.51	4.04	4.32	4.31	6.67	5.56	4.97	2.10	2.54
K_2O	2.51	1.89	3.32	5.29	4.77	3.82	3.95	2.65	2.65	3.66	1.05	4.22	5.53	5.22
P_2O_5	0.33	0.09	0.01	0.02	Bd	0.01	0.02	0.01	0.05	0.03	0.01	0.01	0.13	0.17
LOL	2.20	2.21	0.91	1.01	0.81	1.41	0.56	0.94	1.07	0.46	0.53	0.52	0.80	1.03
Total	100.86	100.01	99.22	99.54	102.95	99.72	98.90	99.53	99.99	99.66	97.86	100.85	98.88	100.61
K/K+Na*	4.61	4.43	3.10	3.88	5.43	3.51	5.04	5.32	5.31	7.67	6.56	5.97	3.10	3.54
Ba/Sr	1.82	1.40	1.44	1.20	1.41	2.25	1.63	1.32	2.08	6.00	1.31	0.73	–	–
Rb/Sr	0.29	0.30	8.78	5.70	14.19	1.88	2.46	1.17	–	9.17	3.10	1.40	–	–
K/Rb	417	201	70	154	103	151	102	149	13.47	276	40	263	–	–
Ba/Rb	6.20	4.60	0.20	0.20	0.10	1.20	0.70	1.10		0.70	0.40	0.50		
Trace elements (ppm)														
Rb	50	78	395	285	383	210	320	148	–	110	220	133	–	–
Ba	309	360	65	60	38	252	212	165	256	72	93	69	–	–
Sr	170	258	45	50	27	112	130	126	123	12	71	95	68	850
Ga	20	14	50	30	32	27	29	21	19	17	21	18	–	–
Nb	4	5	39	50	30	65	70	46	42	27	54	49	35	29
Zr	95	119	66	39	80	259	250	325	320	343	106	390	50	60
Y	11	22	29	32	156	50	45	40	39	33	12	11	75	80
Th	12	11	28	Bd	32	Bd	Bd	21	20	Bd	37	27	–	–
U	Bd	2	8	Bd	9	Bd	Bd	–	4	Bd	9	6	–	–
Sn	5	Bd	750	105	130	540	390	–	1348	780	199	74	–	–
Co	Bd	Bd	Bd	Bd	Bd	8	8	2	Bd	38	11	4	7	7
Sc	17	14	5	9	18	7	5	4	5	12	8	4	7	8
V	15	Bd	4	Bd	6	27	Bd	24	22	8	12	11	–	–
Cu	110	27	600	1100	32	168	224	28	25	343	–	112	60	110
Pb	17	16	38	2	57	15	29	7	8	42	–	66	530	120
Zn	32	50	65	50	104	–	–	78	76	430	–	35	50	50
La	50	45	33	–	39	–	–	62	59	–	46	65	–	–
Ce	40	32	19	–	18	–	–	52	48	–	34	51	–	–
Pr	4	4	2	–	3	–	–	6	7	–	6	7	–	–
Nd	16	14	12	–	14	–	–	22	20	–	25	18	–	–
Sm	5	4	5	–	4	–	–	5	6	–	4	5	–	–

Complete set of Chemical analyses is available from the authors upon request

* $K_2O/(K_2O+Na_2O)$

\# M = Mueilha A = Homr Akarem and I = Igla

– Not determined Bd: Below detection limit

amount of feldspar fractionation defined by the pronounced modal variation in potash feldspar and plagioclase. Alternatively, variable intensity of albitization, greisenization and subsolidus reequilibration of feldsparat at the late stage of consolidation could induce considerable variation in both Na_2O and K_2O contents (*Fig. 7*).

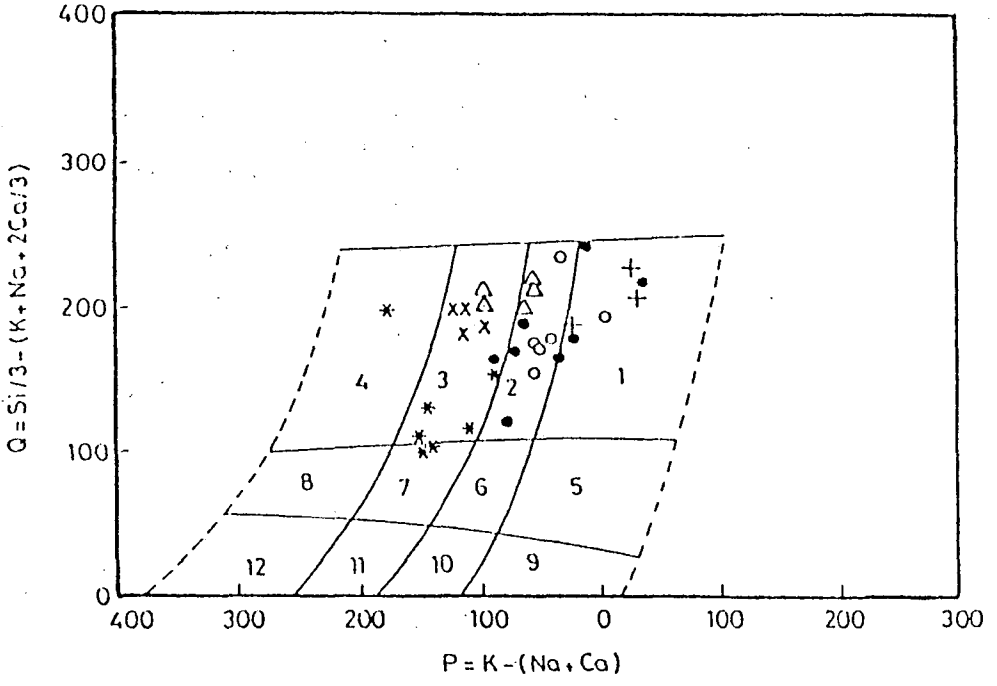

Fig. 4. Q-P diagram of DEBON and LEFORT (1986). Rock symbols are as follows
x = granodiorite; medium grained pink granite, ● = Homr Akarem; ○ = Mueilha; Δ = Igla; ✶ = albitized granite; + = greisenized granite.
1. granite; 2. adamellite; 3. granodiorite; 4. tonalite; 5. quartz syenite; 6. quartz monzonite; 7. quartz monzodiorite; 8. quartz diorite

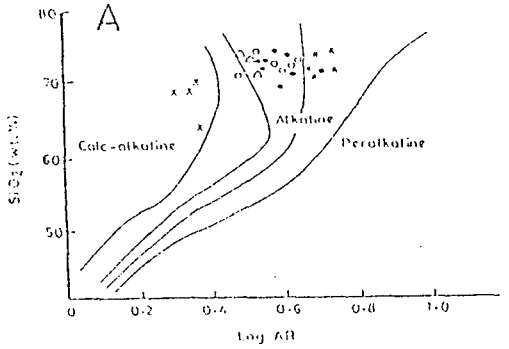

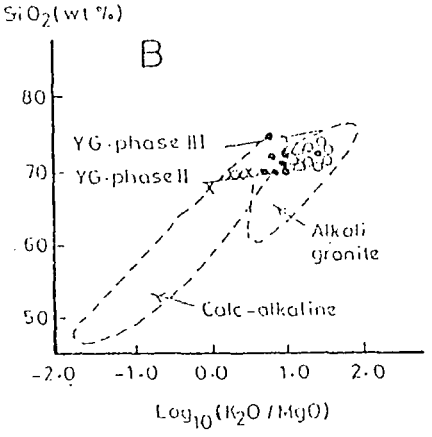

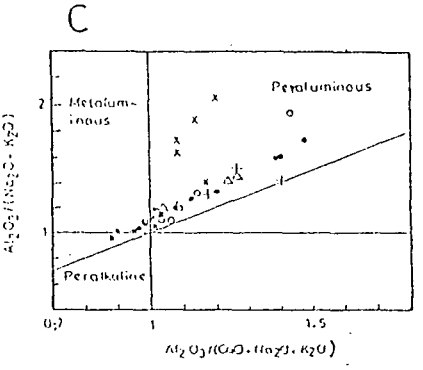

Fig. 5. Compositional variation of the granitic plutons in the SiO_2–LogAR (alkalinity ratio) (A), SiO_2–Log (K_2O/MgO) (B) and in the $Al_2O_3/(Na_2O+K_2O)$–$Al_2O_3/(CaO+Na_2O+K_2O)$. Symbols as in *Fig. 4.*

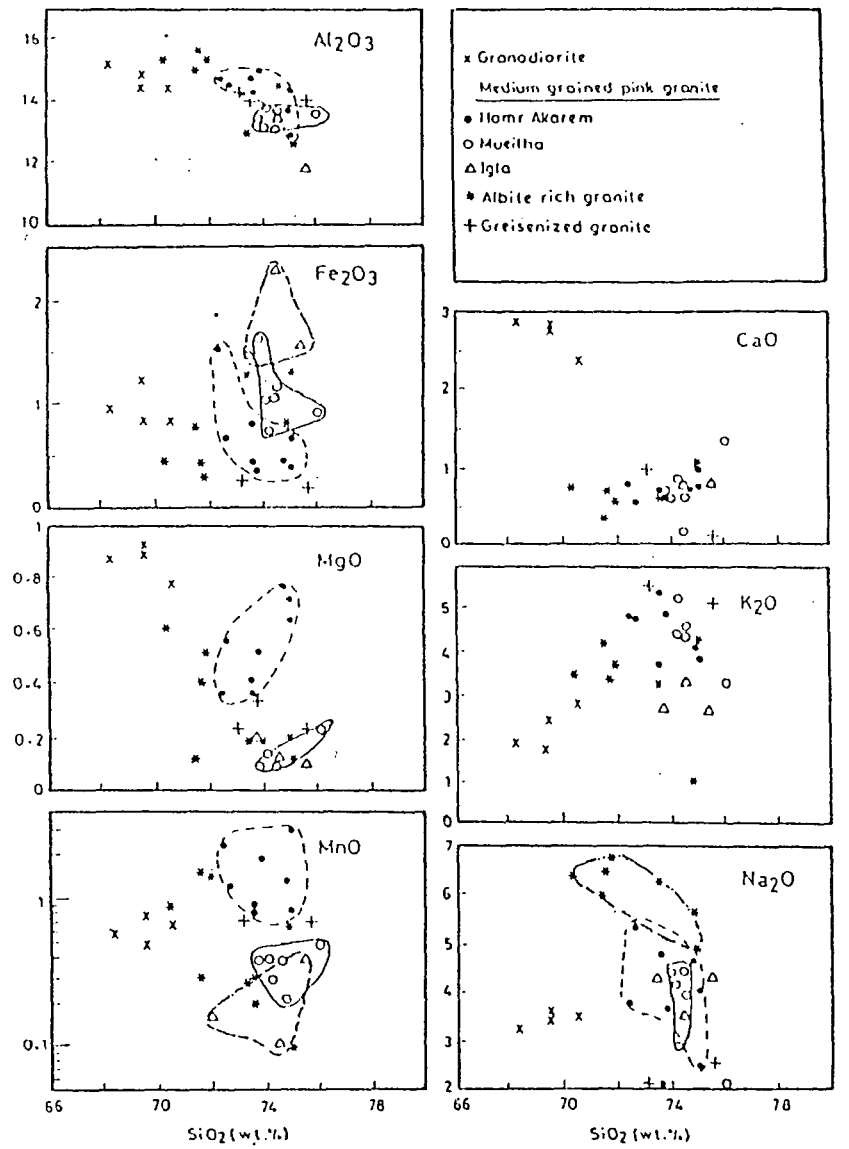

Fig. 6. Major elements versus Silica variation diagrams. Symbols as in *Fig. 4.*

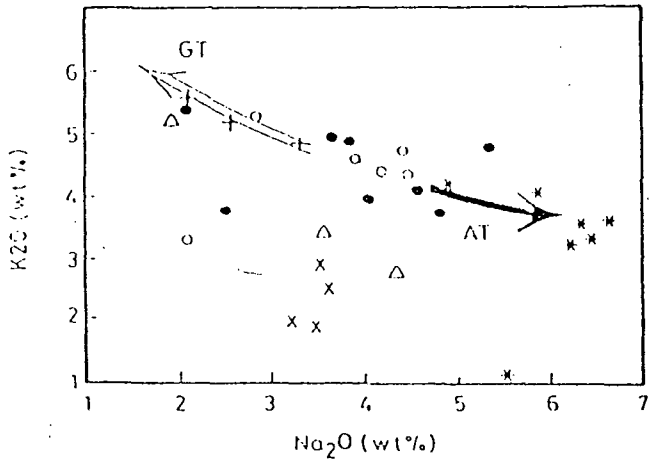

Fig. 7. Binary variation diagram of Na_2O vs. K_2O; the arrows are the optimum trends of albitization (AT) and greisenization (GT)

Trace Element variations

The granitic rocks of the studied plutons show marked and wide variations in their trace element abundances. They show noticeable enrichment in HFS elements (Zr, Y, Zn, Nb, Ga) and HREE (*Fig. 8*), as well as low contents of LIL elements. The albitized rocks are

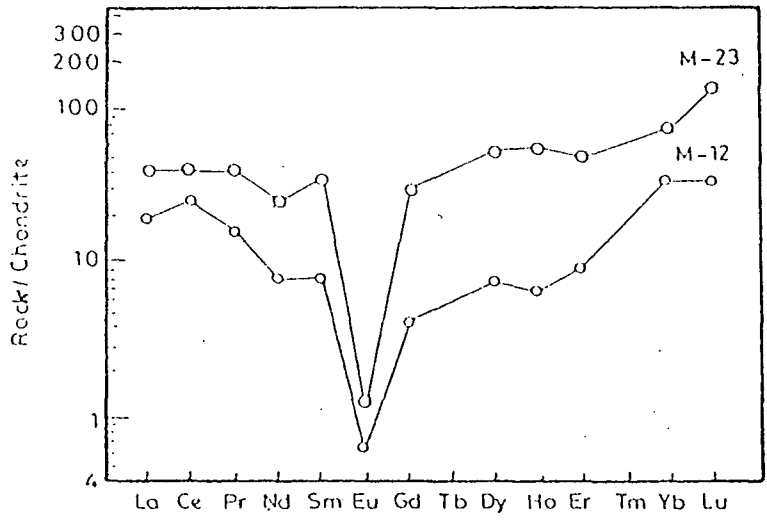

Fig. 8. Chondrite-normalized REE patterns for Mueilha medium-grained pink granite (normalized values of SUN, 1982)

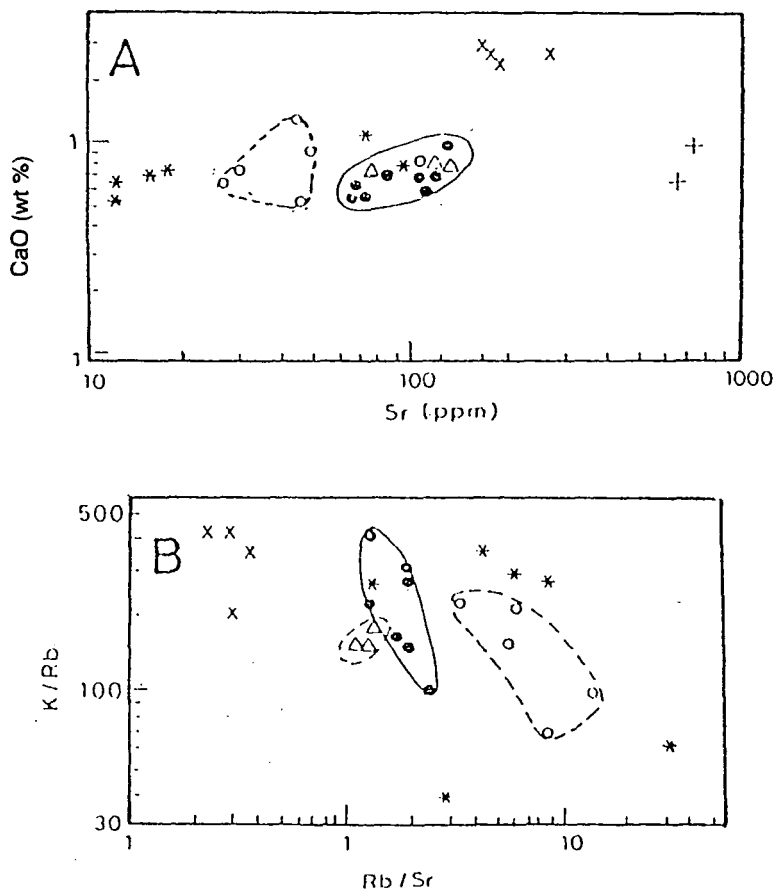

Fig. 9. Binary scatter diagram of (A) Ca vs. Sr, (B) K/Rb vs. Rb/Sr in the three granitic plutons. Symbols as in *Fig. 4.* In A and B, the pink granites of Homr Akarem, Mueilha and Igla are shown as fields outline marked by the rock symbol

still more depletion in Ba, Sr and Rb. The relatively distinct chemical characteristics of the different granitic plutons are illustrated on CaO–Sr and K/Rb–Rb/Sr plots (*Fig. 9A and B*). Each granatic pluton define a distinctive area on most diagrams with little or no evidence of common link between them.

Normalized geochemical patterns for some representative samples from each granitic pluton are shown in *Fig. 10 A–C*. The normalized factor is the hypothetical ocean ridge granite (**ORG**) of PEARCE et al. (1984). The patterns of the granitic rocks have significant enrichment in Rb and Th relative to Nb. According to PEARCE et al. (1984) such patterns can be considered crust-dominated. The patterns of Homr Akarem, Igla and Mueilha granites (*Fig. 10A–C*) resemble the collision granitic rocks (*Fig. 10D*), while on the Nb–Y and Rb–(Y+Nb) discrimination diagrams (PEARCE et al. op. cit.), most of the granitic rocks

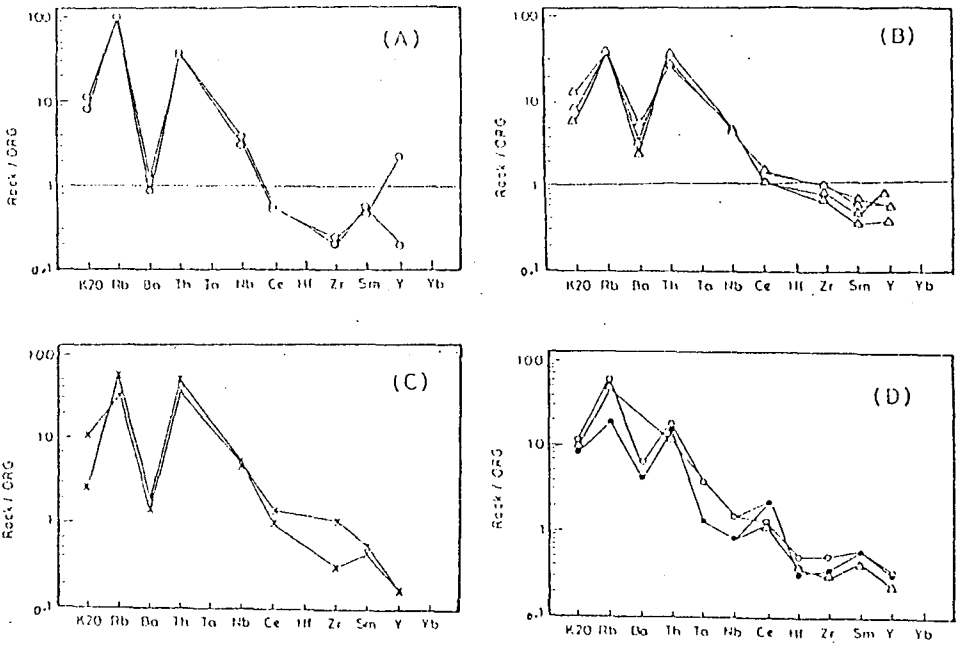

Fig. 10. Geochemical patterns for some representative samples from each granitic pluton, normalized to the oceanic ridge granite (ORG) of PEARCE et al. 1984.
A) Homr Akarem; B) Mueilha and C) Igla granites. D) granites from well-known tectonic setting (from PEARCE et al. 1984). D: ● = Sabaoka, Sudan; ○ = Skaergaard; Δ = Querigate (Pyrenees), based on data given in PEARCE et al. 1984.

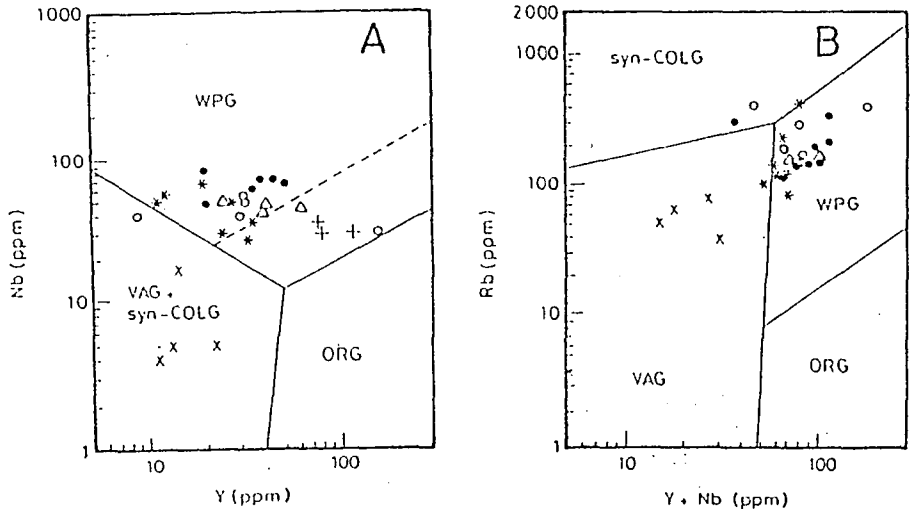

Fig. 11. (A) Nb vs. Y and (B) Rb vs. (Y+N) diagrams for tectonic interpretation of Egyptian younger granites (Field boundaries from PEARCE et al. 1984). Syn-collision granites (Syn-COLG); volcanic are granites (VAG); within-plate granites (WPG) and ocean-ridge granites (ORG). Symbols as in *Fig. 4.*

fall in the field of within-plate (**WP**) granitic rocks (*Fig. 11*). Some post-collision granites commonly plot in the **WP** field (SYLVESTER 1989) and therefore it is difficult to distinguish both post collision and syncollision from the within plate granites on these diagrams.

Lithophile element ratios and fractionation

The abundance of large ion lithophile elements (LIL) (K, Ba, Sr and Rb) in a granitic melt is largely controlled by the major phases such as plagioclase, alkali feldspar and biotite, since they have moderate to high Kd values (>1, ARTH 1976). Hence, the behaviour of these elements give qualitative assessment on the nature of the fractionating

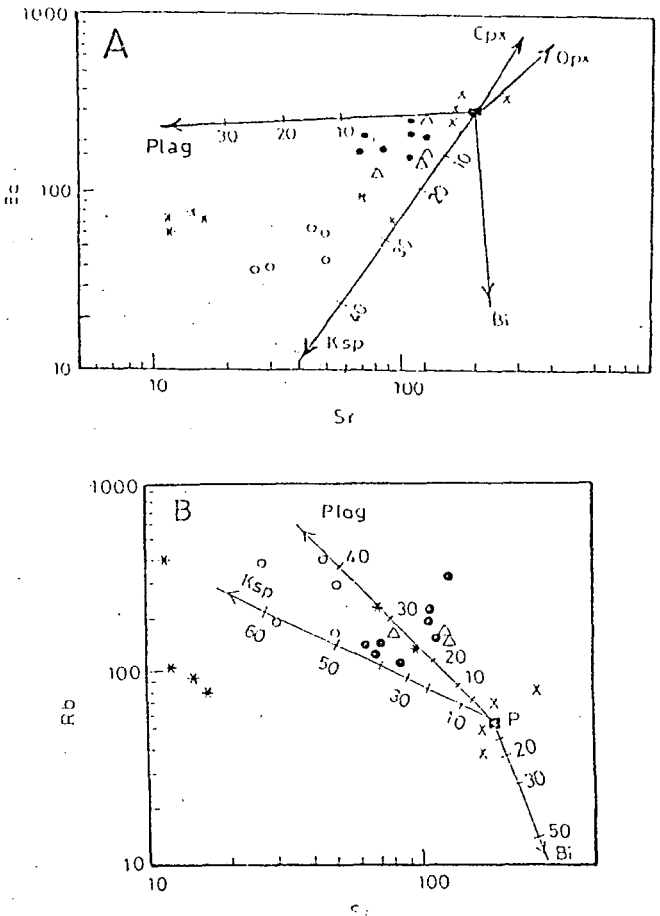

Fig. 12. Logarithmic binary scatter diagrams of (A) Ba vs. Sr and (B) Rb vs. Sr for younger granites. Symbols as in Fig. 4. Vectors denote change in melt composition due to fractional crystallization of named phases. The amount of separating phases (F) is annotated on each vector.

phases during the evolution of their parent magma. On the binary variation diagrams Ba and Rb versus Sr (*Fig. 12A and B*) and K/Rb versus Rb (*Fig. 13*), the granitic rocks show a limited variation in Ba–Sr and Rb–Sr but with vide variation in K/Rb and Rb/Sr. On these binary diagrams sets of fractionation vectors of major minerals are calculated using Ralyeigh fractionation equation ($C^1/C^0=F^{D-1}$). The average composition of granodiorite is used as a parent melt (C^0) while the distribution coefficients (Kds) are taken from published work (ARTH, 1976; HANSON 1978). The composition of the melts (C^1) at different degrees of fractionation (F) for each mineral phase are annotated as percentage on each vector (*Fig. 12A and B*). Comparing the analytical data of the studied granites with these vectors reveal that 20% and 40% separation of plagioclase and alkali feldspar respectively are required for fractionation of Homr Akarem and Igla granites. The Mueilha granite on the other hand is more fractionated (F=40–60%) than the other two granitic plutons (*Fig. 12*).

Granity type and Chemical Specialization

Some isometric granitic plutons of the younger granite province are characterised by a marked enrichment in HFS elements (Zn, Y, Nb, F, Sn, W, Mo, Rb and HREE) (RENNO et al. 1993, MOHAMED et al. 1994). Most of these granitic plutons are often associated with Sn, Mo, W, Be or Nb–Ta mineralization. The investigated granites (Homr Akarem, Igla and Mueilha) belong to this group. The trace elements characteristics of this granitic group correspond to those defined as specialized granites and follow the specialization trend in the Arabaian Shield defined by LE BEL and LAVAL (1986) (*Fig. 13*). The noticeable enrichment in HFS elements, low K/Rb and Ba/Rb are also consistent with their specialization character (TISCHENDORF 1977; MATHEIS et al. 1982; MOHAMED et al. 1994). They are also chemically equivalent to the A-type granite in the sense of WHITE and CHAPELL (1983) and COLLINS et al. (1982). The calculated Ba/Rb ratios for most of the granitic samples are generally less than 0.5. The low Ba/Rb ratio has been used by OLADE (1980) to characterize Sn-bearing from barren granites (Ba/Rb > 0.5) of Northern

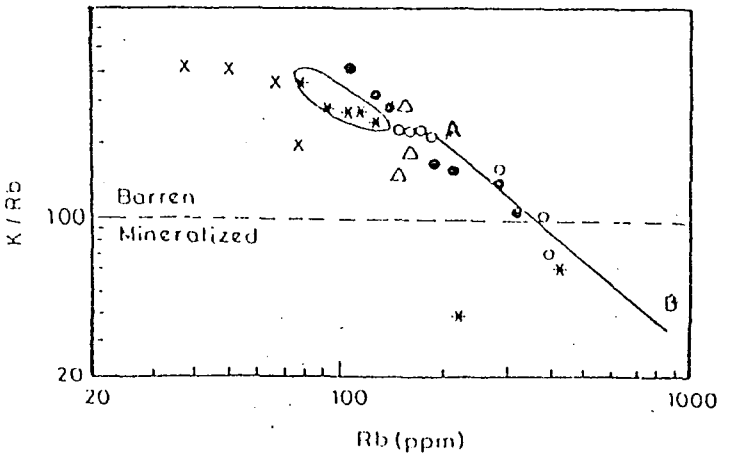

Fig. 13. K/Rb vs. Rb diagram. Heavy line AB represents the trend of specialized granites in Saudi Arabia (LEBEL and LAVAL 1986). Symbols as in *Fig. 4.*

Nigeria. The low Ba/Rb and K/Rb ratios (Table 1) of Homr Akarem and Mueilha granites confirm their chemical specialization (TISCHENDORF 1977) and are also consistent with being Sn-bearing granites. On the contrary, the high Ba/Rb (> 0.5) and K/Rb (> 100) ratios of Igla tin-bearing granite can be attributed either to the mobilization and depletion of Rb by intense post magmatic albitization or to strong fractionation of alkali feldspar and biotite. Rb is commonly accomodated in K-feldspar ($Kd^{Rb}_{k\text{-feldspar}}=0.65$) and biotite ($Kd^{Rb}_{biotite}=3.26$) which are readily altered to albite and muscovite respectively causinga low and wide Rb/Sr range (1.17–14.19), and high Ba/Rb (0.1–1.2) and K/Rb (70–154) ratios.

SUMMARY AND CONCLUSIONS

Tin-bearing granitic plutons were included among the younger granite province in the Egyptian basement complex. The granitic rocks of Homr Akarem, Igla and Mueilha plutons are coarse-grained two mica granites. These granitic masses are associated with Sn, W, Mo, Be and F mineralizations and selectively affected by post-magmatic albitization and greisenization processes. The mineralization occurs in quartz veins, stockworks, greisens and less commonly as dissemination in the host granite. The less altered samples show slight variations in petrography, mineralogy and major elements geochemistry. The altered samples have marked increase in the abundance of quartz, albite and muscovite beside the metallogenetically related minerals such as fluorite, topaz, cassiterite, molybdenite, wolframite and beryl. Unlike, the other younger granites (barren granites) the mineralized ones (Homr Akarem, Igla and Mueilha) show marked chemical pecularities such as high Rb, Zr, Y, Nb, Zn, Ga, Sn, W, Be, HREE, Ba/Rb and Rb/Sr coupled with depletion in Ca, Mg, Fe, Ti, Sr, Ba, Eu, Ba/Sr and K/Rb. These chemical aspects represent late-phase magmatic differentiation and also consistent with metallogenetically specialized granites which elsewhere are oftenly associated with deposits of Sn, Mo, W and rare metals. Greisenization and albitization are the most common alteration processes in the studied granites which can be considered as strong field evidence accompaning these types of mineralizations. Low pressure crystal-melt fractionation of plagioclase, K-feldspar and mica play significant role during the evolution of these granitic rocks. The abnormal enrichment of HFS and HREE elements require the contribution of fluorine-bearing fluid phase at the late stage of magma differentiation.

REFERENCES

AKAAD, M. K. and EL-RAMLY, M. F. (1960): Geological history and classification of the basement rocks of the Central Eastern Desert of Egypt. Geol. Surv. Egypt. No. **9**, 110–115.

AKAAD, M. K. and NOWEIR, A. M. (1980): Geology and lithostratigraphy of the Arabian Desert orogenic belt of Egypt between Lat. 25°35' and 26°30' N. In COORAY, P. G. and TAHOUN, S. A. (eds). Evolution and mineralisation of the Arabian-Nubian Shield. Inst. Appl. Geol. Jeddah, Bull. 3, Pergamon Press 4, 127–135.

ARTH, J. G. (1976): Behaviour of trace elements during magmatic processes – a summary of theoretical models and their applications. J. Res. Us. Geol. Surv. 4, 41–47.

COLLINS, W. J., BEAMS, S. D., WHITE, A. J. R. and CHAPPELL, B. W. (1982): Nature and origin of A-type granites with particular reference to the southeastern Australia. Contrib. Mineral. Petrol. **80**, 189–200.

DEBON, F. and LEFORT, P. (1986): Une classification Chimicomineralogique des roches plutoniques et applications. French translation from Ciencias da Terra (Brazil).

DIXON, T. M. (1981): Age and chemical characteristics of some Pre-Pan-Africa rocks in the Egyptian Shield. Precambrian Res., **14**, 119–133.

EL-GABY, S. (1975): Petrochemistry and geochemistry of some granites from Egypt. N. Jb. Miner. Abh., **124**, 147–189.

EL-GABY, S. List, F. K. and Tehrani, R. (1988): Geology, evolution and metallogenesis of the Pan-African belt in Egypt. In: EL-GABY, S. and GREILING, R. O. (eds.), The Pan-African Belt of Northeast Africa and Adjacent Areas. Vieweg, Wiesbaden, 17–68.

EL-RAMLY, M. F. (1972): A new geologic map for the basement rocks in the Eastern and southwestern Deserts of Egypt. Annals Geol. Surv., Egypt, **2**, 1–18.

FULLAGAR, P. D. and GREENBERG, J. K. (1978): Egyptian younger granites: a single period of plutonism? Precambrian Res., **6**, A-22.

GARSON, M. and KRS, M. (1976): Geophysical and geological evidence of the relationship of Red Sea transverse tectonics to ancient fractures. Geol. Soc. Am. Bull., **87**, 169–181.

GREENBERG, J. K. (1981): Characteristics and origin of Egyptian younger granites: Summary Geol. Soc. Am. Bull., **92**, 224–232.

HANSON, G. N. (1978): The application of trace elements to the petrogenesis of igneous rocks of granatic composition. Earth Planet. Sci. Lett. **38**, 26–43.

HASHAD, A. H., SAYYAH, T. A., EL-KHOLY, S. B. and YOUSEFF, A. (1972): Rb/Sr isotopic age determination of some basement Egyptian granites. Egypt. J. Geol., **16**, (2), 269–281.

HASSANEN, M. A., SAAD, N. A. and KHALEFA, O. M. (in prep.). Mass transfer and volume changes during greisenization and albitization of mineralized granites in Egypt.

HUSSEIN, A. A., ALI, M. M. and EL-RAMLY, M. F. (1982): A proposed new classification of the granites in Egypt. J. Vol. Geoth. Res. **14**, 187–198.

KRS, M., SOLIMAN, A. A. H. and AMIN, A. H. (1973): Geophysical phenomena over deep-seated tectonic zones in southern part of Eastern Desert of Egypt. Ann. Geol. Surv. Egypt. **3**, 125–138.

LE BEL, L. and LAVAL, M. (1986): Felsic plutonism in the Al Amar-Idsas area, Kingdom of Saudi Arabia. J. Afr. Earth Sciences, **4**, 87–98.

MATHEIS, G., EMOFURIETA, W. O. and OHIWEREI, S. F. (1982): Trace element distribution in Tin-bearing pegmatites of southwestern Nigeria. In: EVANS, A. M. (ed.), Metallization Associated with Acid Magmatism. John Wiley & Sons. 205–220.

MESHREF, W. M., ABDEL BAKI, S. H., ABDEL HADY, H. M. and SOLIMAN, S. A. (1980): Magnetic trend analysis in northern part of the Arabian-Nubian Shield and its tectonic implications. Ann. Geol. Surv. Egypt, **10**, 939–953.

MENEISY, M. Y. and LENZ, H. (1982): Isotopic ages of some Egyptian granites. Ann. Geol. Surv. Egypt, **12**, 7–14.

MOHAMED, F. H. (1993): Rare metal-bearing and barren granites, Eastern Desert of Egypt. Geochemical characterization and metallogenetic aspects. J. Afr. Earth Sci., **17**, **4**, 525–539.

MOHAMED, F. H., HASSANEN, M. A., MATHEIS, G. and SHALABY, M. H. (1994): Wadi Hawashia complex, Northern Egypt Shield: Geochemical constraints on the evolution of younger granites and related specialized rocks. J. Afr. Earth Sci., **19**, (in press).

OLADE, M. A. (1980): Geochemical characteristics of tin-bearing and tin-barren granites, Northern Nigeria, Econ. Geol., **75**, 71–82.

PEARCE, J. A., HARRIS, N. B. W. and TINDLE, A. G. (1984): Trace element discrimination diagrams for the tectonic interpretation of granatic rocks. J. Petrol., **25**, 956–983.

RENNO, A. D., SCHMIDT, W. and SHALABY, I. M. (1993): Rare-metal province, central Eastern Desert Egypt II. A-type granites of Abu Dabbab, Igla and Nuweibi. In: THORWEIHE and SCHANDELMEIER (eds.), Geoscientific research in Northeast Africa, Balkema, Rotterdam, 483–488.

ROGERS, J. J. W. and GREENBERG J. K. (1981): Trace elements in continental-margin magmatism, part 3. Alkali granites and their relationship to cratonization. Geol. Soc. Am. Bull. part I, **92**, 6–9.

SAAD, N. A., HASSANEN, M. A. and KHALEFA, O. M. (1994): Mineralogical study of quartz veins and greisens in younger granites, Eastern Desert, Egypt. Bull. Fac. Science, Alex. Univ. (in press).

SABET, A. H., CHABANENCO, V. and TSOGOEV, V. (1973): Tin-tungsten and rare-metal mineralization in the central Eastern Desert of Egypt. Ann. Geol. Surv. Egypt, III, 75–86.

SABET, A. H. and TSOGOEV, V. 1973. Problems of geological and economic evaluatoin of tantalum deposits in Apogranites during stages of prospection and exploration. Ann. Geol. Surv. Egypt, **3**, 87–107.

STERN, R. J. and HEDGE, C. E. (1985): Geochronologic and isotopic constraints on the Precambrian crustal evolution in the Eastern Desert of Egypt. Am. J. Sci., **285**, 97–127.

STERN, R. J., GOTTFRIED, D. and HEDGE, C. E. (1984): Late Precambrian rifting and crustal evolution in the Northeastern Desert of Egypt. Geology, **12**, 168–172.

STRECKSEISEN, A. (1976): To each plutonic rocks its propter name. Earth Sci. Rev. **12**, 1–33.

SUN, S. S. (1982): Chemical composition and origin of the Earth primative mantle. Geochim Cosmochim. Acta. **46**, 179–192.

SYLVESTER, P. J. (1989): Post-collisional alkaline granites. J. Geol., **97**, 261–280.
TISCHENDORF, G. (1977): Geochemical and petrographic characteristics of silicic magmatic rocks associated with rare-metal mineralisation. In: STEMPROK, M., BURNOL, L. and TISCHENDORF, G. (eds.). Metallization associated with Acid Magmatism 2, Usterdni Ustav Geologicky, Prague, 41–98.
WHITE, A. J. R. and CHAPPEL, B. W. (1983): Granitoid types and their distribution in the Lachlan Fold Belt, southeastern Australia. Geol. Soc. Am. Bull. Mem. **159**, 21–34.

Manuscript received 15. Dec. 1994.

Acta Mineralogica-Petrographica, Szeged, XXXVI, 73–87, 1995

INVESTIGATION OF MODERN GEOLOGICAL PROCESSES IN HOLOCENE LACUSTRINE CARBONATES IN THE DANUBE–TISZA INTERFLUVE (HUNGARY)

B. MOLNÁR, L. HUM and J. FÉNYES*

Dept. Geol. and Paleontology, Univ. Szeged*

ABSTRACT

In the middle part of Hungary, lacustrine carbonate mud was deposited along the Danube valley and on the morphologically slightly elevated drift sand ridge east of the Danube in the Holocene. Beside similarities, the carbonates of the two regions display significant differences, as indicated by grain size distribution, mineralogical and gheocemical analyses. The authors propose that these differences are due to different palaeoenvironmental conditions, and to effects of subsequent soil formation. Investigation of the carbonate section reveals modern geological processes in detail.

Keywords: modern geochemical processes, lacustrine carbonate, carbonate, mineralogy and geochemistry

INTRODUCTION

The Danube–Tisza Interfluve is situated in the middle part of Hungary, between the Danube and Tisza rivers. The area is 180 km long and 120 km wide.

The Danube valley was formed by tectonical and erosional processes. It lies 90 to 100 m above sea level (elevation in this study is referred to the Baltic Sea). The valley is filled principally with gravel and coarse-grained sand, and the surface is covered by silt and, in local depressions, by peat. Before regulation of the Danube by training banks in the last century, the area was a 5 to 15 km wide flood plain (*Fig. 1 and 2*).

East of the Danube valley, a drift sand ridge is situated, extending for 70 to 80 km to the east. Its elevation is 100 to 150 m above sea level. It is covered by wind-blown sand and loess. In th Holocene, the prevailing wind formed northwest–southeast running rows of dunes across the area. The crest of these dunes is often as high as 10 to 20 m above the interdunes.

To the east, the drift sand ridge is bordered by the 10 to 15 km wide valley of the Tisza river. It is about 80 m above sea level, and is filled with fluvial sand and silt.

In the depressions among the drift sand dunes and in the Danube valley there are about 100 small natron lakes. Their length varies between 100 m and 6 km. Generally the water depth is only several tens of centimetres, and does not exceed 2 m even in more rainy periods. In the dry period of the last 10 years they totally desiccated. The distribution of Holocene lacustrine deposits clearly indicates the location and number of earlier lakes (*Fig. 1.*).

The summer temperature often exceeds 30°C in the Danube–Tisza Interfluve. Therefore, the water of the shallow lakes also warms up to 30°C. The groundwater-table

* H–6701 Szeged, Egyetem u. 2–6., Hungary

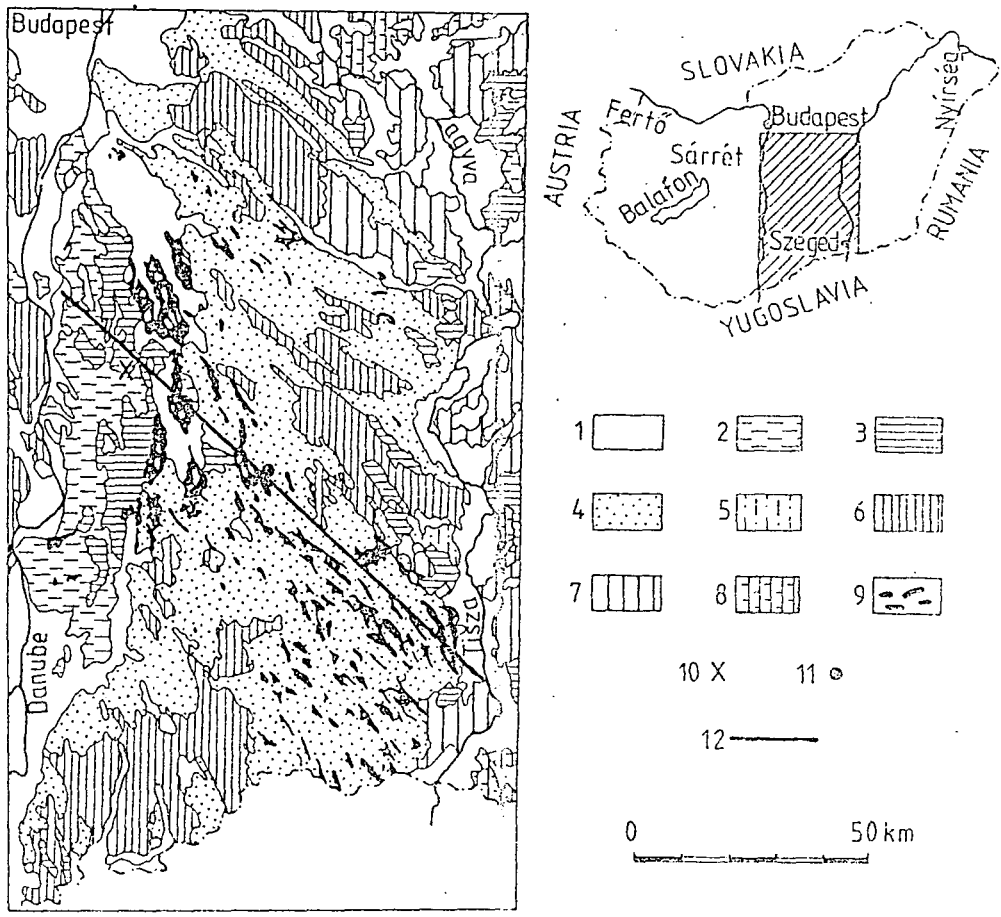

Fig. 1. Geological map of the Danube–Tisza Interfluve and the extension of the present and contemporaneous lacustrine depositional environments (carbonates). (From the map of Hungary on a scale of 1:300.000, K. BALOGH et al. 1956) 1: Alluvium, 2: Redeposited loess, 3: Sodic loess and clay, sand, 4: Wind-blown sand, 5: Loessy sand, 6: Typical loess, 7: Alluvial loess, 8: Clayey loess, 9: Lacustrine carbonate, 10: Kisrét lake, 11: Ródliszék lake, 12: Location of the model geological and geomorphological section of Fig. 2.

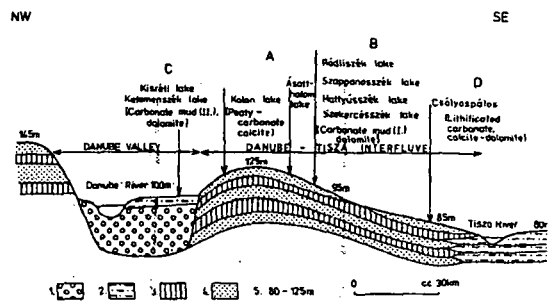

Fig. 2. Model geological and geomorphological section of the Danube–Tisza Interfluve region showing the distribution of lake types. Location of the section in Fig. 1. 1: Gravel, 2: Silt, 3: Loess, 4: Aeolian sand, 5: Elevation above sea level in metres

used to be 1 to 5 m below the surface, even coming to the surface in some depressions between the dunes. Due to the recent dry period, however, it has fallen to 3.to 8 m below the surface. Since in summer time several weeks may pass without precipitation, evaporation of the lake water is intense, and many of the lakes dry up by the end of August even in more humid periods.

The dissolved salt content of the groundwater around the lakes is as high as 500 to 2000 mg/l, in some places even 5000 mg/l. The lake water lost by evaporation is recharged primarily from groundwater, consequently, the total dissolved salt content of the lake water is high: 8000 to 70.000 mg/l. Though the dominant component is Na^+, the amount of Ca^{2+}, Mg^{2+}, and CHO_3^- is also significant. In summer the pH of the lake water is 9 to 11.

As we described elsewhere, high-Mg calcite is produced in these lakes mainly due to evaporation, and a vast portion of this carbonate turns into dolomite through early diagenetic processes (B. MOLNÁR 1980, 1990, B. MOLNÁR & SZÓNOKY 1973).

X-ray, and $\delta^{18}O$ and $\delta^{13}C$ analyses have shown that carbonate precipitation in the Danube valley took place in a different way than in the drift sand ridge (B. MOLNÁR & R. BOTZ 1994).

$\delta^{18}O_{PDB}$-values of the dolomite mud deposited in Ródliszék lake (type "B"), situated in the eastern slope of the drift sand ridge, vary between –3.45 and –0.1‰, while those of the Kisrét lake (type "C") in the Danube valley range from –5.6 to –3.5‰ (*Fig. 2. and 3.*).

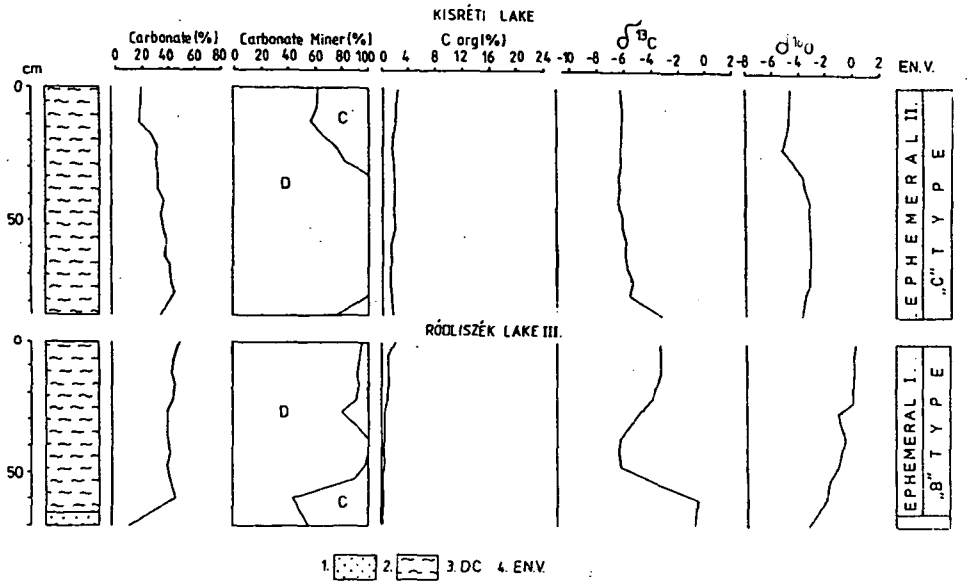

Fig. 3. Results of X-ray and isotope-geochemical analyses of the Kisrét lake and Ródliszék lake carbonate sections. 1: Aeolian sand, 2: Carbonate mud, 3: D=Dolomite, C=Calcite, 4: Depositional environment (B. MOLNÁR and R. BOTZ 1994)

We suggested that this difference is caused by different sources of recharge. Before the regulation of the Danube, lakes in the Danube valley were fed mainly by annual floods of the river. 85% of the water mass of the Danube in Hungary orginates from the Alps. $\delta^{18}O_{SMOW}$ value of the highland rainfall and melt at Vienna is –11.7‰ (D. RANK in J. DEÁK et al. 1972). In contrast, lakes in the drift sand ridge, having water supply from local rainfall and groundwater, have a $\delta^{18}O_{SMOW}$ value of –9.5‰ (J. DEÁK et al. 1992). This difference (–2.53‰ as expressed in terms of $\delta^{18}O_{PDB}$) is responsible in the first place for the –3.0 to –3.5 $\delta^{18}O_{PDB}$ disparity between lakes types "B" and "C", while other factors, like differences in isotopic composition of the local rainfall and groundwater, play a less significant role.

In geology, rock-forming processes are reconstructed from the final product. In our case, we have dolomite mud in both areas, but the generating processes and the conditions were fairly different. In our view, it is important to know these differences in detail, in order to be able to better understand genesis of fossil examples. In the Sedimentological Institute of the University of Heidelberg we had opportunity to carry out a comparative research, the results of which are discussed in this paper.

SELECTION AND SAMPLING OF THE DOLOMITE MUD SECTIONS

On the basis of earlier investigations, two carbonate sections were selected for further comparative study: the Kisrét lake section in Kiskunság National Park from the Danube valley, and the Ródliszék lake section from the drift sand ridge (*Fig. 1.*). Both sections were sampled in 5 cm intervals.

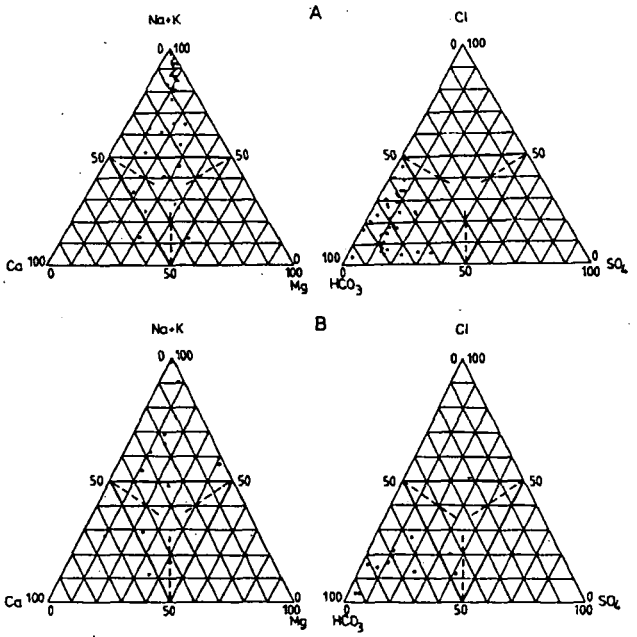

Fig. 4. Chemical components of groundwaters around natron lakes in the Danube valley (A) and in the drift sand ridge (B) (B. MOLNÁR and I. MURVAI 1975, B. MOLNÁR and L. KUTI 1978b)

Chemical composition of the groundwaters, as known from wells next to the lakes, is shown in *Fig. 4*. At the time of well drilling, in September 1974, the groundwater-table was 0.8 to 1.2 m below the surface at Kisrét lake. Its total dissolved salt content was 2000 mg/l averagely. The most important cation was sodium. Sodium was plotted together with potassium in the triangle diagram, the two averaging at 1000 mg/l. Calcium and magnesium was less, together was 10–15 mg/l. In the anions, hydrogencarbonate was dominating, while chloride and sulphate were less significant (B. MOLNÁR and L. KUTI 1978/b).

Chemical composition of groundwaters in Ródliszék area, like in the drift sand ridge in general, is more varied. Though the overall salt concentration is similar to that of the Kisrét area, the amount of sodium and potassium shows considerable scatter, while distribution of anions does not display any significant difference between the two regions (B. MOLNÁR and L. MURVAI 1975).

The Kisrét lake area is characterized by solonchak-solonetz type soils with a humus content of 0.3 to 1.75% (Gy. VÁRALLYAY 1967). Carbonate content of these alkaline soils is significant. In the B2 horizon, at about 20 to 30 cm depth, the maximum salt content of the soil is 6 to 35 mg equivalent. Due to alkalinity (pH = 9 to 10), the dissolved salt content consists mainly of sodium salts, such as Na_2Co_3 and $NaHCO_3$. Surface efflorescenses are rich in NaCl, too.

The drift sand ridge, including the Ródliszék area, is covered by various sorts of soils. Characteristic types are humic sandy soils and sandy regosoils. On lacustrine carbonates, meadow soils were formed, which in turn are replaced by solonchak-solonetz type soils in the southeastern part of the ridge (P. STEFANOVITS 1963). Consequently, changes in chemical features of the soils follow a mosaic-like pattern in the area.

RESULTS

The *Kisrét lake carbonate sequence* is underlain by slightly humic, grey, fine grained wind-blown sand. The lower part (0.75 to 1.05 m) of the carbonate section is light grey, followed by a light yellow (0.50 to 0.75 m) and another light grey (0.20 to 0.50 m) interval. The uppermost 0.2 m is slightly humic, and, consequently, darker grey again (Fig. 5. II). On the basis of hydrometrical and dry sieving analyses, characteristic grain size of the carbonate section down to 1.00 m is under 0.02 mm, that is, belongs to the clay and fine silt fractions. Minor modifications in grain size distribution are reflected by the colour of the rock. The uppermost – humic – part contains more coarse silt and sand than the directly underlying interval. Further parts relatively rich in coarse silt can be found at 0.5 m and at 0.75 to 1.00 m (*Fig. 5. III*).

The ratio of the material soluble in hydrochloric acid is 22% at the bottom of the underlying sand, and 30% at its top, i.e. right below the carbonate. Its maximum value in the carbonate section is 55%. At the interval of 0.75 to 0.85 m, being relatively abundant in fine- and coarse-grained silt, it decreases to 38 and 41%. Its low value (28%) between 0.00 and 0.20 m is probably due to the leaching effect of soil formation (*Fig. 5 IV*).

The mineralogocial composition of the carbonate was analysed by simultaneous thermoanalytical method (*Fig. 6, 7*). (We used a MOM Derivatograph Q-1500 instrument). 26% of the total carbonate was dolomite in the underlying sand (*Fig. 6. 1*). Ratio of dolomite in the total carbonate content of the 0.35 to 1.00 m interval was between 43 and 55% (*Fig. 6. 2–4, Fig. 7. 1*). In the uppermost 15 cm, its value decreases to 11 to 20%, as a consequence of soil formation. As we have pointed out above, the total portion

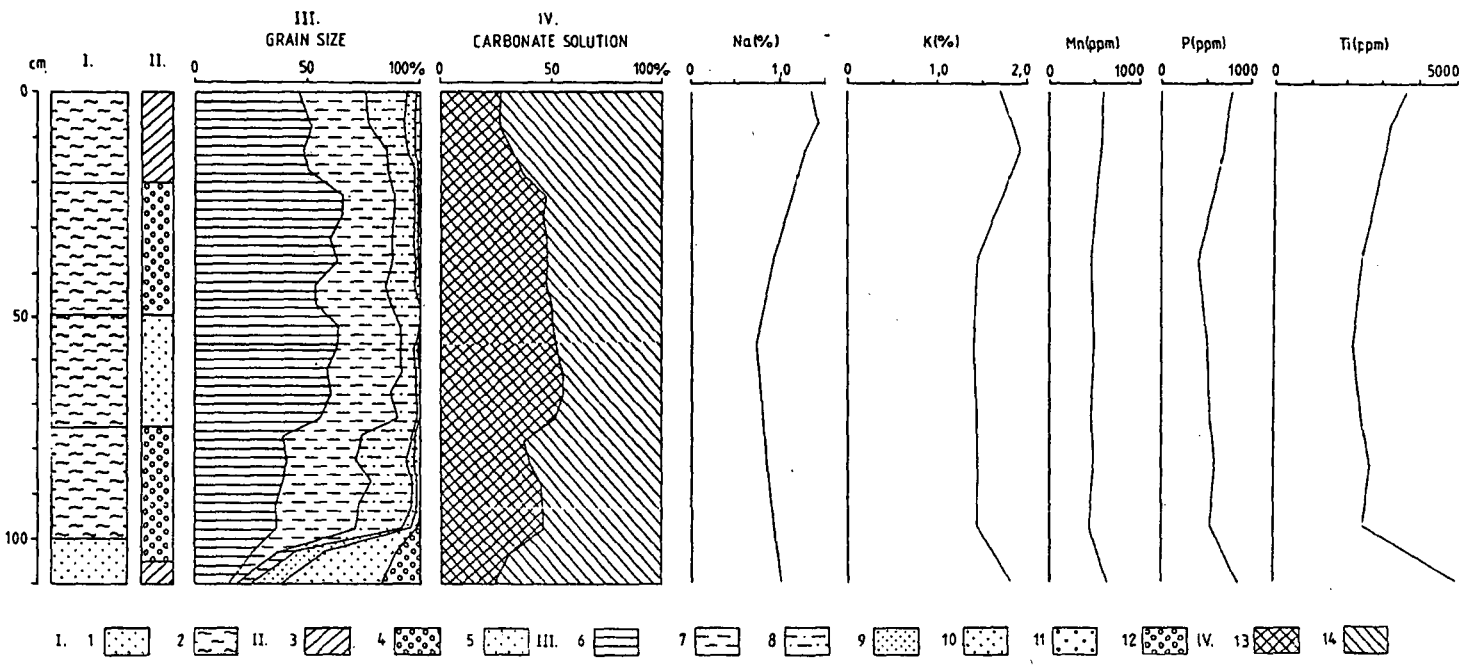

Fig. 5. Results of analyses of the Kisrét carbonate section. I. 1: Fine sand, 2: Carbonate, II. 3: Humic layers, 4: Darker grey, 5: Light grey, III. Grain size distribution, 6: Clay, 7: Fine silt, 8: Coarse silt, 9: Fine sand, 10: Small sand, 11: Medium sand, 12: Coarse sand IV. 13: Portion soluble in hydrochloride acid, 15: Portion insoluble in hydrochloride acid

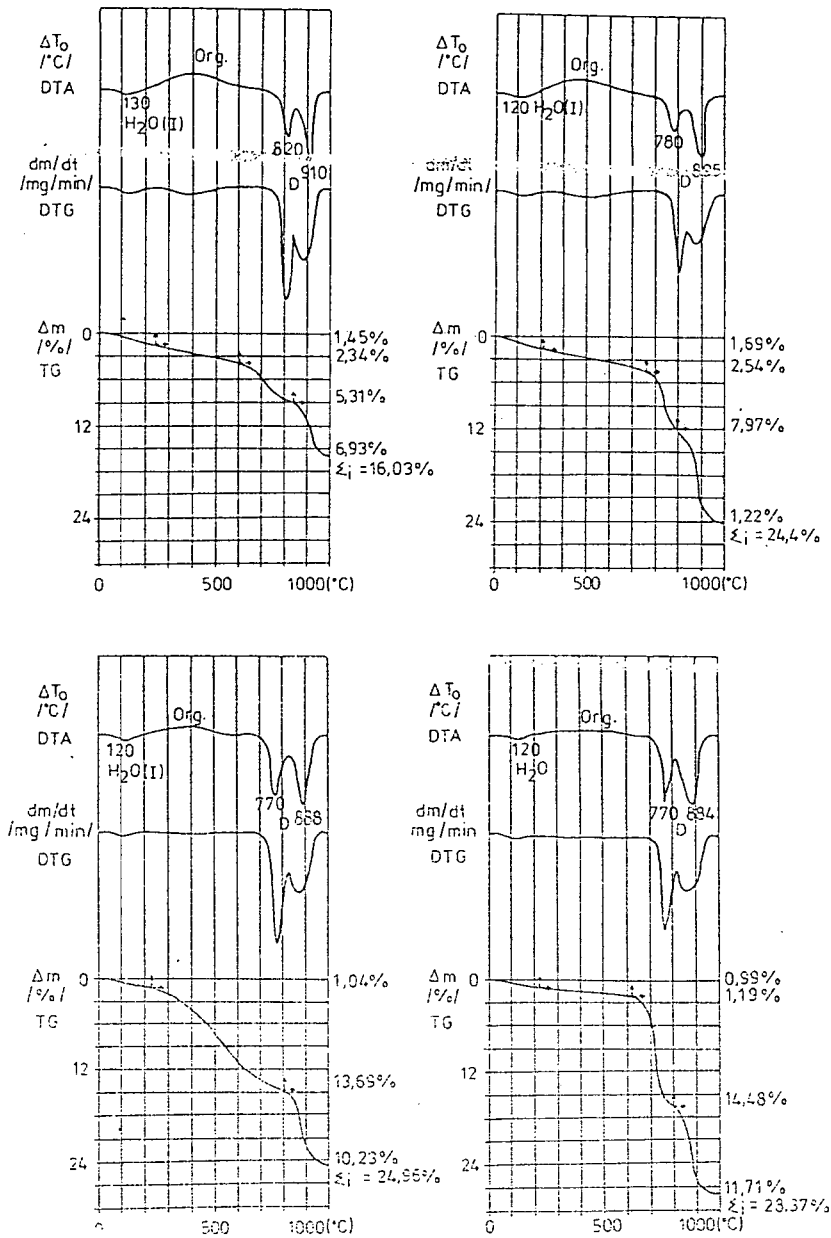

Fig. 6. Thermal analyses of the Kisrét carbonate samples. 1: 1.05–1.10 m, 2: 0.80–0.85 m, 3: 0.70–0.75 m, 4: 0.55–0.60 m. H_2O (I): adsorbed water content, Org.: Decomposition of organic material, P: pyrite, Mg: magnesite, D: dolomite, K: calcite, δ i: Total amount of material lost by reaction, expressed as percentage of the initial test material. Thermograms were determined in air, with a heating rate of 10 °C per minute. The initial amount of test material in the chindholder varied between 500 and 900 mg.

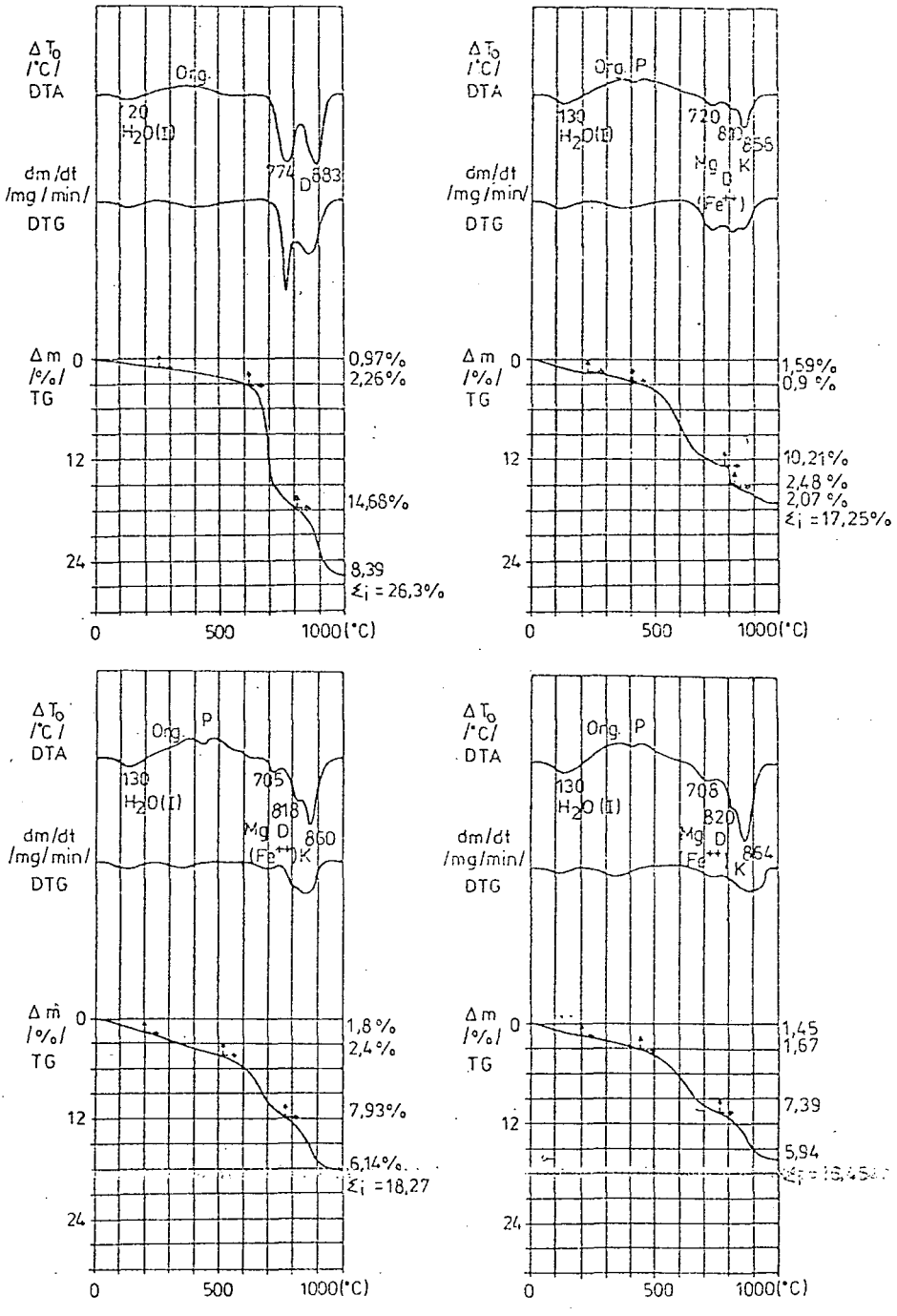

Fig. 7. Thermal analyses of the Kisrét carbonate samples. 1: 0.35–0.40 m, 2: 0.10–0.15 m, 3: 0.05–0.10 m, 4: 0.00–0.05 m. (For legend, see Fig. 6.)

soluble in hydrochloric acid, i. e. the total amount of acid soluble carbonate is also small here. Beside the dolomite-calcite double peak, an additional endothermic peak was recorded in these samples between 705 and 720 °C in the D.T.A. curve. This peak may be attributed to the presence of illite. A several percent illite content of the samples had been justified by X-ray diffraction. It is more probable, however, that the three-peak pattern indicates presence of dolomites with different state of order (B. MOLNÁR and R. BOTZ 1994) (*Fig. 7. 2–4*). Gy. SZÖÖR et al. (1992) suggested that the three peaks show synchronous presence of three phases, namely calcite, dolomite, and magnesite, and prove incorporation of Fe^{2+}. In our case, meteoric water could cause dedolomitization, and precipitation and incorporation of iron.

The Na, K and Mn content of the samples was determined by instrument Perkin Elmer 4100 AAS, while concentration of P and Ti was measured by spectrophotometer (Milton Roy Company Spectronic 1201). Characteristic changes in concentration of these elements are as follows.

The sand, underlying the carbonate section, contains 0.98% Na in feldspars. In the lower half of the carbonate section its amount decreases to 0.73%, and from 0.55 m to the surface it shows a rising trend. A sharp increase was recorded between 0.00 and 0.15 m, due to the solonchak-solonetz type of soil. Concentration of Na is as high as 1.26 to 1.37% here (the latter value belongs to the sample representing the 0.05–0.10 interval) (*Fig. 5*).

K content of the basal sand, also due to feldspars, is 1.8%. It remains steady (1.4 to 1.5%) in the interval of 0.35–1.00 m, while in the uppermost 15 cm, in the soil formation horizon, it displays an increase, similarly to the curve of Na, and reaches 1.73–1.94%.

A similar trend is shown by the concentration of Mn. It is 628 ppm in the underlying sand, varies between 439 and 497 ppm in the interval 0.35 to 1.00 m, and rises to 580 to 586 ppm in the upper 35 cm.

This trend is more pronounced in concentration of P. It is 830 ppm in the basal sand, 401 to 584 ppm in the lower two third of the carbonate section, and 692 to 772 ppm in the uppermost 15 cm.

Concentration of Ti is 5150 ppm in the sand, 2257 to 2715 ppm in the interval between 0.35 and 1.00 m, and 3135 to 3675 ppm in the interval between 0.00 and 0.15 m. Though the Ti concentration curve shows more fluctuations than the others, a basic trend common to the distribution of all these elements can be recognized.

Based on the concentration curves, the section can be subdivided to three parts: the basal sand, the 0.35 to 1.00 m interval, and the uppermost 0.35 m right below the surface.

The *Ródliszék carbonate section* is 0.6 thick, and it is also underlain by fine-grained wind-blown sand. This sand, as well as the lower half of the carbonate section, is light grey in the 0.30 to 0.80 m interval. The 0.00 to 0.30 m interval slightly humic, and darker grey (*Fig. 8 II*).

Predominant grain size in the basal sand is 0.10 to 0.20 mm. It is continuosly decreasing towards the carbonate layer. In the lowermost sample of the carbonate (0.55 to 0.60 m) the ratio of coarse silt and finer material together reaches 60%. This value falls to 38% in the overlying 0.50 to 0.55 m interval. From 0.50 m to 0.15 m the amount of finer fractions is steadily increasing, while in the uppermost 10 cm the ratio of coarse-grained silt is increasing at the expenses of the finer fractions (*Fig. 8 III*).

The ratio of the material soluble in hydrochloric acid is 18% in the basal sand, and it increases upwards. Its maximum value is 48% at the finest-grained 0.55 to 0.60 m interval. In other parts of the carbonate it changes between 36 and 44%. A slight deveease to 36% was measured right below the surface (*Fig. 8 IV*).

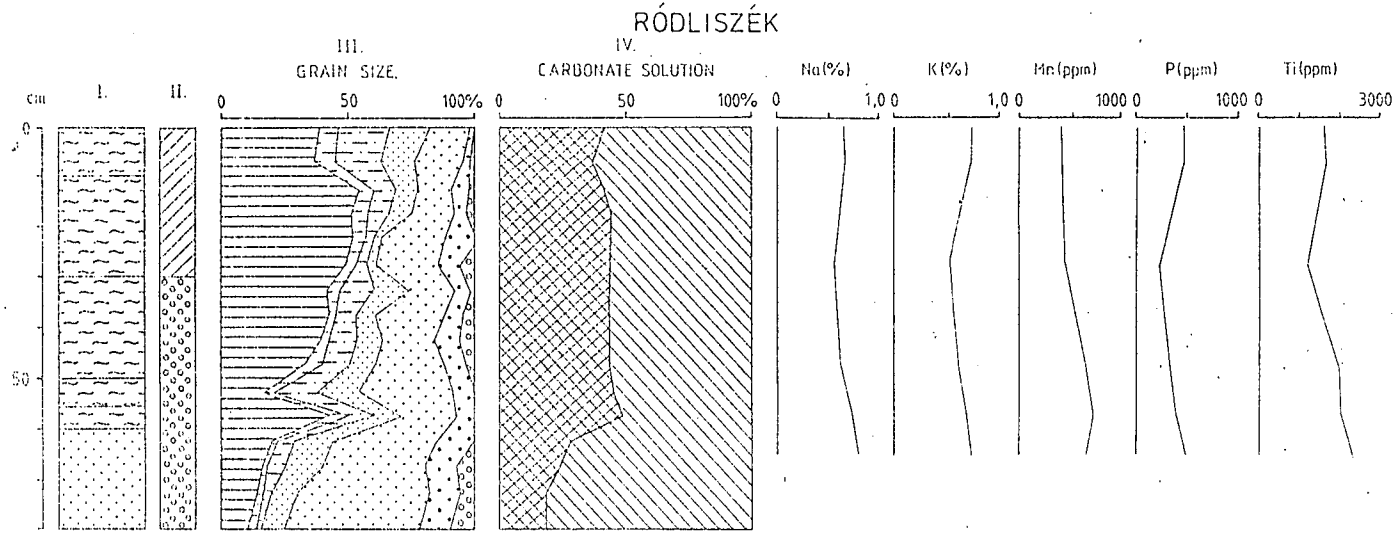

Fig. 8. Results of analyses of the Ródliszék carbonate section. For legend, see Fig. 5.

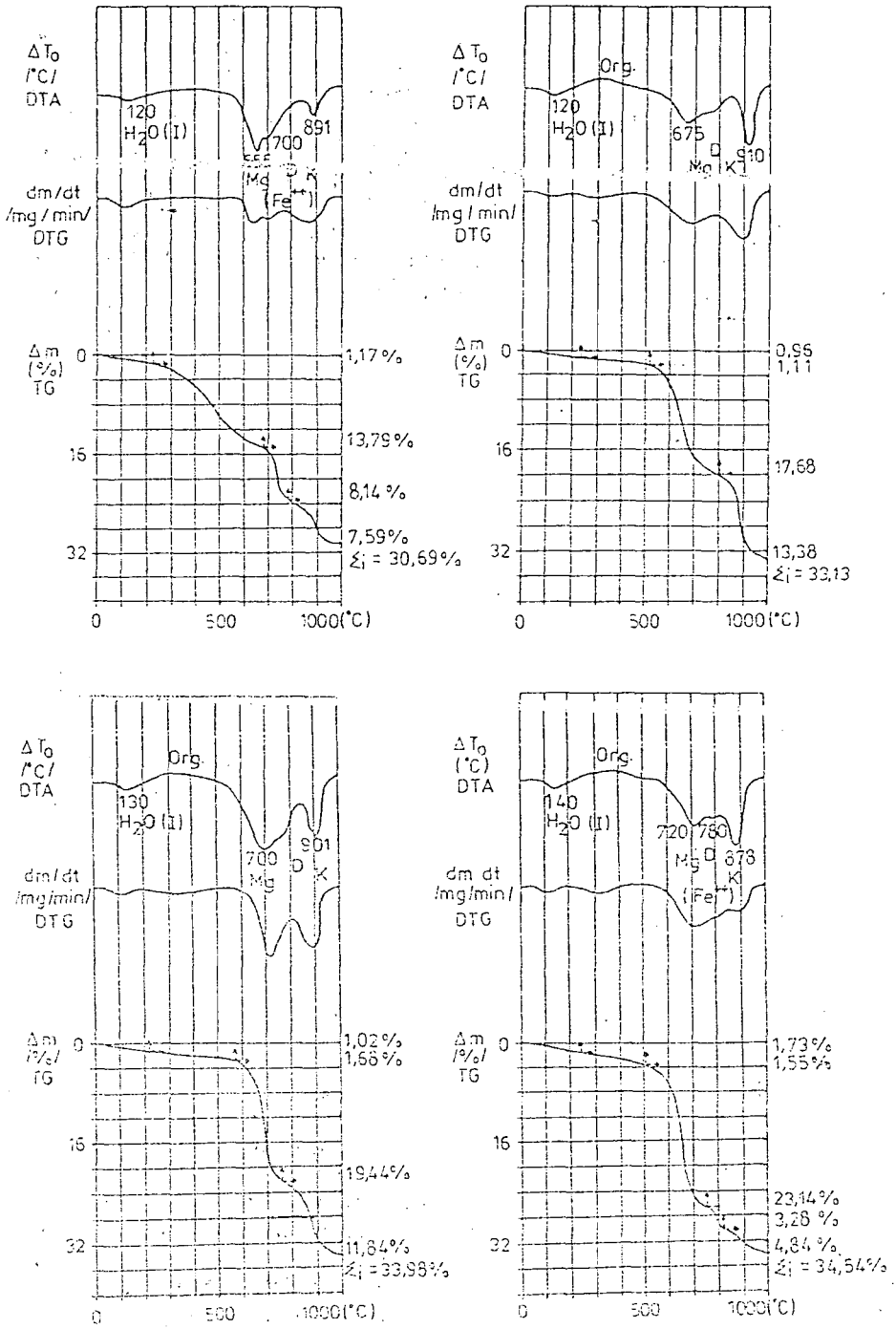

Fig. 9. Thermal analyses of the Ródliszék carbonate samples. 1: 0.60–0.65 m, 2: 0.55–0.60 m, 3: 0.45–0.50 m, 4: 0.25–0.30 m. (For legend, see Fig. 6.)

Thermal analysis of the basal sand samples indicates that its carbonate content consists of dolomite (*Fig. 9. 1*). Similar mineralogical composition was observed in the sample representing the 0.55 to 0.60 m interval of the carbonate layer (*Fig. 9. 2*). Even more definite indication of dolomite was recorded by a double dolomite peak of the D.T.A. curve in the sample from between 0.45 and 0.50 m (*Fig. 9. 3*). Similarly to the Kisrét section, the D.T.A. curve shows an additional third peak along with the calcite and dolomite peaks in samples from the uppermost 30 cm. The third peak was recorded between 693 and 720 °C. We think that this pattern, missing in the deeper parts of the section, is due to dedolomitization and consequent formation of differently ordered lattices and hybrid carbonate minerals (*Fig. 9. 4, and Fig. 10. 1–2*).

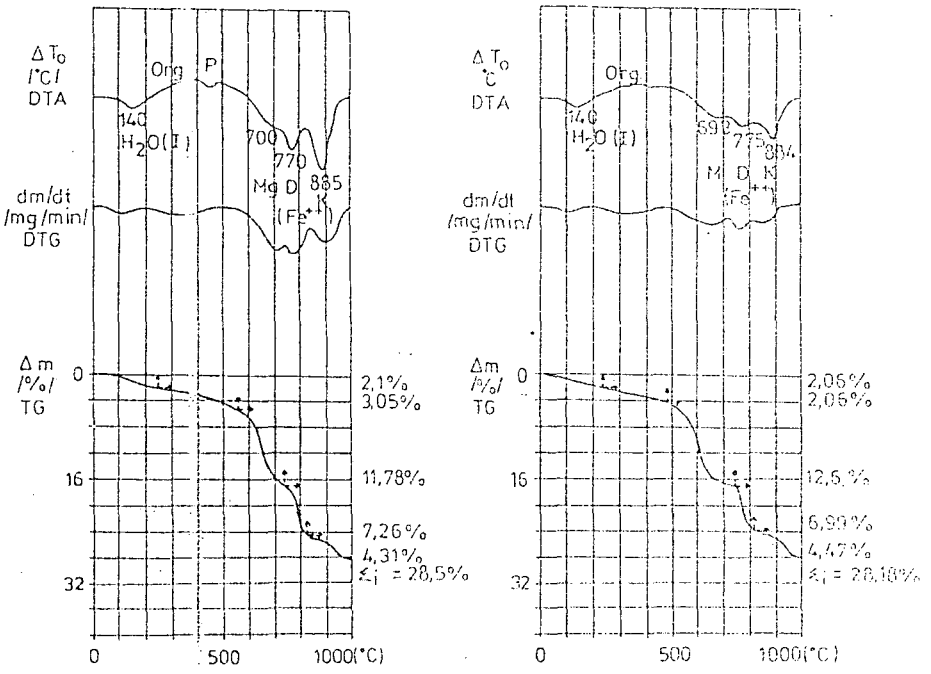

Fig. 10. Thermal analyses of the Ródliszék carbonate samples. 1: 0.05–0.10 m, 2: 0.00–0.05 m. (For legend, see Fig. 6.)

The shape of the Na content curve across the Ródliszék section is very similar to that of the Kisrét section, but the values are smaller. Na concentration in the basal sand is 0.79%. It steadily goes down to 0.55% in the 0.25 to 0.30 m sample, than continuously increases to 0.67% and 0.64% in samples 0.05 to 0.10 and 0.00 to 0.05, respectively.

The Ródliszék section, just like the Kisrét one, is more abundant in K than in Na. The differences between the concentration of the two elements, however, are less significant here. The ratio of K in the sand is 0.85%. It is steadily decreasing to 0.60% in the sample representing the 0.25 to 0.30 m interval, then increasing to 0.74% at the surface.

Mn content of the sand is 656 ppm. It has a maximum value of 716 ppm at the bottom of the carbonate layer, then it is steadily decreasing to 408 ppm at the surface. Unlike in Kisrét section, Mn concentration does not rise near the surface.

The amount of P in the basal sand is 453 ppm, in the lower part of the carbonate layer (0.45 to 0.60 m) is 337 to 395 ppm. It goes down to 227 ppm in sample 0.25 to 0.30 m, than steadily increases to 460 and 496 ppm in the 0.00 to 0.10 m interval. While in the Kisrét section the values are greater and the maximum value is in the sand, the greatest value in the Ródliszék section is recorded in the carbonate right above the sand.

Maximum concentration of Ti (2300 ppm) was observed in the sand. At the bottom of the carbonate layer it is 1977 ppm, and falls to 1195 ppm in 0.25–0.30 m of the section. From 0.25 m to the surface it increases to 1600 and 1670 ppm, In the Kisrét section the amount of Ti was much more significant, and the near-surface increase of concentration was more definite.

COMPARISON OF THE KISRÉT AND RÓDLISZÉK CARBONATE SECTIONS

Both sections are underlain by fine-grained sand. We know from earlier investigations that the Kisrét sand is mixed fluvial and aeolian sand (B. MOLNÁR and L. KUTI 1978a). The Ródliszék carbonate was deposited on wind-blown sand.

Though both sections are dominated by light colours, the Kisrét carbonate is more varied in this respect, having a light yellow interval beside the grey ones. According to earlier investigations, the light yellow colour is due to higher concentration of iron (B. MOLNÁR and R. BOTZ 1994). The near-surface part of both sections is slightly humic.

The grain size distribution is more uniform in the Kisrét section. The amount of sand increases near the surface in both sections. The overall sand content of the Ródliszék section, however, is considerably higher. It has palaeogeographical reasons: the Ródliszék area was a drift sand region even during the deposition of the carbonate, and the wind blew more sand in the lake.

Consequently, the acid soluble part of the Kisrét carbonate is greater. Soil formation is at a more advanced state in Kisrét section, thus the fine fraction of the residue insoluble in hydrochloric acid contains clay minerals, the identification of which has not been done yet.

As to mineralogical composition, the carbonate mud in the basal sand layers is dolomite. This dolomite probably satured the underlying sand layers right after its precipitation from the lake water. The carbonate section itself is also composed of dolomite. The Kisrét material has a more perfect dolimite structure, or crystallinity, than the Ródliszék material. The D.T.A. curve of the latter displays the first endothermic peak at about 675 to 700 °C, instead of the standard 780 to 810 °C. Earlier X-ray diffraction analyses of these samples, however, had unambigously proved the dolomite structure (B. MOLNÁR and R. BOTZ, 1994). This shift of the characteristic peak is due to the extremely high sodium carbonate content of the water from which the dolomite precipitated, and may be related to different crystal grain size. In contrast, the Kisrét lake, receiving the bulk of its input from the Danube, witnessed less dramatic evaporation, therefore its water was less saline, and provided more favourable conditions for crystal formation and growth. This explanation seems to be justified by results of $\delta^{18}O$ analyses; its less negative values in Ródliszék samples indicate more significant effects of evaporation (B. MOLNÁR and R. BOTZ 1994) (*Fig. 3*).

In the D.T.A curves of both sections, triple endothermic peaks were recorded instead of the characteristic double dolomite peaks in near-surface samples. This phenomenon can be a consequence of dedolomitization caused by rainwater, and formation of a secondary carbonate paragenesis with differences in state of order, grain size, and iron content.

Concentration of Na and K are higher in the Kisrét section than in the Ródliszék one. Changes in the amount of these elements follow a similar pattern. Concentration of Mn, unlike in the Ródliszék section, increases near the surface in the Kisrét sequence. Maximum values of P concentration were recorded in the basal sand in Kisrét, and in the overlying carbonate in Ródliszék. In adddition, the overall amount of P is greater in Kisrét. Minimum values of P in Kisrét were observed in the sample representing the interval 0.35 to 0.40 m, while in Ródliszék it was in 0.25 to 0.30 m. The latter sample contains not only the minimum value of P, but the less Na, K and Ti as well; these elements were probably leached from this horizon of the Ródliszék section.

In summary, despite of their different thickness, the two sections display very similar patterns. They both can be divided three correlable parts, as a consequence of nearly identical geological and genetical processes. They have differences, however, in grain size distribution, in details of carbonate association, in the hydrochloride acid soluble part, and in concentration and distribution of some elements. These differences are due to the drift sand environment of the Ródliszék lake, and to different sources of water supply; the Ródliszék lake was fed by groundwater and precipitation, while, as indicated by geochemical facies analysis, the Kisrét lake was fed primarily by the Danube, and only a much less significant amount of its water came from precipitation and groundwater.

ACKNOWLEDGEMENTS

We thank Professor G. MÜLLER, head of the Sedimentological Institute of the University of Heidelberg, and his staff, for rendering possible and supporting our work. This study was funded by OTKA project No. T 014895.

REFERENCES

BALOGH K. et. al. (1956): Magyarország 1:300 ezres földtani térképe (Geologic Map of Hungary) – MÁFI Kiadvány, Budapest.

DEÁK J.–HERTELENDI E.–SÜVEGES M.–BARKÓCZI Zs.–DÉNES Z. (1992): Parti szűrésű kutak vizének eredete trícium koncentrációjuk és oxigén izotóparányuk felhasználásával (Origin of Water in Bank-Filtered Water Supplies) – Hung. Hydrol. Soc. **72**. 4. pp. 204–210.

MOLNÁR B. (1980): Hiperszalin tavi dolomitképződés a Duna–Tisza közén (with English Summary: Hypersaline Lacustrine Dolomite Formation in the Danube–Tisza Interfluve) – Bul. of the Hung. Geol. Soc. **120**. 1. pp. 45–64.

MOLNÁR B. (1991): Moderne Lacustrine Calcite, Dolomite and Magnesite Formation in Hungary. – Publ. of the Department of Quaternary Geol. Univ. of Turku, **70**. Turun Yliopisto, pp. 1–22.

MOLNÁR B.–SZÓNOKY M. (1973): On the Origin and Geohistorical Evolution of the Natron Lakes of the Bugac Region. – Móra F. Múzeum Évk. 1. Szeged, pp. 257–270.

MOLNÁR B.–MURVAI I. (1975): Geohistorical Evolution the Natron Lakes of Fülöpháza, Kiskunság National Park, Hungary – Acta Miner.-Petrogr. Szeged, **22**. 1. pp. 73–86.

MOLNÁR B.–KUTI L. (1978a): A Kiskunsági Nemzeti Park III. sz. területén található Kisréti-, Zabszék- és Kelemenszék-tavak keletkezése és limnogeológiai története (in Hungarian with Germanian Summary: Entstehung und limnogeologische Geschichte der im Gebiet Nr. III. des Kiskunság Nationalparks befindlichen Seen Kisréti-, Zabszék- und Kelemenszék – Journ. of the Hungarian Hydr. Soc. **58**. 5. pp. 216–228.

MOLNÁR B.–KUTI L. 1978b: A Kiskunsági Nemzeti Park III. sz. területén található Kisréti-, Zabszék- és Kelemenszék-tavak környékének talajvízföldtani viszonyai (in Hungarian with Germanian Summary: Grundwassergeoligische Verhältnisse in der Umgebung des auf dem Gebietsteil Nr. III. des Kiskunság Nationalparks befindlichen Seen Kisréti-, Zabszék- und Kelemenszék) – Journ, Hungarian Hydrol. Soc. **58**. 8. pp. 347–355.

MOLNÁR B.–R. BOTZ R. 1994: Geochemical and Stable Isotope Examination of Carbonate Precipitates in Natron Lakes of the Danube–Tisza Interfluve, Hungary – Acta Geol. Hung. (in Press)
STEFANOVITS P. 1963: Magyarország talajai (Soils of Hungary) – Akadémiai Kiadó, Budapest. p. 442.
SZŐŐR Gy.– SÜMEGI P.–FÉLEGYHÁZI E. (1992): Szeged környéki sekély mélységű fúrások anyagának üledékföldtani és őslénytani vizsgálata, fáciestani és paleoökológiai értékelése (in Gy. SZŐŐR (ed.): Fáciesanalitikai, paleobiogenokémiai és paleoökológiai kutatások) – MTA Debreceni Akadémiai Bizottság Kiadványa, Debrecen. pp. 193–203. (In Hungarian)
VÁRALLYAY Gy. (1967): A dunavölgyi talajok sófelhalmozódási folyamatai (with English Summary: Salt Accumulation Processes in the Soils of the Danube Valley) –Agrokémia és Talajtan **16.** 3. pp. 327–356.

Acta Mineralogica-Petrographica, Szeged, XXXVI, 89–100, 1995

THE GEOCHEMICAL CHARACTERISTICS OF LOESSES AND PALEOSOLS IN THE SOUTH-EASTERN TRANSDANUBE (HUNGARY)

L. HUM*–J. FÉNYES*

Department of Geology and Paleontology, Attila József University*

ABSTRACT

This paper deals with a study on loesses and paleosols in the South-Eastern Transdanube. Four types of the sediments (loess, derasional loess, humic loess horizon, chernozem-like steppe soil) from the profiles of the Dunaújváros-Tápiósüly and the Mende-Basaharc loess formations were examined. Loesses can be divided into two groups (weakly weathered loess and weathered loess) on the basis of the element composition, which is also affected by paleoclimatic circumstances and weathering processes. Beside an average element composition, the weakly weathered loess is characterized by high carbonate content and low calcite-dolomito ratio. The characteristic element composition of the loesses is considerably changed during the weathering because some elements accumulate and others decrease. There is characteristically lower carbonate content in paleosols than in loesses, but they have higher calcite-dolomite ratio. The humic loess horizons have geochemically an intermediate character between loesses and paleosols. Mineral and element composition of the chernozem-like steppe soils prove that their pedogenesis was more intensive than that of the humic loess horizons.

Keywords: loess geochemistry, young loess, paleosols, carbonate content, major components, trace elements, correlations.

INTRODUCTION

On the basis of their lithologic properties, loesses of Hungary can be divided into two well-distincted groups: young loess and old loess (PÉCSI 1975, 1985, 1993). Upper part of the young loess is the "Dunaújváros-Tápiósüly subseries" (its age is cca. 12–16 ka B.P.), and the lower part of it is the "Mende-Basaharc subseries" (with an age of cca. 27–120 ka B.P.) (PÉCSI 1975, 1985, 1993).

Several exposures of the loess-paleosols series can be studied in the South-Eastern Transdanube. Loess and derasional loess of the area, which mostly contain humic loess horizons, chernozem-like steppe soil horizons and brown forest soils, can be assigned to the "young loess" series (Dunaújváros-Tápiósüly loess formation and Mende-Basaharc loess formation).

During the last decades sevaral papers have appeared on the geochemistry of loess (GONG et al. 1987, LAUTRIDOU et al. 1984, PETROV et al. 1984, SCHNETGER 1992, TAYLOR et al. 1983, WEN et al. 1985). The young loess of Hungary was studied by PÉCSI-DONÁTH (1985). Geochemical facies analysis of loess in the North-Eastern Great Hungarian Plain was performed by SZŐŐR et al. (1992a, 1992b).

* H-6722 Szeged, Egyetem u. 2–6., Hungary

During the last years 15 sections were sampled for sedimentological, geochemical and paleontological examination using fine stratigraphic methods. Samples were collected by the 25 cm or by the layer. Situation of the sampled profiles is shown by *Fig. 1.*

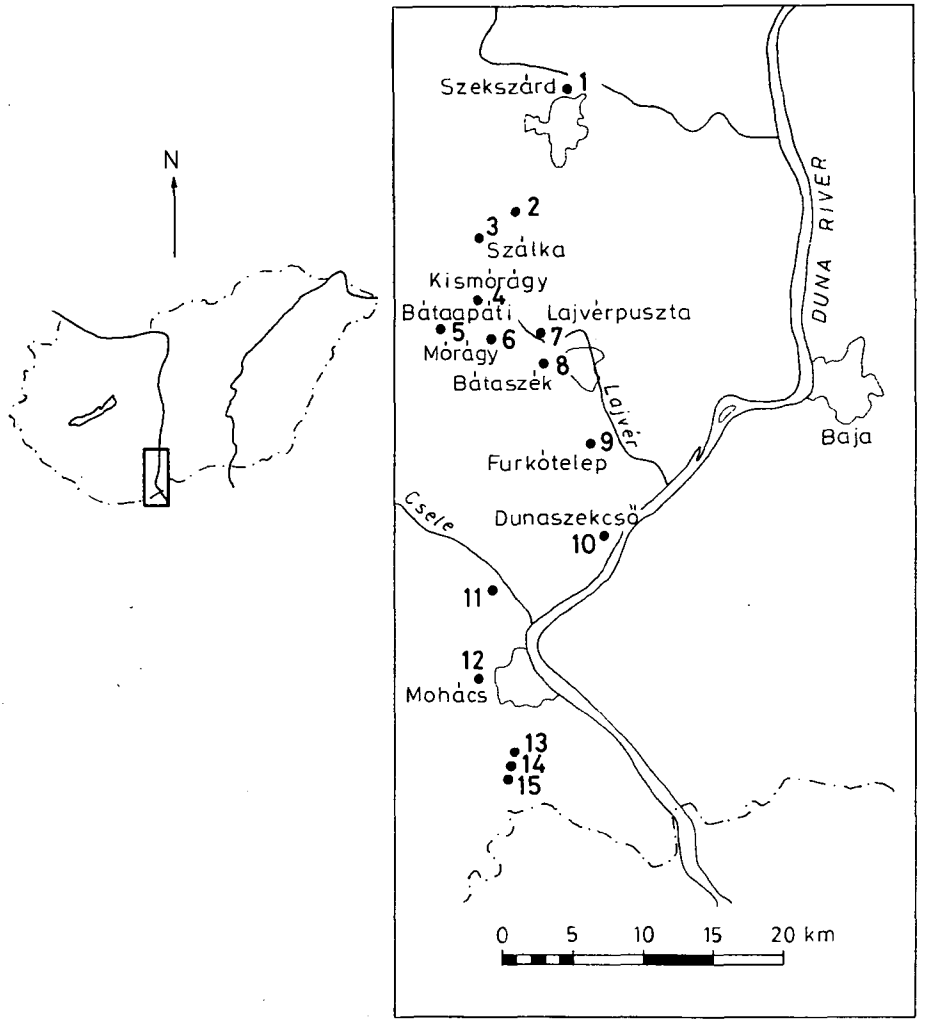

Fig. 1. Location map of the examined profiles

ANALYTICAL METHODS

After determination of grain-size distribution and carbonate content of the samples, mineral and element composition of 66 samples of loess and that of 23 samples of paleosol were examined in the grain-size fraction of less than 71 μm. X-ray measures were used for

determination of the mineral composition; in cases of 25 samples, fraction of less than 5 μm was also examined, and these were prepared with ethylene-glycol for determination of clay minerals. The calcite-dolomite ratios were determined by the method of TENNANT-BERGER (1957). Determination of carbonate and clay minerals was promoted by termoanalytical examinations. Inorganic carbon was removed with HCl, and then organic carbon content was determined by using LECO Carbon-Sulfur Determinator. For the determination of trace and major elements, destructive attack was performed by using HF-$HClO_4$-HNO_3 mixture in Teflon bomb under high pressure. Al, Fe (total), Mn, Mg, Ca, Na, K, Li, Zn and Sr were analyzed by flame AAS (Na, K and Li with emission), and Cr, Pb and Cu were analyzed by graphite-tube AAS (Perkin Elmer 4100). After HF-H_2SO_4 attack in autoclave, Fe^{2+} was measured by titration. Si was measured by RFA, while Ti and P were analyzed by spectrophotometry (using by the Tiron's and the molybdenum yellow methods). All methods are described in HEINRICHS-HERRMANN (1990).

GRAIN-SIZE DISTRIBUTION AND COLOR OF THE SEDIMENTS

Results of the examinations of the grain-size distribution can be summarized as it follows:

– Main grain-size fraction of the loesses ranges from 20 to 50 μm (43–57 weight %), ratios of the clay and the sand fraction range 11–18 and 4–14 weight %, respectively. The derasional loess has a similar grain-size distribution, but ratio of the clay fraction is a little higher (16–20 weight %).

– Because of weathering, grain-size distribution of the paleosols is characterized by quite higher ratio of the clay fraction (19–41 weight %) and lower ratio of the coarse aleurite (26–42 weight %). The chernozem-like steppe soil has the highest clay and the lowest coarse aleurite fractions.

– Grain-size distributions of the different sediments are listed in Table 1.

TABLE I

Grain-size distribution of loesses and paleosols (weight %)

	< 2 μm	2–5 μm	5–10 μm	10–20 μm	20–50 μm	50–100 μm	100–200 μm
Loess	11.2–17.4	3.2–8.1	7.2–13.1	12.5–21.7	43.1–57.4	4.1–14.6	0.2–1.1
Der. loess	16.1–20.4	4.3–5.2	7.4–13.9	11.4–15.2	45.6–49.1	6.2–8.3	0.4–1.5
Humic soil	19.5–20.3	6.4–9.1	5.4–8.2	15.3–18.1	40.3–42.5	7.5–9.3	0.9–2.4
Chern. st. soil.	22.7–43.6	2.9–8.4	10.7–14.5	10.7–14.5	24.6–38.9	5.8–9.7	0.2–2.8

Color of the sediments was determined by the ROCK-COLOR CHART in dry state. Loess samples are dusky yellow (5Y 6/4) and its darker and lighter shades, the humic loess horizon are dark yellowish brown (10Y 5/4) and color of the chernozem-like steppe soils ranges from moderate yellowish brown (10 YR 5/4) through dark yellowish brown (10 YR 4/2) to dusky yellowish brown (10 YR 2/2).

MINERAL COMPOSITION

The X-ray (*Fig. 2*) and the thermoanalytical (*Fig. 3*) measures show that loesses and paleosols dominantly consist of quartz (31,1–48,8%), feldspars (5,2–13,6%), carbonates (2,72–38,20%), micas (muscovite and biotite) and clay minerals of varying quantity (Table

2). By the X-ray diffraction examination of the fractions of less than 5 μm illite, montmorillonite (smectite), chlorite and the illite-montmorillonite mixed layers as dominant components of the clay fraction could be detected in each of the samples, while kaolinite, vermiculite, hydrobiotite and the montmorillonite-chlorite as well as the chlorite swelling mixed layers were of secondary quantity. Clay fraction of the loesses is characterized by illite and montmorillonite content with a relatively low variation, while it is characteristic for the clay fraction of the paleosols that montmorillonite (smectite) and kaolinite contents are higher than that of loesses.

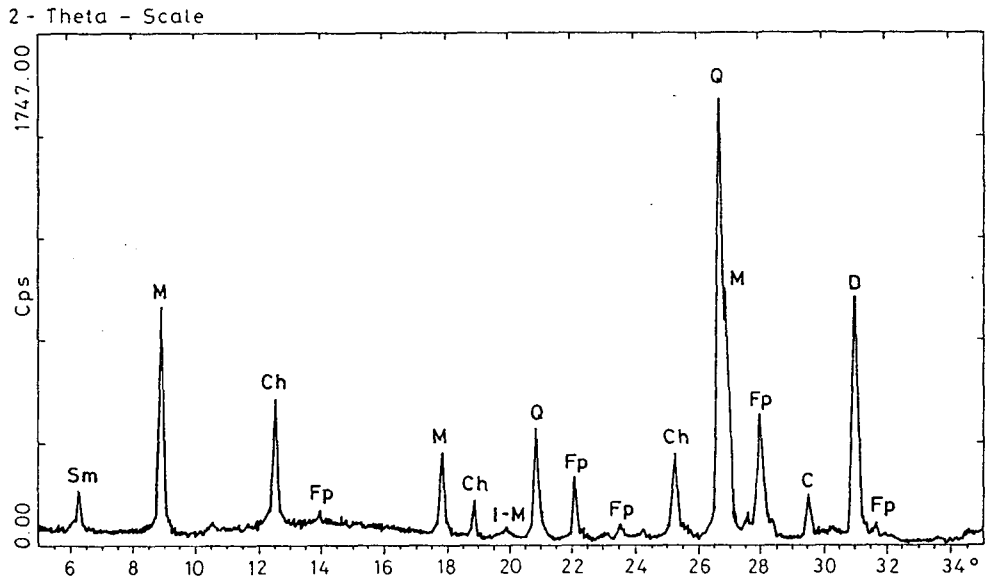

Fig. 2. X-ray curve characteristic for loess. Sample from the 0,50–0,75 m of the profile 14 (South of Mohács) Q = quartz, D = dolomite, C = calcite, Fp = feldspars, M = muscovite, Ch = chlorite, Sm = smectite, I-M = illite-montmorillonite mixed layers

Carbonate content (calcite and dolomite) of the studied loess samples is extremely high (10,7–38,2 weight %, the mean value is 24,36 weight %, the standard deviation is 6,06). According to several authors (SZILÁRD 1983, PÉCSI 1993) samples having carbonate content higher than 22 weight % can rather be considered as loessy formation (carbonate accumulating horizons), however, other authors (FÜCHTBAUER 1988, HÄDRICH 1975) consider sediments of high (as high as 30 and even 40 weight %) carbonate content as loess.

The dolomitic ratio is strikingly high within the carbonate content. According to FÜCHTBAUER (1988) dominant part of the carbonate content is calcite, and dolomite occurs only in special cases. According to international analyses (HÄDRICH 1975, PYE 1983, TAYLOR et al. 1983, SCHNETGER 1992), the calcite-dolomite ratio of the carbonate contents in samples from different places of the world ranges from 2:1 to 3:1. Ratio of the dolomite in the carbonate fraction of the 66 studied loess samples ranges from 49 to 88%, its average is 69,4% (standard deviation: 10,6), therefore the average calcite-dolomite ratio is 1:2. High dolomite content was detected for young loess of Hungary by PÉCSI-DONÁTH

(1985) and GEREI et al. (1985), as well. It can be supposed that this high dolomite content is primary, i. e., it accumulated as dust contemporaneously together with other mineral components of the loess. Average carbonate content of the derasional loess is 19,4 weight % (standard deviation is 5,54).

Paleosols have much lower carbonate content due to its leaching: humic loess horizon: 12,73 weight % (standard deviation: 4,39), chernozem-like steppe soil: 2,95 weight % (standard deviation: 0,89), but calcite has higher ratio (57–82%) than dolomite for these samples. Therefore, calcite-dolomite ratio of the paleosols ranges from 2:1 to 3:1. The higher calcite ratio of the paleosols can explained by the fact that quantity of the calcite increases because of the more solvable dolomite, which has low ordered crystal structure, leaches more rapidly. Mobility of Ca and Mg ion is influenced by pH relations, as well.

TABLE 2

Quartz, feldspar and carbonate contents of loesses and paleosols (%)

	Quartz	Feldspar	Calcite	Dolomite
Loess	31.1–48.8	9.6–13.6	3.1–16.2	7.7–30.0
Der. loess	33.7–40.7	5.2–12.7	1.8–4.5	7.1–14.9
Humic loess hor.	35.3–35.8	3.9–7.6	1.1–5.9	5.3–6.9
Chern. steppe soil	32.2–52.8	4.7–8.8	0.8–5.5	0.4–1.3

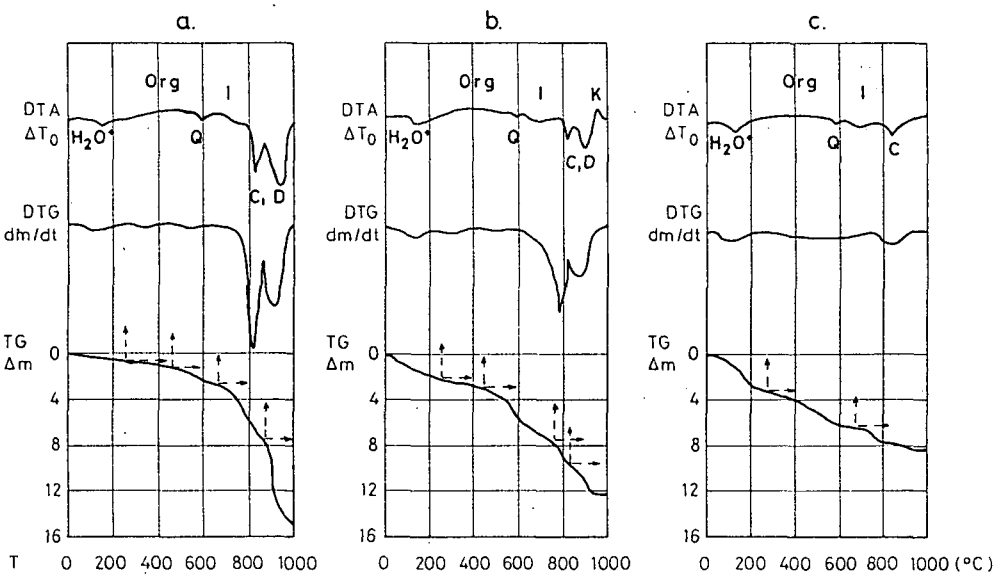

Fig. 3. Thermoanalytical analyses of different sediment types.
a: typical loess from 1,50–1,75 m of the profile 9 near Furkótelep. b: humic loess horizon from 9,00–9,25 m of the profile 10 of Dunaszekcső, c: chernozem-like steppe soil from 5,10–5,35 m of profile 1 north of Szekszárd. H_2O^+ = weakly bound water, Org = organic material, Q = quartz, I = illite, C = calcite, D = dolomite, K = kaolinite

ELEMENT COMPOSITION

Major chemical components of the studied loesses are SiO_2 (49,10–64,53%), Al_2O_3 (8,04–11,82%), CaO (7,30–14,27%), MgO (3,49–5,16%), Fe_2O_3 (2,30–3,46%), Na_2O (0,89–1,35%), K_2O (1,39–1,95%) as well as, in small quantity, TiO_2 (0,50–0,88%), P_2O_5 (0,12–0,19%) and MnO (0,058–0,088%). The organic carbont content ranged from 0,06 to 0,12%. Chemical components of the derasional loesses have same intervals. Average of the iron oxidation indexes of the loesses ($OFe=2Fe_2O_3/FeO$) is 11,03 (standard deviation is 4,64). Quantities of the trace elements are the following: Sr: 222–513 ppm, Li: 20–34 ppm, Cr: 52–86 ppm, Cu: 19–38 ppm, Zn: 44–65 ppm, Pb: 4–14 ppm. These values are correspond to the trace element composition of loess from the different localities of the world (GONG et al. 1984, LAUTRIDOU et al. 1984, PETROV et al. 1984, SCHNETGER 1992, WEN et al. 1985) and that of the Hungarian loesses which have been studied (PÉCSI-DONÁTH 1985).

In the paleosols, contents of SiO_2 (55,69–69,38%), Al_2O_3 (8,52–13,36%), TiO_2 (0,69–0,85%), Fe_2O_3 (2,33–4,12%), MnO (0,066–0,101%), Na_2O (1,01–1,65%), K_2O (1,54–2,20%), P_2O_5 (0,13–0,22%), C_{org} (0,11–0,37%) are high, while those of MgO (1,45–3,78%) and CaO (0,94–11,94%) are quite low as compared to major element contents of the loesses. Increase of the Na_2O content of the paleosols is small, and in some types (fossil soils of old loesses) its decrease can be also observed. Among trace elements of the paleosols, contents of Li (25–40 ppm), Cr (62–94 ppm), Zn (54–82 ppm) and Pb (6–26 ppm) are higher, while those of Sr (167–348 ppm) and Cu (22–27 ppm) are lower (Table 3). Iron oxidation index (O_{Fe}) of the paleosols is 20,10 (standard deviation is 12,13) as an average.

H_2O-content is ranged from1,25 to 3,26% for the loesses, from 2,45 to 3,06% for derasional loesses, from 3,66 to 4,53% from humic loess horizons, and from 4,12 to 6,50 for chernozem-like steppe soils. Distribution of the H_2O content of the different sediments shows a positive correlation with the quantity of the clay minerals.

Geochemical composition of some representative loess and paleosol samples is listed in Table 4.

During the weathering, due to their physical and chemical resistance, SiO_2 and TiO_2 accumulate in the paleosols, and accumulation of Al_2O_3, Fe_2O_3 and alkalines can also be observed. K is adsorbed on the surface of the clay minerals, and Li mainly occurs micas accumulated in soils. Quantity of the alkaline earth metals (Mg, Ca, Sr) strongly decreases in the paleosols because their carbonate minerals are dissolvable and, in this way, washed out from them. As the pedogenesis becomes more and more intensive, solution of the carbonates and accumulation of Al_2O_3 and Fe_2O_3 intensify.

On the basis of the geochemical data FeO/Fe_2O_3, CaO/MgO, $(CaO+K_2O+Na_2O)/Al_2O_3$ and K_2O/Na_2O ratios were calculated (WEN et al. 1985). FeO/Fe_2O_3 and $(CaO+K_2O+Na_2O)/Al_2O_3$ ratios decrease because of the accumulation of Fe_2O_3 and Al_2O_3 during the weathering. Mg can also link to the clay minerals accumulated during the weathering process, and, therefore, quantity of MgO decreases in a small degree. Beside CaO/MgO ratio is higher for the paleosols. Value of the K_2O/Na_2O is increased by weathering, and it reaches its maximum in the paleosols. Potassium is an important constituent of the clay minerals (illite) and can be adsorbed on the surface of the clay minerals, therefore, weathered sediments and paleosols are more rich in potassium.

On the basis of the geochemical data, the studied loesses can be divided into two groups: weakly weathered loesses and weathered loesses. The weathered loess samples are characterized by higher TiO_2, Al_2O_3, Fe_2O_3, K_2O, Li, Cr, Zn and lower CaO, Sr contents.

TABLE 3

Geochemical data of different sediment types

	Weakly weathered loess (24 samples)			Weathered loess (18 samples)		
	Limit	Average	S.D.	Limit	Average	S.D.
SiO_2 %	49.41–64.53	**57.27**	5.47	49.10–62.79	**55.80**	3.96
TiO_2 %	0.50–0.78	**0.67**	0.06	0.58–0.88	**0.73**	0.09
Al_2O_3 %	8.04–9.87	**8.81**	0.45	8.54–11.82	**10.45**	0.96
Fe_2O_3 %	2.30–3.09	**2.64**	0.19	2.64–3.46	**3.17**	0.27
FeO %	0.18–0.71	**0.49**	0.13	0.39–0.64	**0.51**	0.09
MnO %	0.062–0.086	**0.070**	0.005	0.058–0.088	**0.075**	0.009
MgO %	3.88–5.16	**4.47**	0.26	3.49–4.56	**4.01**	0.35
CaO %	9.80–17.17	**11.97**	1.81	7.30–14.27	**9.48**	2.24
Na_2O %	0.89–1.34	**1.21**	0.11	0.96–1.35	**1.27**	0.10
K_2O %	1.39–1.68	**1.52**	0.08	1.48–1.95	**1.78**	0.14
P_2O_5 %	0.12–0.18	**0.15**	0.02	0.14–0.19	**0.16**	0.01
Corg %	0.06–0.14	**0.09**	0.02	0.06–0.12	**0.09**	0.01
Li ppm	20–28	**24**	2	23–34	**29**	4
Cr ppm	52–78	**64**	6	59–86	**73**	8
Cu ppm	22–38	**28**	4	19–33	**27**	4
Zn ppm	44–54	**50**	3	53–65	**58**	4
Sr ppm	306–513	**400**	49	222–414	**324**	56
Pb ppm	4–14	**8**	2	4–9	**7**	1
	Humic loess horizon (4 samples)			Chernozem-like steppe soil (8 samples)		
	Limit	Average	S.D.	Limit	Average	S.D.
SiO_2 %	55.69–59.73	**57.94**	2.04	62.13–69.38	**64.75**	2.83
TiO_2 %	0.69–0.85	**0.80**	0.07	0.78–1.03	**0.93**	0.08
Al_2O_3 %	8.52–12.51	**11.19**	1.85	11.61–13.36	**12.50**	0.67
Fe_2O_3 %	2.33–3.42	**3.03**	0.49	3.64–4.12	**3.83**	0.19
FeO %	0.78–0.97	**0.88**	0.09	0.31–0.75	**0.51**	0.14
MnO %	0.071–0.086	**0.079**	0.06	0.066–0.101	**0.086**	0.013
MgO %	2.72–3.78	**3.34**	0.51	1.45–2.12	**1.90**	0.36
CaO %	6.21–11.94	**8.84**	2.54	0.94–6.37	**3.18**	1.98
Na_2O %	1.13–1.65	**1.42**	0.22	1.01–1.46	**1.29**	0.16
K_2O %	1.54–2.06	**1.84**	0.23	1.84–2.20	**2.03**	0.12
P_2O_5 %	0.17–0.20	**0.19**	0.01	0.13–0.22	**0.17**	0.03
Corg %	0.16–0.37	**0.24**	0.09	0.11–0.32	**0.21**	0.09
Li ppm	23–35	**32**	5	32–40	**37**	3
Cr ppm	62–93	**84**	15	85–94	**90**	3
Cu ppm	25–26	**25**	1	22–27	**25**	3
Zn ppm	54–74	**65**	9	68–82	**74**	5
Sr ppm	281–348	**310**	28	167–288	**233**	11
Pb ppm	6–9	**8**	2	9–26	**11**	6

TABLE 4

Element composition of some representative samples

Weakly weathered loess: 1. Szálka. profile 3. 1.50–1.75; 2. Dunaszekcső, profile 10, 2.40–2.65 m; Weathered loess: 3. Bátaapáti, profile 5, 1.75–2.00 m; 4. Mohács, profile 11, 1.50–1.75 m; Humic loess horizon: 5. Dunaszekcső, profile 10, 7.25–7.50 m; 6. Dunaszekcső, profile 10, 9.25–9.50 m; Chernozem-like steppe soil: 7. Szekszárd, profile 1, 5.10–5.35 m; 8. Mohács, profile 12, 2.85–3.15 m

	1.	2.	3.	4.	5.	6.	7.	8.
SiO_2 %	51,17	52,20	55,20	55,17	56,74	55,69	63,62	63,62
TiO_2 %	0,67	0,69	0,75	0,65	0,82	0,85	0,85	0,92
Al_2O_3 %	8,59	8,87	10,30	9,89	12,33	11,41	11,97	13,36
Fe_2O_3 %	2,70	2,52	3,04	3,04	3,26	3,11	3,73	4,12
FeO %	0,44	0,61	0,51	0,44	0,97	0,83	0,50	0,59
MnO %	0,072	0,070	0,077	0,062	0,079	0,078	0,070	0,093
MgO %	4,56	4,64	4,09	4,22	3,78	2,72	2,16	2,12
CaO %	12,52	12,25	9,30	10,10	7,43	9,78	4,35	3,00
Na_2O %	1,13	1,25	1,35	1,29	1,65	1,38	1,38	1,41
K_2O %	1,49	1,53	1,88	1,68	2,06	1,78	1,99	2,20
P_2O_5 %	0,16	0,13	0,18	0,18	0,18	0,17	0,17	0,14
Corg %	0,10	0,09	0,10	0,09	0,16	0,24	0,32	0,17
Ign. l. %	15,72	15,13	13,19	13,23	10,44	12,08	8,96	8,31
Total %	99,68	99,98	99,96	100,04	99,91	100,12	100,07	99,75
Li ppm	21	26	24	30	34	32	36	39
Cr ppm	64	63	78	69	93	87	85	90
Cu ppm	29	27	25	23	25	25	23	26
Zn ppm	49	49	59	54	74	63	68	79
Sr ppm	447	462	369	322	299	311	252	288
Pb ppm	10	9	8	5	9	7	10	6

Lower FeO/Fe_2O_3, CaO/MgO, $(CaO+K_2O+Na_2O)/Al_2O_3$ and higher K_2O/Na_2O ratios are also characteristics for the weathered loesses (Table 5). Loess samples from exposures of Furkótelep, Dunaszekcső, Lajvérpuszta and from upper parts of the profiles of Szálka and north of Szekszárd belong to the weakly weathered loesses. Exposures near Bátaapáti and Mohács, loesses from the exposure south of Szekszárd, samples from lower parts of the profile north of Szekszárd can be considered as weathered loess. The studied derasional loesses (from the exposure lying northern-west of Mohács) can also be ordered into this group.

Geochemical data of the paleosols of different genesis show important differences. Related to the loesses, humic loess horizons (profiles of Dunaszekcső, Mohács and Lajvérpuszta) have higher TiO_2, Al_2O_3, K_2O, Na_2O, P_2O_5, Cr and Zn contents; and quantities of CaO, MgO and Sr do not show considerable decrease because carbonates are not leached from these levels. Among the four studied sediment types (weakly weathered loess, weathered loess, humic loess horizons, chernozem-like steppe soils), humic loess horizons contain the highest C_{org} contents. Chernozem-like steppe soils have the highest SiO_2, TiO_2, Al_2O_3, Fe_2O_3, MnO, K_2O, Li, Cr, Zn, Pb, and the lowest CaO, MgO and Sr contents (Table 4). As the intensity of the weathering increases, CaO/MgO and $(CaO+K_2O+Na_2O)/Al_2O_3$ ratios for the paleosols become lower and lower, and their values are lowest for the chernozem-like steppe soils. The highest K_2O ratio is characteristic for the chernozem-like steppe soils (Table 5).

TABLE 5

Geochemical ratios of different sediment types

	Weakly weathered loess (24 samples)			Weathered loess (18 samples)		
	Limit	AVG	S.D.	Limit	AVG	S.D.
FeO/Fe_2O_3	0,06–0,27	**0,18**	0,06	0,08–0,22	**0,15**	0,04
CaO/MgO	2,23–4,42	**2,77**	0,54	1,49–3,19	**2,21**	0,40
$CaO+K_2O+Na_2O/Al_2O_3$	1,36–2,42	**1,67**	0,24	0,88–1,61	**1,09**	0,23
K_2O/Na_2O	1,07–1,74	**1,31**	0,16	1,18–1,66	**1,42**	0,10
	Humic loess horizon (4 samples)			Chernozem-like steppe soil (8 samples)		
	Limit	AVG	S.D.	Limit	AVG	S.D.
FeO/Fe_2O_3	0,21–0,30	**0,26**	0,04	0,10–0,20	**0,13**	0,04
CaO/MgO	1,02–3,59	**2,14**	1,07	0,60–3,54	**1,61**	0,52
$CaO+K_2O+Na_2O/Al_2O_3$	0,40–1,13	**0,80**	0,31	0,32–0,80	**0,52**	0,18
K_2O/Na_2O	1,25–1,53	**1,34**	0,13	1,26–1,88	**1,59**	0,19

According to the matrix of the correlation coefficient of weathered loesses, elements, which have different geochemical characters and react to weathering in different way, can unambiguously be distinguished (*Fig. 4*). One group is formed by elements accumulating during weathering (SiO_2, TiO_2, Al_2O_3, Fe_2O_3, MnO, Na_2O, K_2O, Li, Zn, Cr, P_2O_5); these show significant correlation. Elements leaching during weathering (MgO, CaO, Sr) belong to the other group, and these are in significant correlation with each other, too. However, there is only negative correlation between the elements of these two groups (*Fig. 4*).

CONCLUSIONS

Mineral composition of the loesses of this area is characterized by high carbonate content with a dominance of dolomite; the calcite-dolomite ratio is 1:2. This high dolomite content is of primary origin, and, therefore, it was simultaneously deposited together with the other mineral constituens. Carbonate content of the paleosols is lower due to weathering, however, the calcite-dolomite ratio is shifted between 2:1 and 3:1.

Element composition of loesses depends on paleoclimatic and geochemical circumstances as well as on geochemical properties of the elements, and this makes a geochemical classification of loesses possible. Loesses of the studied area can be divided into two groups: weathered loesses and weakly weathered loesses. Comparing with the weakly weathered loesses, the weathered loesses are characterized by higher TiO_2, Al_2O_3, Fe_2O_3, K_2O, Li, Cr, Zn and lower CaO, Sr contents. In the case of the weathered loesses the FeO/Fe_2O_3, CaO/MgO, $(CaO+K_2O+Na_2O)/Al_2O_3$ ratios are lower, while the K_2O/Na_2O ratio is higher.

The geochemical data reflect the intensity of weathering and that of pedogenesis for the paleosols. Therefore, the genetically different paleosols can be distinguished. Humic loess horizon represent an intermediate formation between the loesses and the chernozem-like steppe soils on the basis of their carbonate contents and element composition, as well. Among the sediments studied, the pedogenetic and weathering intensity reaches the maximum in the cases of the chernozem-like steppe soils. This soil type has the highest SiO_2,

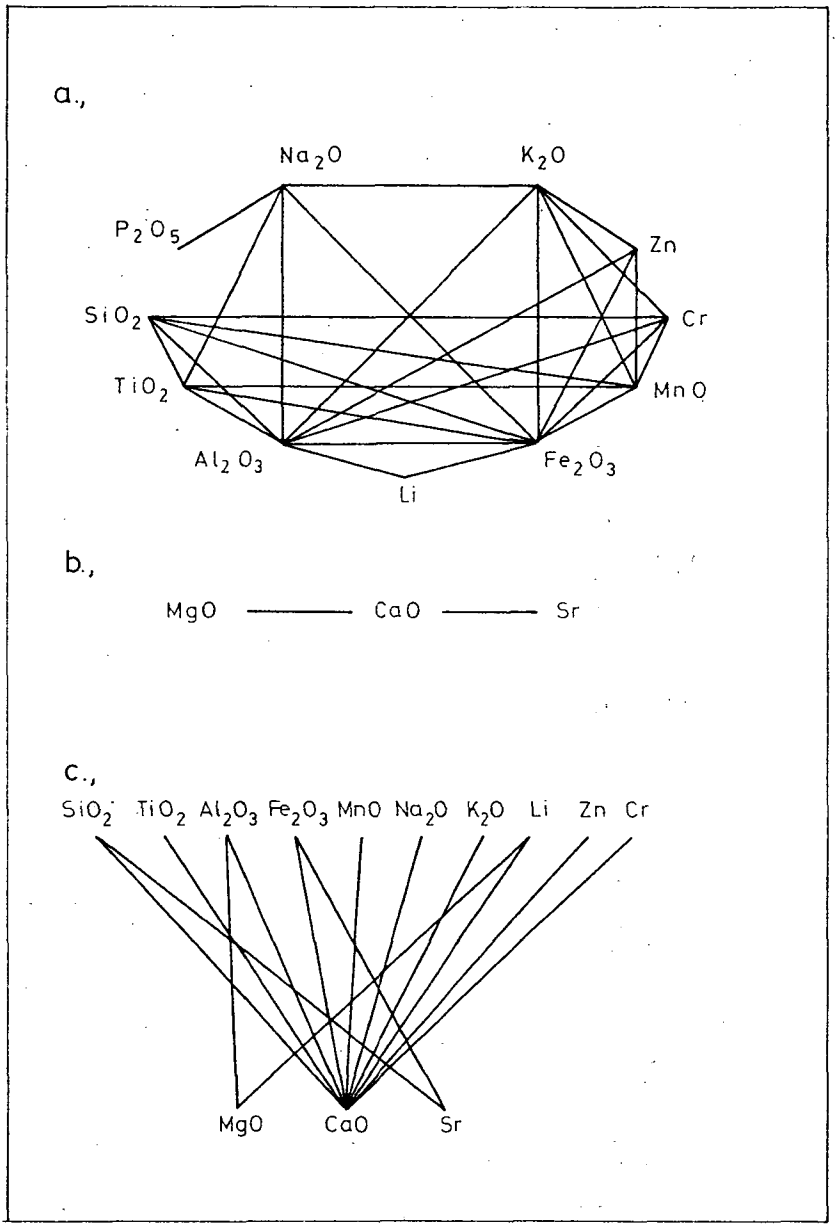

Fig. 4. Correlative profiles of geochemical data of the weathered loesses on the basis of correlation matrix of geochemical data of 18 samples. Coefficiens > 0.5 and significance level > 99.9
a: positive correlative connections of the components accumulating during the weathering
b: positive correlative connections of the components decreasing during the weathering
c: negative correlative connections between the elements accumulating and the elements decreasing during the weathering

TiO_2, Al_2O_3, Fe_2O_3, MnO, K_2O, Li, Cr, Zn, Pb values and the lowest CaO, MgO and Sr contents.

Comparison of the geochemical composition and the stratigraphic position (i. e., stratigraphic correlation on a geochemical base) needs further studies. In this respect, valuable results can mainly be expected from studies of paleosols.

ACKNOWLEDGEMENT

The authors wish to thank Prof. Dr. GERMAN MÜLLER, who made one of us possible to performed studies in the Institut für Sedimentforschung (Heidelberg) led by him. We thank M. GASTNER, S. MARHOFFER and S. RHEINBERGER (*Institut für Sedimentforschung*, Heidelberg) for their help. The research work in Heidelberg was supported by the National Scholarships Board. We also thank the colleagues of the Department of Geology and Paleontology and those of the Department of Mineralogy, Geochemistry and Petrography (JATE, Szeged) for their help.

REFERENCES

FÜCHTBAUER, H. (ed.) (1988): Sedimente und Sedimentgesteine. Schweitzerbart'sche Verlagsbuchhandlung, Stuttgart. 228–231.

GEREI, L., PÉCSI-DONÁTH, É., REMÉNYI, M., SCHWEITZER, F. and SZEBÉNYI, E. (1985): Mineralogical observations on the Paks-Dunakömlőd loess plateau (profiles sampled in 1978, 1979). In: PÉCSI, M. (ed.): Loess and the Quaternary. 83–91., Akadémiai, Budapest.

GONG, Z., CHEN, H., WANG, Z., CAI, F. and LUO, G. (1987): The epigenetic geochemical types of loess in China. In: Liu, T. (ed.): Aspects of loess research. 328–340., China Ocean Press, Beijing.

HÄDRICH, F. (1975): Zur Methodik der Lössdifferenzierung auf der Grundlage der Carbonatverteilung. Eiszeitalter und Gegenwart. **26**, 95–117.

HEINRICHS, H.–HERRMANN, A. G. (1990): Praktikum der analytischen Geochemie. 669 p., Springer, Berlin.

LAUTRIDOU, J. P., SOMME, J. and JAMAGNE, M. (1984): Sedimentological, mineralogical and geochemical characteristics of the loess of Nort-West France. In: PÉCSI, M. (ed.): Lithology and stratigraphy of loess and paleosols. 121–132., Geogr. Research Institute, Budapest.

PETROV, A. G., KRIGER, N. I., GOUNESHIAN, O. G., KOZHEVNIKOV, A. D., MIRONUK, S. G. and ZIMINA G. A. (1984): Geochemical loess history. In: PÉCSI, M. (ed.): Lithology and stratigraphy of loess and paleosols. 133–138. Geogr. Research Institute, Budapest.

PÉCSI, M. (1975): A magyarországi löszszelvények litosztratigráfiai tagolása. Földr. Közl. **23/3–4**., 217–230.

PÉCSI, M. (1985): Chronostratigraphy of Hungarian loesses and the underlying subaerial formation. In: Pécsi, M. (ed.): Loess and the Quaternary. 33–49., Akadémiai, Budapest.

PÉCSI, M. (1993): Negyedkor és löszkutatás. Akadémiai, Budapest. 375.

PÉCSI-DONÁTH, É. (1985): On the mineralogical and petrological properties of the younger loess in Hungary. In: Pécsi, M. (ed.): Loess and Quaternary. 93–104., Akadémiai, Budapest.

PYE, K. (1983): Grain surface textures and carbonate content of late pleistocene loess from West Germany and Poland. Journal of Sedimentary Petrology. **53/3**, 973–980.

SCHNETGER, B. (1992): Chemical composition of loess from a local and worldwide view. N. Jb. Miner. Mh., **1992**, H. 1, 29–47.

SZILÁRD, J. (1983): Dunántúli és Duna-Tisza közi löszfeltárások új szempontú litológiai értékelése és tipizálása. Földrajzi Értesítő. **32/1**, 109–166.

SZÖŐR, GY., BARTA, I., BALÁZS, É., SÜMEGI, P. AND KUTI, L. (1992): Az Északkelet-Alföld negyedkori pelites üledékeinek geokémiai fácieselemzése. In: Szöőr, Gy. (ed.): Fáciesanalitikai, paleobiogeokémiai és paleoökológiai kutatások. 45–64., MTA DAB, Debrecen.

SZÖŐR, Gy., SÜMEGI, P. and BALÁZS, É. (1992): A Hajdúság területén feltárt felső pleisztocén fosszilis talajok geokémiai fácieselemzése. In: SZÖŐR, GY. (ed): Fáciesanalitikai, paleobiogeokémiai és paleoökológiai kutatások, 81–92., MTA DAB, Debrecen.

TAYLOR, S. R., MCLENNAN, S. M., MCCULLOCH, M. T. (1983): Geochemistry of loess, continental crustal composition and crustal model ages. Geochimica et Cosmochimica Acta. **47**, 1897–1905.

TENNANT, C. B., BERGER, R. W. (1957): X-ray determination of dolomite-calcite ratio of a carbonate rock. American Mineralogist. **42**, 23–29.

WEN, G., DIAO, G. and FUQING, S. (1985): Geochemical characteristics of loess in Luochuan section, Shaanxi province. In: PÉCSI, M. (ed.): Loess and the Quaternary. 65–77., Akadémiai, Budapest.

Manuscript received 25 May 1995.

Acta Mineralogica-Petrographica, Szeged, XXXVI, 101–116, 1995

K/Ar RADIOMETRIC DATING ON ROCKS FROM THE NORTHERN PART OF THE DITRÓ SYENITE MASSIF AND ITS PETROGENETIC IMPLICATIONS

E. PÁL MOLNÁR*

Department of Mineralogy, Geochemistry and Petrology, Attila József University

E. ÁRVA-SÓS**

Institute of Nuclear Research of the Hungarian Academy of Sciences

ABSTRACT

Several opinions have been published on the date of the formation of the Ditró syenite massif. Direct contact of this massif and sedimentary rocks can not be found. It is probable that the syenite massif lithostratigraphically formed during the time between the Saalic and the Laramian orogenic cycles. Valuable radiometric data (less than 30) gained by different methods (Pb/Pb, K/Ar, Rb/Sr) have mainly been related to the syenites and nepheline syenites (STRECKEISEN and HUNZIKER, 1974; MÎNZATU, 1980 in JAKAB et al., 1987; JAKAB and POPESCU, 1979; JAKAB and POPESCU, 1984; JAKAB and POPESCU, 1985 in JAKAB et al., 1987). Although valuable data for hornblendites (BAGDASARIAN, 1972) differ from those of syenites, most researches dated the formation of the massif as a whole to the Jurassic on the basis of the radiometric data for the syenites and the nepheline syenites.

In this work 25 K/Ar radiometric data of the rocks (hornblendites, diorites, granites, nepheline syenites, syenites, alkaline feldspar syenites) are evaluated and based on it, devising of a petrogenetic model is attempted.

K/Ar radiometric age of the hornblendites is Middle and Upper Triassic (Ladinian and Carnian), and that of the granites is Upper Triassic (Rhaetian) – Lower Jurassic (Hettangian), the diorites indicate mixed age – Upper Triassic (Rhaetian) and Middle Jurassic (Bajocian), age of the nepheline syenites is Middle Triassic (Ladinian), and that of the syenites and the alkaline syenites is Middle Jurassic (Aalenian) – Lower Cretaceous (Albian). These data indicate two great geological events (intrusions). One happened in the age of the Upper Triassic – Lower Jurassic, and the other was formed in the Middle Jurassic – Lower Cretaceous. These events partly coincide with each other. It is proved by the mixed age of the diorites, which were probably formed by a hybridization of the hornblendites and the syenites during the second event.

INTRODUCTION

The syenite massif of Ditró (46°48' N, 25°30' E) is situated on the S-SW part of Gyergyó Alps (Romania). Diameters of its surface are 19 km and 14 km in NW and SE directions, respectively; its area is 225 km^2 including the bordering zones as well (*Fig. 1.*).

According to our present knowledge the syenite massif of Ditró is a complex magmatic body of E and NE (and perhaps SE and S) inclination, which has divided into some parts.

* H–6701 Szeged, P. O. Box 651, Hungary
** H–4001 Debrecen, P. O. Box 51, Hungary

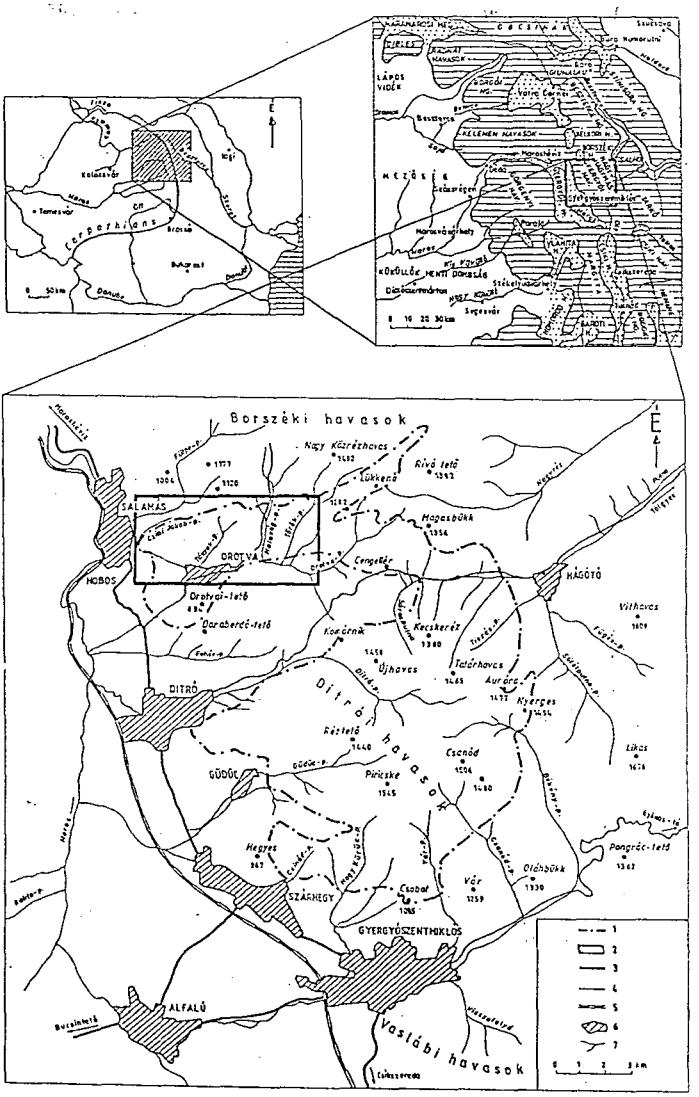

Fig. 1. Narrower and wider geographic environment of the Gyergyó Alps (Transylvania, Romania)
1. Boundary line of the Ditró syenite massif; 2. Study area; 3. Modernized road; 4. Non-modernized road; 5. Railway; 6. Settlement (town); 7. River (creek)

Geophysical (telluric and magnetotelluric) investigations of the Pacani–Tîrgu Neamt–Ditró–Régen geotraverse (VISARION et al., 1987) showed that it is a 2–2.5 km deep allochtonous body and it forms a part of the Bucovina Nappe.

According to the two dimensional model of JAKAB et al. (1987) this 6500 m thick massif is an intrusive, pseudostratified body. Its contact with the surrounding crystalline

rocks can well be traced; inclination of the plane of the contact is low (10–40°) between its surface bordering line and the level line of the –1000m, and it is inclined outward, while it turns toward the massif below the level of the –1000 m (50–80°). The syenite massif is allochtonous, and its reverse fault planes are 3500 and 5000 m deep in the west and in the east, respectively.

The most important mean tectonic element of the massif and its surrounding is fracture zone (G8) running along the line of Salomás–Hodos–Remete–Alfalu (N-W). This zone was detected by gravitational and magnetotellurical measurement, as weel; according to the magnetotellurical measurements, it is inclined toward the west. Probably, it is the "consummation" paleoplane of the Outer Dacides (VISARION et al., 1987), i. e., collision plane of tectonic plates.

The syenite massif of Ditró intruded into the central crystalline rocks of the Eastern Carpathians, and it took part in the Alpine tectonic events together with them (PÁL MOLNÁR, 1994a, c). Within the Bucovina Nappe, the greatest part of the massif is in contact with the Tölgyes Series of the prealpine Putna Nappe. In smaller areas it also touches the Rebra and the Bretila Series. In the immediate vicinity of the massif the situation of the series is as follows (upwards from below): Rebra Series, Tölgyes Series, Bretila Series (PÁL MOLNÁR, 1994a, c). Each of these series is broken through by the syenite massif of Ditró. According to KRÄUTNER et al. (1976), on the basis of K/Ar radiometric dating, ages of formation of the series are as follows: Bretila Series and Rebra, Series – 850±56 Ma; Tölgyes Series – 505±5 Ma.

Any contact of the syenite massif with sedimentary rocks can not be found. According to BALINTONI (1981) Mesozoic sedimentary rocks are absent, among others, under the prealpine Putna Nappe because this nappe was formed before the Trias. He suggests that prealpine nappes broken through y the syenite massif formed during the paroxysm of the Saalic tectogenesis.

The alpine nappes were formed under the influence of the Cretaceous orogenic phases (Austrian, Laramian). Therefore, the syenite massif was lithostratigraphically formed between the Saalic and the Laramian orogenic phases.

OUR MOST IMPORTANT KNOWLEDGES ON THE FORMATION AGE OF THE MASSIF AND ON THE SUCCESSION OF THE PROCESSES WITHIN THE MASSIF

REINHARD (1911) was the first researcher who dealt with the formation age of the syenite massif of Ditró. According to him its rocks are hypabyssal ones of the magma whose effusion formed the rocks of the Görgény Alps, i. e., this hypabyssal magmatic intrusion is younger (post Neocomian) than the last tectonic movements of the Eastern Carpathians.

In 1923 MAURITZ and VENDL stated that there are not any trace of cataclasis with the exception of the joints filled with fine sodalite-cancrinite-muscovite material, therefore, it was the only dynamic influence on the rocks. Consequently, these are traces of young folding and, in this way, it is not possible that the massif was formed before the Mesozoic.

STRECKEISEN (1931) agrees with REINHARD (1911) that the massif was formed after the Middle Cretaceous tectonic movements. He is of opinion that correlation of the rocks of the massif and those of the young Kelemen-Hargita volcanic range is not unambiguous.

IANOVICI (1929–1938), however, denies Reinhard's theory and points out the fact that syenites (Atlantic suite) do not correspond to the eruptive rocks (Pacific suite) of the Kelemen-Hargita range. It was a long time between the syenite intrusion and the Neogene

volcanism of the Eastern Carpathians, and during this period rocks covering the massif were eroded, and, in this way, Neogene andesites, agglomerates and volcanic breccias deposited directly on the syenites. He suggests that the syenite intrusion is Pre-Cretaceous.

According to FÖLDVÁRI (1946) volcanic ranges consisted of Tertiary andesites, dacites and rhyolites have their granitic-dioritic magma chambers in the depth. These granitic-dioritic intrusions, assimilating the Mesozoic limestones of the Nagyhagymás Mountain, formed the nepheline syenitic rocks of the massif. If this theory is true, the syenite intrusion is at least Upper Cretaceous because there are Cretaceous limestones as well in the Nagyhagymás nappe.

From of his field studies and tectonic characters, STRECKEISEN (1952–1954) concludes that alkaline granites and alkaline syenites are of the same age, nepheline syenites are younger, while the "Ditró" essexites and the ultrabasic rocks are the oldest ones. In his opinion these rocks are of common origin.

IONESCU et al. (1966) made the first radiometric age determinations for the rocks of the massif (Table 1). The measurements were performed on zircons and monazites using Pb-α method.

TABLE I

Summarizing table of the radiometric ages of the rocks from the Ditró syenite massif and the related contact zones

Author, year	No.	Number of the sample	Method	The studied rock type, locality	The studied fraction	Age (Ma)
IONESCU et al., 1966	1.	–	Pb-α	**Monacite**	–	326
	2.	–	Pb-α	**Zircon**	–	297
BAGDASARIAN, 1972	3.	5138	K/Ar	**Hornblendite** from lens in gneissic diorites, west of the conjunction of the Tászok and the Orotva creeks.	whole rock	196±6
	4.	5136a	K/Ar	**Hornblendite** from the zone of the gneissic syenites, west of the conjunction of the Orotva and the Simó creeks.	whole rock	161±2
	5.	5134a	K/Ar	**Hornblendite** from xenolite, west of the conjunction of the Orotva and the Halaság creeks.	whole rock	161±10
	6.	5139	K/Ar	**Hornblendite** with plagioclase inclusions, Ditró valley and the spring are of the Putna Creek.	whole rock	177±1
	7.	5137	K/Ar	**Pegmatite syenite**, from veins in hornblendites, east of the conjunction of the Orotva and the Tászok creeks.	whole rock	142±7
	8.	5135	K/Ar	**Syenite**, east from the conjunction of the Orotva and the Simó creeks.	whole rock	128±
	9.	5134	K/Ar	**Syenite**, central part of the Orotva valley.	whole rock	121±2
	10.	5140	K/Ar	**Syenite** from gneissic vein, road between the Ditró valley and the Putna Creek.	whole rock	121.5±0.5
	11.	5133	K/Ar	**Leucogranite**, conjunction of the Orotva and the Hompot creeks.	whole rock	125±10
	12.	5142	K/Ar	**Nepheline** syenite, road between the Ditró valley and the Putna Creek	whole rock	152±1
	13.	5141	K/Ar	**Mica-schist**, basin of the Putna Creek, Ditró-Tölgyes road, km 20.	whole rock	284±14

TABLE 1 contd.

Author, year	No.	Number of the sample	Method	The studied rock type, locality	The studied fraction	Age (Ma)
STRECKEISEN & HUNZIKER, 1974	14.	429	K/Ar	**Nepheline syenite**, Komarnik plateu	biotite	151±9
	15.	1764	K/Ar	**Nepheline syenite**, Ditró Creek, gallery 1.	biotite	153±3
	16.	1195	K/Ar	**Hornfels**, Tászok Creek, 750 m SE	biotite	150±6
	17.	835	K/Ar	**Tinguaite**, Csanód feje, 500 m E	whole rock	161±7
	18.	204	K/Ar	**Tinguaite**, Pricske, 500 m, NE	whole rock	156±6
MÎNZATU et al., 1980	19.	–	K/Ar	**Biotite syenite**, Ditró valley	whole rock	112
	20.	–	K/Ar	–	biotite	117
	21.	–	K/Ar	**Biotite syenite**, Ditró valley, gallery VII.	whole rock	131
	22.	–	K/Ar	**Biotite syenite**, Ditró-Tölgyes, km 11	whole rock	136
	23.	–	K/Ar	**Biotite hornfels**, Auróra, borehole F 144.	whole rock	138
	24.	–	K/Ar	**Biotite hornfels**, Auróra, gallery VII.	whole rock	172
JAKAB & POPESCU, 1979	25.	–	Pb/Pb	**Galenite**. Békény.	–	Jurassic
JAKAB & POPESCU, 1984	26.	–	Rb/Sr	7 rock types (hornblendite, diorite, nepheline syenite, bostonite, liebnerite syenite, microsyenite, biotite lamphrophyre)	whole rock	not intrepretable
JAKAB & POPESCU, 1985	27.	Rb/Sr	Rb/Sr	8 samples of nepheline syenite + liebernite, 8 samples of white nepheline syenite, 5 samples of microsyenite, 5 samples of granite, 5 samples of hornblendite-diorite (Orotva), 5 samples of essexite (Güdüc-Ditró)	whole rock	about 143 not interpretable

In 1966, BAGDASARIAN made a short field trip in the massif and determined the radiometric age of the collected samples using the K/Ar method. His results were published in 1972 (Table 1). In his opinion the age of the diorite-hornblendite complex is Pre-Jurassic. He suggests that age of the syenites and the nepheline syenites are synchronous, and the higher age of the nepheline syenites can be regarded as a result of the cancrinite of this rock because it has influence on the radiometric age because of its higher Ar content.

In 1974 STRECKEISEN and HUNZIKER described the succession of the formation for the different rocks in the massif that they believed to be a magmatic one: (1) lit-par-lit intrusion of dioritoid and gabbroid magmas into the existing crystalline schists; (2) intrusion of the syenitic magma that broke through the rocks of the dioritic complex; in the marginal parts of the massif granitic rocks were formed as a result of the assimilation of the adjacent rocks; (3) intrusion of the nepheline syenitic magma yielding the common hybridization and metasomatic processes; (4) pegmatites, nepheline syenitic aplites, lamprophyres. K/Ar radiometric ages published by them are listed in Table 1. In their opinion the intrusion is not older than Jurassic.

According to MÎNZATU (1980, see in JAKAB et al., 1987) (Table 1) K/Ar radiometric age of the syenites is Lower Cretaceous, and the contact hornfels were formed in the Dogger.

JAKAB and POPESCU (1979) and JAKAB (1982) tried to determine the age of the ores (mostly galenite) associated to the massif using the Pb/Pb method. On the basis of the Pb^{206}/Pb^{207} ratio, comparing the data to those of reference galenites, they regard the formation age of the galenites to be Jurassic (Table 1). They state, however, that Pb/Pb method is not really suitable for dating Post-Hercynian formations.

Rb/Sr radiometric dating (JAKAB and POPESCU, 1984, 1985 in JAKAB et al., 1987) had not concrete results. More than 40 Rb/Sr measurements were performed on the different rocks of the massif but only the age of the red syenites could be determined; it is about 143 Ma. Data for the other rocks could not be interpreted because of the high standard deviation values.

ANASTASIU and CONSTANTINESCU (1978–1980) interpret the formation of the massif as process of several phases. On the basis of the great petrographic variety they suppose two independent hypabyssal magmatic intrusions:

– a basic one of mantle origin (parental),

– a crustal one assimilating Si-poor rock-association.

Formations of these intrusions are spatially similar, but temporally different.

According to JAKAB et al. (1987) the formation history of the massif is the following: (1) The first great process was a magmatic intrusion causing Fe-Mg metasomatism of varying intensity for the crystalline rocks. The metasomatism formed very heterogeneous rocks that are often interjointed. (2) The second great geological event was the intrusion of the nepheline syenites. This process happened at the marginal parts of the massif (excluding the western part). The metasomatic process associated with the intrusion formed, depending on the original compositons, granitoid, melanosyenitic or monzonitic rocks. These rocks have sialic character (as Sr and La isotopes show), all the other rocks of the massif are simatic. (3) During the third, and the last, process of the general alkali metasomatism formed the present state. Its material penetrated the existing basic rocks and created a metasomatic syenite "crown" around them. The alkali metasomatism of the basic rocks led to form diorites, essexites, monzonites, etc. The crystalline schists, depending on their compositions, transformed into essexites, monzonites or syenites.

From the petrographic studies of the hornblendites of the Orotva-Putna zone PÁL MOLNÁR (1992) concludes that problem of the massif can only be solved by the correct interpretation of the ultrabasic rocks.

K/AR RADIOMETRIC DATING THE ROCKS OF THE NORTHERN PART OF THE DITRÓ SYENITE MASSIF

As almost each rock type of the massif can be found on the surface in the N-NW part of the Ditró syenite massif, the K/Ar radiometric measurements were performed on the fresh samples colledted from there. Sampling points of the area is shown by *Fig. 2*, and the results are listed in Table 2.

The classification and the general petrographic characterization of the rocks studied is given in our previous works (PÁL MOLNÁR, 1988, 1992, 1994b, c).

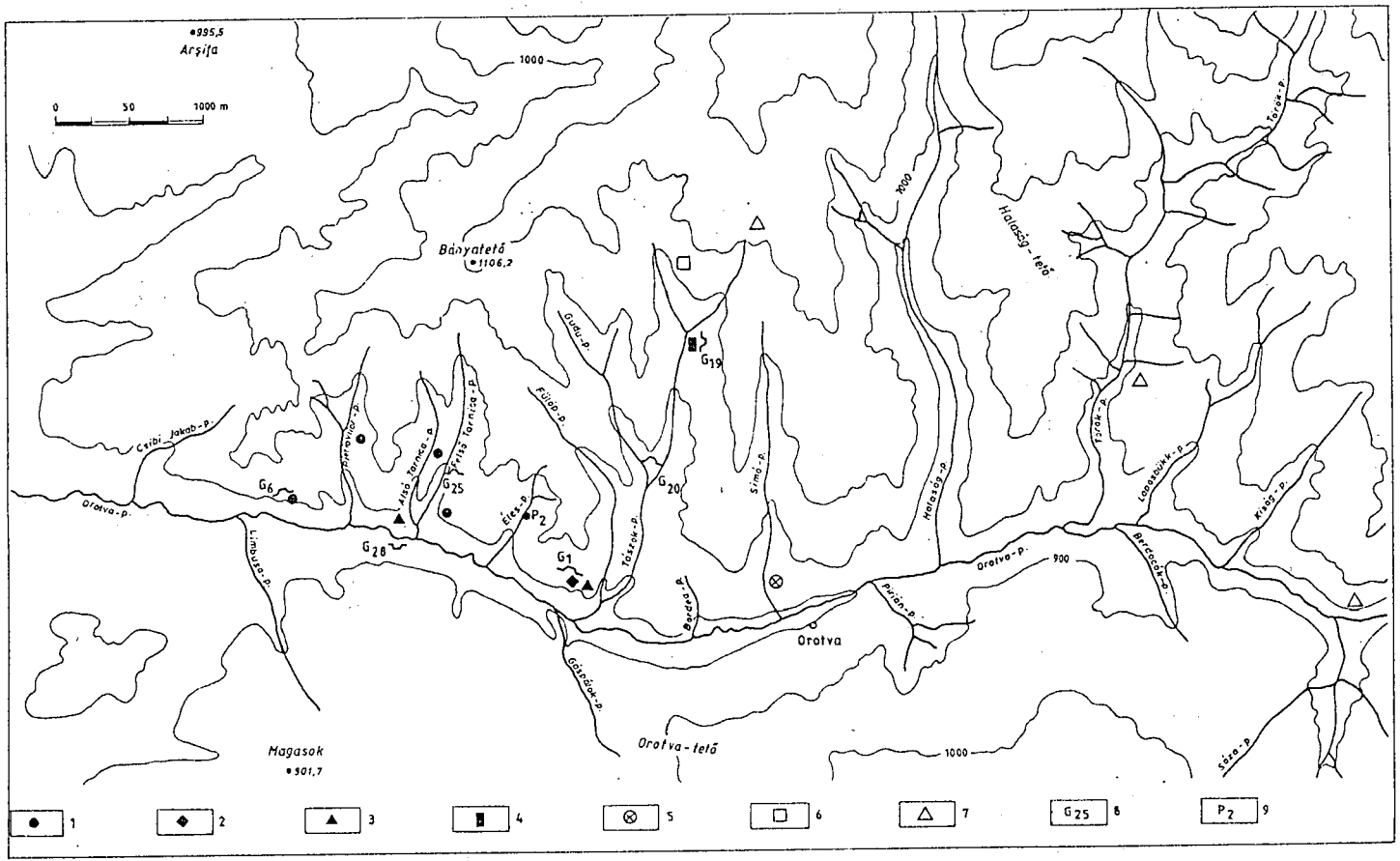

Figure 2. Localities of the sample studied in the basin of the Orotva Creek (northern part of the Ditró syenite massif)
1. hornblendite; 2. meladiorite; 3. diorite; 4. syenite; 5. alkaline feldspar syenite; 6. sodalite nepheline syenite; 7. granite; 8. gallery; 9. pit

TABLE 2

New K/Ar ages of the magmatic rocks from the northern part of the Ditró syenite massif

Number of the sample	Rocks type, locality	Studied fraction	K-content (%)	$^{40}Ar_{rad/g}$ (ncm^3/g)	$^{40}Ar_{rad}$ (%)	K/Ar age (Ma)
6546	Hornblendite with textural ordering Orotva, Felső Tarnica Creek	amphibole	1.158	$1.1417 \cdot 10^{-5}$	77.9	237.4±9.1
6547	Hornblendite with textural ordering Orotva, Pietrarilor Creek	amphibole	1.150	$1.0245 \cdot 10^{-5}$	56.5	216.0±8.8
6548	Hornblendite without textural ordering Orotva, gallery 6	amphibole	1.210	$1.1302 \cdot 10^{-5}$	49.2	226.0±9.6
6705	Pegmatoidic hornblendite Orotva, Felső Tarnica Creek (gallery 25)	amphibole	1.210	$1.1780 \cdot 10^{-5}$	40.5	234.7±10.8
		plagioclase	0.240	$1.5729 \cdot 10^{-6}$	25.4	161.3±9.8
		biotite (Ø> 0.315 mm)	7.440	$4.9074 \cdot 10^{-5}$	97.6	162.4±6.1
		biotite (Ø< 0.315 mm)	4.780	$3.2758 \cdot 10^{-5}$	48.5	168.3±7.2
6549	Meladiorite with textural ordering Orotva, Tászok Creek	amphibole	1.894	$1.6238 \cdot 10^{-5}$	64.7	208.3±8.3
		feldspar	0.551	$3.0753 \cdot 10^{-5}$	52.3	138.2±5.8
6550	Diorite with textural ordering Orotva, Tászok Creek	amphibole	2.960	$2.1309 \cdot 10^{-5}$	88.2	176.6±6.7
		feldspar	1.240	$6.8774 \cdot 10^{-6}$	61.3	137.4±5.5
5667	Diorite with feldspar aggregates Orotva, Alsó Tarnica Creek	amphibole	1.880	$1.6974 \cdot 10^{-5}$	85.8	218.7±8.3
		feldspar	0.520	$5.5430 \cdot 10^{-6}$	38.3	255.4±5.8
6680	Syenite Orotva, Tászok Creek (gallery 19)	biotite	5.616	$2.4163 \cdot 10^{-5}$	83.7	107.6±4.1
		K-feldspar	3.733	$2.7889 \cdot 10^{-5}$	88.5	182.7±6.9
6679	Alkaline feldspar syenite Orotva, Simó Creek	biotite	6.405	$2.6269 \cdot 10^{-5}$	72.3	102.6±4.0
		K-feldspar	5.162	$2.3492 \cdot 10^{-5}$	95.3	113.5±4.3
6678	Sodalite nepheline syenite Orotva, Tászok Creek	biotite	4.154	$3.0968 \cdot 10^{-5}$	94.3	182.4±6.9
		nepheline + sodalite	5.270	$5.0820 \cdot 10^{-5}$	90.2	232.7±8.8
6677	Granite Orotva, Török Creek	biotite	4.443	$3.9891 \cdot 10^{-5}$	84.6	217.6±8.3
		feldspar	3.728	$2.2004 \cdot 10^{-5}$	80.5	146.0±5.6
6703	Granite Orotva, Tászok Creek	biotite	3.044	$2.6757 \cdot 10^{-5}$	79.9	213.5±8.2
		K-feldspar	3.844	$2.1606 \cdot 10^{-5}$	73.9	139.1±5.4
6704	Granite Orotva, Nagyág Creek	biotite	4.482	$3.8038 \cdot 10^{-5}$	95.2	206.3±7.8
		K-feldspar	3.844	$2.2165 \cdot 10^{-5}$	62.9	142.7±5.7

Analytical methods

The least weathered ones were selected from more than 100 rock samples for the K/Ar radiometric dating.

Measurements of K/Ar ages were performed in the Institute of Nuclear Research of the Hungarian Academy of Science (ATOMKI), Debrecen, Hungary.

As the first step of the preparation process the samples for analysis were broken and carefully washed out.

Samples were broken to grains of 0.1–0.315 mm. After a dry sieving, dust was washed out from the samples. The sample part for potassium determination was pulverized before the chemical digestion that necessary for the flame photometric measurement.

Separated mineral fractions were used for the radiometric dating. The separation was performed by magnetic separator, flotation in heavy fluids (bromoform, methylene-iodide), and a "shaking technique", which uses the shape varieties of the different minerals. These techniques were comined with each other. In this way, mostly biotite, amphibole, feldspars and feldspathoids were separated from the samples. If the state of the sample made it possible, several mineral fractions were obtained from one rock.

Ar content of the samples was released by ignition at about 1500 °C in closed vacuum system. Degassing of the samples was performed by high frequency induction heating in molybdenum crucibles, spike enriched in ^{38}Ar to 98% was introduced into the line prior to degassing with a gas pipette. Zeolite, CuO, titanium sponge and traps cooled with liquid nitrogen as well as SAES St 707 getter were used for cleaning the argon. The cleaned argon was directly introduced into a 90° deflection magnetic mass spectrometer of 150 mm radius suitable for static analysis. This instrument was developed at the Institute of Nuclear Research of the Hungarian Academy of Science (ATOMKI), Debrecen. After the determination of the argon isotopic ratio, quantity of the radiogene argon was determined by isotopic dilution analysis using the added ^{38}Ar as a base.

Potassium content was measured by a digital flame photometer. The pulverized minerals were digested in HF, adding some H_2SO_4 and HNO_3 to it. The digested samples were dissolved in 0.25 N Hcl. By the applied dilution, 1% K was equivalent of 1 ppm concentration; 100 ppm Na as buffer and 1000 ppm Li as inner standard was used.

Accuracy was checked by repeated measurements of interlaboratory standards: Asia 1/65 (Soviet), GL-O (French), LP-6 (American) and HD-B1 (German). Details of the instruments, the applied methods and results calibration have been described elsewhere (BALOGH, 1985; ODIN et al., 1982). Ages were calculated with the constants suggested by STEIGER and JÄGER (1977).

Limits of errors given beside the age data show only the analytical errors (standard deviation) because the geological "errors" (argon loss, extra argon, etc.) may not be revealed by study of one sample. Decrease of the geological errors is mainly possible by study on rocks and minerals that are suitable for K/Ar radiometric dating. Amphibole and, in our case, nepheline does not easily release argon (nepheline retains argon very well, experience gained from study on Precambrian rocks shows that its argon retention ability is higher than that of amphiboles), but biotite also has a high argon retention ability. Argon easily escapes from potassium feldspars, in particular, because it is susceptible to exsolution. Consequently, determination of formation age of rocks is primarily available by study of amphibole and biotite. Feldspars generally show the ages of the postmagmatic processes or the secondary geological events (magmatic intrusion, assimilation, hybridization, etc.). Ages measured on hypabyssal magmatic rocks are generally younger than the real ages because of the argon loss of their feldspars. Therefore, these data can only be interpreted as minimal ages. K/Ar ages older than the real ones can rarely occur, mainly in case of minerals of low potassium or that of K-poor rich rocks that crystallized selaing off from the air in great deep and in geological environs which have radiogenic argon. Although in different scale, subsequent tectonic or metasomatic processes rejuvenate all types of the minerals.

K/Ar age

It is well-known that K/Ar ages measured on metamorphic rocks can be interpreted as blocking age in most cases. K/Ar age indicates the date when a rock got under the blocking temperature of the Ar. This temperature is 4–500 °C for the amphibole, about 300

°C for the biotite, and ranges from 120 to 130 °C for the feldspars. If a rock body rapidly emerged (and cooled) after its formation, and it was not affected by other processes, the K/Ar ages of its particular minerals well approach the real geologic age. Henceforth, if the formation age of the rock is mentioned only the Ar blocking age of the particular minerals is considered.

K/Ar radiometric ages were fallen under the geological timetable supposed by HARLAND et al. (1982).

K/Ar ages of the amphiboles separated from hornblendites (samples 6546, 6547 and 6548) range from 216±8.8 to 237±9.1 Ma. As measures were performed on minerals having high Ar retention ability, and taking the fact mentioned above into consideration that ages of the rocks may only be older, the gained Middle Triassic (Ladinian) – Upper Triassic (Carnian) age possibly well approaches the real age of these rocks.

K/Ar age of the amphibole separated from pegmatoidic hornblendite 6705 (Table 2) is 234.7±10.8 Ma, i. e.., Middle Triassic (Ladinian). Feldspars (plagioclase) from the same rocks are 161.3±9.8 Ma, while the ages of the biotites of diameters less and greater than 0.315 mm are 162.4±6.1 Ma and 168.3±7.2 Ma, respectively. Age of the amphiboles, which have very high argon retention ability, corresponds to that of amphiboles from the hornblendite within the limit of error, while the feldspars and the biotites show the age of the secondary effects (Middle Jurassic [Callovian] – Upper Jurassic [Oxfordian]).

Up to the present only Bagdasarian (1972) performed radiometric (K/Ar) measures on the hornblendites (Table 1). Although, because of the argon loss of the feldspars of the rocks his data of whole rock measurements are lower than our ones, however, also suggest a Pre-Jurassic formation for the hornblendites.

In the case of the diorites (samples 6549, 6550, 6567), the two studied fractions (amphibole and biotite) are characterized by quite different data. For meladiorites with textural ordering, age of the amphiboles is 208.3±8.3, while that of the feldspars is 138.2±5.8 Ma. Ages of the amphiboles and feldspars from the diorites with textural ordering were proved to be 176.6±6.7 and 137.4±5.5 Ma, respectively. Amphiboles and feldspars of the diorites with feldspar aggregates gave 218.7±8.3 and 255.4±12 Ma, respectively. Feldspars may lose their argon content without any secondary effects (hence, in general, they are not suitable for K/Ar radiometric dating), but they are sensitive to these processes. It is possible that concurrent Upper Cretaceous (Berriasian, Valanginian) K/Ar ages of the feldspars of meladiorites and diorites (excepting the very high deviating [?] age of the feldspars of the diorites with feldspar aggregates) indicate such a secondary effect. Presumably, this fact can explain the slightly lower (Upper Triassic [Rhaetian] – Middle Jurassic [Bajocian]) K/Ar ages of the amphiboles separated from the same rock in relation to that of the amphiboles of the hornblendites. By the rule of the mathematical statistics, difference between two ages with errors of 67% can be determined if the difference of the data greater than double the sum of the errors. In the present case, highest K/Ar age of the amphiboles of the hornblendites and the lowest one of the amphiboles of the diorites (Table 2) give the following ratio:

$$\frac{237.4 - 176.6}{9.1 + 6.7} = 3.84,$$

therefore, the difference can well be determined. If the average ages of the amphiboles of the diorites and hornblendites are considered, however, this ratio will be below 2 (1.56).

Taking the above mentioned facts into consideration it is possible that argon content of the diorites was partly removed, and the determined K/Ar age is a mixed age. It is also possible that age of the secondary effect corresponds to the K/Ar age of the feldspars.

BAGDASARIAN could not perform measures on the diorites "in absence of potassium", and, therefore, he considered the diorites as old as the hornblendites. JAKAB et al. (1984, 1985 in JAKAB et al., 1987) tried to determined the radiometric ages of the hornblendites and diorites using Rb/Sr method. This method, however, is really suitable for only siliceous rocks even in ultraclean circumstances and using up-to-date mass spectrometer. Other radiometric dating has not been performed yet.

The two analyzed fractions (biotite and potassium feldspars) of the syenite (sample 6680) proved to be 107.6±6.7 and 182.7±6.9 Ma, respectively. The investigated rocks are not derived from the classic syenitic localities (e.g., the central part of the massif), but from the rock-debris of a gallery driven at the Tászok Creek. K/Ar radiometric ages of the syenites (mainly measured on feldspars) are quite similar to each other (Table 1). Comparing our data with K/Ar radiometric ages that were previously measured on the syenites (Table 1: 8, 9, 10, 19, 21, 22), it can be seen that only the value of 182.7±6.9 Ma is differ from the calculated mean age of 133.2±2.8 Ma. This mean age is averaged value of at least three measuring series (Table 2; BAGDASARIAN, 1972; MÎNZATU, 1980 in JAKAB et al., 1987), and measuring method of one of them is not known (MÎNZATU, 1980 in JAKAB et al., 1987). According to the above mentioned facts, the syenites could be formed in the period from the Middle Jurassic (Aalenian) to the Lower Cretaceous (Albian).

The two fractions (biotite and nepheline+sodalite) of the studied sodalite nepheline syenite (ditróite) yield 182.4±6.9 and 232.7±8.8 Ma, respectively. K/Ar age of the biotite fraction is similar to the average value of 152.6±4.3 Ma of the previously determined K/Ar and Rb/Sr ages of nepheline syenites (Table 1: 12, 14, 15, 17, 18, 27) measured on the whole rock.

K/Ar radiometric ages of the two fractions (biotite and potassium feldspars) of the alkaline feldspar syenite (sample 6679) almost correspond to each other: 102.6±4 and 113.5±4.3 Ma, respectively. This refers to the period of the Lower Cretaceous (Aptian, Albian). It very possible that it indicates the real formation age of the alkaline feldspar syenites.

In the case of the granites (samples 6677, 6703, 6704) the biotite and the feldspars were the separated fractions (Table 2). K/Ar radiometric ages of the biotite and the potassium feldspars range from 206.3±7.8 to 217.6±8.3 and from 139.1±5.4 to 146.0±5.6 Ma, respectively. K/Ar age of the biotite of high argon retention ability possibly indicates the minimal Upper Triassic (Rhaetian) – Lower Jurassic (Hettangian) age of the granites, while the Upper Jurassic (Tithonian) – Lower Cretaceous (Berriasian) age of the feldspars refers to a secondary effect.

K/Ar age of the biotite separated from the granites corresponds to that of the amphiboles of the hornblendites within the limit of the errors. Consequently, the hornblendites and the granites emerged (cooled) in he same time, and this process was rapid because minerals of different blocking temperature indicate the same age within the limit of the errors.

Up to the present only one valuable radiometric age (125±10 Ma) has been measured (BAGDASARIAN, 1972) for the granites. This measure was performed on the whole rock, and it is lower than our data.

GENETIC IMPLICATIONS OF THE K/Ar RADIOMETRIC AGES

On the basis of the K/Ar radiometric dating performed on rocks from the northern part of the Ditró syenite massif (principally taking that of the biotite and the amphibole into

consideration, which are of high argon retention ability) the following sussession can be stated:

hornblendite→nepheline syenite→granite→diorite→syenite→alkaline feldspar syenite.

This chronological succession, however, does not mean the succession of the geological processes. Considering data of the feldspars indicating the secondary processes beside the age of the minerals of high argon retention, two greater formations chronological intervals can be determined:

I. Middle Triassic – Lower Jurassic,

II. Middle Jurassic – Lower Cretaceous (*Fig. 3.*).

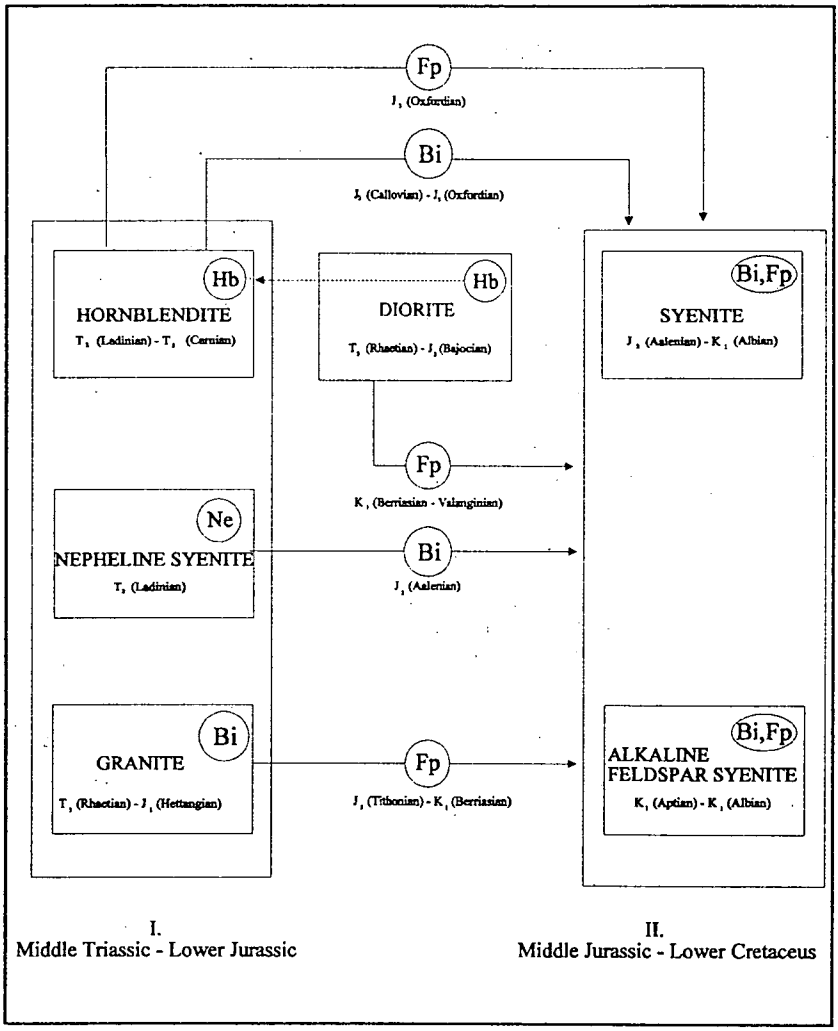

Fig. 3. K/Ar radiometric ages of the rocks of the Ditró syenite massif, and the two formation intervals determined on the basis of this data

Studied fractions: Hb – amphibole (hornblende), Ne – nepheline+sodalite, Bi – biotite, Fp – feldspar

Differences can not be pointed out by statistics between the ages of the minerals with high argon retention ability of the hornblendites, nepheline syenites and granites belonging to the first interval. A petrographical connection of the nepheline syenites and the granites is possible (PÁL MOLNÁR, 1988). However, connection of the hornblendites and granites as well as the nepheline syenites has not been proved yet. Ages of the minerals with lower argon retention ability of the three rock groups also correspond to each other within the limits of the errors. Therefore, their ages were changed by the same geological process.

As it was mentioned, mean K/Ar age of the amphiboles from the diorites corresponds to that of the amphiboles from the hornblendites within the limit of the errors, however, minimal K/Ar age of it corresponds to the maximum K/Ar age of the feldspars from the syenites within the limit of the errors. Difference between the minimal K/Ar age of the amphiboles from the hornblendites and the maximum K/Ar age of the syenites can well be determined. Consequently, it is possible that the K/Ar age of the diorites is a mixed age.

Rocks that can be ordered into second group are the syenites and the alkaline syenites.

A schematic model shown by *Fig. 4* can be created on the basis of the K/Ar radiometric ages of the rocks studied. According to this model two great geological events

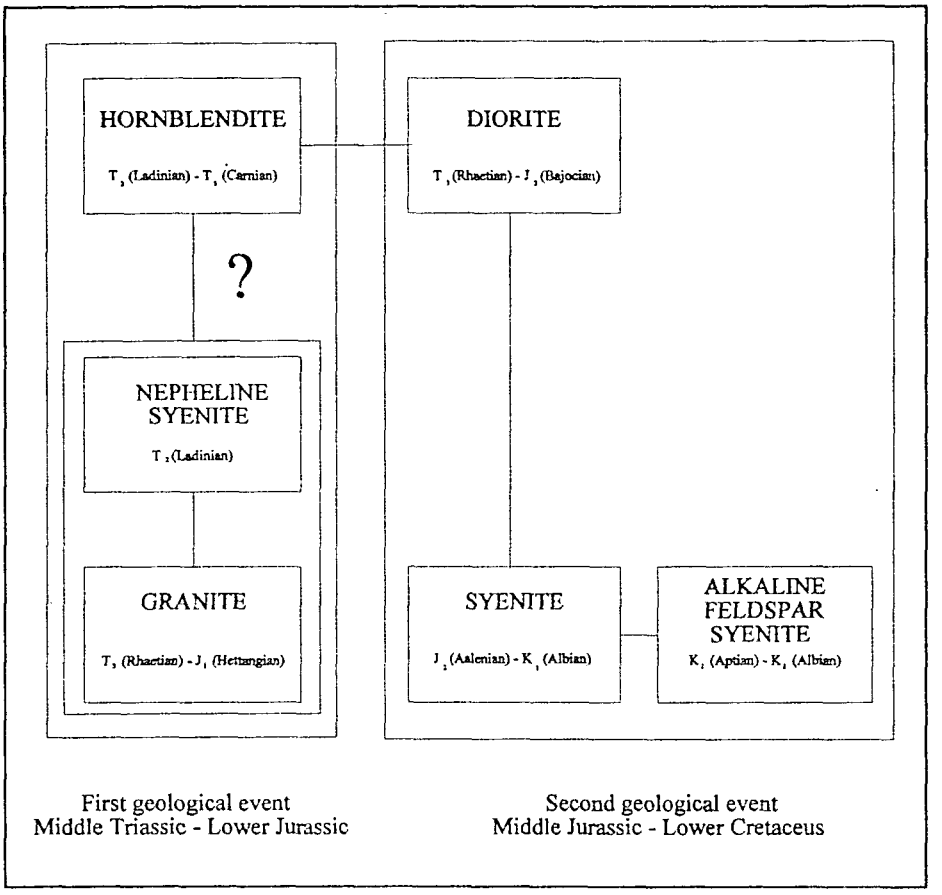

Fig. 4. Genetic model of the Ditró syenite massif on the basis of the K/Ar data

(magmatic intrusion) can be identified. During the first one, appearance of the hornblendites was followed by the formation of the nepheline syenites and the granites. In the second event the syenites and the alkaline feldspar syenites intruded as well as the diorites were formed. In spite of the fact that mineralogical composition of the diorites is similar to that of the hornblendites (PÁL MOLNÁR, 1994c), the diorites formed during the second event. Their structure suggests an injection bordering zone (PÁL MOLNÁR, 1994c). It is possibly the case of mixing hornblendites and syenites.

The alkaline feldspar syenites occur both in the syenites and the hornblendites as veins (PÁL MOLNÁR, 1988), therefore, they represent the magmatic vein phase finishing the second geological event.

CONCLUSIONS

Evaluation of 25 K/Ar radiometric dating of the studied 6 rock types has thrown a new light upon the formation of the Ditró syenite massif.

The previous radiometric datings (Pb/Pb, K/Ar, Rb/Sr) were mainly performed on the syenites and the nepheline syenites (STRECKEISEN and HUNZIKER, 1974; MÎNZATU, 1980 in JAKAB et al., 1987; POPESCU, 1979; JAKAB and POPESCU, 1984, 1985 in JAKAB et al., 1987). Radiometric ages of the hornblendites outcropping in other parts of the massif were studied by BAGDASARIAN (1972), and he suggested the formation of the rocks before the Jurassic period. Although radiometric age of the diorites (essexites) was studied (JAKAB et al., 1984, 1985 in JAKAB et al., 1987), however, valuable results were not yielded. On the basis of these results it was the dominant idea that the Ditró syenite massif was formed in the Jurassic period.

According to our studies, there were two greater geological events in the Ditró syenite massif: one in the Middle Triassic – Lower Jurassic, and another in the Middle Jurassic – Lower Cretaceous period.

K/Ar age of the amphiboles of the hornblendites is Middle Triassic (Ladinian) – Upper Triassic (Carnian) (first geological event), and that of the feldspars and the biotite is Middle Jurassic (Callovian) – Upper Jurassic (Oxfordian) (second geological event, the age of the formation of the syenites). K/Ar age of the amphiboles of the diorites id Upper Triassic (Rhaetian) – Middle Jurassic (Bajocian) (first geological event, the age of the formation of the hornblendites), and that of the feldspars from this rock is Lower Cretaceous (Berriasian, Valanginian) (second geological event, age of the formation of the syenites). K/Ar age of the nepheline+sodalite fraction of the nepheline syenites is Middle Triassic (Ladinian) (first geological event), that of their biotites is Middle Jurassic (Aalenian) – Lower Cretaceous (Albian) (second geological event). Both fractions (biotite and potassium feldspars) of the alkaline feldspar syenites are Lower Cretaceous (Aptian, Albian) (second geological event). K/Ar age of the biotites from the granites is Upper Triassic (Rhaetian) – Lower Jurassic (Hettangian) (first geological event), that of the potassium feldspars is Upper Jurassic (Tithonian) – Lower Cretaceous (Berriasian) (second geological event, age of the formation of the syenites).

Our results confirm the hypothesis that the syenite massif was formed by a multi-stage process; i. e., it was formed either by two entirely independent magmatic intrusions (?) or, perhaps, by an obduction (ultrabasic rocks) and an intrusion (nepheline, syenite, granites) and, subsequently, another intrusion which partly influenced the rocks formed by the first geological event (syenites, alkaline feldspar syenites, monzonites). Mixed ages of the diorites prove that these rocks are into connection with both the hornblendites and the

syenites, therefore, they are hybrid rocks. The hybridization undoubtedly connects with the second geological event.

Evidence of this genetic model and that of the difference or the connection between the hornblendites and the granites, the hornblendites and the nepheline syenites, the hornblendites and the syenites, the nepheline syenites and the granites, as well as, the syenites and the alkaline feldspar syenites can only be proved by major and trace element geochemistry, radiogene isotopic ratio, and petrogenetic model calculations.

ACKNOWLEDGEMENTS

The authors wish to thank Professor TIBOR SZEDERKÉNYI and Dr. SÁNDOR MOLNÁR for the financial assistance of the K/Ar radiometric measurements and Dr. KADOSA BALOGH for his helpful discussions. Dr. PÉTER RÓZSA is thanked for the translation.

REFERENCES

ANASTASIU, N., CONSTANTINESCU, E. (1979): Structura şi petrogeneza masivului alcalin de la Ditrău, Raport geologic final. (Structure and petrogenesis of alkaline massif of Ditró). Doc. Dept. of IPEG "Harghita", Miercurea-Ciuc, Manuscript.

ANASTASIU, N., CONSTANTINESCU, E. (1980): Structure du massif alcalin de Ditrău. An. Univ. Buc. Seria Geol., **XXIX**., 3–22.

BAGDASARIAN, G. P. (1972): Despre vîrsta absolută a unor roci eruptive şi metamorfice din masivul Ditrău şi Munţii Banatului din România. (A study on the absolute age of igneus and metamorphic rocks of the Ditró and the Bánát Hills.) Stud. Cerc. Geol. Geofiz. Geogr. Ser. Geol., **17/1**, 13–21.

BALINTONI, I. (1981): Date noi asupra poziţiei structurale a metamorfitelor din bazinul văii Putnei (Carpaţii Orientali). [New data on spatial structure of metamorphites from the Putna basin (Eastern Carpathians).] Dări de Seamă ale Şedinţelor Inst. Geol. Geofiz., **LXVI/5**, 25–36, Bucureşti.

BALOGH, K. (1985): K/Ar dating of Neogene volcanic activity in Hungary: technics, experiences and methods of chronological studies. ATOMKI Reports D/1, 277–288.

FÖLDVÁRI, A. (1946): A ditrói nefelinszienit masszívum koráról és kontakt hatásáról. [Age and contact-metamorphic effects of the nephelite syenite stock of Ditró (Transsylvania).] Rel. Ann. Inst. Geol. Hung., B disp, **8/1–2**, 11–32.

HARLAND, W. B., COX, A. V., SMITH, A. G. (1982): A geologic time scale. Cambridge University Press.

IANOVICI, V. (1933): Étude sur le massif syénitique de Ditrău, région Jolotca, district Ciuc (Transylvanie). Rev. Muzeului Geol. Min. Univ. Cluj, **4/2**, 1–53.

IANOVICI, V. (1934): Sur les rockes andésitiques de Ditrău (dép. de Ciuc, Transylvanie). Ann. Scient. Univ. Jassy, **20**, 86–97.

IANOVICI, V. (1938): Considérations sur la consolidation du massif syénitique de Ditrău, en relation avec la tectonique de la région. C. R. Acad. Sci. Roum., ***II/6***, 689–694.

IONESCU, J., TIEPAC, I., UDRESCU, C. (1966): Determination de l'age absolut par la metod Pb. Inst. Geol. St. Tehn. Ec., Seria B, 44, 55–63.

JAKAB, Gy. (1982): Studiul mineralogic şi geochimic al mineralizaţiilor metalifere dintre Voşlobeni şi Corbu. Tez. doct. (The mineralogical and geochemical investigations of metalic mineralization between Vasláb and Holló), Univ. Al. I., Cuza, Iassy, Manuscript.

JAKAB, GY., GARBAŞEVSCHI, N., BALLA, Z., ZAKARIÁS, L., PÉTER, J., STRUNGARU, T., HEREDEA, N., SILEANU, T., ARONESCU, M., POSTOLACHE, C., MOCANU, V., TEULEA, G., HANNICH, D., TIEPAC, I. (1987): Sinteza datelor obţinute prin prospecţiuni geologice complexe, lucrări miniere şi foraje, executate pentru minereuri de metale rare şi disperse, feroase şi neferoase în masivul de roci alcaline de la Ditrău, jud. Harghita. (Synthesis of informations from complex geological mapping, concerning especially the rare elements, ferrous and non ferrous minerals in the alkaline massif of Ditró, Hargita county.) Doc. Dept. of IPEG "Harghita", Miercurea-Ciuc, Manuscript.

JAKAB, GY., POPESCU, G. (1979): Date noi privind vîrsta şi geneza mineralizaţiilor hidrotermale din cristalinul seriei de Tulgheşi, zona Gheorgheni-Bilbor (Carpaţii Orientali). [New Data Concerning the Age and

Genesis of the Hydrothermal Mineralizations in the Tulgheş Series, Gheorgheni-Bilbor Zone (East Carpathians).] Dări de Seamă ale Şedinţelor Inst. Geol. Geofiz., **LXVI**, 37–44, Bucureşti.

KRÄUTNER, H. G. (1976): Das metamorphe Paläozoikum der rumänischen Karpaten. Nova Acta Leopoldina, **45/224**, 335–350.

MAURITZ, B., VENDL, M. (1923): Adatok a ditrói szienitmasszívum abisszikus kőzeteinek ismeretéhez. (Daten zur Kenntnis der abyssischen Gesteine des Syenitmassivs von Ditró.) Mat. term. tud. Értesítő, **XL**, 99–113.

MÎNZATU, S., ARDELEANU, P. (1980): Raport: Cercetări radiometrice de detaliu în masivul Ditrău. (Report: Detailed radiometric investigations in the Ditró Massif.) Doc. Dept. of IPEG "Harghita", Miercurea-Ciuc, Manuscript.

ODIN, G. S., ADAMS, C. J., ARMSTRONG, R. L., BAGDASARYAN, G. P., BAKSI, A. K., BALOGH, K., BARNES, I. L, BOELRIJK, N. A. I. M., BONDADONNA, F. P., BONHOMME, M. G., CASSIGNOL, C., CHANIN, L., GILLOT, P. Y., GLEDHILI, A., GOVINDARAJU, K., HARAKAL, R., HARRE, W., HEBEDA, E. H., HUNZIKER, J. C., INGAMELLS, C. O., KAWASITA, K., KISS, E., KREUZER, H., LONG, L. E., MCDUGALL, I., MCDOWELL, F., MEHNERT, H., MONTIGNY, R., PASTEELS, P., RADICATI, F., REX, D. C., RUNDLE, C. C., SAVELLI, C., SONET, J., WELIN, E., ZIMMERMANN, J. L. (1982): Interlaboratory standards for dating purposes. In Odin, G. S. (ed): Numerical Dating in Stratigraphy, pp. 123–149, Wiley & Sons, Chichester, New York, Brisbane.

PÁL MOLNÁR, E. (1988): Studiul mineralogic şi petrologic al complexului Jolotca din masivul alcalin de la Ditrău, cu privire specială asupra mineralelor purtătoare de fier. (Mineralogical and petrographical study of the Orotva Complex of the Ditró syenite massif, with special respect to the iron-bearing minerals with iron content.) Lucr. dipl., Univ. Babeş-Bolyai, Cluj-Napoca, Manuscript.

PÁL MOLNÁR, E. (1992): Petrographical characteristics of Ditró (Orotva) hornblendites, Eastern Carpathians, Transylvania (Roumania): a preliminary description. Acta Min. Petr., Szeged, **33**, 67–80.

PÁL MOLNÁR, E. (1994a): A Ditrói szienitmasszívum kialakulása a földtani megismerés tükrében. (History of scientific cognition of the origin of Ditró syenite massif.) MTA SzAB Kiad., Szeged.

PÁL MOLNÁR, E. (1994b): Petrographical characteristics of Ditró (Orotva) diorites, Eastern Carpathians, Transylvania (Roumania). Acta Min. Petr., Szeged, **35**, 95–109.

PÁL MOLNÁR, E. (1994c): Adalékok a Ditrói szienitmasszívum szerkezeti és kőzettani ismeretéhez. (Contributions on structural and petrological knowledge of Ditró syenite massif.) MTA SZAB Competition, Manuscript.

REINHARD, M. (1911): Sur l'age de l'intruzion du syénite néphélinique de Ditró, Transylvanie. C. R. Inst. Géol. Rou., **2**, 116.

STEIGER, R. H., Jäger, E. (1977): Subcommission on geochronology: convention on the use of decay constans in geo- and cosmochronology. Earth Planet. Sci. Lett., **36**, 359–362.

STRECKEISEN, A. (1931): Über das Nephelinsyenit-Massiv von Ditro (Rumänien). Neues Jahrb. f. Mineral., **64/A** (Brauns-Festband), 615–628.

STRECKEISEN, A. (1952): Das Nephelinsyenit-Massiv von Ditro (Siebenbürgen), I. Teil. Schweiz. Min. Petr. Mitt., **XXXII**, 251–309.

STRECKEISEN, A. (1954): Das Nephelinsyenit-Massiv von Ditro (Siebenbürgen), II. Teil. Schweiz. Min. Petr. Mitt., **34**, 336–409.

STRECKEISEN, A., HUNZIKER, I. C. (1974): On the origin of the Nephelinsyenit Massiv of Ditró (Transylvania, Romania). Schweiz. Min. Petr. Mitt., **54**, 59–77.

VISARION, M. (1987): Studii geologice şi geofizice complexe pe geotraversa Paşcani-Tg. Neamţ-Topliţa-Reghin. (Complex geological and geophysical study in the geotraverse of Paşcani-Tg. Neamţ-Topliţa-Reghin.) Doc. Dept of Inst. Geol. Geofiz., Bucuresti, Manuscript.

Manuscript received 13 June, 1995.

Acta Mineralogica-Petrographica, Szeged, XXXVI, 117–128, 1995

RETROGRADED ECLOGITE IN THE CRYSTALLINE BASEMENT OF TISZA UNIT, HUNGARY

T. M. TÓTH

Institut of Mineralogy, Geochemistry and Petrology, Attila József University*

ABSTRACT

Crystalline basement of Eastern part of Tisza Unit in Hungary has been said to be built up of amphibolite facies rocks. However, some samples of these contain relics of an earlier high pressure event and sporadically eclogitic remnants also occur. A symplectitic rock from borehole Kőrösladány-5 includes garnet fragments (Py ≈ 30%), phengite, rutile and also pseudomorph after alkali pyroxene. These traces corresponding to other mineralogical observations imply a one-time B or C type eclogitic material.

INTRODUCTION

Crystalline basement of Tisza Unit (Pannonian Basin) consists of mica schist and gneiss as the most common metamorphic rocks. There are also some amphibolite bodies forming thin intercalations in the other metamorphites. The mineralogical composition and textural features of these rocks refer to a Barrow type metamorphism with a peak condition of medium pressure and temperature. In the southern part of the Unit (Codru nappe) andalusite bearing metamorphites occur as well, suggesting a LP phase of metamorphic history (SZEDERKÉNYI, 1984). There has also been very little data of high pressure metamorphism in the northern part of Tisza Unit. The first information on HP rocks was an eclogitic sample found in the borehole Görcsöny-1 (RAVASZNÉ BARANYAI, 1969). This rock is retrograded and contains only pseudomorph after garnet and pyroxene referring to the preceding quality of it. In addition to this sample some relict parageneses were found in amphibolitic rocks in the eastern part of Biharian Autochthonous, which point to an earlier high pressure metamorphic phase (M. TÓTH, 1995a). As a result of a microscopic work both traces of eclogite and blueschist facies metamorphism were found. However, since all samples are sufficiently altered, only a detailed mineralogical study may confirm the existence of the earlier HP metamorphism.

In the near past I was allowed to measure significant minerals of an altered eclogite sample by electron microprobe at the University of Berne in Switzerland. The purpose of this paper is presentation of this sample and interpreting its significance in the crystalline basement of Tisza Unit.

* H-6701 Szeged, P. O. Box 651, Hungary

GEOLOGICAL SETTING

Tisza Unit is located in south and south-east Hungary and also may be traced in Rumania, Serbia and Croatia. In the Palaeozoic time it was a part of the European basement and got to its present setting due to Alpine movements. During Alpine orogenesis a complicated nappe structure formed in the Tisza Unit. The subsequent nappes differ from each other petrologically and may be traced on the surface in the Apuseni Mountains. In Hungary the existence of "Biharian Autochthonous" and Codru nappe has been inferred so far (SZÁDECZKY–KARDOSS, 1970; SZEDERKÉNYI, 1984; BALÁZS et al., 1984). Since metamorphic rocks in the Hungarian part of Tisza Unit are covered by more than 2000 m thick young sediments, only crystalline rocks from borecores may be examined.

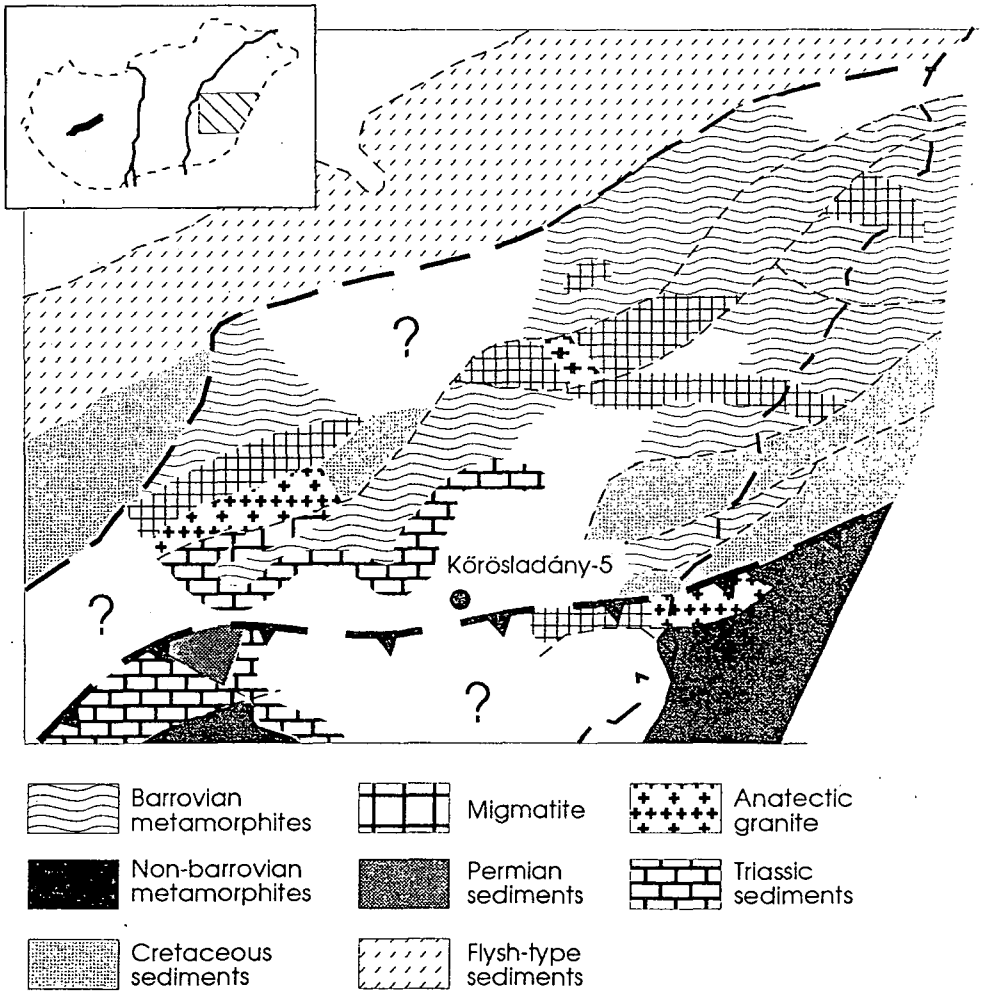

Fig. 1. Simplified geological map of Eastern Tisza Unit and location of borehole Kőrösladány-5

The sample in question came from borehole Kőrösladány-5 (*Fig. 1*) which is in the area of Biharian Autochthonous (SZEDERKÉNYI, 1984) not far (about 10 km-s) from the border of Codru nappe. Surrounding borecores consist mainly of micaschist and gneiss. Relative to other parts of Tisza Unit, in this small sub-area, amphibolite is also a frequent rock type. Detailed geochemical examination showed the protolith of these metabasic rocks back-arc basin type tholeiite (M. TÓTH, 1994). Further geochemical and multivariate mathematical methods inferred that amphibolite samples preserve subsequent stages of a former-tholeiitic differentation trend (M. TÓTH, 1995b). Amphibolite samples from boreholes in question all represent a primitive or partially differentiated T-MORB basalt. Petrologically all these metamorphosed basalt samples, but one, have equilibrium texture and consist of minerals of common amphibolite paragenesis (LAIRD, ALBEE, 1981): Ca-amphibole, plagioclase, with or without garnet, epidote, quartz. However, these samples also suggest uncertain signs of previous high pressure (M. TÓTH, 1995a). Hornblende often contains a big quantity of albite rimmed inclusions of magnetite referring to a reaction product of an earlier sodic amphibole (YARDLEY, 1982). Mica schist and gneiss have not been reported yet to show any relict high pressure paragenesis, though these rock types have not been investigated in detail yet.

There is only one sample which contains high pressure minerals and relict textural characteristics referring to an earlier eclogite facies metamorphism.

MINERALOGICAL FEATURES OF THE RETROGRADED ECLOGITE SAMPLE

The sample is characterized by a conspicuous duality. The bigger part of it has symplectitic texture (*Fig. 2/a*). Mineralogical composition of a pseudomorph is fairly difficult to recognize under microscope. It consists of a set of very fine grained amphibole, plagioclase and white mica. As amphibole is almost colourless its composition must be close to tremolite. Sometimes chlorite and epidote may be identified. All of these symplectites have a zoned structure. The fine grained core is rounded by coarser grains of plagioclase. Between these relics of earlier minerals newly formed amphibole occurs forming a duality of a rock (*Fig. 2/a*). These amphibole grains have a pale green colour opposite to those in the pseudomorphous part of the rock. Occasionally small garnet grains occur in this rock with many opaque minerals (magnetite, ilmenite) and also some biotite around them (*Fig. 2/b*). The frequency of this secondary paragenesis suggests that the rock before the alteration may have contained conspicuous amount of big garnet grains.

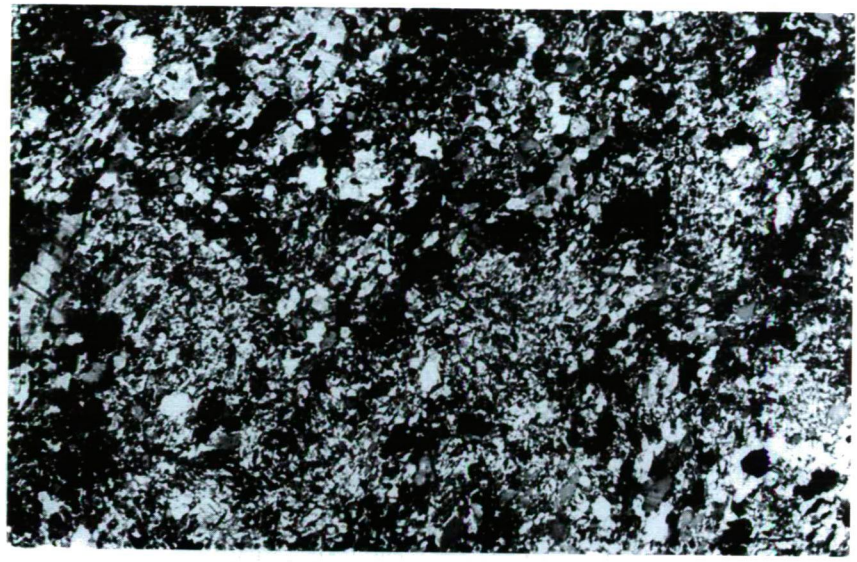

Fig. 2. (a) Secondary amphibole and plagioclase around fine grained symplectite of tremolite, albite and white mica.

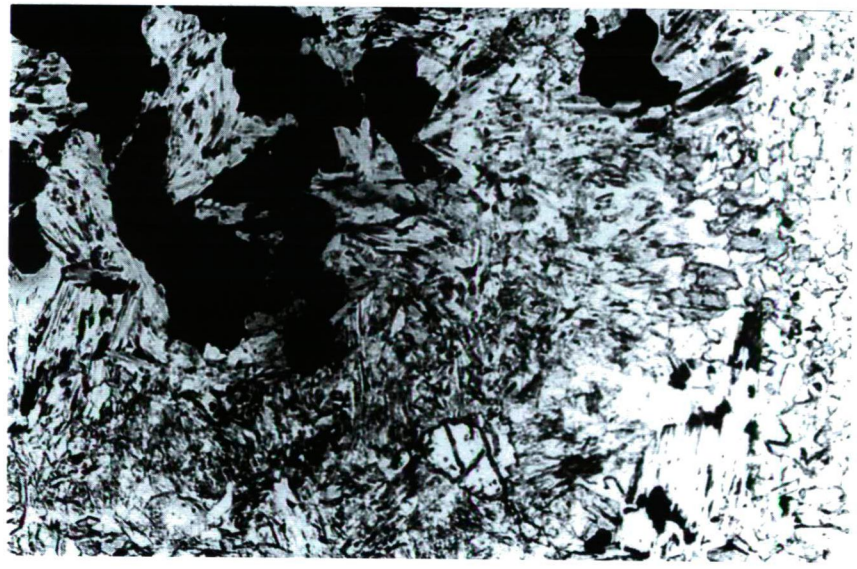

Fig. 2. (b) Small garnet relict as well as secondary biotite and opaque minerals

GARNET

The rock sample studied contains only a very few garnet grains, all small in size. However, garnet is always surrounded by the minerals mentioned above implying that these garnet fragments are the remains of a previously larger grain existed in an earlier stage of metamorphic history. Relict garnet grains are not zoned chemically, and they all have a very similar composition. Representative garnet analyses are given in Table 1, while calculated end-members are plotted in *Fig. 3*. The relatively high pyrope content (about 30%) of garnet shows that this mineral may have formed under eclogite facies. The typical composition of garnet examined belong to the border of B and C type eclogite fields (COLEMAN et al., 1965).

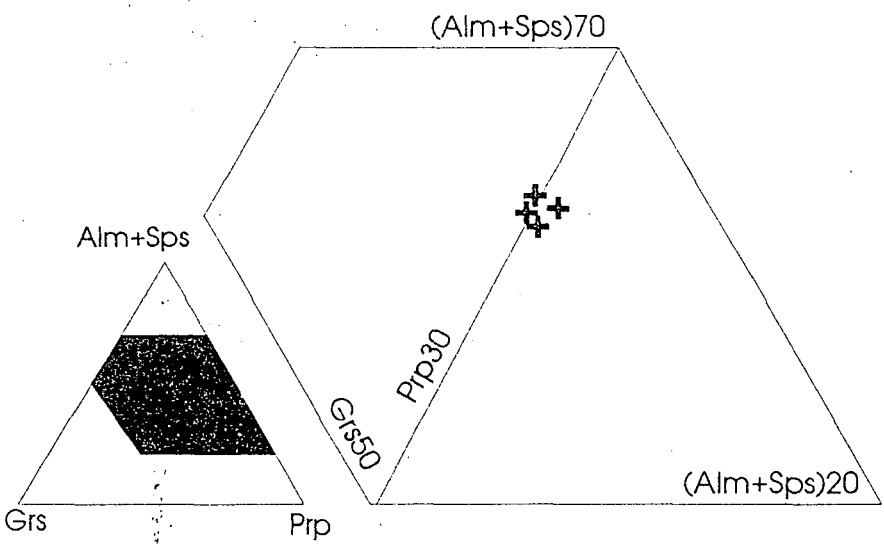

Fig. 3. Garnet analyses plotted in the (Alm+Sps)–Prp–Grs triangular diagram of COLEMAN et al. (1965)

TABLE 1

Representative chemical analysis of characteristic minerals

	Garnet	Amphibole$_1$	Amphibole$_2$	White mica	Ilmenite
SiO_2	39.06	49.70	40.55	49.51	0.00
TiO_2	0.04	0.25	0.49	0.00	60.34
Al_2O_3	22.60	5.31	15.29	28.25	0.00
FeO	20.59	13.58	15.45	2.13	36.84
MnO	0.40	0.26	0.26	0.00	2.51
MgO	7.74	13.88	9.45	3.05	0.00
CaO	8.65	10.90	10.44	0.06	0.18
Na_2O	0.00	0.47	1.65	0.05	0.00
K_2O	0.00	0.14	0.61	10.35	0.00
Total	99.08	94.49	94.19	93.40	99.88

AMPHIBOLE

Amphibole has two typical occurences in the sample examined. There are colourless amphibole paths very small in size in the symplectitic part of the rock forming the first amphibole generation. There is also a secondary generation of amphiboles around the margins of symplectites. These latter grains are strongly pleochroic, and differ from symplectite amphiboles in both shape and size. Representative amphibole analyses of both types are given in Table 1. Different important parameters are plotted on *Fig. 4*. This figure suggests that the two kinds of amphibole from an exact series of development. In general, symplectitic ones are close to tremolite in composition. These grains are magnesian and have little tetrahedral alumina, they contain essentially no sodium in the M4 site and only few alkalies in the A site. This composition may be expected for a low pressure and relatively low temperature phase (LAIRD, 1982). Secondary amphiboles, however, are pargasites and the diagrams on *Fig. 4*. clearly show the development of

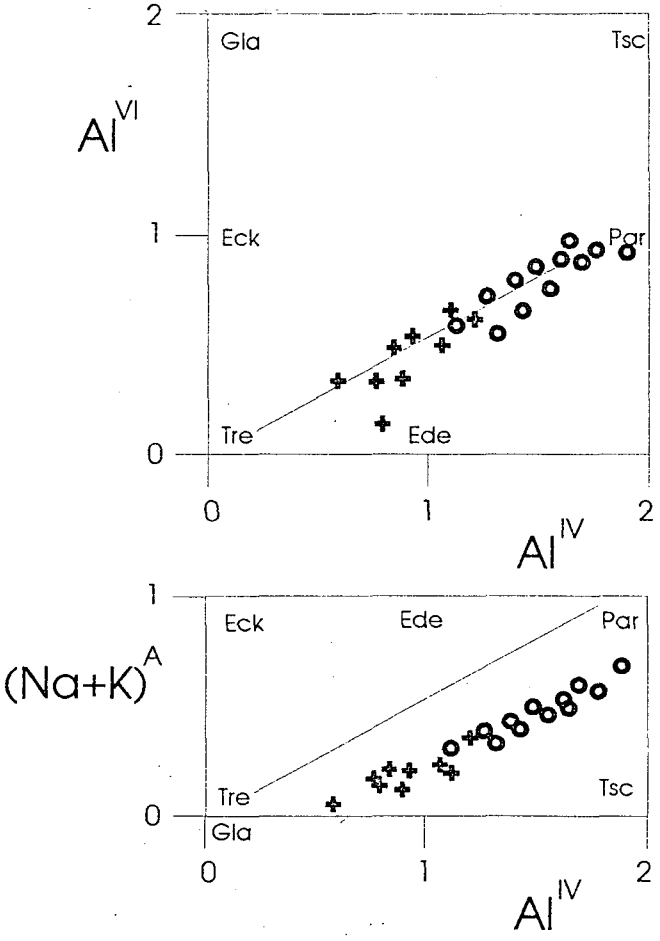

Fig. 4. Plotting of amphibole analyses in Al^{IV}–Al^{VI} and Al^{IV}–$(Na+K)_A$ diagrams. Evolutional trends suggest the significance of tschermak and edenite substitution. Sign "+" represents sypmlectitic grains while sign "o" secondary grains

amphibole grains from tremolitic towards the near pargasitic composition. That is, tschermak (Mg_{-1} Si_{-1} Al^{IV} Al^{VI}) and edenite (λ_{-1} Si_{-1} Na^{A} Al^{IV}) substitution must have played a significant role in change of amphibole composition, refererring to increasing temperature during metamorphic history (BANNO, 1964; BARD, 1970; HIETANEN, 1974).

PLAGIOCLASE

Both fine grained symplectite and the secondary part of the rock contain plagioclase in significant amount. Symplectites always contain plagioclase and most of these relict structures are surrounded by plagioclase grains yielding a zoned building of them. Plagioclase also occurs together with pargasitic amphiboles as secondary mineral. Chemically two discrete groups of feldspar are present, albite (An < 5%) and a more Ca-rich face (35% < An < 45%) (Fig. 5.). Though this distinction is evident, the tendency of their occurrence in space is obscure. As a secondary mineral only the An-rich plagioclase can be found, however, symplectites contain grains of both compositions. Probably, albite forms the original symplectitic face, while An-rich plagioclase occurs due to increasing temperature of metamorphism.

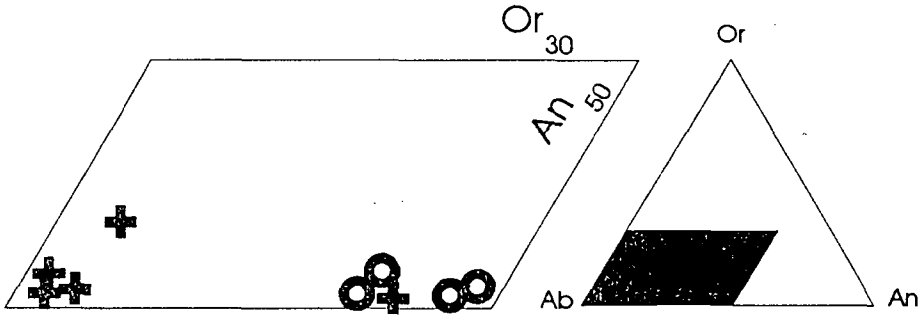

Fig. 5. Plagioclase analyses plotted on Ab–An–Or triangular diagram. Sign "+" represents symplectitic grains while sign "o" secondary grains

OTHER MINERALS

In addition to tremolite and albite, symplectites also contain different amounts of white mica. These grains are muscovites with a various phengitic component, silica in tetrahedral position differs between 3.2 and 3.3 with one outstanding value (3.46) (Fig. 6.). The high phengite content of the white mica may imply this mineral to be an eclogitic remnant. Na-content of the mica (paragonite) is low, < 15%.

The breakdown of garnets, presented in detail above, yielded biotite and ilmenite. Biotite is magnesian (X_{Fe} < 0.5) and relatively poor in Ti (0.17–0.22). Ilmenite occurs always in intergrowth with very fine-grained rutile needless suggesting that the original garnet, as eclogitic garnets commonly do, contained rutile inclusions. Mn-concentration in ilmenite (pyrophanite) is rather high (MnO > 2.5%).

The sample examined also contain a small amount of chlorite, epidote, tremolite and magnetite forming small symplectites together with albite.

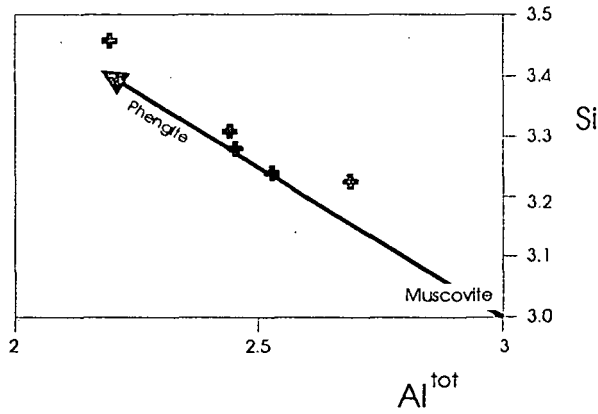

Fig. 6. Evolution of white mica on the Altot–Si diagram

THERMOBAROMETRY

Since, not even a little part of the examined sample shows an equilibrium texture, neither of possible geothermometers or geobarometers (garnet-biotite, plagioclase-amphibole, GRISP, etc.) may be applied. However, the compositional change of different relict and newly formed minerals may let us estimate the physical conditions of the metamorphic history. Chemical composition of the few garnet fragments suggests that the original metamorphic rock before any retrograde alteration may have been a B or C type eclogite (*Fig. 3.*). Theoretically, the temperature border between the two varieties is at 550 °C as an initial temperature of metamorphism may only be accepted approximately. Estimation of pressure in low temperature eclogite is problematical even in the case of stable eclogite (GHENT, STOUT, 1994). Supposed white mica (phengite) is also a relict eclogitic mineral, its chemical composition may give more information about the initial conditions of the eclogite facies metamorphism. The low paragonite-content of white mica implies temperature not lower than 450 °C based on diagrams of SASSI et al. (1994). Presuming the temperature about 500 °C, the Si-content of phengite yields pressure in the range of 10–13 kbar (MASSONE, SCHREYER, 1987).

The occurence of the tremolite+epidote+magnetite+albite+chlorite paragenesis in the retrograded eclogite may point to the previous existence of crossite as original component of eclogite (BROWN, 1977; YARDLEY, 1982; MARUYAMA et al., 1986). Assuming the appearance of alkali amphibole as initial high pressure constituent one can confirm that eclogite was metamorphosed under low to medium temperature (< 550 °C) (MARUYAMA et al., 1986 and references therein).

Although the sample examined contain no pyroxene grain, the previous existence of this mineral may be assumed. The first step of retrograde breakdown of eclogitic pyroxene is the formation of a less jadeite-rich pyroxene and a Na-rich plagioclase. Later, the secondary pyroxene grains are substitued by amphibole, white mica and more plagioclase. These processes result in a symplectitic intergrowth of amphibole and plagioclase (O'BRIEN, 1993).

The fact that no orthopyroxene formed in the place of original eclogitic clinopyroxene as a secondary mineral suggests that retrogression may have been characterized by

decreasing temperature (O'BRIEN, 1993). This estimated tendency of breakdown history is confirmed also by the chemical character of garnet replacing minerals: ilmenite and biotite. The Mn-content of ilmenite (proportion of pyrophanite) is higher the lower the metamorphic temperature of formation is (POWNCEBY et al., 1987a, 1987b). This value in the ilmenite grains from our sample is much higher than it would be expected in the realm of amphibolite or granulite facies. The low content of titanium in biotite implies the greenschist grade formation of it (GUIDOTTI, 1984) verifying the low breakdown temperature of the original eclogitic garnets. All these things considered, the breakdown of the original eclogite was controlled by decreasing both pressure and temperature.

Therefore, the mineral assemblage of symplectites, mainly tremolite and albite, represents the lowest P and T phase of metamorphic history. The appearance of these two significant minerals refers to the conditions of greenschist facies. The temperature of this phase must not have been higher than 450–480 °C and assumed pressure not higher than 5 kbar (*Fig. 7.*).

The only fresh minerals in the sample are Ca-amphibole with high pargasite content and plagioclase (An_{35-45}) representing physical conditions of amphibolite facies. Both tschermak substitution in amphibole and Ca enrichment in feldspar infer that greenschist facies was succeeded by increase of temperature. The stable amphibole-plagioclase paragenesis corresponds to that of amphibolite common in surrounding borecores. Metamorphic condition of these metabasic rock is calculated to be 580–600 °C and 4–6 kbar (SZEDERKÉNYI, 1984).

A sketch of the three subsequent phases of estimated metamorphic development of the retrograded eclogite sample is given in *Fig. 7.*

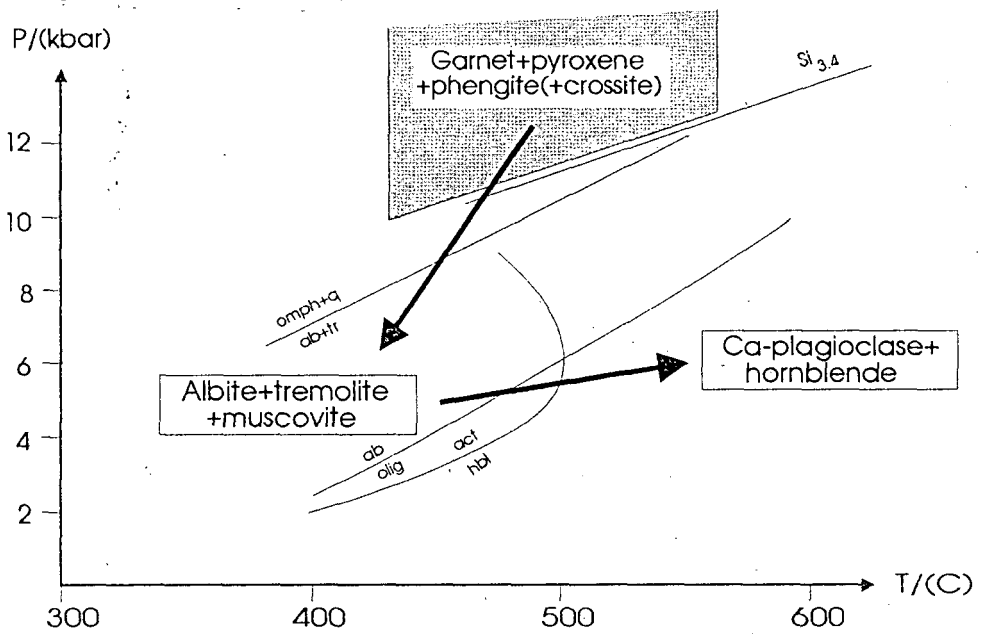

Fig. 7. Estimated PT-path of the eclogite from borehole Kőrösladány-5, stability fields of subsequent mineral parageneses and boundaries of important reactions. Albite-oligoclase and actinolite-hornblende transitions (MARUYAMA et al., 1983); isopleth of Si in phengite (MASSONE, SCHREYER, 1987); omphacite+quartz = albite+tremolite (NEWTON, 1986)

CONCLUSIONS

Based on detailed mineralogical investigation the retrograded eclogite sample from the borehole Kőrösladány-5 proved to be a B or C type eclogite. Unfortunately, the rock contain no stable high pressure paragenesis, so only the estimation of the physical condition of development is possible. Based on it, the rock was formed under low to medium temperature (450–550 °C), while the evaluated pressure was as least 10–13 kbar. The breakdown of the eclogite was controlled by decreasing temperature yielding vermicular symplectites of tremolite, albite and white mica in the place of previous clinopyroxene. The last progressive metamorphic effect was an amphibolite facies overprint corresponding to other metabasic rocks in the surrounding boreholes.

Previous works inferred that the protolith of amphibolite and other metabasic rocks from the investigated area was tholeiitic basalt formed in a back-arc basin (M. TÓTH, 1994). Recent papers on metamorphic as well as exhumation development of back-arc basins showed a special cooling history of such regions (*Fig. 8.*) (JOLIVET et al., 1994 and references therein). In the case of Naxos and Corsica the typical P-T path is characterized by low peak temperature (about 450 °C) and not very high peak pressure (lower than 14 kbar). The original HP-LT associations broke down to greenschist facies parageneses.

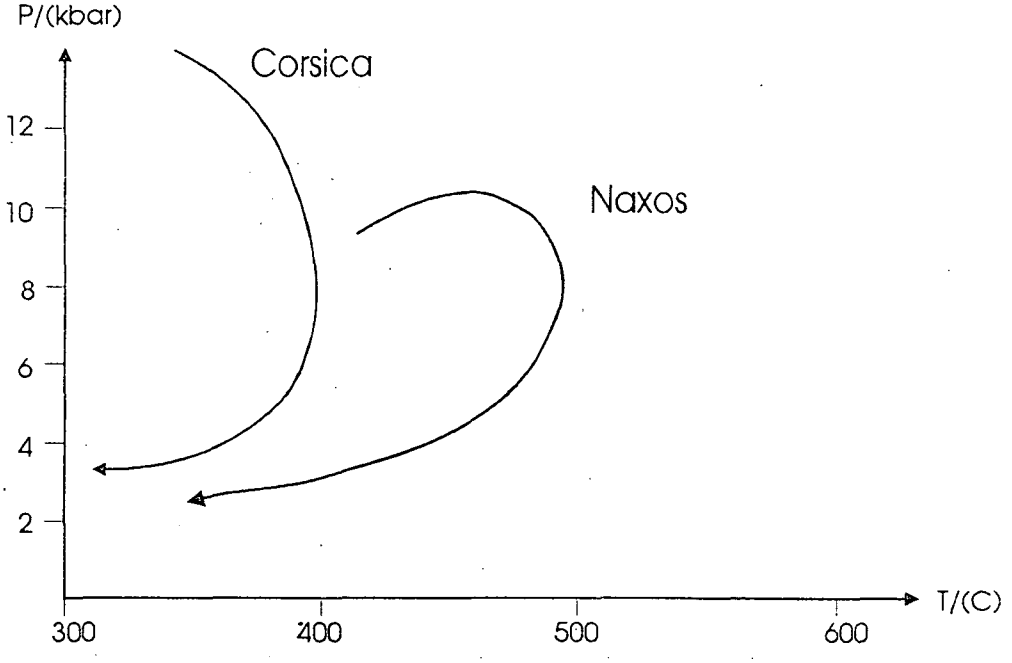

Fig. 8. Metamorphic development and cooling history of back-arc basins during exhumation (after JOLIVET et al., 1994).

All these features are similar to those were concluded from the retrograded eclogite from borehole Kőrösladány-5. Therefore, the metamorphic evolution of this sample corresponds to the previous findings that the investigated area of Tisza Unit belonged to a one-time marginal basin.

There are some papers as well as unpublished data which call attention to similar petrological, chronological etc. characteristics between Tisza Unit and the eastern part of European Variscides, especially Bohemian Massif. In addition to investigation of these correspondences the comparison of metamorphic evolution of HP rocks in the two areas seems important. In the Bohemian Massif the peak pressure and temperature of eclogitic rocks as well as the breakdown temperature of them decreases from south to north (O'BRIEN, 1993, MEDARIS et al., 1995). This tendency yields the common occurrence of granulite facies rocks in the Moldanubian part of the massif, while in Sudetes C-type eclogite (SMULIKOWSKI, SMULIKOWSKI, 1985) and in Lugicum also blueschist occurs (GUIRAUD, BURG, 1984). Supposed the Tisza Unit the eastern continuation of European Variscan Belt, based on the similar characteristics of HP rocks, the small area examined in this paper may have belonged to the northern part of Bohemian Massif.

ACKNOWLEDGEMENT

Gy. Lelkes-Felvári is thanked for calling my attention to the examined rock sample. The author wish to express appreciation to Schweizerischer Nationalfonds (Credit 21-26579.89) for supporting of microprobe analysis at University of Bern. The authors researches in Switzerland were financially supported by Hungarian Scholarship Committee.

REFERENCES

BALÁZS, E. ed. (1984): Az Alföld prekambriumi-, paleozóos-, triász-, jura és alsókréta korú képződményeinek összefoglaló áttekintése a mezozóos és idősebb összletek szénhidrogén prognózisa szempontjainak megfelelően; I. Prekambrium-paleozoikum. (Conclusion of the Precambrian, Paleozoic, Triassic, Jurassic and Lower-Cretaceous formations of the Great Hungarian Plane in accordance with hydrocarbon prognostic of mesozoic and older formations; I. Precambrian, Paleozoic); SZKFI, Manuscript.

BANNO, S. (1964): Petrologic studies on Sanbagawa crystalline schists in the Bessi-Ino district, central Shikoku, Japan. Journal of the Faculty of Science, University of Tokyo, II/15, 203–319.

BARD, J. P. (1970): Compositions of hornblendes during the Hercynian progressive metamorphism. Journal of Petrology, **18**, 53–72.

COLEMAN, R. G.; LEE, D. E.; BEATTY, L. B.; BRANNOCK, W. W. (1965): Eclogites and eclogites: their differences and similarities. Geological Society of America Bulletin, **76**, 483–508.

GHENT, E. D.; STOUT, M. Z. (1994): Geobarometry of low-temperature eclogites: applications of isothermal pressure-activity calculations. Contributions to Mineralogy and Petrology, **116**, 500–507.

GUIDOTTI, C. (1984): Micas in the metamorphic rocks. In: Micas, Reviews in Mineralogy 9B, Chelsea.

GUIRAUD, M.; BURG, J. P. (1984): Mineralogical and petrological study of a blueschist metatuff from the Zelezny Brod Crystalline Complex, Czechoslovakia. Neues Jahrbuch Miner. Abh., **149**, 1–12.

HIETANEN, A. (1974): Amphibole pairs, epidote minerals, chlorite and plagioclase in metamorphic rocks, northern Sierra Nevada, California. American Mineralogist, **59**, 22–40.

JOLIVET, L.; DANIEL, J. M.; Truffert, C.; Goffé, B. (1994): Exhumation of deep crustal metamorphic rocks and crustal extension in arc and back-arc regions. Lithos, **33**, 3–30.

LAIRD, J. (1982): Amphiboles in metamorphosed basaltic rocks. In: Amphiboles, Reviews in Mineralogy 9B, Chelsea.

LAIRD, J.; ALBEE, A. L. (1981): Pressure, temperature, and time indicators in mafic schist: their application to reconstructing the polymetamorphic history of Vermont. American Journal of Science, **281**, 127–175.

M. TÓTH, T. (1994): Geochemical character of amphiboles from Tisza Unit on the basis of incompatible trace elements. Acta Mineralogica-Petrographica, Szeged, XXXV: 27–38.

M. TÓTH, T. (1995a): Magas nyomású metamorfózis nyomai a Tisza Egység aljzatában. (Traces of high pressure metamorphism of the amphibolites from Tisza Unit, Eastern Hungary) Földtani Közlöny, in press (Both Hungarian and English).

M. TÓTH, T. (1995b): Pre-metamorphic history of amphibolites from Kőrös Complex, Pannonian Basin: A geomathematical approach. Mineralogy and Petrology, in press.
MARUYAMA, S.; SUZUKI, K.; LIOU, J. G. (1983): Greenschist-amphibolite transition equilibria at low pressures. Journal of Petrology, **24**, 583–604.
MARUYAMA, S.; CHO, M.; LIOU, J. G. (1986): Experimental investigations of blueschist-greenschist transition equilibria: Pressure dependence of Al_2O_3 contents in sodic amphiboles – A new geobarometer. In: Blueschists and eclogites, Geological Society of America Memoir **164**, 1–16.
MASSONE, H. J.; SCHREYER W. (1987): Phengite geobarometry based on limiting assemblage with K-feldspar, phlogopite and quartz. Contributions to Mineralogy and Petrology, **96**, 212–224.
MEDARIS, G. Jr.; JELINEK, E.; MÍSAR, Z. (1995): Czech eclogites: Terrane settings and implications for Variscan tectonic evolution of the Bohemian Massif. European Journal of Mineralogy, **7**, 7–28.
NEWTON, R. C. (1986): Metamorphic temperatures of Group B and C eclogites. In: EVANS, B. W.; BROWN, E. H. eds.: Blueschists and Eclogites; The Geological Society of America Memoir 164.
O'BRIEN, P. J. (1993): Partially retrograded eclogites of Münchberg Massif, Germany: records of a multy-stage Variscan uplift history in the Bohemian Massif. Journal of Metamorphic Geology, **11**, 241–260.
POWNCEBY, M. I.; WALL, V. J.; O'NEILL, H. ST. C. (1987a): Fe-Mn partitioning between garnet and ilmenite: experimental calibration and applications. Contributions to Mineralogy and Petrology, **97**, 116–126.
POWNCEBY, M. I.; WALL, V. J.; O'NEILL, H. ST. C. (1987b): Fe-Mn partitioning between garnet and ilmenite: experimental calibration and applications; Erratum. Contributions to Mineralogy and Petrology, **97**, 539.
RAVASZNÉ BARANYAI, L. (1969): Eclogite from the Mecsek Mountains, Hungary. Acta Geologica Academiae Scientiarium Hungaricae, **13**, 315–322.
SMULIKOWSKI, K.; SMULIKOWSKI, W. (1985): On the porphyroblastic eclogites of the Snieznik Mountains in the Polish Sudetes. In: Chemistry and petrology of eclogites, Chemical Geology, **50**, 201–222.
SZÁDECZKY-KARDOSS, E. (1970): Subsidence and structural evolution mechanism in the Pannonian Basin. Acta Geologica Academiae Hungaricae, **14**, 83–93.
SZEDERKÉNYI, T. (1984): Az Alföld kristályos aljzata és földtani kapcsolatai. (The crystalline basement of the Great Hungarian Plane and its geological connections); Academic doctor theses, Hungarian Academy of Sciences, Budapest (In Hungarian).
YARDLEY, B. W. D. (1982): The early metamorphic history of the Haast schist and related rocks of New Zealand. Contributions to Mineralogy and Petrology, **81**, 317–327.

Manuscript received 13 June, 1995.

Acta Mineralogica-Petrographica, Szeged, XXXVI, 129–142, 1995

PETROGRAPHICAL STUDY OF SUBVOLCANIC ROCKS SURROUNDING OF MÓRÁGY AND ÓFALU (SE-TRANSDANUBE, HUNGARY)

CS. SZABADOS*

Department of Mineralogy, Geochemistry and Petrography, Attila József University

ABSTRACT

Rock types described as bostonites by MAURITZ and CSAJÁGHY (1952), JANTSKY (1972) are characterized in this paper. They can be subdivided into two groups: (1) Light-reddish, brownish-coloured, fine-grained rock characterized by trachytic texture with potassium feldspar microlites in the groundmass showing a subparallel arrangement among K-feldspar phenochrysts forming by flow parallely with the wall-rock. This type occurs only in dykes which penetrate the granite mass. On the basis of petrographical examinations this group is classified as alkalitrachyte. (2) Greenish, greyish-coloured, fine-grained rock characterized by a micro-holocrystalline, porphyritic texture. It forms a small laccolith-like subvolcanic body in the quarry of Kismórágy No. 5. and like a centre, dykes run from here to every directions. On the basis of petrographical examinations this group is classified as trachyandesite (or latite).

INTRODUCTION

The researched rocks outcrop in the territory of Mórágy, Kismórágy, Bátaapáti and Ófalu (*Fig. 1.*), but they occur in the boreholes of Alsónána No. 1 and 2., too. As pebbles they also appear in the NE Mecsek Mountains (SZAKMÁNY and JÓZSA 1994).

The origin and age of these rocks are unsettled question. MAURITZ and CSAJÁGHY (1952) regarded them bostonites on the basis of their mineralogical composition and major element content which can be ranged them into the products of granitoide magmatism or the Early Cretaceous volcanism.

Using the bostonite term is fitting if the origin of these rock-types are really granitoid. Bostonite ("soda-trachyte-aplite", TRÖGER 1935) is the silky, leucocratic, faneritic, hypabyssal syenitic dyke-rock. It is characterized by a trachytic or flow texture in which lath-like feldspar grains are arranged in a rough, but no perfect, parallelism or in radiating patterns. The groundmass consist mostly of alkali feldspar at least in 90% portion. The porphyritic version contains feldspar phenocrysts. The feldspar may be orthoclase, microcline, sanidine, anorthoclase or albite. Biotite, alkali amphibole or pyroxene form the scarce ferromagnesian minerals. Quartz in small amounts (max. 10%) is almost always present, particularly in the matrix. According to ROSENBUCH (1907) every type which has more than 90% alkali feldspar (plagioclase is or no), may be classified as bostonite rock. This term has been used rarely in the modern literature, moreover the Glossary of Geology (1980) does not recommend the usage of bostonite name.

K/Ar age of examined rocks is ranged in Early Cretaceous (106–117 Ma, ÁRVÁNÉ S. E. 1987). A "Bostonite" and an Early Cretaceous alkaline basalt dyke contact penetrated by

* H-6701 Szeged, P. O. Box 651, Hungary

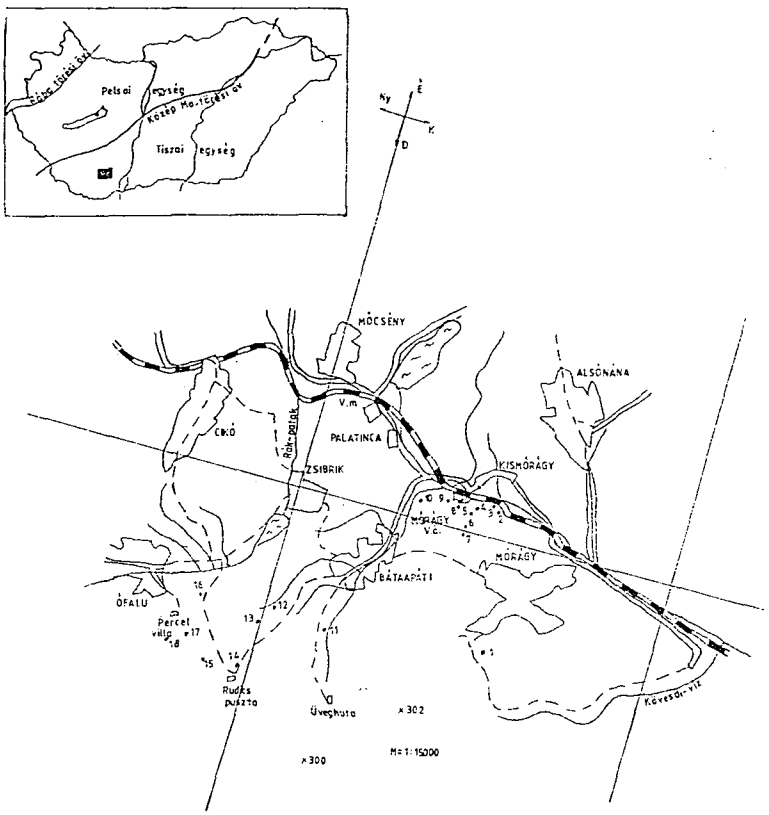

Fig. 1. Occurrence of the subvolcanic trachytic rocks in the investigated area
1. Mórágy quarry (reddish dyke), 2. Kismórágy quarry (reddish dyke), 3. Kismórágy quarry (reddish dyke), 4. Kismórágy quarry, No. 6. (greenish dyke), 5. Kismórágy quarry, No. 5. (greenish laccolith), 6. Kismórágy quarry, No. 3. (reddish dyke), 7. Kismórágy quarry, No. 1. (reddish dyke), 8. Kismórágy quarry, No. 10. (greenish vein), 9. Kismórágy quarry (reddish dyke), 10. Kismórágy, outcrop (reddish dyke), 11. Bátaapáti, outcrop (reddish dyke), 12. Bátaapáti Köves-creek, outcrop (reddish dyke), 13. Bátaapáti Köves-creek, outcrop (reddish dyke), 14. Rudics farm, outcrop (reddish dyke), 15. Ófalu, Aranyos-valley, outcrop (reddish dyke), 16. Studer valley, outcrop (reddish pebbles), 17. Ófalu, Aranyos-valley, outcrop (reddish dyke), 18. Ófalu, Till farm-valley, outcrop (reddish dyke).

the borehole Alsónána No. 1. suggests that the bostonite is younger than the Early Cretaceous volcanism (JANTSKY 1979). So, these (bostonite) rocks can be regarded Early Cretaceous alkalitrachytes, trachytes.

Aim of this paper to give a mineralogical-petrographic and tectonic characterization of these rocks using also field observations.

PETROGRAPHICAL CHARACTERIZATION

On the basis of the field observations, colour, mineralogical composition and textural features this trachytic group can be divided into two types: (1) Reddish-brownish coloured dyke rocks, (2) greenish-coloured laccolith-like rocks.

1. Reddish-brownish dyke-rocks

Aphyric, from fine-grained to slightly porphyric, visibly fluidal arrangement compact rocks occuring as 0.1 m to 20 m thick veins or dykes which penetrate the granite (*Fig. 1.* No. 1, 2, 3, 5, 7, 9–15). Generally these penetrations are in relations with faults and close to their contacts typical granite mylonite stripes with calcite veinlets are characteristic. However, some dykes invade into metamorphic rocks, too (Ófalu Formation in the valleys East of Ófalu *Fig. 1.* No. 17, 18).

Spatial arrangement of dykes shows a predominant E-W orientation (*Fig. 1.* No. 1, 6, 12), but N-S and NE-SW ones also occur (*Fig. 1.* No. 2, 3, 7, 9, 15, 17). Dip of dykes are steep, 75°–90°. Their rocks contain naked eye feldspar phenocrysts, rarely. Tabular sanidine in 1 cm size, and red-stained tabular orthoclase crystals are embedded into the microcrystalline groundmass. But the smaller portion of these phenocrysts are empty cavities or pseudomorph calcites surrounded by limonite coat.

On the basis of their granulation these rocks can be divided into two subtypes:

(1) Fine-grained, light coloured rocks without phenocryst located into the thin (0,6 m thick) veins (*Fig. 1.* No. 6, 18).

(2) Phorphyric, fine-grained, dark-coloured rocks having a coarser groundmass than that of the previous type (*Fig. 1.* No. 1, 17, 18). A naked eye fluid texture is characteristic.

1.1. Description of typical outcrops of dyke rocks

1.1.1. Dyke in the granite quarry at Mórágy free time centre

A 2.8–3.4 m thick dyke outcropping the southern side of quarry having a 6–8 m height is open along its strike in 10 m length (*Fig. 2.*). This rock penetrate the granite next to a fault having 360°/85–90° dip. The northern side of dykes is fractured. A 1–2 cm thick calcite vein marks the contact of dyke and granite. A 1–2 m thick and strongly sheared granite wall-rock accompany the dyke with a network of calcite veinlets.

Megascopically the rock is reddish in colour and ranged into the 2. type.

Microscopically it shows a microholocrystalline trachytic texture (*Fig. 3*) and the microlites of groundmass manifest more or less fluidal arrangement. The oriented samples shows that the dyke material flowed from East to West (before the rock solidification). The groundmass consist mostly of lathy, elongated perfectly crystallized alkali feldspar, mainly sanidine. The lath-like feldspars are arranged parallely, but near the phophyritic crystalls they follow their outlines. Average grain size of groundmass material measures 24×240 μm. They form 85% portion of the rock. Sanidine phenocrysts are scarce and their average size is 144×780 μm. (*Fig. 4.*). Xenomorphic quartz fills the interstitial places between sanidines in the groundmass giving 10% portion of the rock. Idiomorphic quartz in typical hexagonal prism also occurs. Limonitization and hematitization are rather common. Limonite (2% of the groundmass) display as unshaped, reddish-brownish-coloured patches originating from the breakdown of pyrite but in several parts of the rock small fresh pyrite hexaeders are preserved. In the groundmass are a lot of very small grains of zircon (8×7 μm). Opak minerals are also visible sporadically in less than 2% portion. Secondary minerals are calcite and calcedony after decay of feldspars (1% of the groundmass). On the basis of mineralogical composition this rock can be classified as alkaliquartztrachyte.

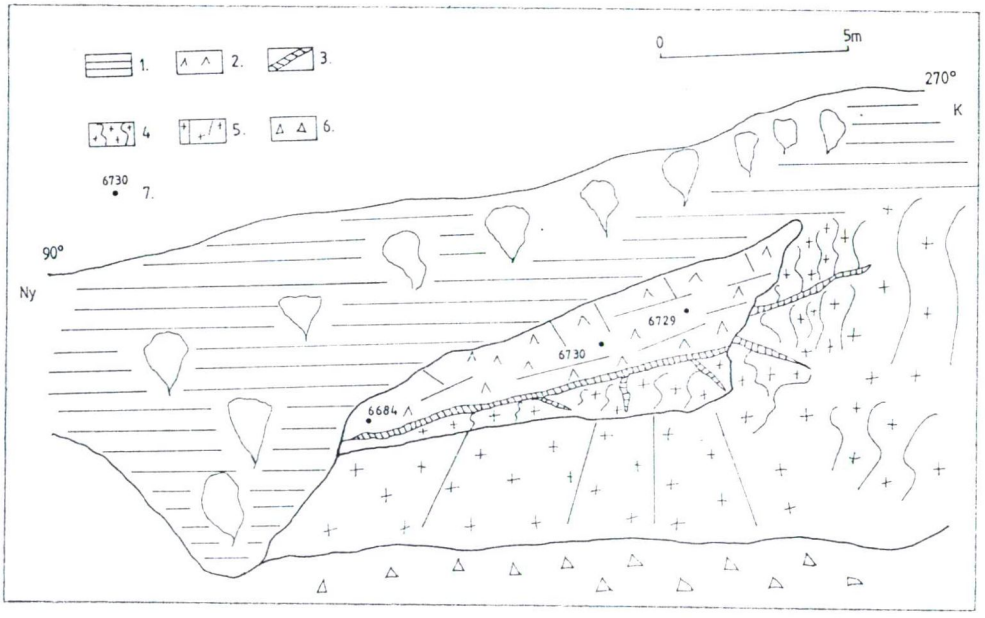

Fig. 2. Sketch about the alkaline dyke rock with trachytic texture in the granite. Mórágy quarry. Legend: 1. soil, 2. reddish-coloured dyke, 3. calcite vein, 4. granite mylonite, 5. medium-grained granite, 6. debris, 7. sampling locality and number of samples.

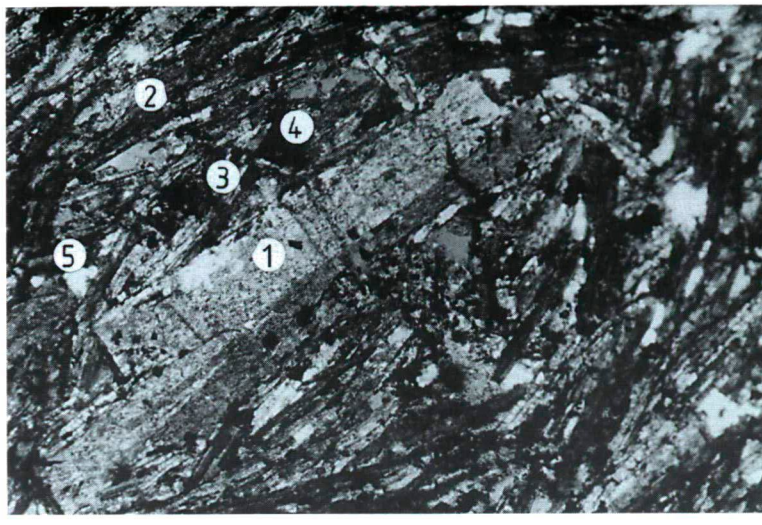

Fig. 3. Microholocrystalline trachytic texture with phenocrysts of sanidine from the Mórágy quarry. 1. phenocrysts of sanidine, 2. fluidal arrangement of alkali feldspar laths, 3. limonite, 4. pyrite, 5. quartz. 100x, +N.

Fig. 4. Sanidine penetration from Mórágy quarry. 100x, +N.

1.1.2. Dyke in the granite quarry at Kismórágy No. 3.

The examined dyke rocks occur quarries located behind the Mórágy railway station (*Fig. 5.*). One of the typical occurrences is shown by *Fig. 6.* Here the dyke is 0.6 m thick only and intruded into a fault which has a 6–8 m high and broad slickenside. It is accompanied by 0.5 m thick tectonic breccia wall-rock with 10/85–90° dip, consisting of alkalitrachyte and granite mixture. Dip of the dyke is the same, and indentical with that of dyke of Mórágy granite quarry. Megascopically the rock is fine-grained type (1. type). Due to a lot of fissures and cooling stripes the dyke material is strongly altered.

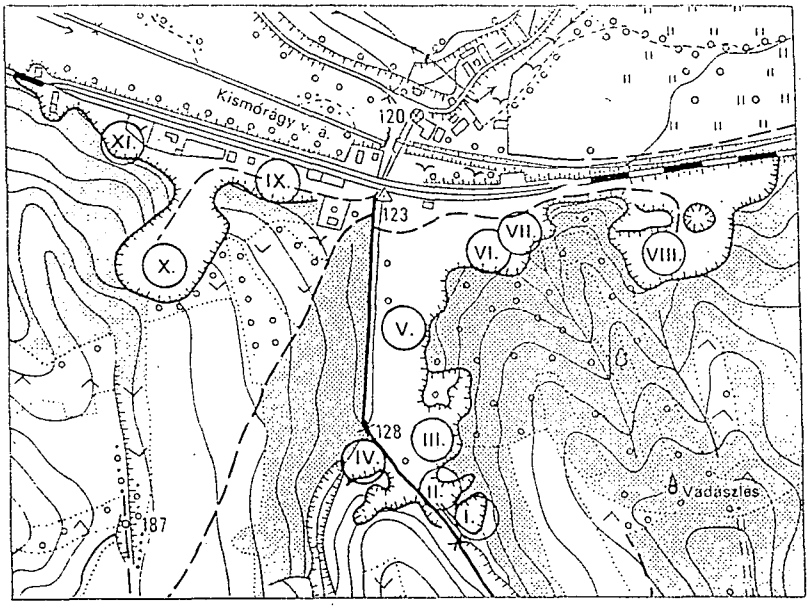

Fig. 5. Sketch about granite quarries at Kismórágy (SZEDERKÉNYI in FÜLÖP 1994)

The microscope shows a microholocrystalline, porphyric, trachytic texture corresponding to that of dyke of Mórágy quarry. Alkali feldspars of groundmass give about 90% portion of the rock, but they are strongly linonitized, calcitized and sericitized. These secondary minerals form 10–15% portion of the rock. Secondary quartz is less than 5% forming little xenomorph grains. Mafic minerals are do not occur or invisible.

The laths of alkali feldspar of groundmass are only 10×70 μm long. The oriented sampling shows that the dyke material flowed from East to West before the melt solidified in the same way as the dyke of Mórágy did. This dyke contains feldspar phenocrysts, too. Optically these are negative, their crackings are very dens and they probably are orthoclase, but in highly sericitized state. Their average grain size measures 2250×1560 μm. On the basis of mineralogical composition this rock can be classified as alkalitrachyte.

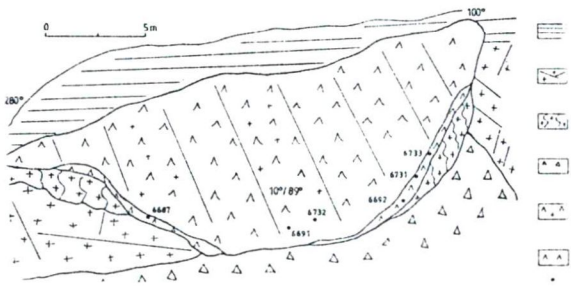

Fig. 6/a. Sketch of alkali dyke rock with trachytic texture and his breccia in the granite. Kismórágy quarry, No. 3. Legend: 1. soil, 2. fractured granite, 3. granite mylonite, 4. debris, 5. reddish-coloured dyke and slickenside accompained by granite breccia wall-rock, 6. reddish-coloured dyke, 7. sampling locality and number of samples

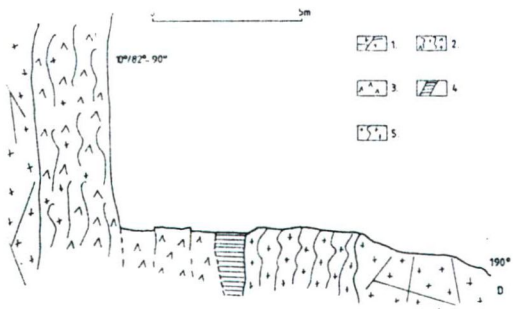

Fig. 6/b. Sketch of alkali dyke rock from frontial situation. Kismórágy quarry No. 3.
Legend: 1. fractured granite, 2. red dyke and slickenside of accompained granite breccia wall-rock, 3. red dyke, 4. calcite vein, 5. granite mylonite.

1.1.3. Ófalu: Aranyos-valley and Till farm-valley

East of Ófalu in several valleys reddish-coloured, trachytic textured dykes or sills occur penetrated into the metamorph rocks. In the occurence of Aranyos valley (500 m towards South of Percel farm, right side of the bank of creek) the dip of dyke is 310°/83° and it length is 20 m (*Fig. 7.*). Due to the tectonical fracturing the border of this dyke is not definable.

Megascopically the hard and relative fresh rock is red, brown coloured and ranged into the 2. type. 1×0.2 cm large sanidine naked eye phenocrysts are visible with tipical cross-cracking.

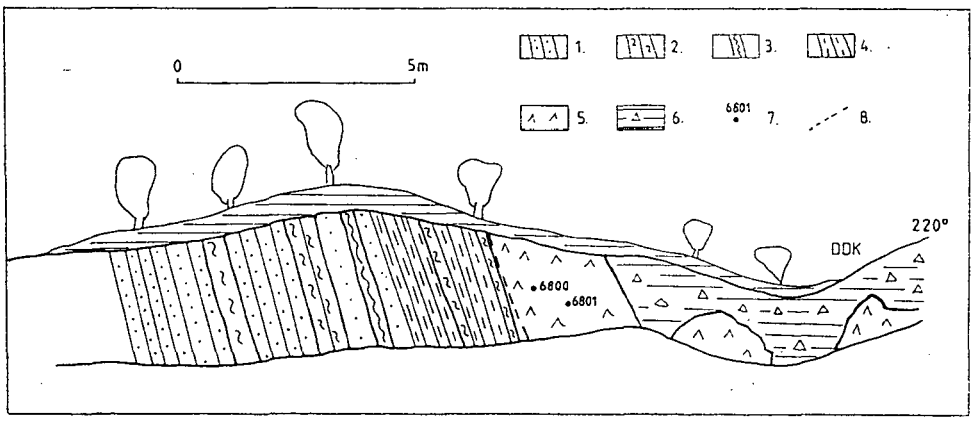

Fig. 7. Sketch of alkali dyke rock with trachytic texture in metamorphic surroundings, Ófalu, Aranyos-valley. Legend: 1. metasandstone, 2. sericitized micaschist, 3. migmatite, 4. clay schist and silica schist with chert, 5. reddish-coloured dyke, 6. soil, 7. sampling locality and number of samples, 8. fault.

Microscopic feature of this rock is also trachytic with fluidal arrangement of strongly sericitized feldspar groundmass. Phorphyric sanidine crystals characterized by 100 plane and typical cross-cracking (*Fig. 8.*) occur with a fairly big frequency. Their average size measures 2460×1140 μm. A lot of phenocrysts are altered and surrounded by wreath of very small zircon minerals. On the basis of mineralogical composition this rock can be classified as alkalitrachyte.

In the Till farm-valley (700 m towards the South of the farm, located on the both side of the creek) at the hydrological object a dyke and abundant debris of this dyke occur. Length of the outcropped dyke in the metamorphic sericite schist is 4 m, and its material is strongly fractured. Rather dense red spottedness is conspicuous on the rock. In the centre of every patch 1×0.5 cm big feldspar table is observable (*Fig. 9.*).

Microscopic features are similar to that of the rock of Aranyos-valley, but here the phorphyries are orthoclase crystals. The rock is strongly altered, the feldspars are surrounded by wide solution stipes with red-coloured, unshaped limonites. On the basis of mineralogical composition this rock is also classified as alkalitrachyte.

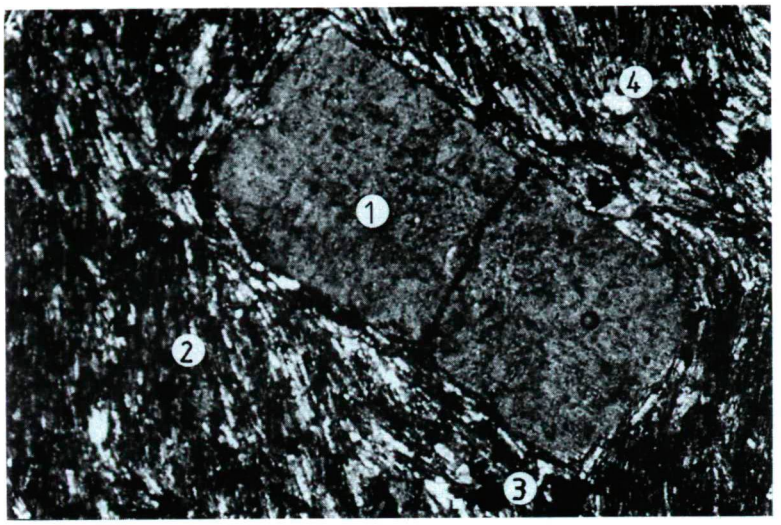

Fig. 8. Sanidine phenocryst in the microholocrystalline trachytic groundmass from Ófalu, Aranyos-valley.
Legend: 1. sanidine, 2. fluidal arrangement of alkali feldspar laths, 4. pyrite, 4. quartz. 50x, +N.

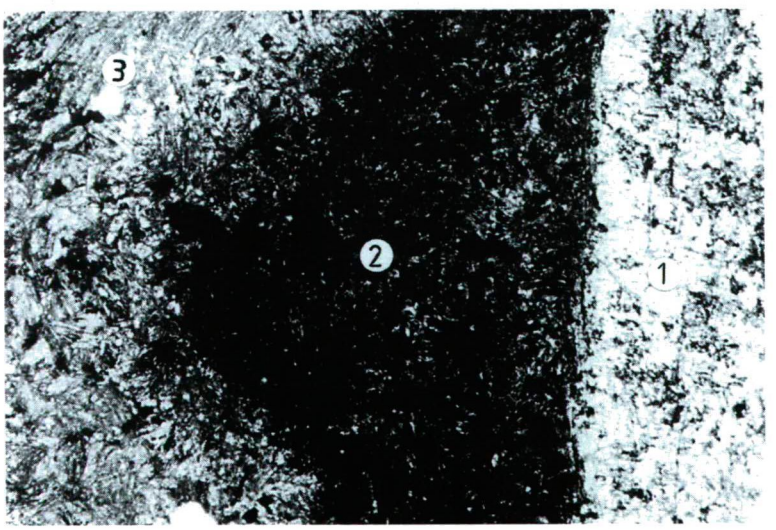

Fig. 9. Weathering of feldspar phenocryst. Till farm-valley.
1. feldspar, 2. limonitized, weathered part, 3. alkali feldspar laths of groundmass. 50x, +N.

2. Greenish-coloured, microholocrystalline, porphyric rock forming a subvolcanic (laccolith) body

These rocks occur in Kismórágy No. 5, 6, 10 quarries, exclusively (*Fig. 5.*). The bigest outcrop is found in the quarry No. 5. (*Fig. 10.*). In this quarry the rock-body shows very complicated surface having 30°, 70° or 90° dip. It resembles to a small 40 m long and 5–20 m high and 10–20 m broad laccolith body with a dome configuration. Eastern side of the outcrop a fault is found with 360°/60° dip. Left from it a "layered dyke" occurs. Inner part of this "layered dyke" becomes gradually decayed and it turns into clayey consistency. 1–2 cm thick calcite crust and 2–3 cm thick undefinable greenish-coloured, gelatinous material

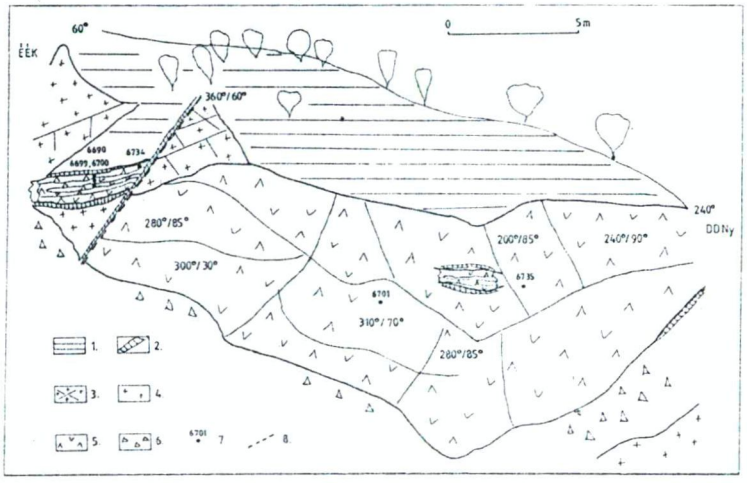

Fig. 10. Sketch of subvolcanic laccolith in Kismórágy quarry, No. 5.
Legend: 1. soil, 2. calcite vein, 3. fractured granite, 4. coarse-grained granite, 5. green-coloured intrusion (laccolith), 6. debris, 7. sampling locality and number of samples, 8. fault.

cover the rock body which may exist as a remnant of an inner contant of laccolith. Its exocontact zone is hidden in the strongly fractured closing granite. Probably the elevating melt of laccolith crushed and arched the granite above the dome. Apart from the local fracturing, the closing large granite mass was impermeable, therefore volatiles of the laccolith were trapped within the subvolcanic body and covering brecciated granite causing a powerful decomposition in them. During the period of this autometasomatism the iron content of the laccolith could not oxidizing so the greenish colour became widespread.

Besides the laccolith subvolcano the greenish-coloured trachyandesites as 1–3 m thick dikes also occur in the Kismórágy quarry No. 6. (*Fig. 11.*) and No. 10. In the latter has

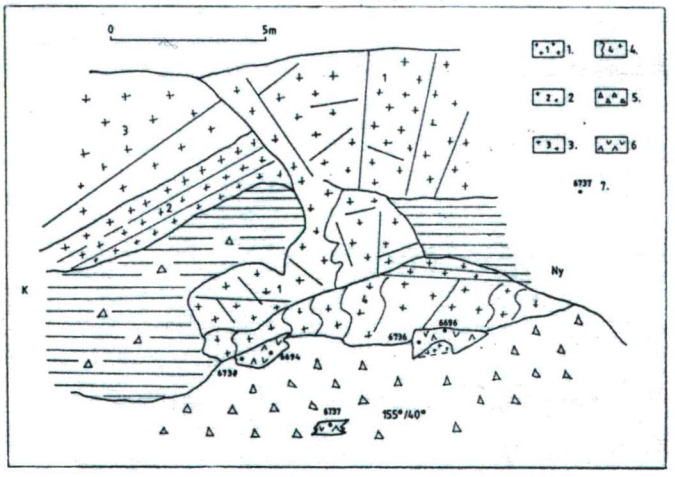

Fig. 11. Sketch of subvolcanic dyke rocks from Kismórágy quarry, No. 6.
Legend: 1. medium-grained granite, 2. fine-grained granite, 3. coarse-grained granite, 4. granite-mylonite 5. debris, 6. green-coloured dyke rocks, 7. sampling locality and number of samples

152°/40° dip and the dyke is represented by strongly-folded rock. These greenish-coloured dykes occupy more than 150 m^2 area in the quarries. A direct connection between the laccolith and dykes is not recovered yet.

Megascopically, every trachytic rocks of mentioned quarries are similar to each other i. e.: fine-grained, greenish-, greyish-coloured, homogeneous, massive rocks with fine calcite network.

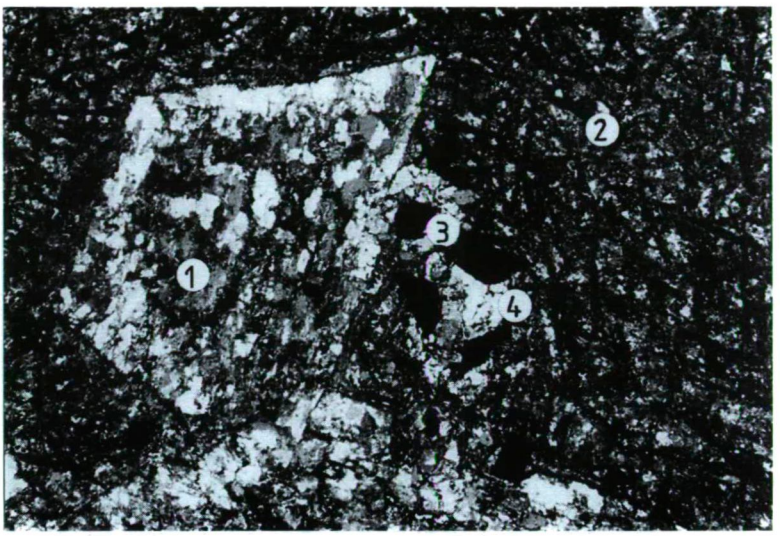

Fig. 12. Tabular feldspar in the sericitized, glassy groundmass from Kismórágy quarry, No. 5. 1. feldspar phenocryst, 2. radiating feldspar crystal germs, 3. pyrite, 4. calcite. 50x, +N.

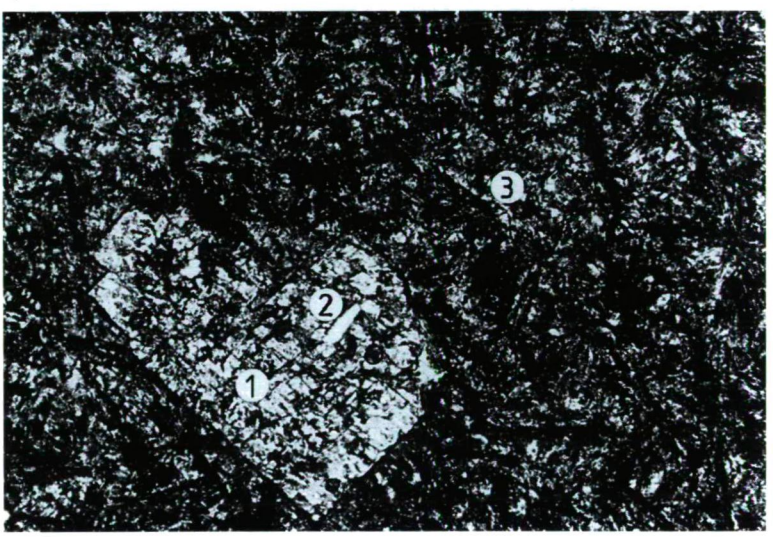

Fig. 13. Sericitized tabular feldspar phenocryst with apatite embedded into the microholocrystalline groundmass from Kismórágy quarry, No. 6. 1. feldspar, 2. apatite, 3. groundmass. 50x, +N.

The microscope shows an altered microholocrystalline porphyric texture with trachytic base. In the groundmass there are a lot of crystal germs and sometimes glass (*Fig. 12.*), suggesting a quick cooling. Needle-shaped minerals in the groundmass (feldspar is 80×10 μm) settled down radially and their quantity reach the 70–90%. Slight fluidal arrangement is characteristic in the dyke rocks, exclusiveley. The groundmass is strongly calcitized, cloritized, sericitized and clayey. Opak minerals are fairly abundant (3% of the groundmass). Pyrite, limonite (5% of the groundmass) are visible mainly next to the feldspar phenocrysts (*Fig. 12.*). Apatite also occurs and, it measures 90×25 μm (*Fig. 13.*). Mafic minerals were probably amphiboles but nowadays they exist only as pseudomorphs consisting of limonite, opacite and mainly calcite (10–30% of the groundmass). These pseudomorphs are surrounded by carbonatic or clay minerals as well as limonite. The phenocrysts are tabular feldspars and amphibole pseudomorphs. Their bigest measurement is 3300×1600 μm. Quartz is less than 3%.

On the basis of mineralogical composition this rock is qualified as subvolcanic trachyandesite (or latite) which have phenocrysts of plagioclase and K-feldspar in nearly equal amounts, little or no quartz and from fine-crystalline to glassy groundmass. The latter consists of undeterminable feldspars.

CONCLUSIONS

Two different trachytic subvolcanic rock-types are recognized in the valleys of Mórágy, Kismórágy, Bátaapáti, and Ófalu. On the basis of their relations, modal composition, macroscopic and microscopic features, using the IUGS nomenclature they can be classified as follows:

1. Alkalitrachytes. Reddish-coloured, fine-grained, oxidized rocks which occur only as dykes. Their srikes E-W are in general, but subordinatelly N-S and NE-SN ones also occur. Macroscopic features of these rocks are really similar to that of the scarcely occuring "bostonite" reference rocks. The microscope shows microholocrystalline, porphyritic, trachytic texture and alkali feldspar microlites more or less fluidal arrangement with phenocrysts of sanidine.

2. Trachyandesites (or latites). Greenish-coloured, fine-grained strongly calcitized rocks which occur in two kind of forms: local intrusion (probably laccolith) and related dykes. The microscope shows a microholocrystalline, porphyritic texture with trachytic base. The phenocrysts are strongly altered feldspars, probably plagioclase and sanidine or orthoclase in nearly equal amounts. The groundmass are from microcrystalline to glassy which may consists of obscure feldspars.

These petrographic estimations require through geochemical confirmation carried out on every rock-type written in this paper.

REFERENCES

ÁRVÁNÉ S. E., BALOGH K., RAVASZNÉ B. L., RAVASZ Cs. (1987): Mezozoós magmás kőzetek K/Ar kora Magyarország egyes területein. MÁFI Évi jelentés. 1985. évről, 295–307.

ÁRVÁNÉ S. E., RAVASZNÉ B. L. (1992): A Mecsek és a Villányi hegység között feltárt kréta telérkőzetek K/Ar kora. MÁFI Évi jelentés. 1990. évről, 229–240.

BATES R. L., JACKSON J. A. (1980): Glossary of Geology

FÜLÖP J. (1994): Magyarország geológiája, Paleozoikum. II. Akadémiai Kiadó, 306–317.

GHANEM, M. A., RAVASZNÉ, B. L. (1969): Petrographie study of the crystalline basement rocks Mecsek Mt. Hungary. Acta Geol. Ac. Sci. Hung., 191–219.

HETÉNYI R., HÁMOR G., FÖLDI M., JANTSKY B. (1976): Magyarázó a Mecsek-hegység földtani térképéhez 10000-es sorozat. Ófalu, 31–39.
HUNTER, M., ROSEMBUCH, H. (1890): Über Monchiqit, ein Camptonitisches Ganggestein aus der Gefolgschaft Elaolithsyenite. Tschermarks Petr. Mitt. **11**, 447.
JANTSKY B. (1950): A mecseki kristályos alaphegység földtani viszonyai. MÁFI Évi Jelentés. 1950. évről, 65–77.
JANTSKY B. (1979): A mecseki gránitosodott kristályos alaphegység földtana. MÁFI Évkönyv LX., **30**, 147, 150.
JÁRÁNYI K. (1970): A Mórágy környéki gránitoid kőzetek vizsgálata, különös tekintettel a gránitosodás folyamatára. Manuscript. ELTE Budapest, 52–54.
JOHANSEN, A. (1937): A descreptive petrography of the igneous rocks. The University of Chicago Press. Vol III, 26–27. Vol IV, 22–23.
LE MAITRE, E. W. (1989): Classification of igneous rocks and glossary of terms. Blackwell Scientific Publications, London.
KOCSI Z. (1995): A Mórágyi rögben található alsó kréta korú bosztonitok térbeli elhelyezkedése és petrográfiája. Manuscript. JATE Szeged.
MAURITZ B., Csajághy G. (1952): Alkáli telérkőzetek Mórágy környékéről. Földtani Közlöny **82**, 137–142.
PANTÓ Gy. (1980): Ritkaföldfémek geokémiája és néhány alkalmazási területe. Doktori Értekezés. MTA Könyvtár, Bp. 101–121.
ROSENBUCH, H. (1907): Mikroskopische Physiographie der Mineralien und Gestein I. Stuttgart. Band II, 600–607.
SORENSEN, H. (1974): The alkaline rocks. John Wiley and Sons Ltd. New York.
SZAKMÁNY GY., JÓZSA S. (1994): Rare pebbles from the miocene conglomerate of Mecsek Mountains. Hungary. Acta Miner. Petr. Szeged XXXV, Supplementum, 53–64.
SZÉKINÉ F. V. (1952): A magmás kőzetek szerepe a komlói kőszénöszletben. MTA Műszaki O. K. 5/3, 187–209.
TRÖGER I. E. (1935): Spezielle Petrographie Eruptivgesteine. Verlag der Deutschen Mineralogischen Gesellschaft V. Berlin, 81.

Acta Mineralogica-Petrographica, Szeged, XXXVI, 143–152, 1995

EVOLUTION OF CHONDRITIC PARENT BODIES I: CORRELATION AMONG FERROUS COMPONENTS

SZ. BÉRCZI*, ÁGNES HOLBA** and B. LUKÁCS**

*Dean's Office & Astronomy Dept., R. Eötvös University
**Central Research Institute for Physics

ABSTRACT

The thermal and chemical evolution of the precursors of chondritic meteorites are discussed by using the data of recent chemical analyses performed in the NIPR, Tokyo, Japan, mainly on Antarctic meteorites.

INTRODUCTION

Meteorites are small bodies, but many of them show clear signs of previous intensive thermal evolution and transformation, which is quite possible if they are fragments of bigger objects, the so called parent podies. A few parent bodies have been identified: e. g. some very few meteorites are fragments of Luna and Mars, and it is quite possible that eucrites come from the asteroid Vesta. However all these meteorites are differentiated achondrites.

Chondrites still preserve partially the primordial structure. So their parent bodies must have been smaller. One can guess that they were comets or medium or small asteroids, with much less chance to be individually identified. Still some general properties of these parent bodies can be traced back from the chondrites.

Such a reconstruction needs a large number of data to be collected, mainly for texture and chemical composition. In 1995 a Japanese group published the database largest up to now for chemical compositions. We try to draw some conclusions from this database about the thermal and chemical evolution in the parent bodies. We also were able, by the courtesy of the NIPR, Tokyo, to perform optical investigations on representatives of all standard chondrite types, on a thin section collection from Antarctic meteorites.

The present approach will be empirical. In Sect. 2 we recapitulate the classification of chondrites, in Sect. 3 the Japanese database is discussed, and in Sect. 4 we make some statistical evaluation based on this database. Sect. 5 contains the results and discussions.

ABOUT THE VAN SCHMUS-WOOD CLASSIFICATION

Meteorites are traditionally classified triadically according to the main chemical components as

* H–1088 Rákóczi út 5., Budapest, Hungary
** H–1525 Bp. 114. Pf. 49., Budapest, Hungary

1) Irons (mainly FeNi)
2) Stony-Irons (mosaics of FeNi and the next group); and
3) Stones (mainly silicates).

The main component of stone meteorites is some silicate, i. e. a SiO_2 lattice with metal oxides inside. The stones are further subdivided dually according to the presence of small beads of silicates called chondrules (of sizes from 0.1 mm up to mm's). Then we get:

A) Achondrites (chondrules missing); and
B) Chondrites (chondrules present).

Third, chondrites can be further divided according to the dominant silicates in the matrix and in the chondrules, plus the state of the chondrules. Before going into details, we summarize the classification up to this point according tot he ROSE–PRIOR–MASON–ANDERS scheme (BÉRCZI, 1991) on *Fig. 1.*

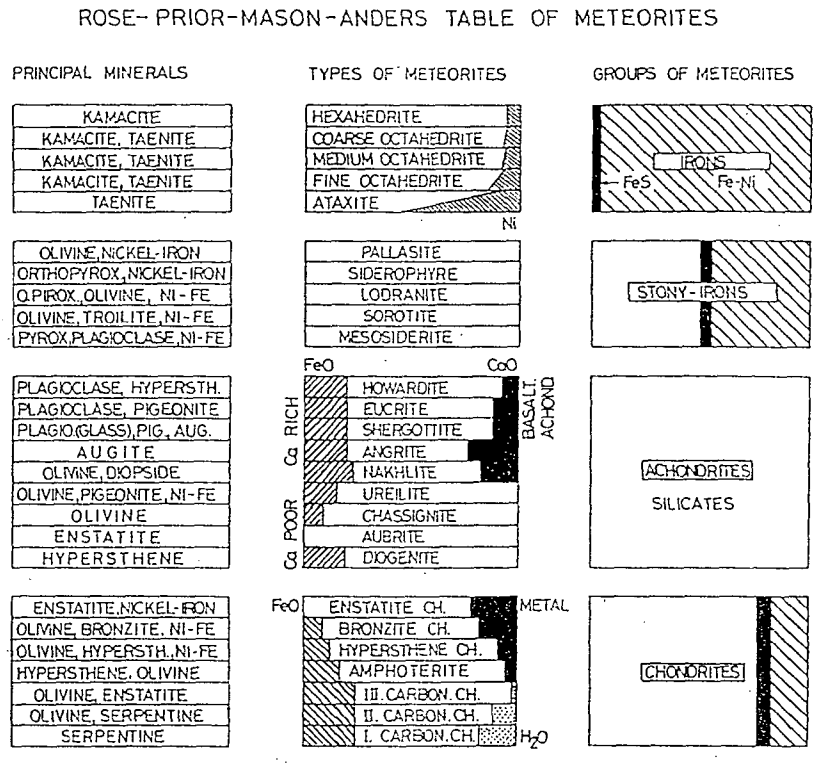

Fig. 1. The ROSE–PRIOR–MASON–ANDERS scheme.

Classical classifications of meteorites into irons, stony-irons and stones, and further distinction in the last group to chondrites and achondrites are shown on the right edge column. In middle column the meteorite types with their names are given. On the left column the main mineral components of the corresponding meteorites – in the same row – are given. Generations of investigators worked on this classification of which here ROSE, PRIOR, MASON and ANDERS were emerged.

Further developments of this system happened, when lunar and Martian meteorites were identified. To lunar meteorites 13 distinct samples belong in 1995 January. (see for instance: YANAI, KOJIMA, 1991) To Martian meteorites 10 distinct samples belong in 1995 January. Most of them belonged earlier to the Nakhlite, Shergottite, Chassignite group (the SNC meteorites), but later such type of meteorite was found among diogenties, too. (see i. e. MITTLEFEHLDT, 1994.)

According to common opinion, chondrites seem to be less evolved than achondrites. Achondrites are understood as bodies where the chondrules have been obliterated by heat & c. Here we concentrate on chondrites. They were classified first by PRIOR (1916), who summarized their main chemical characteristics in the PRIOR Rules. UREY and CRAIG (1953) named two groups of chondrites according to their non-oxidized vs. oxidized Fe content. These two central groups on the 2-dimensional plot are the L (low) and H (high) ones, meaning the non-oxidized (metallic and sulphide) component.

WIIK further developed both PRIOR Rules and UREY–CRAIG classification (WIIK, 1956). He subdivided the carbonaceous chondrites into three types. Then MASON (1962) subdivided the two UREY–CRAIG groups, and included carbonaceous chondrites. So a system emerged with 5 types, mainly according to the percentage of the non-oxidized Fe in the total mass of the meteorite. From above down the 5 types were

$$E \rightarrow H \rightarrow L \rightarrow LL \rightarrow C$$

In accordance with the PRIOR Rules the non-oxidized Fe content strongly correlates with the type of silicate dominating in the pyroxenes of the meteorite as (MASON, 1962):

E → enstatite
H → bronzite
L → hypersthene
LL → pigeonite

(In C's serpentine is frequent.) By this observation one could determine the type without chemical analysis from microscopy of thin sections. It remains open how strict is this correlation.

In the early 60-ies J. A. WOOD and E. ANDERS studied in details the texture of chondrites and they recognized, that thermal transformations can be deciphered from different textural features of meteorites with the same type. From these studies grow out the next important step in the chondrite classification. VAN SCHMUS and WOOD (1967) introduced the notion of petrologic class, a number from 1 to 6 as

1) Still no chondrules (very much volatiles).
2) Sharp chondrule boundaries, more volatiles.
3) Sharp chondrule boundaries, less volatiles.
4) Slightly blurred chondrule boundaries.
5) Obscure chondrule boundaries.
6) Badly defined chondrule boundaries (hardly seen).

Recently a Class 7 has been introduced too in which chondrules cannot be seen at all, but still the general texture is similar to that of chondrites of Class 6. A possible explanation is that this sequence shows the higher and higher heat impact in the history of the body, washing out the sharp boundaries by diffusion.

When WIIK (1956) recognised, as thum rule, from 30 selected chondrites that, removing volatiles, there seems to be a tendency to get only two values for total Fe content: cca. 27% for E's, H's and C's, and cca. 22% for L's and LL's, the possibility of evolutionary models were opened (see e. g. SZTRÓKAY 1966).

However all these results were obtained from very limited samples below 100 specimens, and it is easy to see that in the full VAN SCHMUS–WOOD classification the number of possible classes is between 20 and 30 (petrologic classes 1 and 2 are known only for C's up to now), therefore the classes were so poorly populated that the statistical analysis was almost hopeless.

THE CATALOG OF ANTARCTIC METEORITES

The National Institute of Polar Research in Tokyo started to collect meteorites from the icefields of the Antarctic interior in 1969. Conservation conditions are the best there on Earth, all of them are easily discriminated from the environment, and accumulating for tens of thousand of years. So the statistics is best for Antarctic meteorites. A group working first under K. YANAI and now under H. KOJIMA is continuously classifying and analysing the meteorites and the recent stage of research was published in 1995 in a Catalog (YANAI, KOJIMA and HARAMURA, 1995). The Catalog contains some 8000 meteorites in the NIPR collection, of which more than 3000 have been classified into the VAN SCHMUS–WOOD scheme, and standard wet chemical analysis has been performed for 549. This is the biggest available homogeneous sample whose chemical compositions are known.

By using this huge database one can get many data characterizing the various chondrite types with at least modest statistical reliability. Here we note that the distribution of the analysed chondrites is such that more populated C and LL classes contain samples in the order of 10, L and H ones are more numerous and the most populated class is L6 with 94 meteorites. We have started a statistical analysis of the data and give here some preliminary results concentrated on Fe contents.

SOME CHARACTERISTIC DATA OF THE CHONDRITE COMPOSITONS

Fig. 2 gives the average values of Fe concentration in FeO, Fe_2O_3, FeS and metallic phase, relative to the Si content. One can see that the total Fe contents of E's, H's and C's are rather similar (cf. WIIK's observation), but there are some differences between L's and LL's (at some petrologic classes they are statistically significant). Also, one sees that FeS is substantial in early C's and E's, but nowhere else.

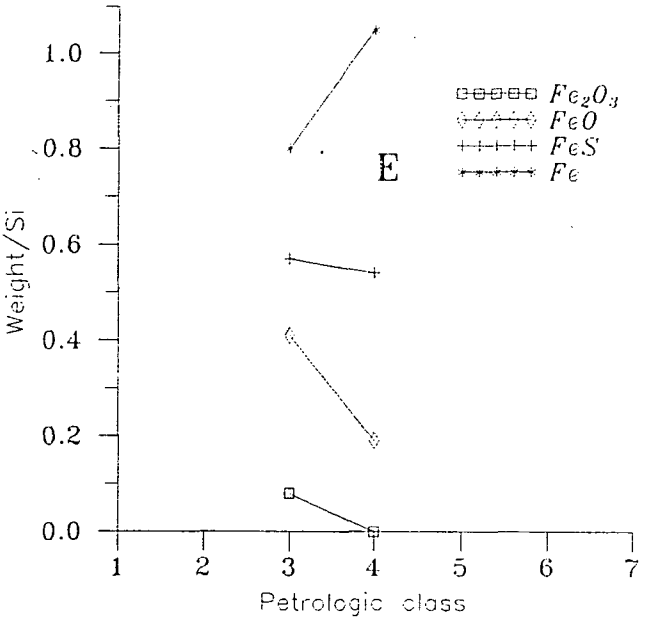

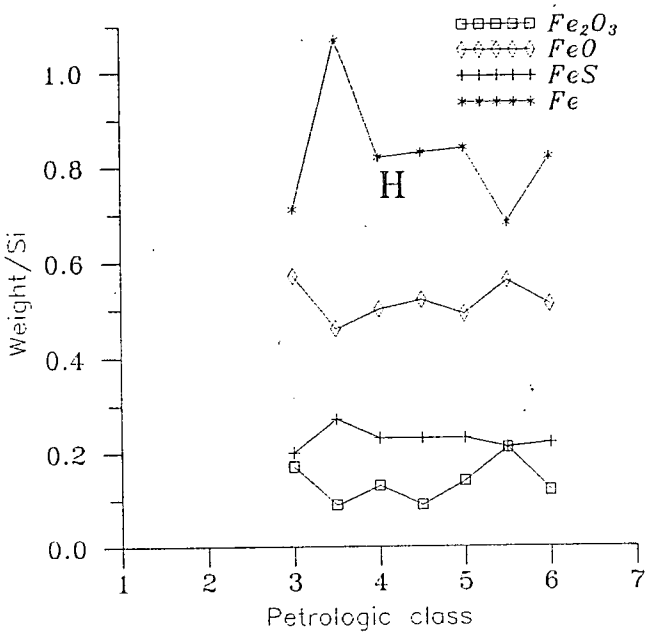
Fe_2O_3
FeO
FeS
Fe
H
Weight/Si
1.0
0.8
0.6
0.4
0.2
0.0
1
2
3
4
5
6
7
Petrologic class

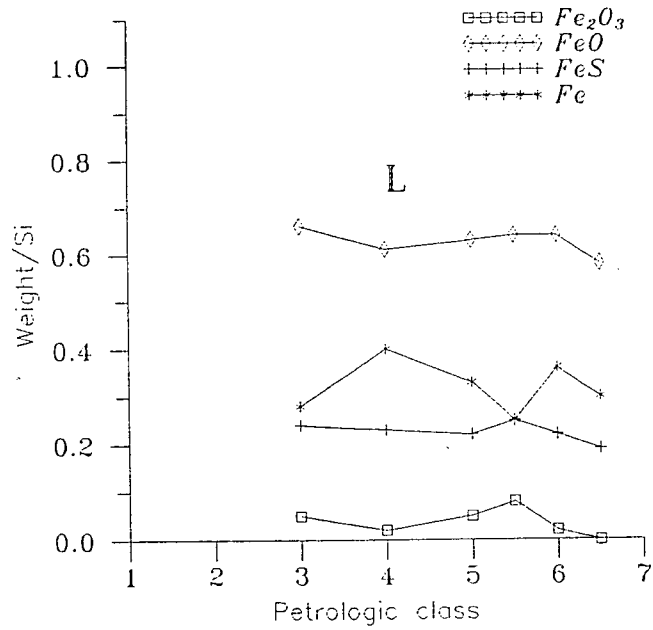
Fe_2O_3
FeO
FeS
Fe
L
Weight/Si
1.0
0.8
0.6
0.4
0.2
0.0
1
2
3
4
5
6
7
Petrologic class

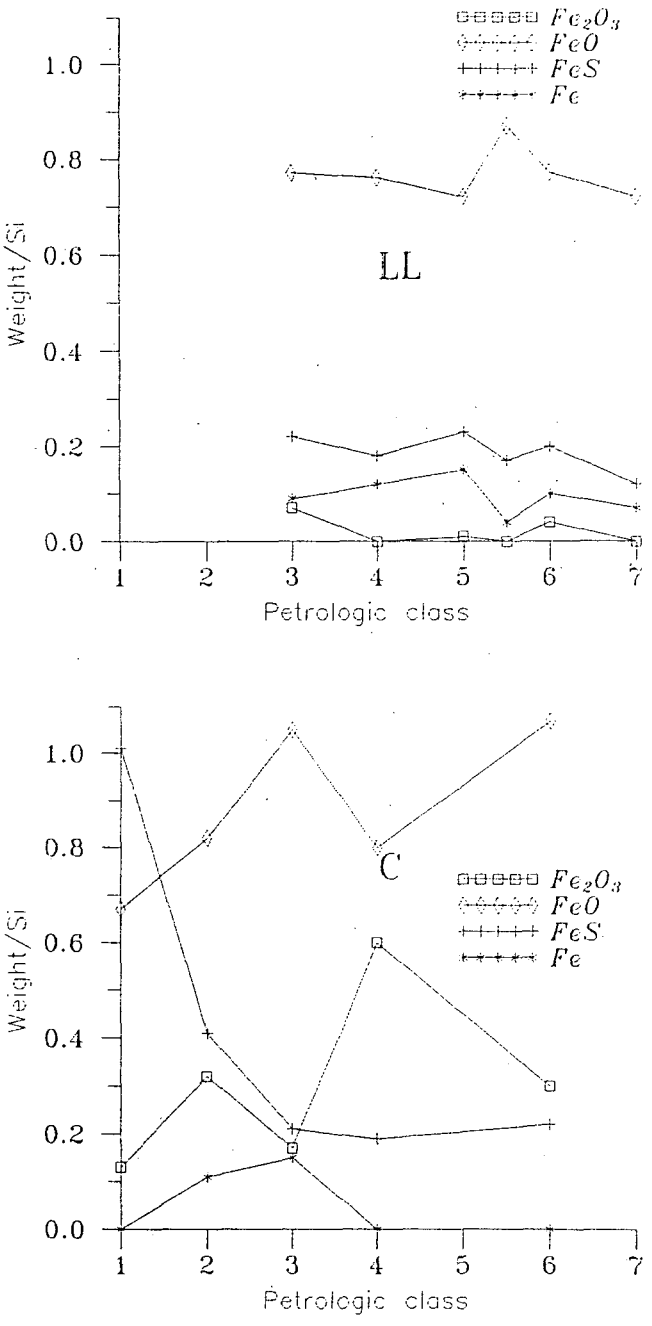

Fig. 2. The Fe/Si weight ratios for 4 different chemical positions of Fe vs. petrologic class, separately for E, H, L, LL and C chondrites, according to the averages of meteorites in the NIPR analysis.

Now, for the reconstruction of the past history of the chondrites, it is important to see the correlations between the different ferrous compounds; they reflect the processes which transferred the common Fe stock from one form to another. Correlation coefficient between two quantities x and y on the same manifold is defined as (EZEKIEL and FOX, 1969).

$$r_{xy} = (\langle xy\rangle - \langle x\rangle\langle y\rangle) / (\sigma_x\sigma_y) \qquad (4.1)$$

This quantity is between +1 and –1 by construction, and values near to +1 are signals for strong positive connections between the individual fluctuations of the two quantities. High negative values indicate similarly strong connection, but in opposite direction. Values near 0 do not prove disconnectedness, but strongly suggest that. In first approximation the statistical mean error of r is

$$\delta r = (1-r^2) / \sqrt{n} \qquad (4.2)$$

where n is the size of the sample. Significant *negative* correlation between 2 ferrous compounds at least suggest that the two compounds may go into each other in a process, and strong positive correlations are suspected for similar behaviour in the dominant processes.

The correlation coefficients read as:

TABLE 1

Correlation coefficients r between the concentrations of Fe in different chemical positions. Always the Fe content is meant

Type	r						$n^{-1/2}$
	FeO, Fe_2O_3	FeO, Fe	FeO, FeS	Fe_2O_3, Fe	Fe_2O_3, FeS	Fe, FeS	
E3	–0.42	–0.85	–0.60	–0.04	–0.40	+0.73	0.44
H3	–0.20	–0.56	+0.11	–0.63	–0.30	+0.17	0.29
H3–4	–0.65	–0.27	+0.45	–0.41	–0.62	–0.23	0.50
H4	–0.26	–0.36	–0.36	–0.59	+0.11	+0.16	0.12
H4–5	+0.11	–0.41	–0.61	–0.84	+0.12	+0.04	0.33
H5	–0.38	–0.41	–0.17	–0.59	–0.07	–0.10	0.15
H6	+0.53	–0.77	+0.74	–0.86	+0.62	–0.76	0.21
L3	–0.14	–0.52	–0.55	–0.43	–0.15	+0.30	0.22
L4	–0.40	–0.22	–0.36	–0.43	+0.13	–0.05	0.19
L5	–0.59	+0.38	+0.11	–0.78	–0.35	+0.42	0.24
L5–6	–0.80	+0.50	–0.47	–0.92	–0.14	+0.52	0.58
L6	–0.41	–0.25	–0.34	–0.41	+0.17	+0.01	0.10
LL3	–0.61	–0.41	–0.51	+0.08	+0.02	+0.11	0.32
LL4	–0.62	–0.61	–0.32	+0.28	+0.30	–0.26	0.33
LL5	–0.43	–0.79	–0.65	+0.49	–0.15	+0.20	0.33
LL6	–0.93	–0.18	–0.37	+0.03	+0.16	+0.55	0.24
C2	–0.76	–0.19	–0.05	–0.18	–0.32	–0.24	0.24
C3	–0.72	–0.39	+0.03	–0.33	+0.02	–0.16	0.32

For the omitted types there are no enough samples for calculating the correlation coefficient. The last column is to see the significance of the coefficients.

There is no room to discuss all the correlations in all types. We choose only several characteristic classes.

For E3's the only significant r's show that Fe and FeS are both concurrents of FeO. In H4 everything else concur with FeO. In L4 both Fe_2O_3 and Fe are concurrents of FeO. The same is true for L6, but there Fe and Fe_2O_3 change together. In LL3 again FeO concurres

with everything else; the same is true for LL6, but there also Fe and FeS change together, just as for L6. C2, however, is quite different: Fe_2O_3 changes oppositely to FeO and FeS, and Fe changes oppositely to FeS too.

Even with the present huge database in some VAN SCHMUS–WOOD classes the measured correlations are not significant. One can guess that for significant results in each class 50–100 analysed samples would be needed, and this number will be reached when some 3000 meteorites will have been analysed.

RESULTS AND DISCUSSIONS

First let us see again *Fig. 2*. Our hope is that this Figure tells something about the relations among the different chondritic types. Namely, chondrites may differ in initial conditions and in subsequent evolution as well. The only clear point is that higher petrologic classes got higher heat impact. But we practically do not know anything about the origin of main types. Namely, C, H and E chondrites may have been developed from their own primordial progenitors (say C1, H1 and E1), but, since petrologic classes 1 and 2 are known only among C's, it is also possible to imagine some evolution from C2 to H3 or E3 as well. Obviously, average C's cannot be progenitors of LL's and L's because of the different total Fe/C ratio, conserved without global differentiation.

Now, *Fig. 2* shows that the letters of the van Schmus–Wood scheme differ mainly in the degree of oxidation of Fe. This is not surprising at all, since these types are defined according to the FeO content of the pyroxenes and olivines. Now, if some part of the Fe is reduced then the resulting Fe is not a part of the silicate lattice. So a higher metallic (+sulphide) content of the *whole* meteorite must be strongly correlated with a lower FeO content in pyroxenes and olivines.

However, dependences on the petrologic class are more complicated. Let us first see the oxides and the metallic phase. First, FeO always dominate Fe_2O_3; the latter is minor constituent except for some C's. So in the early thermal history of parent bodies the environment was mainly reducing. Still, FeO/Fe is not monotonous with the petrologic class. So some oxidizing agent must have been present too. Except for E's and C's, the ratios of free and bound Fe's show some oscillations (see *Fig. 3*). Note that FeO generally anticorrelates with both Fe_2O_3 and Fe. This suggests that FeO is the original source, and both hypothetical processes influence the quantity of FeO and that of something else.

The sulphide Fe/Si ratio is generally about 0.2. There are two exceptions: the low petrologic class C's, where the ratio rapidly decreases with the petrologic class and reaches the asymptotic value at C3, and E's, whose sulphide contents are similar to those of C2's (slightly in the direction of C1's). So the process reducing FeS was not effective beyond the heat impact of petrologic class 3, and was not effective at all in E's. E3's more or less smoothly follow C2's, if one can invent circumstances in which something (C?) strongly reduces the Fe oxides, while nothing influences the sulphide. Unfortunately the early environment is rather unknown, and anyways, it was exotic compared to those about which we have experience. Iron sulphides are not used in human iron metallurgy, and definitely not in reducing atmospheres.

At the highest petrologic classes metallic Fe and FeS both decrease. The simplest explanation is iron loss by iron melting, possibly starting in this stage. The liquid may leave the silicate body via the gravity of the parent body; note that Fe and FeS are similar to melting points, and also neither of them are in the silicate lattice. So they are lost together, and this is seen in L5, L5–6 and LL6 (but, interestingly, not seen in H6 and L6).

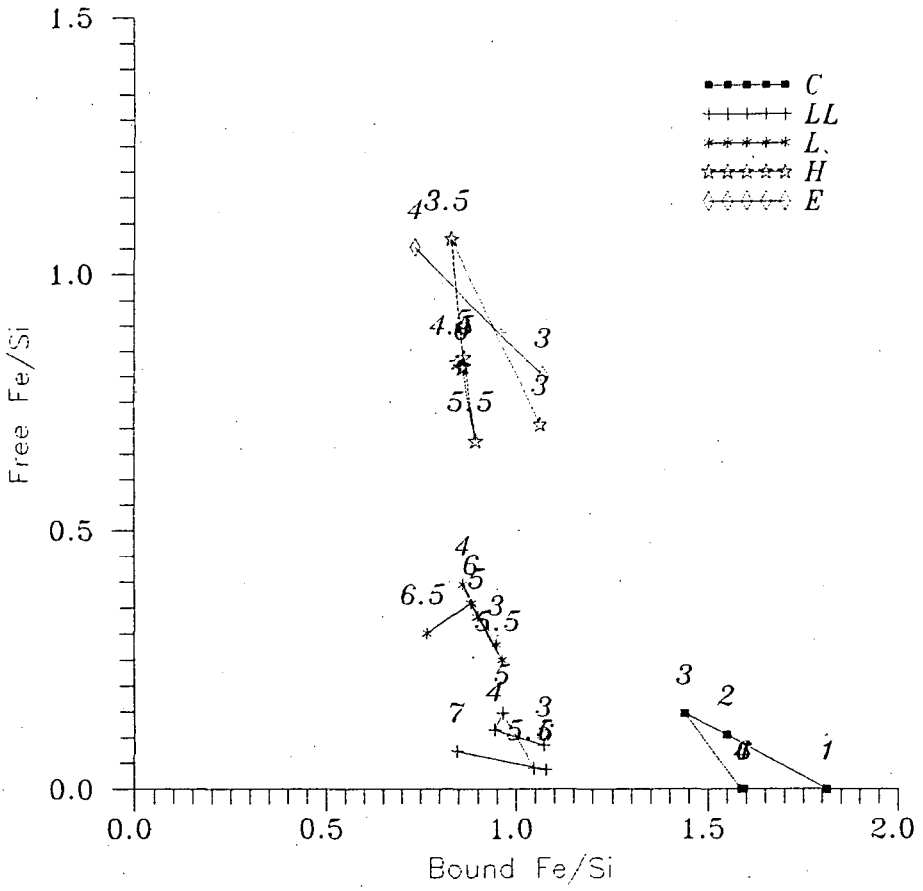

Fig. 3. Average free Fe/Si vs. bound Fe/Si weight ratios for the different classes of chondrites of the NIPR analysis. Petrologic classes are indicated by labels above the points.

Finally, the data suggest that some "transitional" classes do not fit into the VAN SCHMUS–WOOD scheme. The analysers found a few percent of chondrites awkward for petrologic class, which they classified, as best available solution, between two well definied petrologic classes. Now, *Fig. 2* clearly show that H3–4 is not transitional between H3 and H4, and the same is conjectured for LL5–6 and H5–6. These chondrites need further analysis. They may even not be H's or LL's; at least the total Fe/Si content of the average H3–4 is extremely high.

The present treatment was purely empirical. The possible explanatory models will be discussed in a subsequent paper.

ACKNOWLEDGEMENTS

Authors would like to thank the NIPR, Tokyo, Japan, specially Dr. KOJIMA for illuminating discussions and to Drs. KOJIMA and YANAI to lend us earlier copies of the NIPR Antarctic Thin Section Set.

Partly supported by MKM 3356/94.

REFERENCES

BÉRCZI SZ., (1991): Kristályoktól bolygótestekig. Akadémiai, Budapest.

EZEKIEL M. and FOX K. A. (1969): Methods of Correlation and Regression Analysis (Linear and Curvilinear). J. Wiley and Sons, New York.

MASON B. (1962): Meteorites, J. Wiley and Sons, New York.

MITTLEFEHLDT D. W.: (1994): Abstracts of 19th Symp. Antarctic Meteorites, Tokyo, 1994. p. 59.

PRIOR G. T. (1916): Mineral. Mg. **18**, 26.

VAN SCHMUS W. R. and WOOD J. A. (1967): Geochim. Cosmochim. Acta **31**, 747.

SZTRÓKAY K. (1966): Földt. Közl. **XCVII**, 3.

UREY H. C. and CRAIG H. (1953): Geochim. Cosmochim. Acta **4**, 36.

WIIK H. B. (1956): Geochim. Cosmochim. Acta **9**, 279.

YANAI K., KOJIMA H. (1991): Photographic Catalog of Antarctic Meteorites, NIPR, Tokyo.

YANAI K., KOJIMA H. and HARAMURA H. (1995): Catalog of the Antarctic Meteorites, NIPR, Tokyo.

Illustrations

Figures should be used only where they are essential to elucidate text.

The illustrations should be numbered according to their sequence in the text, and in the text references should be made to each figure.

All illustrations should be given separately, not stuck on sheets and not folded. The number of the figure and the authors name should be noted on the reverse side of the photographs and on the lower frontside of drawings, indicating at the same time the top of the figure where it is necessary.

Captions for all figures should be given typewritten on a separate list at the end of the manuscript. Drawn text in the figures should be kept to a minimum.

Drawings should be made on tracing paper by Indian ink. The thickness of the lines and the size of the lettering should enough to allow a necessary reduction.

Photographs of good contract and intensity on glossy paper are only acceptable. Colour photographs or drawings cannot be accepted.

Use bar scale on all illustrations instead of numerical scales that must be changed if reductions are necessary.

References

All references to publications made in the text should be made by quoting the authors's name (without initials) and year of publications in paranthesis.

The list of references at the end of the manuscript should be arranged alphabetically by author'a names and chronologically per author.

If the referred publications are written by more than two authors, in the text only the name of the first author should be indicated, the other co-authors are denoted by "et al.", however, in the list of references the names of authors and all co-authors should be mentioned.

In the list of references all references should be written, e. g. Balogh, K., A. Barabás (1972): The Carboniferous and Permian of Hungary. Acta Miner. Petr. Szeged, XX/2, 191–207.

At references to books beside the author's name, year of publication, title and the publishing house should also be mentioned.

In the case of references for symposium volumes, special issues or multi-authors books, the following system should be used: Roser, B. P., C. W. Childs, and G. P. Glasby (1980); Manganese in New Zealand. In: I. M. Varentsov and Gy. Grassely (Editors): Geology and Geochemistry of Manganese, Vol. II. Akadémiai Kiadó, Budapest, 199–211.

Manuscripts that are not adequately prepared will be returned to the author(s).